MATHEMATICAL MODELS OF ACUTE INFLAMMATION AND A FULL LUNG MODEL OF GAS EXCHANGE UNDER INFLAMMATORY STRESS

by

Angela Marie Reynolds

B.S., Loyola College of Maryland, 2002

Submitted to the Graduate Faculty of

the Department of Mathematics in partial fulfillment

of the requirements for the degree of

Doctor of Philosophy

University of Pittsburgh

2008

UNIVERSITY OF PITTSBURGH

MATHEMATICS DEPARTMENT OF THE UNIVERSITY OF PITTSBURGH

This dissertation was presented

by

Angela Marie Reynolds

It was approved by

Dr. G. Bard Ermentrout, Department of Mathematics

Dr. Gilles Clermont, Department of Critical Care, UPMC

Dr. Jonathan Rubin, Department of Mathematics

Dr. David Swigon, Department of Mathematics

Dissertation Director: Dr. G. Bard Ermentrout, Department of Mathematics

MATHEMATICAL MODELS OF ACUTE INFLAMMATION AND A FULL LUNG MODEL OF GAS EXCHANGE UNDER INFLAMMATORY STRESS

Angela Marie Reynolds, PhD

University of Pittsburgh, 2008

This thesis focuses on the development and analysis of mathematical models of acute inflammation. These models were developed to understand multiple organ dysfunction syndrome (MODS), which is a common cause of death in intensive care unit patients. MODS is characterized by sequential organ failure caused by an overactive immune system. Therefore, our modeling focused on the acute immune response, which is the generic initial response. Understanding the complex interaction during this response will facilitate the development of effective treatments for MODS.

We first derived a small scale model for the acute inflammation to understand simple dynamics between pro- and anti-inflammation. We use this reduced model to explore the role of anti-inflammatory mediators, which were once hypothesized as a treatment for MODS with less success than predicted. After the analysis of this reduced model, we expanded this model into two more complex models.

The first includes specific measurable immune mediators, unlike the four variable model. This model also takes in account the interactions between the tissue and blood, which are essential during an inflammatory response. It is a minimum model for an organ. We used this model to explore the spread of inflammation between organs by linking two tissues units to the same blood supply.

The second models the effects of inflammation on gas exchange in the lung. The lung is typically the first organ to fail during MODS. We developed a model for a single respiratory unit ~25 alveoli). Linking the respiratory units (RUS) under various anatomical conditions

we model the full lung. Methods were developed in order to reduce computation times of the RU model. With shorter computation times we were able to implement more accurate ventilation perfusion mismatch in the full model. To increase biological fidelity of the model we have created a closed loop form of the RU model that accounts for variable arterial PO2 levels.

We have created multiple models that explore various aspects of MODS. We look at the role of anti-inflammation, spread of inflammation and inflammation within the lung in order to understand the complex interactions prompting organ failure.

TABLE OF CONTENTS

LIST OF TABLES

LIST OF FIGURES

ACKNOWLEDGMENTS

I would like to thank my committee members:

To Dr. G. Bard Ermentrout- My advisor since I started at the University of Pittsburgh. You are the reason I came to Pittsburgh and I thank you because it turned out to be a great fit. More importantly though, thank you for being a great advisor. You steered me to a project I would like (not neuroscience), gave me advice and support throughout every bump and snag I hit, all the while keeping me laughing. Thanks for being available for questions. I appreciate the fact that I could always come to your office and ask a question even without a scheduled meeting. Oh yeah, thanks for never forgetting Julian mishap. I will probably think of you every time I hear the name Julian for the rest of my life.

To Dr. Gilles Clermont - a member of my thesis committee and my main biology advisor. I have enjoyed working together with you on inflammation minus some parameter fitting. I could not have asked for a better advisor/collaborator. I truly hope our projects will keep us working together for awhile. Thanks for saving me from life as a TA. I am grateful for the opportunity to work with you as a GSR, from which I have learned more than I ever thought I would. Also, thank you for De-Angela-izing my many abstracts, poster, and papers.

To Dr. Jonathan Rubin - a member of my thesis committee and vital contributor to my research projects. Thanks for your advise and support on my various projects. I could always count on you to keep our meetings on topic.

To Dr. Ermentrout, Dr. Clermont and Dr. Rubin: Thank you for teaming up and working with me on my various projects. For a long time I probably held the record for the most professors at weekly research meeting. I have a had a great time working with all three of you and greatly appreciate all I have learned during my years here. I benefitted greatly from working with some many great researchers simultaneously. I will miss our meetings and am jealous of the next student who works with the three of you.

To David Swigon - a member of my thesis committee, whose knowledge of inflammation and work with his own students made him the ideal fourth member of my committee. Thank

you for agreeing to be a member of my committee and fitting my defense into your tight summer schedule.

I would also like to thank my family and friends:

My parents, who have been there for me not matter what my whole life and have always supported my decision to continue school. You were there for me whenever I needed you. I couldn't have done this without you.

My sister, Paula, who is my closest friend. Talking to you has keep me sane throughout this adventure.

My grandparents, thank you for your calls and visits while I was in Pittsburgh. I am so glad you all were able to make it here for graduation. Also, thanks for all the encouraging words (and teasing). They motivated to finish before I started collecting social security.

My whole extended family, thanks for all of your calls and advise throughout my time here at the University of Pittsburgh. Though I was far away, I never felt alone and knew there was always someone I could call.

Cheng Ly, without you my last year at Pittsburgh would have been my worst. Everyone had moved away, but meeting you has made it my best. Thanks for all your help and support through the last few months. Without you I would have lost it somewhere between job interviews and first draft submission.

Jyotsna Diwadkar, *Dana Mihia & Silvia Daun,* I am lucky to have met such wonderful people here at Pitt. Thank you for your help, you guys where there when I need you the most, whether it was grading for me during the prelims or proof-reading. I couldn't have asked for a better group of friends.

Judy Day, I enjoyed not only working with but having you as a friend, officemate and Math GSO co-president. Our dual parameter fitting were the best time I ever had parameter fitting. I hope we can some day work together again. Also, thanks for paving the way for me as a GSR on these inflammation projects.

Stephanie Hoogendoorn and Fatma Gurel Kazanci, my academic sisters, thanks for your advise and help throughout the years.

1.0 INTRODUCTION

Multiple organ dysfunction syndrome (MODS) is a common cause of death in intensive care units (ICU). The mortality rate for one organ failure is 18%, two or three organ failure is 52% and mortality rates continue to increase with further organ failure [11] [42] [79]. MODS is characterized by an overactive immune response that causes sequential failure of organs. MODS occurs often in sepsis patients. These patients have a systemic response to an infection [79]. During MODS, treatment of the initial insult does not typically eliminate the immune response. The immune system remains active and inflammation spreads from one organ to the next. Therefore, typical treatment protocols focus on the support of failing organs. In hopes of obtaining a better understanding of the immune response and developing better treatment options, we have turned to mathematics.

Typical treatments of MODS involve organ specific support with the administration of antibiotics when infection is clinically observed or identified [74]. Lung and cardiac functions are often compromised during sepsis and MODS. To combat this loss of lung function patients are put on oxygen therapy to increase their oxygen levels. Severe loss of lung function requires the use of a ventilator, which mechanically breaths for the individual. To increase cardiac function, fluids are typically given. This increases blood volume which leads to increases in venous return of blood to the heart, which then causes increase in cardiac output [27]. Support of both these organs is required to restore perfusion, oxygenation of blood and blood pressure ([73], Seely, A, personal communication). Fluids increase the flow of blood increasing blood pressure. Blood pressure can also be increased with the use of vasopressor agents, which increase resistance in the blood vessels ([27]). Combinations of these treatment are used in patients in order to optimize blood pressure while minimizing side effects of the treatments. Failure of other organs requires organ specific support, such as dialysis for renal

failure.

These standard treatments do not alter the immune response driving the organ failure. Anti-inflammatory treatments, such as the administration of cortisol were explored in the past, but showed not increase in survival ([78], [63], [65]). Developing treatments which alter the immune response is difficult because of the complex interactions between the immune components. Mathematical models offer tools to investigate the mechanisms driving the immune response and to explore the effects of manipulating immune component levels. We have developed multiple models for inflammation in order to explore various aspects of MODS.

Inflammation is characterized by an activated immune system, therefore its intensity is measured by the levels of immune cells and mediators. There are two types of immune responses the immediate, hard-wired innate response and the more specific adaptive response. During an infection by pathogen the innate response is the first triggered and results in the syndrome of acute inflammation. This same response is triggered by wide variety of pathogen [70]. Immune cells in the vicinity of the infection become activated increasing their ability to fight pathogen. These activated cells: 1) produce proteins called pro-inflammatory cytokines, which recruit additional immune cells to the infection site, 2) produce proteins called anti-inflammatory cytokines, which inhibit the ability of the immune cells to produce cytokines and fight infection, 3) trigger the adaptive immune response. The adaptive response is a specific response to the type of pathogen. The adaptive immune system will selectively activate cells capable of fighting the pathogen causing the inflammation [34].

Experiments can modulate cytokine and cell levels to explore their role in inflammation. This gives insight into intracellular mechanisms and cell to cell interaction. However, the complexity of the immune system makes predictions of the entire immune response in vivo difficult. Therefore, we turned to mathematics to gain insight into the full system from knowledge of the simple cell to cell interactions.

We focused on the development and progression of MODS. During MODS, inflammation often persists after elimination of the pathogen. So, we developed models for the acute inflammation. Many models for acute inflammation have been developed containing varying degrees of complexity. For example, the Kumar et al. model is a small model which

captures clinical outcomes of acute inflammation [38]. The Vodovotz et al. model is large scale and includes variables for both innate and acute inflammation [75]. We have taken a gradual approach in the design of our models. We first derived a small scale model for acute inflammation to understand simple dynamics between pro- and anti-inflammation. The precursor to this model, Kumar et al., did not contain a variable for anti-inflammation. We have included anti-inflammation as a specific variable, since modulating anti-inflammatory cytokines was once hypothesized as a treatment for MODS. After we analyzed this reduced model, we expanded it into two more complex models. The first takes into account the diffusion between the blood and tissue compartments. The second models the effects of inflammation on gas exchange in the lung.

These ordinary and partial differential equations models were constructed through a modular approach where the dynamics of subsystems were analyzed. This approach allows one to ensure that biologically known dynamical features of interaction between model components are present in the model. Modeling MODS is a multiscale problem where understanding both cell to cell and also organ to organ interactions is essential. However, multiscale modeling is computationally intense. Therefore, when expanding the reduced model into the compartmental model, complexity in the cell to cell interactions was added as needed to capture the proper biological behavior. We did not include all signals and regulators of acute inflammation, but did include a few specific cytokines. Multiscale modeling within the lung was necessary to properly capture gas exchange dynamics. This lead to a model which is computationally intensive and required reduction techniques for practical simulations.

In the following chapters we develop and analyze these three models for acute inflammation: the reduced model, compartmental model (tissue/blood model), and the full lung model. In chapter 2 we present the reduced model, which is our small scale model for the acute inflammation. It is a four dimensional system of ODEs, which models the activation of the innate immune response and the production of pro- and anti- inflammatories. These inflammatories give rise to positive and negative feedback on the pro-inflammatory response. We use this reduced model to explore the effects of modulating anti-inflammatory mediators.

In chapter 3, we expand the reduced model to include both the blood and tissue compartments. This blood/tissue model is referred to as the compartmental model. Additionally,

we breakdown pro- and anti- inflammation from the reduced model into specific cells and cytokines. This is a simple model for an organ and organ to organ interactions when linking two tissue units to the same blood supply. Using the multiple organ model, we explore the effect of altering diffusive and macrophage properties on the spread of inflammation.

The lung is typically the first organ to fail during MODS [42]. Thus, we model the lung as a multiple compartment unit in chapter 4. We cannot use the compartmental model, because it consist of two compartments and within the lung interactions occur between the air, tissue, and blood. Typically, models for gas exchange in the lung do not explicitly model the tissue compartment. However, we have included it because inflammation accumulates in the tissue and affects the diffusion of gas molecules. We developed a PDE model for gas exchange and inflammation on a single respiratory unit ($\approx$ 25 alveoli), which accounts for space along the capillary. We linked multiple respiratory units under various ventilation perfusion ratios in order to model the full lung. With this model we explore the effects of inflammation and shunting. Shunting is when the alveolar air space collapses eliminating the gas exchange on a respiratory unit.

In chapter 5 we explore reduction methods for the full lung model to shorten simulation times. First, a spatial reduction is developed that allows us to track the blood gas pressures at the end of capillary. We also developed a temporal reduction, which eliminates the breathing mechanism. This reduction is the most effective at reducing computation times. Therefore, the resulting non-breathing model is used to study ventilation perfusion mismatch introduced under more complex means than in the full breathing model. Additionally, we increased biological accuracy of the full lung model without breathing by linking the arterial (entering the lung) pressure of O_2 and CO_2 to the O_2 and CO_2 pressures exiting the lung, creating a closed loop model for the lung.

2.0 A REDUCED MATHEMATICAL MODEL OF THE INNATE INFLAMMATORY RESPONSE

2.1 INTRODUCTION

Acute biological stress, such as severe infection or trauma, leads to the development of an acute inflammatory response. This syndrome typically includes increases in heart and respiratory rates, fever, and activation of the innate immune response. The goal of this response is to promote adaptation of the organism to stress, eliminate threats to survival such as pathogens, and promote tissue repair and healing. However, an excessive or inappropriate inflammatory response will lead to collateral tissue damage, organ dysfunction, a prolonged healing phase, or possibly death. This state of excessive inflammation is particularly common in association with extensive physiological organ support as provided in modern intensive care units [26] [68]. Organisms have developed regulatory mechanisms to contain the molecular and cellular cascades initiated by excessive inflammation. In general, pro-inflammatory elements that are key to ridding organisms of large numbers of pathogens also mobilize a negative feedback, or anti-inflammatory response, which downregulates the initial inflammatory wave (Figure 1). Specific details of pro- and anti-inflammatory responses may be sculpted by the nature and magnitude of the initiating insults, as well as by genetic predispositions.

In prior work a reduced mathematical model of the pro-inflammatory response was constructed by Kumar et. al. consisting of a response instigator (pathogen) and early and late pro-inflammatory mediators [38]. While that model captured a variety of clinically relevant scenarios associated with the inflammatory response to infection, the goal of the present work is to gain insight into the presumed advantage and robustness instilled by the presence of a time dependent anti-inflammatory response. While anti-inflammation inhibits the

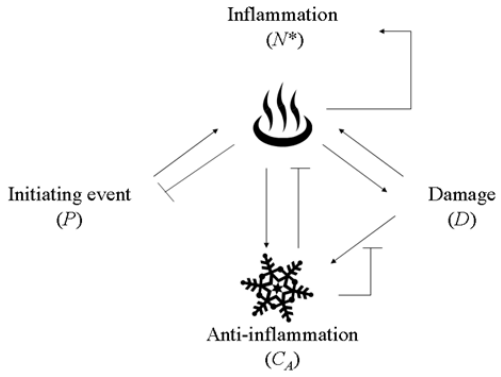

Figure 1: Interactions included in our four variable model of the acute inflammation. Arrows and bars represent upregulation and inhibition, respectively. The bar between anti-inflammation and inflammation corresponds to the inhibition of both the production of inflammation and the ability of inflammation to interact with all other involved species.

subsequent build-up of pro-inflammation and the damage to tissue that may be caused by pro-inflammation, it also mitigates the subsequent production of anti-inflammatory mediators. Thus, the overall effects of anti-inflammation on the outcome following pathogenic infection, and how these effects depend on parameters such as pathogen growth rate and the anti-inflammatory response rate itself, may be difficult to predict by intuition alone but are well-suited for dynamical systems analysis.

As the first step in performing this mathematical analysis, we derive a reduced model of the acute immune response that incorporates pro- and anti-inflammation presented in Reynolds et. al [58]. This model does not include components of the adaptive immune response, such as T-cells and specific anti-bodies. Therefore, this model describes the generic response to pathogenic insult [33]. Our derivation proceeds through several stages, based on the calibration of subsystems to generally accepted features of the interactions of particular immune system components, as observed in previous experimental studies. We construct a reduced model of inflammation from these subsystems, where the impact of dynamic anti-inflammation is evaluated through simulations and bifurcation studies. Our results illustrate the health advantage conferred by a dynamic anti-inflammatory response and suggest that the rates of this response may be well tuned to yield optimal outcomes following pathogenic

infection. Our findings also point to risks associated with manipulation of the levels of the anti-inflammatory mediator present, either before an initial infection or following an initial infection that is on its way to, but has not yet reached, a healthy resolution. We conclude with a discussion in which we elaborate on these and other possible therapeutic implications of our results.

2.2 METHODS

Our reduced model of the acute inflammatory response consists of a system of four differential equations in which the dependent variables represent the levels of pathogen (P), activated phagocytes (N^*) such as activated neutrophils, tissue damage (D), and anti-inflammatory mediators (C_A) such as cortisol and interleukin-10 [58]. This model describes the interactions depicted in Figure 1. We develop this model by first considering the two-variable subsystems N^*/P and N^*/D, treating C_A as a parameter, then combining these subsystems to form a three-variable subsystem, and finally incorporating the dynamics of the anti-inflammatory mediator to create the reduced model. We adopted a subsystem approach to ensure that the interactions of the model variables are consistent with biological observations.

Baseline parameter values for both the subsystems and the reduced model are provided in Tables 1 and 2 are selected to remain within the given ranges and constraints found in the experimental literature. This baseline parameter set is used for all simulations except where noted in the text. Parameters that could not be documented from existing data were estimated such that the subsystems behave in a biologically appropriate manner for plausible levels of the anti-inflammatory mediators. Furthermore, when the pathogenic insult is replaced by endotoxin as an initiating event, as presented in [18], the resulting model qualitatively reproduces the responses of immune mediators measured experimentally during repeated endotoxin administrations. Units for the model variables and many of the associated parameters cannot be determined, since the variables represent various types of cells, signaling proteins such as cytokines, and/or other mediators concurrently. More precisely, these variables quantify the response of the immune function they represent rather than, for example, an exact cell count. Therefore, units of most parameters related to these variables

are not in conventional form, but rather in terms of the associated variable.

Throughout the analysis of the reduced model and its subsystems, we will be tracking the existence and values of fixed points, determining the parameter regimes in which particular fixed points are stable, and locating bifurcations. A fixed point is a point where the derivatives of all variables in the system are zero, also known as a critical point or equilibrium point. This occurs where the nullclines of the system intersect. We will refer to a fixed point as stable if the real part of each eigenvalue associated with the linearized system at that fixed point is negative. In the systems that we consider, it is exactly the stable fixed points that represent possible asymptotic steady states attained by open sets of initial conditions. A bifurcation occurs when a change in a parameter alters the number of fixed points and/or their stability, and thus changes the number and nature of the asymptotic steady states of the system [66].

The reduced model displays three physiologically relevant equilibrium points, which correspond to biological states of health, aseptic death, and septic death, respectively. The health state is a fixed point with $P = 0$, $N^* = 0$, $D = 0$, and $C_A = s_c/\mu_c$, which, when stable, is the desirable asymptotic behavior. The aseptic death state, which corresponds to an outcome where pathogen has been eliminated but with high and persistent immune activation and damage, is a fixed point where $P = 0$, $N^* > 0$, $D > 0$ and $C_A > 0$. The third possible equilibrium is septic death, where all variables are nonzero, which corresponds to a state in which there is insufficient immune activation to clear pathogen. Note that a healthy outcome viewed as a return to an equilibrium point is an idealized construct. In fact, the complex biological systems we are considering are out of equilibrium and a return to mediator levels within the basin of attraction of the health state is a desirable outcome. However, in the reduced model, solutions with initial conditions in the basin of attraction of health asymptotically approach health. Thus, for simplicity we refer to the fixed point, $(0, 0, 0, s_c/\mu_c)$ as the health state.

Name	Value	Description	Comments	Sources
k_{pm}	$0.6/M$units/ hr	Rate at which the non-specific local response (M) eliminates pathogen (P)	Estimated to be considerably less efficient than a phagocyte driven response, and therefore can be overwhelmed with a modest to large inocula of pathogen.	
k_{mp}	$0.011/P$units/ hr	Rate at which the non-specific local response (M) is exhausted by pathogen (P)		
s_m	0.005 Munits/hr	Source of non-specific local response (M)	Chosen to balance known natural half-life of non-specific antibodies (see below)	
μ_m	$0.002/hr$	Decay rate for the non-specific local response	Range based on the reported half-lives of immunoglobulin G and A, non-specific antibodies probably key in the non-specific local immune response.	([34] [80])
k_{pg}	Variable	The growth rate of pathogen		([64]; [70])
p_∞	20×10^6 pg/cc	Maximum pathogen population	Estimated from a lethal model of E. Coli rat peritonitis	Vodovotz, personal communication
k_{pn}	$1.81/N^*$units/ hr	Rate at which activated phagocytes (N^*) consume pathogen	Based on observed mean rate of phagocytosis by macrophages in the presence of unlimited supply of targets.	[13]
k_{np}	$0.1/N^*$units/ hr	Activation of resting phagocytes (N_R) by pathogen		
k_{nn}	$0.01/N^*$units/ hr	Activation of resting phagocytes by already activated phagocytes and their cytokines		
s_{nr}	$0.08/N_R$units/ hr	Source of resting phagocytes	This parameter was chosen to ensure a stable concentration of resting phagocytes in the absence of inflammation.	
μ_{nr}	0.12/hr	Decay rate of resting phagocytes (macrophages and neutrophils)	We used a half-life of 6 hrs.	[14]
μ_n	0.05/hr	Decay rate of activated phagocytes (macrophages and neutrophils)	Activated cells have a prolonged half-lives due to delayed apoptosis, $\mu_n < \mu_{nr.}$	[14]
k_{nd}	$0.021/D$ units/hr	Activation of phagocytes by tissue damage (D)	The peak of the activated phagocyte response elicited from pathogen (k_{np}) is greater than that triggered by damage (k_{nd})	[3]

Table 1: Parameters for the reduced model of acute inflammation

Name	Value	Description	Comments	Sources
k_{dn}	$0.35/D$ units/ hr	Max rate of damage production by activated phagocytes (and/or associated cytokines/free radicals)		
x_{dn}	$0.06/N^*$ units/ hr	Determines level of activated phagocytes (N^*) needed to bring damage production up to half its maximum		
μ_d	0.02/hr	Decay rate of damage; combination of repair, resolution, and regeneration of tissue	We calculated the parameter data of the half-life of HMG-1, a histone tethering protein leaked dy damaged cells.	[76]
c_∞	0.28 $C_A$units	Controls the strength of the anti-inflammatory response	Set such that $f(x) = x/\left(1+(C_A/c_\infty)^2\right)$ corresponds to $\approx$ 75% inhibition when C_A reaches maximum value in respones to an insult.	[32]
s_c	0.0125 $C_A$units/hr	Source of the anti-inflammatory mediator	Organims have constitutive levels of anti-inflammatory effectors. The source parameter was chosen to balance their documented half-life.	
k_{cn}	0.04 $C_A$units/hr	Maximum production rate of the anti-inflammatory mediator		
k_{cnd}	48 N^*units/Dunits	Relative effectiveness of activated phagocytes versus damage in inducing the production of anti-inflammatory mediators		
μ_c	0.1/hr	Decay rate of the anti-inflammatory mediator	Anti-inflammatory signals have downstream cellular effects not explicitly modeled herein, lasting longer than the effector cytokine or molecule producing it. Therefore, our parameter value was set at the lower limit of reported half-lives of anti-inflammatory effectors. This still probably is a higher bound for this parameter.	[6], [12], [24], [31]

Table 2: Table of parameters continued.

$M + P \xrightarrow{k_{pm}} M$	P is destroyed at the rate k_{pm} when it encounters M.
$M + P \xrightarrow{k_{mp}} P$	M is consumed at the rate k_{mp} when it encounters P.
$* \xrightarrow{s_m} M$	Source of M.
$M \xrightarrow{\mu_m}$	Death of M.

Table 3: Table 2 Reactions involving the local immune response (M) and pathogen (P)

2.2.1 The non-specific local immune response: the M/P subsystem

A normal individual in a healthy state has a baseline capacity to respond and resolve local infections. This resides in the presence of cells, such as tissue macrophages as well as other non-specific physical and biological defenses, such as defensins and non-specific antibodies. [51] [54] [57] This non-specific local response is rapid and effective, but can be overwhelmed with large inocula or rapidly dividing pathogens. To account for this non-specific local removal of pathogen, we assume the reactions in Table 3, with the non-specific local response (defensins, non-specific antibodies and tissue macrophages) and pathogen levels represented by the variables M and P, respectively.

From the reactions in Table 3, based on mass action kinetics, we derive the following preliminary equations:

$$\begin{aligned} \frac{dM}{dt} &= s_m - \mu_m M - k_{mp} MP \\ \frac{dP}{dt} &= -k_{pm} MP \end{aligned}$$

For simplicity, we assume that the local response reaches quasi-steady-state and substitute $M = s_m/(\mu_m + k_{mp}P)$ into the pathogen equation. Further, to incorporate the dynamics of the pathogen population into our model, we used a logistic growth term, $k_{pg}P(1 - \frac{P}{P_\infty})$ Therefore, we obtain the pathogen equation, equation (2.1).

$$\frac{dP}{dt} = k_{pg}P(1 - \frac{P}{P_\infty}) - \frac{k_{pm}s_m P}{\mu_m + k_{mp}P} \tag{2.1}$$

Here, the pathogen growth rate and the carrying capacity of the pathogen population are represented by k_{pg} and P_∞, respectively. The units for k_{pg} are per hour while P_∞ has the same units as P, 10^6pg/cc. $P = 0$ is always a fixed point of equation (2.1). We find that a saddle-node bifurcation gives rise to two additional fixed points, say $p_1 < p_2$, which exist for $k_{pg} > 4k_{mp}s_m P_\infty/(P_\infty k_{mp} + \mu_m)^2$, or equivalently for $k_{pg} > 0.059$ with the parameters in Tables 1 and 2. When they first arise, p_1, p_2 are positive. Direct linearization and algebraic manipulation show that $P = 0$ is stable for $k_{pg} < k_{pm}s_m/\mu_m = 1.5$, where it loses stability in a transcritical bifurcation with p_1, and that the largest fixed point is stable whenever it exists. Thus for $0.059 < k_{pg} < 1.5$, this subsystem is bistable.

2.2.2 The N^*/P subsystem

A key component of the acute immune response is the removal of the pathogen by phagocytic immune cells, such as activated neutrophils and macrophages. Resting phagocytes are activated by pathogen and by previously activated phagocytes via the binding of endotoxin and pro-inflammatory cytokines [33]. Once activated, a phagocyte becomes efficient at eliminating pathogens. When the growth rate of the pathogen is low, activated phagocytes are capable of clearing the pathogen in normal individuals. However, if the growth rate is high, then a sufficiently large inoculum of pathogen can induce a persistent infection despite the attack by activated phagocytes. This dependence on k_{pg} and the interaction between resting and activated phagocytes are essential in developing the N^*/P subsystem, which consists of equations (2.2) and (2.3).

$$\frac{dP}{dt} = k_{pg}P(1 - \frac{P}{P_\infty}) - \frac{k_{pm}s_m P}{\mu_m + k_{mp}P} - k_{pn}N^*P \tag{2.2}$$

$$\frac{dN^*}{dt} = \frac{s_{nr}R_1}{\mu_{nr} + R_1} - \mu_n N^* \tag{2.3}$$

$$\text{where } R_1 = k_{nn}N^* + k_{np}P$$

To derive equations (2.2)-(2.3) we first take into account the activation of the resting phagocytes (N_R). In particular, from the system of reactions given in Table 4, we derive the

$N_R \xrightarrow{k_{np}P + k_{nn}N^*} N^*$	Activation of the resting phagocytes (N_R) is induced by the presence of pathogen (P) and by positive feedback from the activated phagocytes (N^*) via pro-inflammatory cytokines.
$* \xrightarrow{s_{nr}} N_R$	Source of N_R.
$N_R \xrightarrow{\mu_{nr}}$	Death of N_R.
$N^* \xrightarrow{\mu_n}$	Death of N^*.

Table 4: Reactions involving resting (N_R) and activated phagocytes (N^*)

following equations:

$$\begin{aligned} \frac{dN_R}{dt} &= s_{nr} - \mu_{nr}N_R - R_1 N_R \\ \frac{dN^*}{dt} &= R_1 N_R - \mu_n N^* \\ \text{where } R_1 &= k_{nn}N^* + k_{np}P \end{aligned}$$

When a resting phagocyte encounters an agent capable of activating it, however, the activation process is rapid. Thus, we assume that the variable N_R is in quasi-steady-state, reducing the N_R/N^* system to a single equation, equation (2.3). When this equation is combined with the pathogen equation, equation (2.1), derived above, and an additional term is included to encode the direct consumption of pathogen by activated phagocytes, we obtain system, equations (2.2)-(2.3).

Linearization of equations (2.2)-(2.3) about the health fixed point $(P, N*) = (0, 0)$ yields real eigenvalues that are negative for $k_{pg} < k_{pm}s_m/\mu_m$ and $\mu_m > s_{nr}k_{nn}/\mu_{nr}$. Since the second of these inequalities holds for the parameters in Tables 1 and 2, the condition $k_{pg} < k_{pm}s_m/\mu_m$ is once again the criterion for the stability of health, as in the M/P subsystem.

We provide a further analysis of the fixed points of equations (2.2)-(2.3) below, but first, to more accurately model the immune response, we introduce the anti-inflammatory mediator in this subsystem. At this point, we simply encode anti-inflammatory effects in a

parameter C_A. By treating the anti-inflammatory mediator as a parameter, we can manually manipulate it to verify that sustained variations in its level induce biologically appropriate alterations in the N^*/P dynamics, such that this subsystem will behave appropriately once dynamic anti-inflammatory mediators are incorporated.

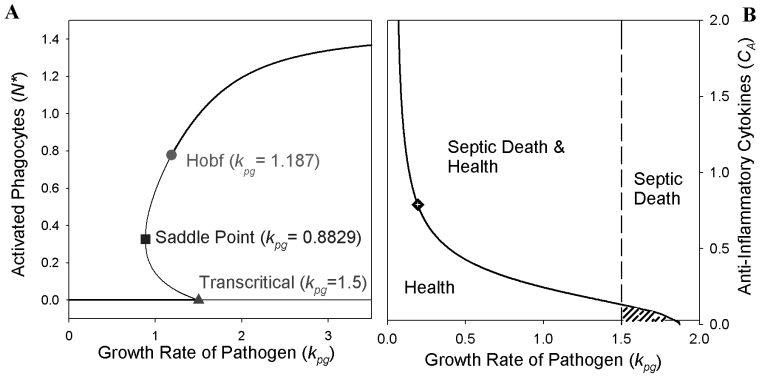

Figure 2: Bifurcation diagrams for the N^*/P subsystem. (A) The bifurcation diagram generated for $C_A = 0.2$ with bifurcation parameter k_{pg}. There is a Hopf bifurcation at $k_{pg} = 1.187$, where the system becomes bistable between septic death and health, and a transcritical bifurcation at $k_{pg} = 1.5$, where health loses stability. (B) Two parameter bifurcation diagram. We follow the existence of stable septic death (the bold line) and the transcritical bifurcation (the dashed line) from (A), with C_A as the second parameter. This divides the k_{pg}-C_A plane into regions labeled by the set of stable outcomes that exist. In the shaded region there are no stable fixed points and the system oscillates. The diamond represents the point where the bifurcation giving rise to stable septic death changes from a Hopf (below the diamond) to a saddle-node bifurcation (above the diamond).

In normal individuals, the anti-inflammatory mediator inhibits the activation of phagocytes and reduce the ability of activated phagocytes to attack pathogen [71]. We incorporate this inhibition into the N^*/P subsystem by replacing R_1 with $f(R_1)$ and N^* with $f(N^*)$ in equation (2.2), for $f(V) = V/\left((1 + \left(\frac{C_A}{c_\infty}\right)^2\right)$. The parameter c_∞ is set such that when the anti-inflammatory mediators reach their maximum level in response to an infection, their inhibitory effects are roughly equivalent to a seventy-five percent reduction in the inhibited element, as seen in [32]. While it would have been reasonable to consider different levels of inhibition by the anti-inflammatory mediator for each interaction, we consider uniform inhibition for simplicity.

For low pathogen growth rate (k_{pg}), the resulting N^*/P subsystem has only the stable health state, whose existence is independent of C_A. There is a saddle node bifurcation at $k_{pg} = 0.8829$ for the parameters in Tables 1 and 2 with C_A fixed to 0.2. The corresponding

bifurcation diagram is displayed in Figure 2A, which was created, as were all other figures in this paper, using XPPAUT [23]. Of the pair of fixed points born in the saddle node bifurcation, the lower (with respect to N^*) is a saddle separatrix, while the upper, corresponding to septic death ($P > 0, N^* > 0$), is initially unstable. As k_{pg} increases further, there is a Hopf bifurcation at $k_{pg} = 1.187$, which stabilizes septic death. Finally, health loses stability through a transcritical bifurcation at $k_{pg} = 1.5$. The stable branch that is created corresponds to negative levels of pathogen and activated phagocytes and is therefore not included in the bifurcation figure. In summary, for $1.187 < k_{pg} < 1.5$ and $C_A = 0.2$, this subsystem features bistability between health and septic death.

This bifurcation structure remains qualitatively similar for nearby values of C_A, while for sufficiently elevated C_A levels, septic death is stable as soon as it appears and we no longer observe a Hopf bifurcation. We examined the criteria for existence of stable septic death in a two parameter bifurcation k_{pg}-C_A plane. A curve divides the plane in two regions (solid curve in Figure 2B). For parameter values on the left of the curve, stable septic death does not exist, while on the right, it does. Also in Figure 2B, at $k_{pg} = 1.5$, there is a dashed vertical line that denotes where the health state loses stability. This line further divides the plane, creating a total of four regions: health, health/septic death, septic death, and a shaded region. The first three regions are labeled by the stable states that corresponding parameter values support. In the shaded region, septic death does not exist, and health is unstable. Therefore, there is no stable fixed point and trajectories oscillate. This does not represent a biologically observed state; however, once we combine subsystems below, oscillations will no longer occur.

In Figure 3, we see the effect of C_A on the level of activated phagocytes (N^*) in the septic death state when it first becomes stable. From Figure 2B, we know that as C_A increases, the k_{pg} value at which the stable septic death state appears decreases. Biologically, this corresponds to a prediction that holding C_A at a larger constant level induces a greater inhibition of the immune response, allowing a less virulent pathogen to induce a septic death outcome. In theory, this inhibition of N^* could allow an initial enhancement of the build-up of P, which would subsequently evoke a large rise in N^*, leading to a high-N^* septic death state; alternatively, the combination of higher C_A and low k_{pg} could suppress the level of

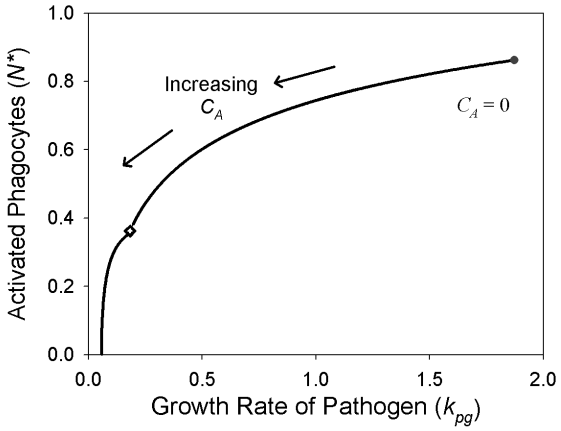

Figure 3: Activated phagocytes levels at the bifuraction for the onset of septic death. A plot of the solid curve from (B) in (N^*, k_{pg}) space shows the level of activated phagocytes reached at the onset of stable septic death as a function of k_{pg}. Again a diamond marks the change from a Hopf bifurcation (above the diamond) to a saddle-node bifurcation.

N^* seen in septic death. Figure 3 shows that in fact the latter possibility occurs, such that the activated phagocytes levels reached in septic death decrease, along with the pathogen growth rate, as the anti-inflammatory increases.

For parameters corresponding to the region of septic death/health in Figure 2B, the N^*/P subsystem is bistable. As noted above, a saddle separatrix, specifically the stable manifold of a saddle fixed point, separates the two stable states, as we see Figure 4A-B for $C_A = 0.2$. Notice the boxed region in Figure 4A. Zooming in on this region, as in Figure 4B, we see that the P nullcline and the stable manifold of the saddle point divide the P axis into three regions. Suppose that an initial pathogen load, P_0, is introduced to the system, which had previously been in the health state. When P_0 falls in the first region, to the left of the P nullcline, the non-specific local response is able to eliminate the pathogen without any transient pathogen growth. If P_0 falls in the middle region, between the P nullcline and the stable manifold, then the pathogen is able to overcome the local response and initially grow before the activated phagocytes respond and clear the infection. If P_0 is in the final region, to the right of the stable manifold, then the immune response is unable to heal the individual. When the subsystems are combined, and the anti-inflammatory mediator is allowed to evolve dynamically, we shall see that these regions persist, with qualitatively similar properties.

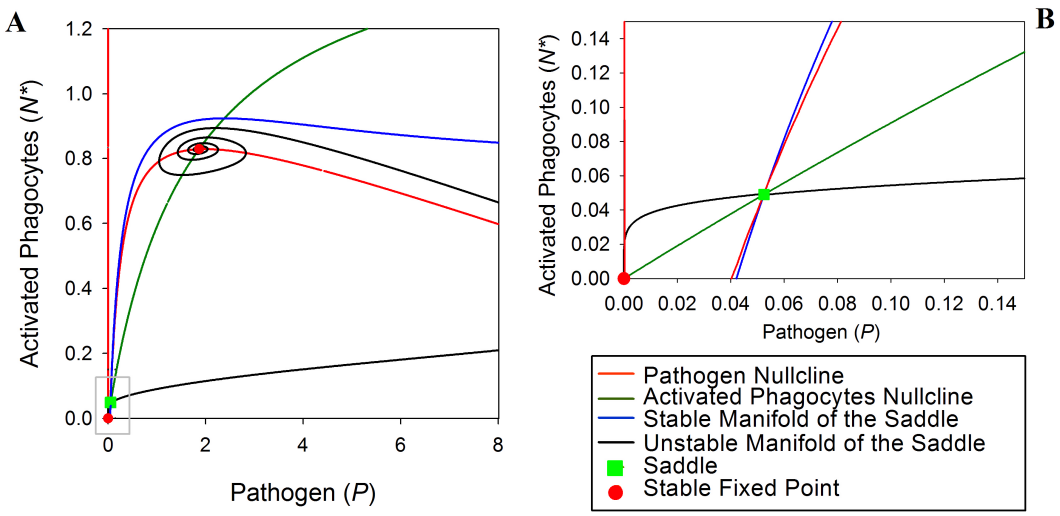

Figure 4: Nullclines for the N^*/P subsystem. (A), (B) A plot of the nullclines for this subsystem with $C_A = 0.2$ and $k_{pg} = 1.25$. The system is bistable between the health and septic death fixed points with a saddle point separating them. The unstable and stable manifolds of the saddle point are included in (A) and by zooming in on the boxed region, we see in (B) that the P axis is divided into three regions by the P-nullcline and the stable manifold of the saddle point.

Thus, this analysis of the N^*/P system with constant anti-inflammatory mediator is helpful in understanding the role of the activated phagocytes in the pro-inflammatory response to pathogen.

2.2.3 The N^*/D subsystem

When activated phagocytes respond to an infection, their presence in the tissue not only kills pathogens, but may also lead to collateral tissue damage [26] [68]. Damaged tissue releases pro-inflammatory cytokines, which causes further phagocyte activation. This positive feedback interaction between phagocytes and damage also exists in the absence of pathogen and can be triggered by other stimuli, such as tissue trauma. Therefore, the N^*/D system should be bistable between health and aseptic death over a range of the anti-inflammatory mediator. Modeling the interactions between activated phagocytes and damage, we developed the

N^*/D subsystem, which consists of equations (2.4) and (2.5).

$$\begin{aligned} \frac{dN^*}{dt} &= \frac{s_{nr}R_2}{\mu_{nr}+R_2} - \mu_n N^* && (2.4)\\ \frac{dD}{dt} &= k_{dn}f_s(N^*) - \mu_d D && (2.5)\\ \text{Where } R_2 &= k_{nn}N^* + k_{nd}D \\ \text{and } f_s(V) &= \frac{V^6}{V^6 + x_{dn}^6}. \end{aligned}$$

As in the N^*/P system, equations (2.2)-(2.3), the activated phagocyte equation in the N^*/D system is derived by first considering a system of equations that includes the resting phagocytes and subsequently assuming that the resting phagocytes are in quasi-steady-state. The only difference between the N^* equations, equations (2.3) and (2.4), appears in the activation of resting phagocytes, which we now take to be affected by D rather than P. Correspondingly, R_1 from equation (2.3) is replaced by $R_2 = k_{nn}N^* + k_{nd}D$ in equation (2.4).

At low counts, activated phagocytes do not cause significant damage. However, as they accumulate in response to an infection, the activated phagocytes will cause tissue damage to accrue. Finally, once levels of activated phagocytes are sufficiently high, damage saturates, such that the activation of additional phagocytes has little impact on damage creation. We model this nonlinearity in the induction of damage by activated phagocytes via the Hill type function, fs, in equation (2.5). The coefficient in f_s must be chosen to be sufficiently large to produce a reasonable basin of attraction for health in the N^*/D system (see Appendix A for further explanation). We subtract the term in equation (2.5) to represent tissue repair, resolution, and regeneration. Linear stability analysis of the health state, $(N^*, D) = (0, 0)$, shows that the eigenvalues are negative for $\mu_n > s_{nr}k_{nn}/\mu_{nr}$, which is the same condition that arose for the N^*/P subsystem and always holds for our baseline parameter set.

As in the N^*/P subsystem, we introduce the anti-inflammatory mediator (C_A) into the N^*/D subsystem as a parameter to ensure that our other parameter choices give the desired bistability for all physiological levels of C_A. As in the previous subsystem, the inclusion of the anti-inflammatory mediator leads to inhibition of activated phagocytes by two means. Specifically, the activation process itself is inhibited, which we model by replacing R_2 with

$f(R_2)$ in equation (2.4), where f is the same saturating function defined for inhibition in the N^*/P subsystem. The ability of activated phagocytes to cause damage is also inhibited by the anti-inflammatory mediator, which we model by replacing N^* with $f(N^*)$ in the Equation (2.5).

As in the N^*/P subsystem, the nullclines of the modified N^*/D subsystem intersect such that there are two stable fixed points separated by a saddle node for appropriate values of C_A. Similarly to Figure 4A-B, Figure 5 shows the nullclines and invariant sets of the N^*/D subsystem with $C_A = 0.2$. The stable manifold of the saddle point defines the threshold between health and aseptic death. The parameters and the Hill coefficient are chosen so that this threshold allows activated phagocytes to adequately respond to an inoculum of pathogen without triggering aseptic death.

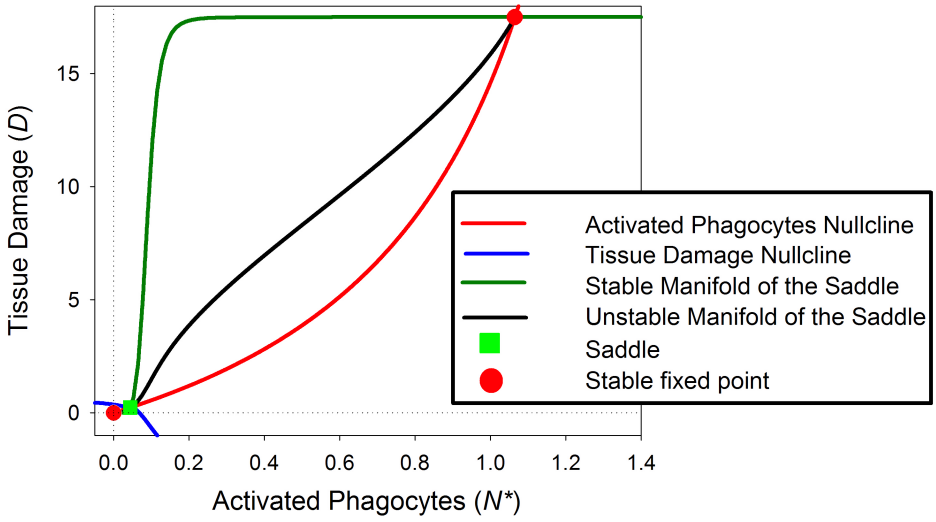

Figure 5: Nullclines for the N^*/D subsystem. A plot of the nullclines shows that the stable health and aseptic death fixed points are separated by a saddle point. The stable and unstable manifolds of the saddle point also are included.

In the bifurcation diagram for the anti-inflammatory mediator in Figure 6, we see that the N^*/D subsystem displays bistability between health and aseptic death for $C_A < 0.626$. Note that as the level of C_A increases the level of activated phagocytes reached at aseptic death is decreased. This trend makes sense, since the anti-inflammatory mediator inhibit the activation of phagocytes. Eventually, this inhibition prevents the system from equilibrating

at a state where N^* remains elevated; specifically, as C_A increases, the nullclines pull apart and eventually do not intersect. This occurs at the saddle node $C_A = 0.626$ and causes this subsystem to lose bistability. We note that this value lies above the physiological relevant range for C_A and also is consistent with the intuition that high C_A levels prevent the explosion of N^* needed for aseptic death.

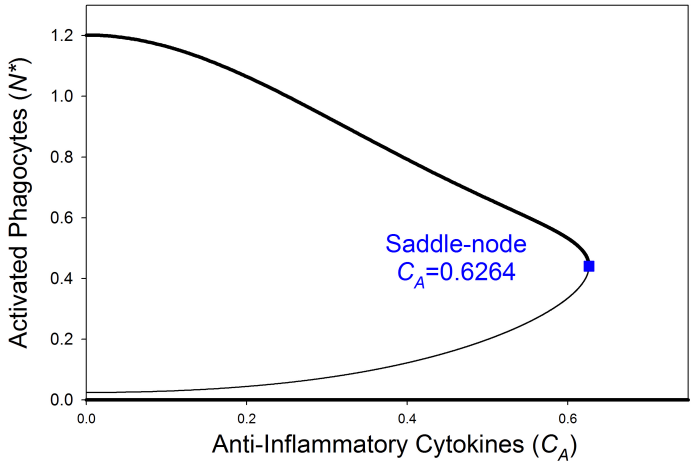

Figure 6: Bifurcation diagram for the N^*/D subsystem. A bifurcation diagram with the bifurcation parameter C_A, showing bistability between health and aseptic death that is lost through a saddle-node bifurcation as C_A increases through 0.6264.

2.2.4 The Three-Variable Subsystem

We combine the above two systems by including effects of both pathogen and damage on the rate at which the resting phagocytes are activated. To do this, we let $R_3 = k_{nn}N^* + k_{np}P + k_{nd}D$ and again assume that the resting phagocytes are in quasi steady state to obtain the system of equations (2.6)-(2.8).

$$\frac{dP}{dt} = k_{pg}P(1 - \frac{P}{P_\infty}) - \frac{k_{pm}s_mP}{\mu_m + k_{mp}P} - k_{pn}N^*P \tag{2.6}$$

$$\frac{dN^*}{dt} = \frac{s_{nr}R_3}{\mu_{nr} + R_3} - \mu_nN^* \tag{2.7}$$

$$\begin{aligned} \frac{dD}{dt} &= k_{dn} f_s(N^*) - \mu_d D \\ \text{Where } R3 &= k_{nn} N^* + k_{np} P + k_{nd} D \text{ and } f_s(V) = \frac{V^6}{x_{dn}^6 + V^6} \end{aligned} \tag{2.8}$$

Model (2.6)-(2.8) exhibits the combined dynamics of the previous two subsystems. The conditions for stable health are unchanged from the N^*/P subsystem, since $D = 0$ at the health fixed point. In particular, health is stable for low pathogen growth rate (k_{pg}), but loses stability at a transcritical bifurcation at $k_{pg} = 1.5$ as k_{pg} is increased. Since this instability is induced by the pathogen dynamics, it follows that even after this stability loss, the healthy state retains a two-dimensional stable manifold, such that small perturbations in the non-pathogen components lead to healthy resolutions. For low or moderate growth rate, the system inherits the existence of stable aseptic death from the bistability of the N^*/D subsystem. Consequently, for low pathogen growth rate, the physiological outcomes after pathogenic infection are health, achieved when the initial pathogen level is low, and aseptic death, arising when the initial inoculum of pathogen is large enough that the resulting phagocytic response results in large tissue damage.

As in the N^*/P subsystem, increasing pathogen growth rate leads to a bifurcation that introduces the possibility of septic death. Figure 7 shows a bifurcation diagram with $C_A = 0.2$, in which we see that this bifurcation is a Hopf at $k_{pg} = 1.707$. This diagram also shows the transcritical bifurcation that destabilizes the health state at $k_{pg} = 1.5$; the second branch of equilibria participating in this bifurcation is not shown, since it corresponds to a non-physiological state with negative pathogen and activated phagocytes. Since health is already unstable for $k_{pg} < 1.707$, there are only two possible stable outcomes, aseptic death and septic death, until $k_{pg} = 2.769$, when aseptic death loses stability through a second transcritical bifurcation. Aseptic death loses stability when k_{pg} becomes so large that the immune system cannot clear the pathogen, preventing stability of a state with a nonzero pathogen level and leaving septic death as the only stable state for the system.

Despite the bistability between aseptic and septic death for $1.707 < k_{pg} < 2.769$, initial conditions with only pathogen elevated, and all other variables at healthy levels, always lead to septic death for fixed C_A. The aseptic death outcome is attainable if tissue trauma ($D_0 > 0$) occurs in the absence of pathogen or if the initial level of activated phagocytes

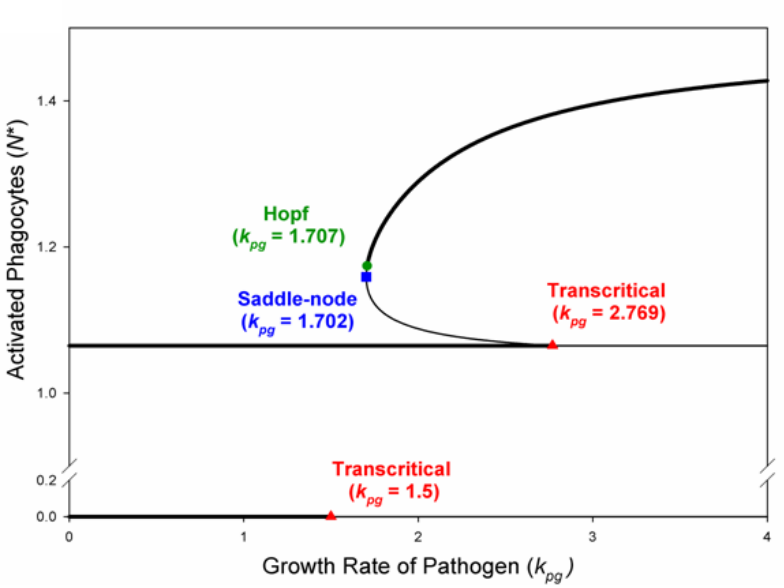

Figure 7: Bifurcation diagram for the three-variable subsystem for k_{pg} with $C_A = 0.2$. Health and aseptic death both lose stability through transcritical bifurcations, at $k_{pg} = 1.5$ and $k_{pg} = 2.769$, respectively. At $k_{pg} = 1.702$ there is a saddle-node bifurcation giving rise to two initially unstable fixed points. At $k_{pg} = 1.707$, a Hopf bifurcation creates a stable state, which corresponds to septic death.

($N_0^* > 0$) is elevated (with or without pathogen). A pre-activated immune system allows the infection to be cleared, avoiding septic death. However, activated phagocytes continue to be elevated in response to the pathogen, and this triggers aseptic death.

Next, we follow the bifurcation points in a two-parameter bifurcation diagram in the k_{pg}-C_A plane (Figure 8). The existence of septic death is represented by the solid curve. For a combination of parameters on the right of this curve, this system enters septic death (given a sufficient inocula for pathogen), while on the left septic death does not exist. The transcritical bifurcation where healthy loses stability is represented by the vertical dashed line at $k_{pg} = 1.5$. To the right of this line the health state is stable. The transcritical threshold corresponding to the loss of stability of aseptic death is represented by a blue dashed curve. Also, for C_A levels above the horizontal, dashed line, aseptic death does not exist due to the same saddle point bifurcation we showed in the N^*/D subsystem. Therefore, aseptic death is not a possible outcome above the horizontal, dashed line or to the right of the blue dashed curve. Combining these bifurcation structures we are able to label each region, as we did in Figure 2B, by the stable states they support.

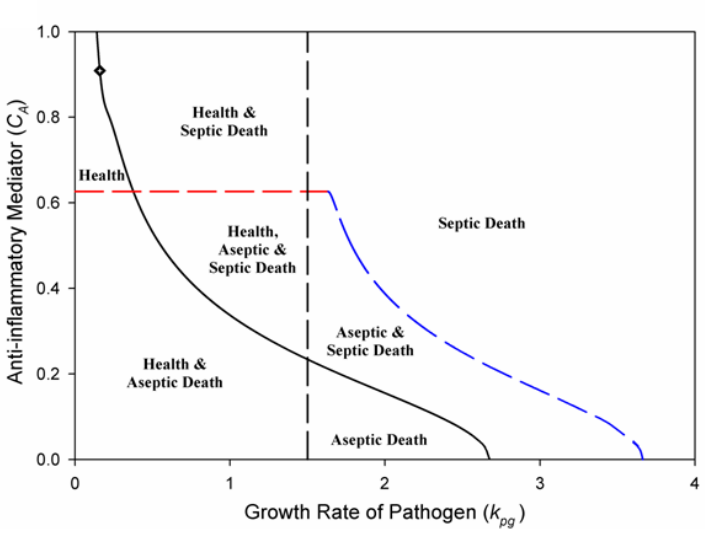

Figure 8: Two paramter bifurcation diagram for the three-variable subsystem for k_{pg} and C_A generated by following the bifurcations from Figure 7. The black solid curve represents the onset septic death. The diamond is the a switch from a Hopf (below) to a saddle-node bifurcation. Each region is labeled by the possible outcomes in that parameter regime. Transcritical bifurcations are the dashed curves. The dashed, horizontal line corresponds to where the aseptic death state loses existence due to a saddle-node bifurcation as C_A is increased.

From the two parameter bifurcation diagram in Figure 8, we observe that for $C_A > 0.234$, the bifurcation giving rise to the existence of septic death occurs at a $k_{pg} < 1.5$. Therefore, if $0.234 < C_A < 0.626$ (indicated by the horizontal, dashed line in Figure 8, there is a range of k_{pg} for which all three outcomes are stable. As in the case with $C_A = 0.2$ and bistability between aseptic and septic death, the path to aseptic death is sensitive to initial conditions and there is a propensity to enter septic death when only pathogen is initially introduced.

2.2.5 The Four-Variable Model

We complete the model derivation by introducing time-dependence to the anti-inflammatory mediator C_A, thereby obtaining our four-variable reduced model of the acute immune response. The production of the anti-inflammatory mediator is associated with the presence of activated phagocytes [19] and elevated markers of tissue damage [67]. As discussed in the development of the various subsystems considered above, the anti-inflammatory mediator (C_A) regulates the immune response by inhibiting the production and effects of activated

phagocytes and damage. More specifically, the presence of C_A decreases the ability of activated phagocytes to react to other cell types, reducing their effectiveness against pathogen, their induction of damage, and their production of additional C_A [19]. The recruitment of C_A by tissue damage (D) is similarly inhibited. Further, C_A compromises all means of activation of resting phagocytes.

As in the various subsystems, inhibition of activated phagocytes by the anti-inflammatory mediator (C_A) is incorporated in the model by replacing N^* with $f(N^*) = N^* / \left(1 + \frac{C_A}{c_\infty}\right)^2$ in equations (2.6) and (2.8). The inhibition of the activation of resting phagocytes is modeled by replacing R_3 with $R = f(R_3) = f(k_{nn}N^* + k_{np}P + k_{nd}D)$. Note that f limits to zero as C_A approaches infinity, and therefore if C_A levels are manipulated to be sufficiently high (above the maximum reached in response to an infection), then they will correspond to nearly complete inhibition of immune activation, which is experimentally observed [16].

The C_A equation contains a source of C_A, denoted s_c, and a term modeling the production of anti-inflammatory mediator from damage and activated phagocytes, which takes the form $k_{dn}(N^* + k_{cnd}D)/(1 + N^* + k_{cnd}D)$, before inhibition is incorporated. This expression is a Michaelis-Menten type term, in which k_{cnd} controls the effectiveness of damage, relative to activated phagocytes, in producing C_A. Including inhibition in this term, we obtain $k_{dn}f(N^* + k_{cnd}D)/(1 + f(N^* + k_{cnd}D))$.

Finally, incorporating these changes and additions into our three variable model, equations (2.6)-(2.8), results in our four variable model, which consists of equations (2.9)-(2.12). We shall refer to equations (2.9)-(2.12) as the reduced model, because it describes a highly abstracted representation of the complexity of the acute immune response.

$$\frac{dP}{dt} = k_{pg}P(1 - \frac{P}{P_\infty}) - \frac{k_{pm}s_mP}{\mu_m + k_{mp}P} - k_{pn}N^*P \tag{2.9}$$

$$\frac{dN^*}{dt} = \frac{s_{nr}R}{\mu_{nr} + R} - \mu_nN^* \tag{2.10}$$

$$\frac{dD}{dt} = k_{dn}f_s(f(N^*)) - \mu_dD \tag{2.11}$$

$$\frac{dC_A}{dt} = s_c + k_{dn}\frac{f(N^* + k_{cnd}D)}{1 + f(N^* + k_{cnd}D)} - \mu_cC_A \tag{2.12}$$

$$
\begin{aligned}
\text{Where } R &= f(k_{nn}N^* + k_{np}P + k_{nd}D), \\
f(V) &= \frac{V}{1 + \left(\frac{C_A}{c_\infty}\right)^2}, \\
\text{and } f_s(V) &= \frac{V^6}{x_{dn}^6 + V^6}
\end{aligned}
$$

2.3 RESULTS

The reduced model, equations (2.9)-(2.12), exhibits the same physiological fixed points as discussed above for the three-variable model. The health state is a fixed-point with $P = 0$, $N^* = 0$, $D = 0$, and $C_A = s_c/\mu_c$. The anti-inflammatory mediator is non-zero in this state, corresponding to the background level of these cytokines that exists in healthy individuals. In aseptic death, $P = 0$, but N^*, D, and C_A are nonzero. All variables are non-zero in septic death. Model dynamics for initial conditions leading to health, aseptic death or septic death are depicted in Figures 9A, 9B and 10A, respectively.

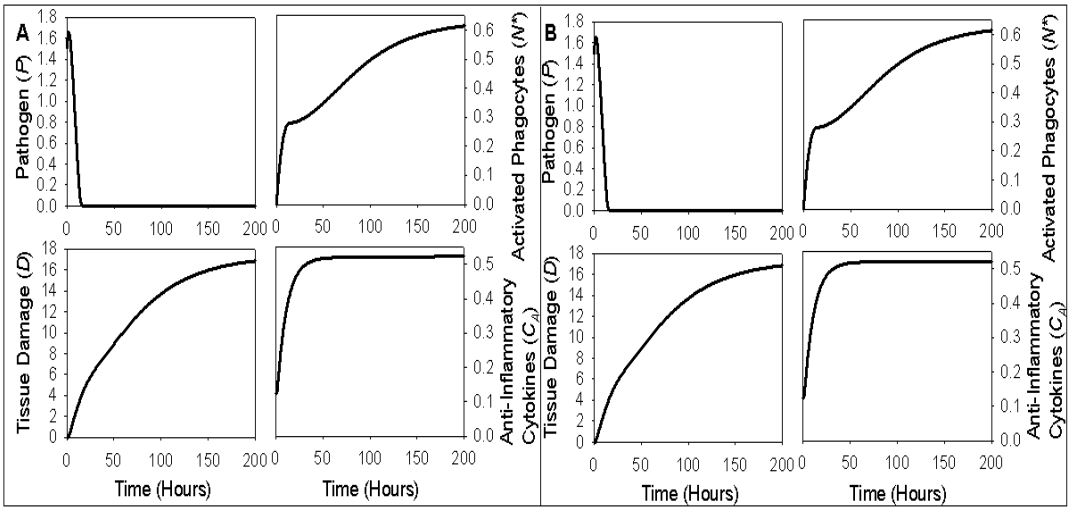

Figure 9: Transients from the evolution of the reduced model with a healthy and an aseptic death outcome. A) Health, simulation were run with $k_{pg} = 0.3$/hr and initial conditions $P = 1$, $N = 0$, $D = 0$, and $C_A = 0.125$. B) Aseptic death with $k_{pg} = 0.3$ and initial conditions $P = 1.5$, $N = 0$, $D = 0$, and $C_A = 0.125$.

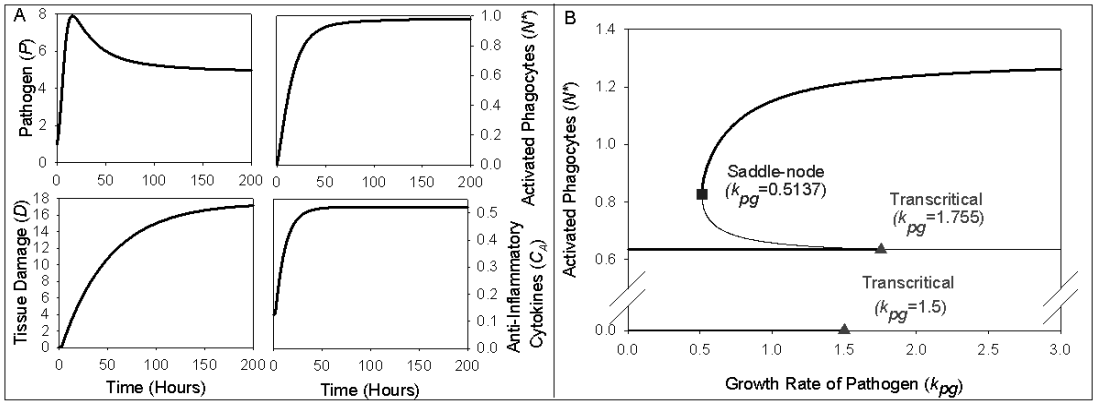

Figure 10: Transients from the evolution of the reduced model with septic outcome and the bifurcation diagram for the four-variable reduced model. (A) Septic death with $k_{pg} = 0.6$, such that septic death is a possible outcome, and initial conditions $P = 1$, $N = 0$, $D = 0$, and $C_A = 0.125$. (B) Bifurcation diagram, septic death comes into existence via a saddle-node bifurcation at $k_{pg} = 0.5137$. Health and aseptic death lose stability by transcritical bifurcations at $k_{pg} = 1.5$ and 1.755, respectively. Emerging stable states are not shown, since they are non-physiological. For $k_{pg} < 0.5137$, the model is bistable between health and aseptic death. The model has all three states stable for $0.5137 < k_{pg} < 1.5$. There is bistability between aseptic and septic death for $1.5 < k_{pg} < 1.755$. Finally, above $k_{pg} = 1.755$, the only stable state is septic death.

The qualitative dependence of the existence of stable states on the pathogen growth rate k_{pg} is maintained as in the three-variable model. As k_{pg} is increased, the septic death state comes into existence via a Hopf bifurcation at $k_{pg} = 0.514$ and the aseptic death state loses stability at $k_{pg} = 1.755$, as can be seen in the bifurcation graph presented in Figure 10B. As in the subsystems, health loses stability at a transcritical bifurcation at $k_{pg} = 1.5$. The second branch of equilibria involved in this transcritical bifurcation corresponds to a non-physiological state and is not included in the Figure 10B.

Utilizing both the three-variable subsystem, with the anti-inflammatory mediator treated as a parameter, and the reduced model, we explore several aspects of the role of C_A: (1) we investigate the effects of allowing C_A to dynamically depend on other model variables, which we compare to results found by holding the anti-inflammatory response at various constant levels, (2) we vary parameters that govern the speed of the anti-inflammatory response, (3) we analyze the effects resulting from the presence of initially elevated or depleted C_A levels when an infection is introduced, and (4) we consider the effects of reducing or elevating (resetting) C_A after an infection has progressed for multiple hours and then allowing the

full model to evolve, a manipulation that simulates a therapeutic intervention with an anti-inflammatory mediator.

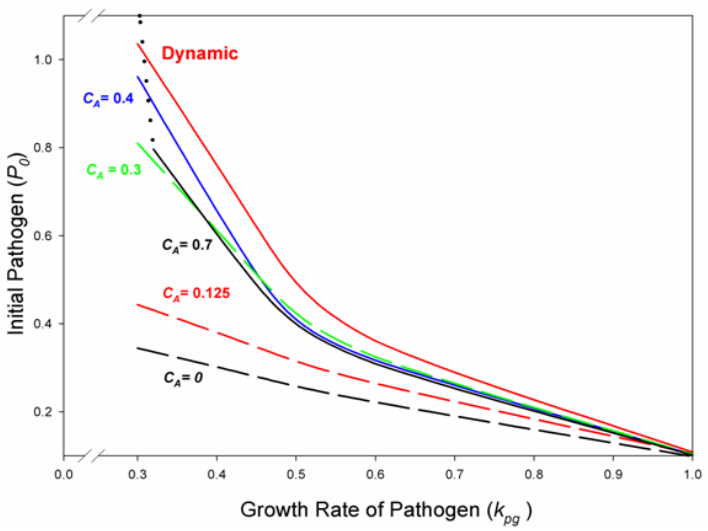

Figure 11: The basin of attraction for the health state depends on C_A. For each constant C_A level shown, the three-variable subsystem was used to determine the level of initial pathogen were the onset of death occurs (aseptic or septic), over a range of k_{pg}. Using the reduced model, with initial conditions with background initial conditions, the same was done, giving rise to the curve labeled 'Dynamic'. The dotted portion of the $C_A = 0.7$ curve (black) represents a range of where healthy is the only outcome.

We first ask whether the dynamics of the anti-inflammatory response are important, or whether a similar protection against runaway inflammation is achieved by the inclusion of a constant presence of the anti-inflammatory mediator in the model. In Figure 11, we compare the outcomes associated with a dynamic C_A response and those found with a variety of constant levels of C_A. At different k_{pg} values, we determine the level of initial pathogen that is the threshold between health and death (aseptic or septic). The curve associated with $C_A = 0$ lies below all other curves: the presence of the anti-inflammatory mediator, whether dynamic or constant, allows a larger initial pathogen load or growth rate to be tolerated over all physiologic (> 0) values of the pathogen growth rate, k_{pg}. An interesting result arising from simulation of the reduced model is that a dynamic anti-inflammatory mediator is almost always more effective than constant levels of the anti-inflammatory mediator at producing a healthy outcome following infection. Indeed, the curve associated with dynamic C_A in Figure 11 is above all other curves for most k_{pg} levels. The only exception is that at low growth

rate ($k_{pg} < 0.307$), the curve for $C_A = 0.7$ (very high C_A) ends and is continued by a dotted line, which crosses above the curve for dynamic C_A. In this region, with $C_A = 0.7$, the only outcome is health, and hence the threshold between health and death is no longer defined. For infections of such low virulence, even large anti-inflammatory levels will not thwart inflammation to a degree that allows runaway infection and death. Teleologically, our model demonstrates that a dynamic anti-inflammatory response increases the robustness of the immune response to infection, allowing the body to recover over a broad range of pathogen growth rate, yet in a way that minimizes life-threatening tissue damage.

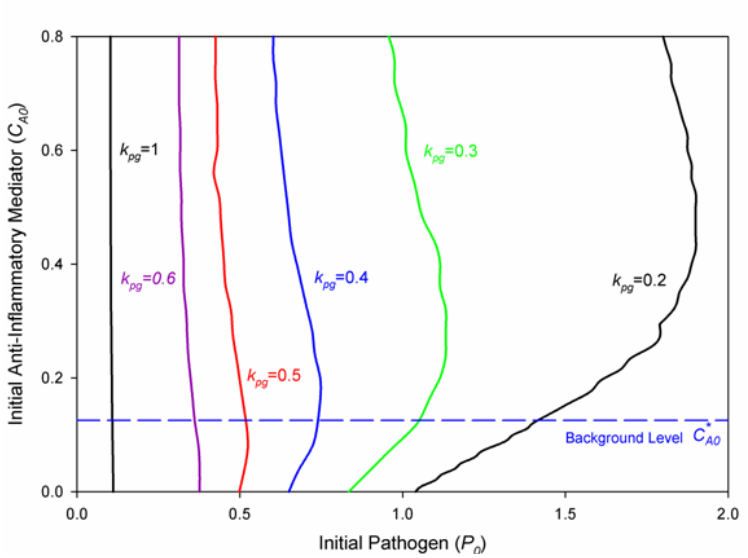

Figure 12: The threshold between health and death depends on the initial anti-inflammatory mediator and pathogen levels in the reduced model. At each k_{pg} value indicated we find the initial C_A level that is the threshold between health and death outcomes, given that N^* and D initially are at zero. Initial conditions to the left of each curve lead to health. Those to the right give rise to either death. The blue dashed line indicated the baseline level of C_A.

Given that a dynamic anti-inflammatory response is advantageous, we now consider how the rate of this response affects the overall outcome following infection. Considering a trajectory that is in the basin of attraction of health but close to the threshold between health and death, we altered the time scale of C_A by modifying the rate constants reflecting the production (k_{cn}) and decay rate (μ_c) of the anti-inflammatory mediator simultaneously. A slight increase in these rates helped the system to restore health sooner, but larger increases favored septic death. On the other hand, slowing down the anti-inflammatory dynamics

causes the trajectory to proceed to aseptic death. Similar results are obtained over a broad range of pathogen growth rates.

Next, we use the reduced model to explore the impact of baseline anti-inflammatory mediator levels on response to infection. First, we vary the initial level of C_A (C_{A0}) for a given initial level of pathogen (P_0) and determine the threshold between health and death at this P_0. This was repeated for multiple values of P_0 at fixed k_{pg} values. As depicted in Figure 12, this process defines, for each k_{pg} value, a boundary between health and death illustrated by the corresponding curve. Because the local non-specific immune response in our model is not inhibited by C_A, the threshold between health and death cannot fall below the level of pathogen that the local response is capable of clearing, regardless of the initial levels C_A. Thus, a vertical asymptote, close to the $k_{pg} = 1$ curve, is reached for large k_{pg}. The dotted line in Figure 12 indicates the level of C_{A0} found in the healthy state (background), call it C^*_{A0}. From Figure 12, we see that the effect of C_{A0} is generally stronger at lower k_{pg}. For such k_{pg}, a reduction in C_{A0} from C^*_{A0}moves the threshold for death to lower P_0. Conversely, increasing C_{A0} allows the system to handle higher P_0. However, the changes that occur for higher k_{pg}, while milder, are opposite to these. Moreover, even for low k_{pg}, the threshold for death shifts back to lower P_0 when C_{A0} is made sufficiently large. Indeed, it appears that the background C_A level, C^*_{A0} , is fairly optimally situated to allow for maximal or near-maximal threshold P_0 for a fairly broad range of high pathogen growth rates values, without undue compromise of protection at lower k_{pg}. Interestingly, however, this background level is not globally optimal.

For solutions to the reduced model with initial conditions in the basin of attraction of the health state, C_A returns to baseline significantly later than all other variables (Figure 9A). Therefore, after an infection is cleared, there is a period of time when only C_A is elevated, a window of relative immune suppression. Figure 12 allows us to consider the effects of introducing a second infection during this window. Although, for high k_{pg}, the baseline level of C_A leads to a larger basin of attraction for health than does elevated C_A, the elevated levels of C_A found immediately after an infection are only mildly detrimental. At these levels, C_A offers significant protection against a subsequent infection of a low or moderate k_{pg} (see also [18]).

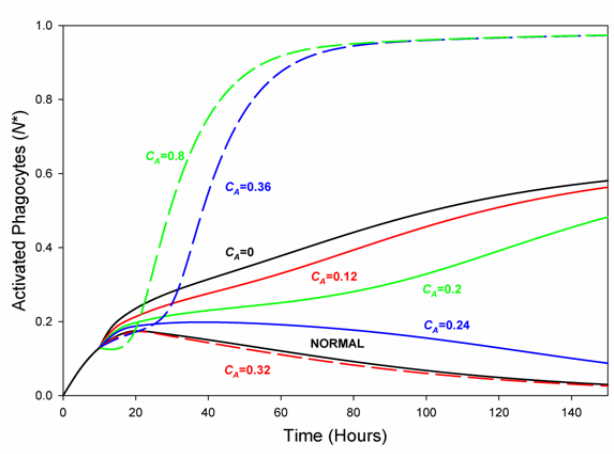

Figure 13: Figure 9: Altering the anti-inflammatory mediator levels after an infection has progressed can dramatically alter outcome. In this example, we allow an infection, triggered by an initial pathogen injection of 0.36 with $k_{pg} = 0.6$/hr, to progress for ten hours. After this, the anti-inflammatory mediator (C_A) is increased (dashed lines) or decreased (solid lines) without altering pathogen, activated phagocytes, and damage levels. The curve labeled 'NORMAL' is the time course obtained without manipulation of the C_A level from its normal level of 0.303, and all other curves are labeled by their adjusted C_A levels, as introduced at ten hours.

Multiple clinical trials have been conducted in which an anti-inflammatory mediator is administered as treatment to individuals with severe clinical sepsis (i.e., typically a highly inflamed state), where death is a frequent outcome ([4], [42]). To mimic treatment aimed at modulating the anti-inflammatory mediator after an initial infection, we devised an in silico experiment where initial pathogen is injected into the reduced model, equations (2.9)-(2.12). The infection is allowed to evolve for several hours at which point we instantly decrease or increase the level of C_A, to simulate a therapeutic intervention aimed at depleting or raising the availability of C_A. The simulation then proceeds according to equations (2.9)-(2.12). Initially, we ran simulations where the intervention was performed at eight, ten, and twelve hours after pathogen injection. The results depicted in Figure 13, obtained for the ten hour intervention, are representative of the case with moderate pathogen growth rate, where the simulation still results in health restoration, yet the solution lies near the threshold between health and aseptic death. In Figure 13, a sufficiently small depletion of C_A (e.g. $C_A = 0.24$) still yields a healthy outcome, but resolution to health takes longer. More substantial depletion of C_A (e.g. $C_A = 0 - 0.2$) pushes the system to aseptic death:

activated phagocytes clear the infection successfully yet are insufficiently inhibited, such that persistent collateral tissue damage results. If instead C_A values are instantly raised beyond 0.35, the simulation leads to septic death due to an excessive inhibition of activated phagocytes, which cannot mount a substantial attack on the pathogen. Therefore, over the time window explored, a modest increase in the anti-inflammatory mediator may indeed be slightly beneficial (e.g. $C_A = 0.32$ in Figure 13), but it is important to prevent an overly large increase. This finding could be particularly crucial in clinical circumstances where the body cannot mount a sufficient anti-inflammatory response ([4], [5]). In such situations, a modest transient increase in anti-inflammation mediator would change the outcome from aseptic death to health, but larger increases would be problematic.

Finally, we explored the sensitivity of these results to pathogen growth rate and timing of intervention. For larger k_{pg}, the thresholds between health, aseptic death, and septic death are quite close together. As we raise k_{pg} from the example in Figure 13, we find that interventions featuring significant increases in C_A continue to promote septic death, while significant decreases favor aseptic death. However, for sufficiently large k_{pg}, aseptic death becomes less of a threat, while there is a propensity for a pathogenic explosion leading to septic death. In these cases, the removal of most or all of the C_A present at the time of intervention is optimal for yielding a return to health. We note that if the delay before intervention is increased for moderate k_{pg}, then a greater C_A input is needed to avoid aseptic death, since N^* builds up during the time before intervention. In cases of high k_{pg}, excessive delays before removal of C_A can eliminate their ameliorative effects by prolonging the period of insufficiently restrained pathogen growth. These results highlight further that the outcome of anti-inflammatory therapy will be highly sensitive to the nature of the infection being treated and the details of the therapeutic protocol.

2.4 DISCUSSION

We have derived a reduced model of the acute inflammatory response to infection that includes an anti-inflammatory mediator. Simulation and bifurcation analysis of this model suggest that anti-inflammation plays several important roles in the restoration of health.

First, anti-inflammation expands the basin of attraction of health compared to that present in models lacking anti-inflammation [38], which is a desirable feature, given that we expect health to be a robust state. Second, we demonstrate an advantage, in terms of healthy resolution of infection, conferred by the dynamic nature of the anti-inflammatory response, in comparison to a tonic response. This advantage holds in all situations except for the mildest of infections, which, in any case, do not present a vital threat. This is illustrated in current clinical practice, where distressing symptoms associated with mild infections are alleviated by the co-administration of antibiotics and anti-inflammatory mediators. The reduced model also underlines the importance of the different response rates of substances promoting inflammation, represented in the model by N^*, and of the anti-inflammatory mediator that limit this response. Specifically, our results suggest that these rates are fairly well tuned to optimize healthy outcomes to pathogenic infection. Further, we have used simulations of our model to explore how variations in levels of the anti-inflammatory mediator present initially or at some time after initial infection affect the restoration of health following an inflammatory response.

We followed a systematic, modular approach to model development, building our reduced model from subsystems, each one with biologically plausible dynamics. Indeed, by building up this model through modules, we gain a clear understanding of how each element and interaction in the system contributes to the overall network dynamics. We also ensure that the final model behaves in a way that is consistent with situations in which particular features are absent, such as tissue damage without pathogen exposure, or are experimentally manipulated.

Our results illustrate the point that administration of an anti-inflammatory mediator during the response to an infection may compromise outcome (Figure 13). The administration of pharmacological doses of steroids, which are potent natural anti-inflammatory mediators, in severely septic patients has clearly resulted in worse survival. ([63], [65]) This situation corresponds in our model to either the maintenance of tonic elevated levels of the anti-inflammatory mediator or the transient administration of the anti-inflammatory mediator, in patients who would otherwise survive or evolve to aseptic death, causing septic death (Figure 13). The association between significant immune suppression and infectious

complications is clearly an ongoing concern for several groups of patients. Fortunately, the anti-inflammatory mediator, in addition to being conducive to the healing phase of injury, also plays a role in the acute phase of infection as well. A significant body of recent evidence suggests that low-dose immunosuppression with an anti-inflammatory mediator may in fact improve outcome in patients with severe infection, particularly in patients with an insufficient anti-inflammatory response ([4], [5]). Our simulations highlight the dependence of the outcomes of such interventions on pathogen virulence (Figure 12) and timing of intervention, as discussed in the previous section. Therefore, studies such as we have performed may be useful for subsequent investigations of anti-inflammatory therapeutic agents. For example, the only approved therapeutic agent for patients with severe sepsis, recombinant human activated Protein C, has anti-inflammatory properties ([9], [35], [50]) and the proper degree of modulation with this agent, alone or in combination with others, remains a very active focus of clinical research ([15], [43]). How the various features of the inflammatory response interact to govern the outcome following multiple insults, including pathogen, trauma, endotoxin, or other stimuli, warrants intensive computational exploration ([18]).

The biological relevance of our analysis and conclusions are limited by the significant oversimplification present in our reduced model and the difficulty in translating functions such as "pro-inflammation", "anti-inflammation" and "damage" into measurable quantities. Future directions for study include a more detailed biological characterization of anti-inflammatory substances, since they differ widely in the timescale and specificity of their activity, and a detailed mathematical analysis of the use of anti-inflammatory mediators as "therapeutic" agents, depending on timescale as well as time and intensity of intervention. The experimental and clinical relevance of these efforts will continue to grow as methods are developed to better link reduced models and more complex models, both from top-down and bottom-up approaches.

3.0 COMPARTMENTAL MODEL OF ACUTE INFLAMMATION

3.1 INTRODUCTION

The reduced model of acute inflammation was sufficient for exploring the role of anti-inflammatories. However, in order to more accurately model acute inflammation within an organ, we expand the reduced model to account for the interplay between blood and tissue during acute inflammation. Though pathogen is typically introduced via the tissue, the blood supplies immune cells need to eliminate severe infections. During the inflammatory response, local tissue macrophages are activated. These activated macrophages produce cytokines that diffuse into the blood and trigger a local influx of activated neutrophils, facilitating the elimination of pathogen [48]. The interplay between compartments is essential in eliminating infection and restoring homeostasis during severe insults. Additionally, we model specific cytokines and immune cell types, which have been measured clinically.

We developed this model by initially focusing on the immune mediators within tissue and then expanding the model to include the blood components. Additionally, we examined individual terms to properly model their effects on the full model. Once the structure of the equations was established for a single unit of tissue the parameters were fitted using heuristics from data for IL-10, TNF, neutrophils, macrophages and pathogen. Stable outcomes (health, aseptic death, and septic death) and dynamics are similar to the results seen in the reduced model. However, we have included specific cytokines, cells, and tissue integrity rather than variables representing all pro-inflammatories, all anti-inflammatories, and general damage. We included in this model the interactions shown in Figure 14.

Once the single tissue unit model was developed, capturing the cell to cell level interactions, we linked multiple tissues to the same blood supply to model the communication

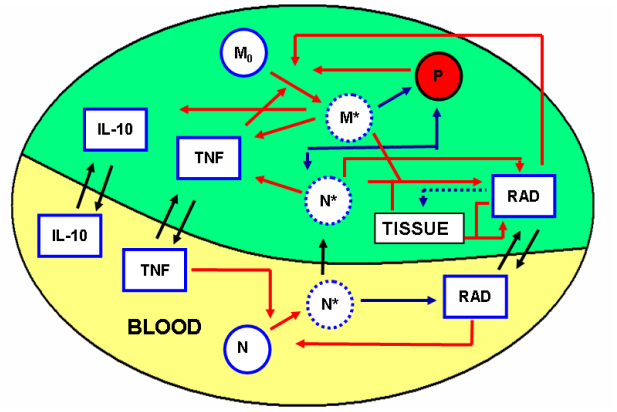

TNF	Tumor Necrosis factor	N*	Activated Neutrophils	P	Pathogen
IL10	Interleukin-10	M	Resting Macrophages	RAD	Radicals
N	Resting Neutrophils	M*	Activated Macrophages		

Figure 14: Interactions included in the compartmental model. Diffusion is represented by black arrows and immune interactions are represented by the red (up-regulation) and blue (down-regulation) arrows. In addition, the anti-inflammatory cytokine IL-10 inhibits all interactions including neutrophils and macrophages, the species with dashed border.

between organs via the blood. During MODS there is propagation of inflammation from one organ to the next. This tissue/blood model is a minimal model for most human organs. The lung does not have this construct, having three compartments. Therefore, in the following chapter we develop a three compartmental model of the lung. Here, in this chapter we focus on organs which consist of tissue interacting with the blood only. This covers a variety of organs, including as the kidney and liver.

These organs have significant differences, many of which we introduced into this model. Primarily, we consider differences in blood-tissue permeability and the background level of macrophages residing in the tissue. These difference are considered, since both diffusion and macrophages play a major role in the immune response. Permeability controls the neutrophil response and the exchange of mediators between organs and the blood. Macrophages play a significant role. They fight local infection and produce immune mediators, which diffuse into the blood. The liver has high levels of macrophages and typically fails after the kidney during MODS, which has fewer macrophages [42].

3.2 DEVELOPMENT OF THE MODEL

3.2.1 Isolated Tissue

Initially, we focused on the interactions including pathogen, macrophages and antibodies within the tissue. The effects of both tissue macrophages and antibodies were included in the reduced model. However, they were grouped together into a single variable. In this model, they are represented by distinct variables. The resting and activated tissue macrophages are represented by the variables, M and M^*, respectively. All other antibodies and cells activated at the onset of infection are referred to as the background immune response, B. This background response, B, can immediately eliminate low levels of pathogen, P. Given the immediate response of B and its ability to eliminate P, the B variable is assumed to be in steady state. This assumption gives rise to the term, $-s_b k_{pb} P/(\mu_b + k_{bp} P)$ in the P equation, equation (3.1), which has the same form as the analogous term in the reduced model. Also, as in the reduced model, we assume logistic growth of pathogen giving us the first term in the P equation, equation (3.1). See Tables 5-12 for further explanation of the parameters.

$$\frac{dP}{dt} = k_{pg} P(1 - \frac{P}{p_\infty}) - \frac{s_b k_{pb} P}{\mu_b + k_{bp} P} - k_{pm} M^* P \tag{3.1}$$

$$\frac{dM}{dt} = -\mu_m M - k_{mp} M P + s_m \tag{3.2}$$

$$\frac{dM^*}{dt} = -\mu_{m*} M^* + k_{mp} M P \tag{3.3}$$

The tissue macrophages are not capable of fighting infection until they are activated by either pathogen or pro-inflammatory cytokines. Therefore, when a resting tissue macrophage, M, meets a pathogen, P, we have $M + P \rightarrow M^* + P$ where M^* is activated tissue macrophage. This reaction gives rise to the second term in both the M and M^*equations, equations (3.2) and (3.3). Activated macrophages are capable of eliminating pathogen. For this reason, we also have $M^* + P \rightarrow M^*$, which gives rise to the third term in the P equation, equation (3.1). The first terms in equation (3.2) and equation (3.3) model the decay of macrophages. Note that, as in the reduced model the activated cells have slower decay rates, $\mu_m > \mu_{m*}$. The bone marrow provides a source of resting macrophages, s_m, see equation (3.2). Therefore,

resting cells are in the tissue at background and their source supplies resting cells during the infection.

Once activated, macrophages produce both pro- and anti-inflammatory cytokines. Pro-inflammatory effects were included in the reduced model, however, there were no specific cytokines. Here, we modeled the pro-inflammatory cytokine, TNF. The compartmental model also focuses on a specific anti-inflammatory, interleukin-10 (IL-10). These two cytokines were chosen because they have high biological relevance and are commonly measured in experiments for many animal types. The first terms in equations (3.4) and (3.5) describe the decay of the cytokine and the second terms model production from activated macrophages.

$$\frac{dTNF}{dt} = -\mu_t TNF + k_{mat} M^* \tag{3.4}$$

$$\frac{dIL10}{dt} = -\mu_i IL10 + k_{mai} M^* \tag{3.5}$$

Once produced, TNF can bind to resting macrophages and cause activation. Therefore, we include the reaction $M + TNF \rightarrow M^*$ into this system. TNF does not appear on the right side of the arrow, since it is consumed during activation. This reaction gives rise to the second term in the M, M^*, and TNF equations, equations (3.7)-(3.9). This activation is assumed to be nonlinear, since multiple TNF bind to a macrophage in order to activate it. Note that, we refer to both the variable and the actual cytokine by TNF, but the variable appears as TNF. The same convention is used for IL-10.

$$\frac{dP}{dt} = k_{pg} P(1 - \frac{P}{p_\infty}) - \frac{s_b k_{pb} P}{\mu_b + k_{bp} P} - k_{pm} f_i(M^*) f(P, x_{m*p}, h_{m*p}) \tag{3.6}$$

$$\frac{dM}{dt} = -\mu_m M - k_{mtcell} f_i(M) f(TNF, x_t, h_t) - k_{mp} f_i(M) f(P, x_{m*p}, h_{m*p}) + s_m \tag{3.7}$$

$$\frac{dM^*}{dt} = -\mu_{m*} M^* + k_{mtcell} f_i(M) f(TNF, x_t, h_t) + k_{mp} f_i(M) f(P, x_{m*p}, h_{m*p}) \tag{3.8}$$

$$\frac{dTNF}{dt} = -\mu_t TNF - k_{mtmol} f_i(M) f(TNF, x_t, h_t) + k_{mat} f_{it}(f(M^*, x_{m*t}, h_{m*t})) \tag{3.9}$$

$$\frac{dIL10}{dt} = -\mu_i IL10 + k_{mai} f_i(f(M^*, x_{m*i}, h_{m*i})) \tag{3.10}$$

$$\begin{aligned}
\text{where } f_i(M^*) &= M^* \left(\frac{(1-c_i)}{1+\left(\frac{il10}{il10_\infty}\right)^{h_i}} + c_i \right), \\
f_{it}(M^*) &= M^* \left(\frac{(1-c_{it})}{1+\left(\frac{il10}{il10t_\infty}\right)^{h_{it}}} + c_{it} \right) \\
\text{and } f(v, x_v, h_v) &= \frac{v^h}{v^h + x_v^h}
\end{aligned}$$

IL-10 effects the ability of macrophages to be activated, to deplete pathogen, and to produce cytokines. Therefore, M^* is replaced by $f_i(M^*) = M^*(1-c_i)/\left(1+\left(\frac{il10}{il10_\infty}\right)^{h_i}\right) + c_i$ and M with $f_i(M)$ in all terms but those modeling decay and production of TNF in equations (3.6)-(3.10). The parameter c_i determines the maximum inhibition of M^*. When $IL10 \to \infty$, $M^* \to c_i M^*$. This is a Hill-type term with $IL10_\infty$ determining the level at which $IL10$'s inhibition of M^* is at half strength. This function form is used for all inhibition included in our compartmental model.

The main role of TNF is to act as a trigger to the onset of the innate immune response, once it diffuses into the tissue. TNF is produced only in the early stages of infection whether or not the insult is survivable [44]. In order to model this early production of TNF, the production term has a higher level of inhibition than the other reactions involving macrophages. Using the function for the inhibition of the production of TNF, $f_{it}(M^*) = M^*(1-c_{it})/\left(1+\left(\frac{il10}{il10t_\infty}\right)^{h_{it}}\right) + c_{it}$, which has the same form as $f_i(M^*)$ but with $c_{it} << c_i$, so that production is nearly thwarted when $IL10$ is high. Also $il10_{t\infty} < il10_\infty$ so the that onset of the inhibition of production occurs at a lower $IL10$. We replace M^* with $f_{it}(M^*)$ in the TNF production term in equation (3.9).

Macrophages are the only producers of cytokines in our model. In order to control the dynamics of the cytokine populations we introduced nonlinearities via a Hill-type production term, see equations (3.9) and (3.10). This combined with f_{it}, allows the model have a significant levels of TNF that occurs after approximately twelve hours during a mild survivable insult. Also, the Hill-type term for $IL10$ production allows M^* to be more effective during the initial stage of infection.

Unlike in the reduced model, variables are measured in the units used clinically. Therefore, pathogen now ranges from 0 to 20,000. Assuming linear terms for activation of macrophages by pathogen and the elimination of pathogen as we did in equations (3.1)-(3.3) gives rise to improper dynamics. If the rate constant is set such that the proper dynamics occurs at low pathogen, then at high pathogen the elimination and activation terms are so large that death outcome is eliminated. If the rates of these reactions are reduced to adjust for large population we do not get proper levels of activation and elimination at the onset of inflammation. Consider the elimination of P by M term, $k_{pm}f_i(M^*)P$, as the rate of elimination per M^*, $k_{pm}P$, multiplied by $f_i(M^*)$. In this form, this rate is linear in P. At low pathogen levels there is dependence on concentration, since concentration determines the likelihood that M^* encounters P. However, at high pathogen, pathogen is readily available and the rate at which pathogen is eliminated should be determined by the ability of the activated macrophages to fight the infection. Therefore, in order to model elimination properly we replace $k_{pm}f_i(M^*)P$ in equation (3.1), with $k_{pm}f_i(M^*)P^{h_{m*p}}/(P^{h_{m*p}} + x_{m*p}^{h_{m*p}}) = k_{pm}f(P, x_{m*p}, h_{m*p})f_i(M^*)$. This can simply be viewed as there being a maximal rate at which macrophages can eliminate pathogen. This maximum is achieved when the concentration of pathogen is sufficiently high. The same derivation is used for activation of macrophages by pathogen. There is a maximal rate at which a resting macrophage can be activated, so P is replaced by $f(P, x_{m*p}, h_{m*p})$ in all activation terms. Including these changes we the have final form of the equations for the tissue components in the absence of diffusion, see equations (3.6)-(3.10).

3.2.2 Immune components within the blood

The activation of macrophages and the ensuing production of TNF produces a signal to the neutrophils, which are phagocytic cells that once activated are highly capable of destroying pathogen. In this model we assume that activated, but not resting, neutrophils can diffuse into the tissue. Therefore, activation of neutrophils by pathogen and TNF occurs only in the blood. The reactions of the activation and resulting terms are of the same form as the activation of macrophages, see the second term in equations for N_b, N_b^* and TNF_b, equations (3.12), (3.13) and (3.14). Note the first term in equations (3.12)-(3.15) model the intrinsic

decay of these variables.

$$\begin{aligned}
\frac{dP_b}{dt} &= k_{pbg}P_b(1-\frac{P}{p_{b\infty}}) - \frac{sb_b k_{pbb}P_b}{\mu_{bb}+k_{bbp}P_b} - k_{pn}f_{ib}(N_b)f(P_b,x_{n*p},h_{n*p}) && (3.11)\\
\frac{dN_b}{dt} &= -\mu_{nb}N_b - k_{ntcell}f_{ib}(N_b)f(TNF_b,x_{tb},h_{tb}) && (3.12)\\
&\quad -k_{mpb}f_{ib}(N_b)f(P_b,x_{n*p},h_{n*p}) + s_{nb}\\
&\quad +k_{snb}f(cN_b^*+dN^*,x_{snb},h_{snb})\\
\frac{dN_b^*}{dt} &= -\mu_{nb*}N_b^* + k_{ntcell}f_{ib}(N_b)f(TNF_b,x_{tb},h_{tb}) && (3.13)\\
&\quad +k_{npb}f_{ib}(N_b)f(P_b,x_{n*p},h_{n*p})\\
&\quad -(1-r_b)k_{pncell}f_{ib}(N_b^*)f(P_b,x_{n*p},h_{n*p})\\
\frac{dTNF_b}{dt} &= -\mu_{tb}TNF_b - k_{ntmol}f_{ib}(N_b)f(TNF_b,x_{tb},h_{tb}) && (3.14)\\
\frac{dIL10_b}{dt} &= -\mu_{ib\,\max}IL10_b && (3.15)\\
\text{where } f_{ib}(N_b^*) &= \frac{N_b^*(1-c_{ib})}{1+\left(\frac{il10_b}{il10_{b\infty}}\right)^{h_{ib}}} + c_{ib} \text{ and } f(v,x_v,h_v) = \frac{v^h}{v^h+x_v^h}
\end{aligned}$$

As with resting macrophages there is a source of resting neutrophils from the bone marrow. For the neutrophil population, however, we assume that the bone marrow increases the source of the resting neutrophils in response to increasing inflammation. To include this effect we modeled the source with the final term in equation (3.12). This term is a nonlinear function of the total amount of blood and tissue activated neutrophils, N_b^* and N^*, respectively. Note the subscript b is used to denote components in the blood and no subscript denotes those in the tissue.

The structure of the equation for pathogen in the blood is the same as the one for pathogen in the tissue. We still assume logistic growth and the presence of the background immune mediators capable of eliminating the pathogen immediately. Therefore, the first two terms in the blood pathogen equation, equation (3.11), are the same as in the tissue pathogen equation, (3.6).

Inhibition of neutrophil activation is similar to the inhibition of macrophage activation, but dependent on $IL10_b$ with the level of inhibition determined by c_{ib} and $IL10_{b\infty}$. The $IL10_b$ equation is included here, due to the inhibition of neutrophils . The source of $IL10_b$

to the blood is via diffusion. The modeling of diffusion is discussed in the next section, so here the only term in the $IL10$ equation, equation (3.15), is its decay.

Neutrophils are able to destroy pathogen. Therefore we have the reaction, $P + N^* \rightarrow r_b N^*$, where $r_b \leq 1$. During the elimination of pathogen the activated neutrophils are depleted. The parameter r_b determines the proportion of activated neutrophils which are destroyed during elimination. Accounting for this and the inhibition of neutrophils, we develop the last term of both the pathogen and activated neutrophil equations, equations (3.11) and (3.13).

3.2.3 Tissue Integrity

When inflammation occurs in tissue, the tissue becomes damaged by the presence of radicals, such as nitric oxide. Therefore, in this model we track the level of radicals and the integrity of the tissue with the variables, RAD and TI, respectively. $TI = 1$ in the absence of inflammation. If significant radicals accumulate, RAD increases, and TI will drop to zero, representing fully damaged tissue incapable of repairing itself. In order to model the ability of tissue to repair itself, we initially set $\frac{dTI}{dt} = k_{tg} TI(1 - \frac{TI}{T_\infty})(TI - a)$, with $0 < a < 1$. This is similar to logistic growth with the extra factor. k_{tg} is the repair rate of the tissue and T_∞ is set to one, representing 100%. This equation and has three fixed points, $TI = 0$, $TI = a$, and $TI = 1$. This TI equation is bistable between $TI = 0$ (fully damage) and $TI = 1$ (100% integrity) with the threshold between these outcomes determined by the unstable fixed point a. If TI falls below a it is unable to repair and falls to zero. We set $a = 0.1$, therefore if tissue integrity falls below 10% it is unable to recover. Adding the depletion of TI when it meets a radical, $-k_{rtt} RAD\ TI$ to this growth term, we have the TI equation, equation (3.16).

$$\frac{dTI}{dt} = k_{tg} TI(1 - \frac{TI}{T_\infty})(TI - a) - k_{rtt} RAD\ TI \tag{3.16}$$

$$\begin{aligned} \frac{dRAD}{dt} &= -\mu_r RAD + k_{rtr} RAD\ TI + k_{nar} f_{in}(N^*) \\ &\quad + k_{natr} N^* TI + k_{rntp} N^* P\ TI + k_{rtmp} M^* P\ TI \end{aligned} \tag{3.17}$$

In this model, all damage to tissue is assumed to be caused via radicals, which are produced in four ways. The presence of activated neutrophils in the tissue causes tissue damage that releases radicals ($k_{natr}N^*TI$). Tissue is also damaged as both activated macrophages and neutrophils eliminate pathogen producing radicals ($k_{rntp}N^*P\ TI$ and $k_{rtmp}M^*P\ TI$). Radicals are also released by activated neutrophils ($k_{nar}f_{in}(N^*)$). Radicals cause further damage to the tissue increasing their own levels, $k_{rtr}RAD\ TI$. These terms all appear in the radical equation, equation (3.17). The first term in this equation is the intrinsic decay of RAD. Only the term $k_{nar}f_{in}(N^*)$ is inhibited, since it is a cell function of the N^* and IL-10 inhibits all cell functions of macrophages and neutrophils. All other damage terms are not the result of cell function, but rather population size and therefore they are not inhibited. Radical production is not dependent on the level of the activated macrophages since in healthy tissue they are present in the tissue in resting state. Once produced, radicals cause depletion of TI, $k_{rtt}RAD\ TI$ in equation 3.16. Radicals also activate macrophages in the tissue and neutrophils in the blood once they have diffused. The terms associated with these actions occur in the final form of the equations for M, M^*, N_b, and N_b^*, equations (3.23), (3.24), (3.33), and (3.34).

3.2.4 Diffusion

During an immune response the endothelial layer of the tissue changes its permeability allowing cells, pathogen, and molecules to diffuse more efficiently. These changes are dependent on levels of TNF and the accumulation of tissue damage. In order to model this, we create a variable for inflammation of the tissue layer, Z. This variable is needed since diffusion cannot be directly dependent on TNF and/or TI. Changes in permeability have a longer half-life than the immune mediators TNF and the repair rate of TI. Therefore, we developed the Z variable such that its growth is dependent on the level of TNF and $1-TI$ and set its decay to be less than the decay of TNF and the rate of tissue repair, $\mu_z < \mu_t$ and $\mu_z < k_{tg}$. The

Z equation is given by equation (3.18).

$$\frac{dZ}{dt} = (k_{tz}f(TNF, x_{tz}, h_{tz}) + k_{zti}(1 - TI))(1 - Z) - \mu_z Z \tag{3.18}$$

$$d_n(Z) = d_{bn}(1 + d_{fn}Z) \tag{3.19}$$

$$d_{mol}(Z) = d_{bmol}(1 + d_{fmol}Z) \tag{3.20}$$

$$d_p(Z) = d_{bp}(1 + d_{fp}Z) \tag{3.21}$$

Diffusion is then modeled for activated neutrophils, molecules, and pathogen with the functions, (3.19), (3.20), and (3.21), respectively. Each of these functions has the form $d_x(Z) = d_{bx}(1 + d_{fx}Z)$. The parameter d_{bx} is baseline diffusion of x in the absence of inflammation and $d_{fx}Z$ is the facilitation of diffusion during inflammation. Activated neutrophils diffuse into tissue by a process called migration. They roll along the surface of the tissue, only entering inflamed tissue. To model this, we set d_{bn} to be very small with large d_{fn}. Small molecules, radicals, TNF, and IL-10 readily diffuse in the absence of inflammation. Therefore, changes in endothelial cells do not increase molecules diffusion as much as neutrophil diffusion. Accordingly, d_{bmol}, the baseline diffusion of molecules, is large with small d_{fmol} relative to d_{bmol}. Individual pathogens are larger than molecules, so we also set $d_{bp} < d_{bmol}$.

When modeling diffusion, we also accounted for the formation of pathogen colonies and the compartment volumes. Pathogen within the tissue forms colonies at high concentrations. Therefore, the diffusion is dependent on the surface area of the population. The surface area is not the only determining factor. Other constraints limit the diffusion such that it is less than that corresponding to surface area alone. To capture this dependence of pathogen diffusion from tissue to blood on the surface area of P, we define a function for the rate at which P diffuses from the tissue, $d_{pt}(P) = a_t P^{2/3}/(1 + b_t P^{1/3})$. We derive this function form by assuming that the volume of the colony formed is proportional to the concentration of the pathogen , P. Hence, the radius and the surface area of the colony are proportional to $P^{1/3}$ and $P^{2/3}$, respectively. This determined the numerator of $d_{pt}(P)$, $a_t P^{2/3}$. To capture other constraints on diffusion we divided this by $(1 + b_t P^{1/3})$. The exponent 1/3 on the bottom is chosen so that in the limit as $P \to \infty$, $d_{pt}(P) < P^{2/3}$. Due to the flow of blood these pathogen colonies do not occur as easily in the blood. Therefore we assume the rate of diffusion from blood to tissue is linearly dependent on P_B and modeled with $d_{pb}(P_b) = a_b P_b$.

Additionally, we need to account for the volumes of each compartment. First, let us focus on the simplest case, the passive diffusion of molecules. Parameters are defined such that $d_{mol}(Z)([X]_b - [X])$ is the rate at which molecules of X diffuse. Note that, this is dependent on the difference in concentration, but it defines the exchange of molecules. Therefore, when this term has to be divided by the volume of the compartment we get the change in concentration for that compartment. For example, $d_{mol}(Z)(IL10_b - IL10)/V_T$ is the diffusion term for IL-10 that appears in the $IL10$ equation with V_T denoting tissue volume. This method is used to derive the diffusion terms for radicals, TNF, and IL-10, see the equation and parameter section, Section 4.6.1.

Neutrophils diffuse via migration, therefore the rate of diffusion is not dependent on the difference in concentration. Instead it is dependent on the concentration of the blood neutrophils available for migration. Hence, the diffusion term in the blood takes the form $-d_n(Z)N_b^*/V_B$ with V_B equal to blood volume, and $d_n(Z)N_b^*/V_T$ in the tissue. These terms occur in the N_b^* and N^* equations, (3.34) and (3.25). Once the neutrophils enter the tissue, they are capable of eliminating pathogen. As in the blood, they are destroyed during this process. So, the elimination terms for P and N^* have the same form in the blood and tissue, see equations (3.25) and (3.22).

Above we saw that rate of pathogen diffusion from the blood is determined by $d_{pb}(P_b)$ and its diffusion from the tissue by $d_{pt}(P)$. Therefore, the actual terms for pathogen diffusion are of the form, $d_p(Z)(d_{pb}(Pb) - d_{pt}(P))/V_x$, with $V_x = V_B$ or V_T. These terms appear in the equations of P and P_b, equations (3.22) and (3.32).

3.2.5 Decay of Inhibition

IL-10 dynamics are essential in eliminating the immune response after the pathogens are eliminated. They are solely produced by macrophages. However, IL-10 is elevated until after macrophages are eliminated. If the decay rates of IL-10 in the tissue and the blood are simply modeled as $-\mu_i IL10$ and $-\mu_{ib} IL10_b$ as in equations (3.10) and (3.15) and we assume the documented decay rates for IL-10, $IL10$ returns to zero before M^* does. When this occurs, the low levels of damage produced during a macrophage response are able to

sustain the M^* population, since inhibition has dropped. In order to model $IL10$ correctly we assume that the decay rate of $IL10$ is a function of $IL10$, such that high $IL10$ corresponds to a minimal decay rate. We replace $-\mu_{i\max}$ with $-\mu_{imax}$+(μ_{imax}-μ_{imin})$il10^{hi}/(x_i^{hi} + il10^{hi}) = -\mu_{imax} + (\mu_{imax} - \mu_{imin})f(IL10, x_i, h_i)$ to get Equation (3.27). The same type is used for $IL10_b$, giving the equation (3.36).

3.2.6 Equations and Parameters

Here we summarize the equations and parameters for the full blood/tissue compartment model.

Tissue Equations:

$$\begin{aligned}\frac{dP}{dt} &= k_{pg}P(1-\frac{P}{p_\infty}) - \frac{s_b k_{pb} P}{\mu_{b+k_{bp}P}} - k_{pm}f_i(M^*)f(P, x_{m*p}, h_{m*p}) \qquad (3.22)\\ &\quad -k_{pn}f_{in}(N^*)f(P, x_{n*p}, h_{n*p}) + d_p(Z)\frac{d_{pb}(P_b) - d_{pt}(P)}{V_T}\\ \frac{dM}{dt} &= -\mu_m M - k_{mtcell}f_i(M)f(TNF, x_t, h_t) \qquad (3.23)\\ &\quad -k_{mrcell}f_i(M)RAD - k_{mp}f_i(M)f(P, x_{mp}, h_{mp}) + s_m\\ \frac{dM^*}{dt} &= -\mu_{m*}M^* + k_{mtcell}f_i(M)f(TNF, x_t, h_t) \qquad (3.24)\\ &\quad +k_{mrcell}f_i(M)RAD + k_{mp}f_i(M)f(P, x_{mp}, h_{mp})\end{aligned}$$

$$\begin{aligned}\frac{dN^*}{dt} &= -\mu_{n*}N^* - (1-r)k_{pncell}f_{in}(N^*)f(P, x_{n*p}, h_{n*p}) + \frac{d_n(Z)N_b^*}{V_T} \qquad (3.25)\\ \frac{dTNF}{dt} &= -\mu_t TNF - k_{mtmol}f_i(M)f(TNF, x_t, h_t) \qquad (3.26)\\ &\quad +k_{mat}f_{it}(f(M^*, x_{m*t}, h_{m*t})) + \frac{d_{mol}(Z)(TNF_B - TNF)}{V_T}\\ \frac{dIL10}{dt} &= (-\mu_{imax} + (\mu_{imax} - \mu_{imin})f(IL10, x_i, h_i))IL10 + k_{mai}f_i(M^*) \qquad (3.27)\\ &\quad +\frac{d_{mol}(Z)(IL10_b - IL10)}{V_T} + k_{mai}f_i(f(M^*, x_{m*i}, h_{m*i}))\\ \frac{dRAD}{dt} &= -\mu_r RAD + k_{rtr}RAD\ TI + k_{nar}f_{in}(N^*) + k_{natr}N^*TI \qquad (3.28)\\ &\quad +k_{rntp}N^*P\ TI + k_{rtmp}M^*P\ TI + \frac{d_{mol}(Z)(RAD_b - RAD)}{V_T} \qquad (3.29)\end{aligned}$$

$$\frac{dTI}{dt} = k_{tg}TI(1-\frac{TI}{T_\infty})(TI-a) - k_{rtt}RAD\ TI \tag{3.30}$$

$$\frac{dZ}{dt} = k_{tz}(f(TNF, x_{tz}, h_{tz}) + k_{zti}(1-TI))(1-Z) - \mu_z Z \tag{3.31}$$

Blood Equations:

$$\begin{aligned}\frac{dP_b}{dt} &= k_{pbg}P_b(1-\frac{P}{p_{b\infty}}) - \frac{sb_b k_{pbb}P_b}{\mu_{bb+k_{bbp}P_b}} - k_{pnb}f_{ib}(N_b^*)f(P_b, x_{n*pb}, h_{n*pb}) \\ &\quad + d_p(Z)\frac{d_{pt}(P) - d_{pb}(P)}{V_B}\end{aligned} \tag{3.32}$$

$$\begin{aligned}\frac{dN_b}{dt} &= -\mu_{nb}N_b - k_{ntcell}f_{ib}(N_b)f(TNF_b, x_{tb}, h_{tb}) \\ &\quad - k_{npbcell}f_{ib}(N_b)f(P_b, x_{npb}, h_{npb}) \\ &\quad - k_{nrb}f_{ib}(N_b)RAD_b + s_{nb} + k_{snb}f(cN_b^* + dN^*, x_{snb}, h_{snb})\end{aligned} \tag{3.33}$$

$$\begin{aligned}\frac{dN_b^*}{dt} &= -\mu_{nb*}N_b^* + k_{ntcell}f_{ib}(N_b)f(TNF_b, x_{tb}, h_{tb}) \\ &\quad + k_{npb}f_{ib}(N_b)f(P_b, x_{npb}, h_{npb}) + k_{nrb}f_{ib}(N_b)RAD_b \\ &\quad - (1-r_b)k_{pncell}f_{ib}(N_b^*)f(P_b, x_{n*pb}, h_{n*pb}) - \frac{d_n(Z)N_b^*}{V_B}\end{aligned} \tag{3.34}$$

$$\begin{aligned}\frac{dTNF_b}{dt} &= -\mu_{tb}TNF_b - k_{ntmol}f_{ib}(N_b)f(TNF_b, x_{tb}, h_{tb}) \\ &\quad - \frac{d_{mol}(Z)(TNF - TNF_B)}{V_B}\end{aligned} \tag{3.35}$$

$$\begin{aligned}\frac{dIL10_b}{dt} &= (-\mu_{ib\max} + (\mu_{ib\max} - \mu_{ib\min})f(IL10_B, x_i, h_i))IL10_B \\ &\quad + \frac{d_{mol}(Z)(IL10 - IL10_b)}{V_B}\end{aligned} \tag{3.36}$$

$$\frac{dRAD_b}{dt} = -\mu_{rb}RAD_b + k_{narb}f_{inb}(N_b^*) + \frac{d_{mol}(Z)(RAD - RAD_b)}{V_B} \tag{3.37}$$

Hill Function:

$$f(v, x_v, h_v) = \frac{v^h}{v^h + x_v^h}$$

Name	Value	Description
k_{pb}, k_{pbb}	$0.461/B$ units hr	Rate at which the non-specific local response in tissue (B)/blood (B_B) eliminate pathogen in the tissue (P) and blood (P_B)
k_{bp}	$0.0001/P$ units/ hr	Rate at which B is exhausted by P
k_{bbp}	$0.02/P$ units/ hr	Rate at which B_B is exhausted by P_B
s_b, s_{bb}	$0.0075B$ units/hr	Source of B and B_B
μ_b, μ_{bb}	$0.0023/hr$	Decay rate for the B and B_B
k_{pg}	Various	The growth rate of P/P_B
$p_\infty/p_{b\infty}$	$20,00$ P units	Maximum P/P_B population
k_{pm}	2.8 P units/hr/M^* units	Rate at which activated macrophages (M^*) eliminate P
k_{mp}	40/hr	Rate at which pathogen activates of resting phagocytes (M) by P
x_{m*p}/x_{mp}	20 P units	Determines level of P needed to bring elimination of P by M^* and activation of M to half their maximums
h_{m*p}	3	Hill coeffecient for the elimination and activation terms containing P.

Table 5: Table of parameters for the compartmental model

Inhibition Functions:

$$f_i(x) = x\left(\frac{(1-c_i)}{1+\left(\frac{il10}{il10_\infty}\right)^{h_i}}+c_i\right) \qquad f_{it}\ (x) = x\left(\frac{(1-c_{it})}{1+\left(\frac{il10}{il10t_\infty}\right)^{h_{it}}}+c_{it}\right)$$

$$f_{in}(x) = x\left(\frac{(1-c_{in})}{1+\left(\frac{il10}{il10n_\infty}\right)^{h_{in}}}+c_{in}\right) \qquad f_{inb}(x) = x\left(\frac{(1-c_{inb})}{1+\left(\frac{il10_b}{il10nb\infty}\right)^{h_{inb}}}+c_{inb}\right)$$

Diffusion Functions:

$$d_n(Z) = d_{bn}(1+d_{fn}Z) \qquad d_{pt}(P) = \frac{a_t P^{2/3}}{1+b_t P^{1/3}}$$

$$d_{mol}(Z) = d_{bmol}(1+d_{fmol}Z) \qquad d_{pb}(P_b) = a_b P_b$$

$$dp(Z) = d_{bp}(1+d_{fp}Z)$$

Parameter values are presented in the Tables 5-12.

Name	Value	Description
s_m, s_{nb}	10 /M units/hr	Source of M and resting blood neutrophils (N_B)
μ_m, μ_{nb}	0.12/hr	Decay rate of M and N_B
μ_{m*}, μ_{n*}, μ_{nb*}	0.05/hr	Decay rate of activated macrophages $M^*$and activated neutrophils N^* in the blood and tissue
k_{mtcell}	20/hr	Rate at which TNF (TNF) activates M
k_{mtmol}	$5P$ units/M-units hr	Rate at which TNF is consumed during the activation of M
x_t	20 P units	Determines level of TNF needed to bring activation by M by TNF to half its maximum
h_t	2	Hill coeffecient for the activation of M by TNF.
k_{mrcell}	0.01/RAD-units/hr	Rate at which radicals (RAD) activate M

Table 6: Table of parameters for the compartmental model continued

Name	Value	Description
k_{pn}	5.8/hr	Rate at N^* eliminates pathogen (P)
k_{pncell}	5/hr	Rate at N^* is destroyed when it eliminates pathogen (P)
r	0.98	Population of the N^* that survives the elimination of P
x_{n*p}	1500 P units	Determines level of P needed to bring elimination of P by N^* to half its maximum
h_{n*p}	3	Hill coeffecient for the elimination term by N^* containing P.
μ_t/μ_{tb}	1.8/hr	Decay rate for TNF and TNF_B
k_{mat}	3,000 P units/hr	Rate of TNF production by M^*
x_{m*t}	80 M^* units	Determines level of M^* needed to bring TNF production to half its maximum
h_{m*t}	2	Hill coeffecient for the producttion term of TNF by M^*
$\mu_{i\max}/\mu_{ib\max}$	0.34/hr	Maximum decay rate for $IL10$ and $IL10_B$
$\mu_{i\min}/\mu_{ib\min}$	0.005/hr	Minimum decay rate for $IL10$ and $IL10_B$
k_{mai}	1,000 P units/hr	Rate of $IL10$ production by M^*
x_{m*i}	140 M^* units	Determines level of M^* needed to bring $IL10$ production to half its maximum
h_{m*i}	2	Hill coeffecient for the production term by TNF by M^*
x_i	8 P units	Determines level of $IL10/IL10_B$ needed to cause its decay rate to decrease to half its maximum
h_i	2	Hill coeffecient for the production term by TNF by M^*

Table 7: Table of parameters for the compartmental model continued.

Name	Value	Description
μ_r/μ_r	4/hr	Decay rate for RAD and RAD_B
k_{rtr}	0.1/hr	Rate at which RAD is produced when RAD is in the tissue
k_{nar}/k_{narb}	$0.01RAD$ units/N^*units/hr	Rate at which RAD/RAD_B is released by N^*/N_B^*
k_{natr}	RAD units/N^*units/hr	Rate at which RAD is produced when N^* is in the tissue causing damage
k_{rntp}	0.2 RAD units/N^*units/hr/P units	Rate at which RAD is produced when N^* eliminates P is in the tissue
k_{rtmp}	$1 \times 10^{-5} RAD$ units/N^*units/hr/P units	Rate at which RAD is produced when M^* eliminates P is in the tissue
k_{tg}	2/hr	Repair rate of the tissue intergrity(TI)
T_∞	1	TI maximum, corresponds to 100% intergrity
a	0.1	Below $TI = a$, tissue is unable to repair itself.
k_{rtt}	$0.01/RAD$units/hr	Rate at which RAD deplete TI
k_{tz}	$0.5/hr$	Rate at which TNF and tissue damage $(1 - TI)$ cause inflammation (Z)
x_{tz}	20 P units	Determines level of TNF needed to bring production of Z by TNF to half its maximum
h_{tz}	2	Hill coeffecient for the production term of Z by TNF
k_{zti}	0.1	Relative effectiveness of TNF versus tissue damage in producing Z
μ_z	$0.01/hr$	Decay rate of Z

Table 8: Table of parameters for the compartmental model continued.

Name	Value	Description
k_{pnb}	0.04/hr	Rate at N_B^* eliminates pathogen (P_B)
$k_{pnbcell}$	5/hr	Rate at N_B^* is destroyed when it eliminates pathogen (P_B)
r_b	0.98	Population of the N_B^* that survives the elimintaion of P_B
x_{n*pb}	0.1 P units	Determines level of P_B needed to bring activation of N_B and P elimination by N_B^* to half their maximums
h_{n*pb}	1	Hill coeffecient for the blood pathogen elimination term by N_B^*
k_{ntcell}	2/hr	Rate at which TNF_B activates N_B
k_{ntmol}	0.8 P units/M units/hr	Rate at which TNF_B is consumed during the activation of N_B

Table 9: Table of parameters for the compartmental model continued

Name	Value	Description
x_{tb}	2 P units	Determines level of TNF_B needed to bring activation by N_B by TNF_B to half its maximum
h_{tb}	2	Hill coeffecient for the activation of N_B by TNF_B
k_{nrb}	$0.1/RAD$ units//hr	Rate at which radicals (RAD) activate N_B
k_{snb}	3 N -units/hr	Rate at which the source of N_B increases
c	1	Effectiveness of N^* and increasing the source of resting neutrophils (s_{nb})
d	1	Effectiveness of N_B^* and increasing the s_{nb} of N
x_{snb}	200 N^*-units	Determines level of $N^* + N_B^*$ needed to bring increases in s_{nb} to half their maximum
h_{snb}	2	Hill coeffecient for the production term of Z by TNF

Table 10: Table of parameters for the compartmental model continued.

Name	Value	Description
c_i	0.05	Maximum inhibition level of f_i, inhibition of macrophage functions
c_{it}	1×10^{-6}	Maximum inhibition level of f_{it},inhibiton of TNF production
c_{in}	0.15	Maximum inhibition level of f_{in}, inhibiton of tissuse neutophils
c_{inb}	0.15	Maximum inhibition level of f_{inb},inhibtion of blood neutrophils
h_i	3	Hill coeffecient for f_i
h_{it}	5	Hill coeffecient for f_{it}
h_{in}	1	Hill coeffecient for f_{in}
h_{inb}	1	Hill coeffecient for f_{inb}
$il10_\infty$	200 $il10$-units	Determines level of $IL10$ needed to bring macrophage inhibtion to half its maximum
$il10_{t\infty}$	60 $il10$-units	Determines level of $IL10$ needed to bring the inhibition of TNF production
$il10_{n\infty}$	80 $il10$-units	Determines level of $IL10$ needed to bring tissue neutrophils inhibition to half its maximum
$il10_{nb\infty}$	80 $il10b$-units	Determines level of $IL10_B$ needed to bring blood neutrophils inhibition to half its maximum

Table 11: Table of parameters for the compartmental model continued.

Name	Value	Description
d_{bn}	0.005 L/hr	Baseline diffusion of neutrophils
d_{fn}	50	Effectiveness of Z in increasing neutrophil diffusion
d_{bp}	1	Baseline diffusion of pathogen
d_{fp}	1	Effectiveness of Z in increasing pathogen diffusion
d_{bmol}	10 L/hr	Baseline diffusion of molecules (RAD, TNF, and $IL10$)
d_{fmol}	1	Effectiveness of Z in increasing molecule diffusion
a_t	50 L/hr/(P units)$^{-1/3}$	Constant in the numerator of d_{pt}
b_t	0.8 (P units)$^{-1/3}$	Constant in the denominator d_{pt}
a_b	2000/hr	Rate of pathogen diffusion in the d_{pb}

Table 12: Table of parameters for the compartmental model continued

3.2.7 Multiple Tissues

When linking two tissues to a single blood unit, we assumed the same structure for all equations in both tissues. The blood equations are unchanged other than the diffusion and the source of resting neutrophil terms. Diffusion terms have the same structure, but now account for diffusion in and out of both tissues. For example, $d_{mol}(Z)(IL10 - IL10_b)/V_B$, the diffusion of IL-10 as it appears in the $IL10_b$ equation, is replaced with $d_{mol1}(Z_1)(IL10_1 - IL10_B)/V_B + d_{mol1}(Z_2)(IL10_2 - IL10_B)/V_B$, when we are considering two tissues connected to the same blood supply. Note that the variable, function, and parameter names contain a 1 or 2 to denote the tissue unit they are from. We are considering each tissue unit to represent an organ, so we will refer to the tissue units as organ 1 and organ 2.

The source of N_b is dependent on the total activated neutrophils. So in the linked form of the model this term becomes $s_{nb} + k_{snb}f(cN_b^* + dN^*, x_{snb}, h_{snb})$. Initially, all parameters are assumed to be the same for each organ and their values are given in Tables 5-12. Differences in the organs will be introduced via the baseline diffusion parameters, d_{bp} and d_{bn} and via the source of macrophages, s_m. We focus on the diffusion and resting macrophages, because these are known to differ from organ to organ and have significant roles in curing inflammation.

3.3 RESULTS

3.3.1 Single Organ

The single organ has three outcomes, health, aseptic and septic death. Health corresponds to a fixed point with all immune components equal to zero except $TI = 1$ (tissue integrity is 100%), $M = \frac{s_m}{\mu_m}$ and $N_b = \frac{s_{nb}}{\mu_{nb}}$. Health is stable for $k_{pg} < 1.5$. Note that k_{pg} is the pathogen growth rate. Aseptic death is a fixed point for all k_{pg} with tissue integrity equal to zero ($TI = 0$), inflammation high ($Z \neq 0$) and all other variables recovering to their healthy state values. Pathogen has been eliminated, but the damage accumulated during the elimination of pathogen has destroyed the tissue. Septic death is a fixed point with tissue integrity zero, resting cells depleted and all other variables elevated including inflammation and pathogen. In septic death the immune system is unable to eliminate pathogen and it remains activated due to the presence of pathogen. Septic death becomes stable at $k_{pg} \approx 0.425$. Therefore, the model is bistable for $k_{pg} < 0.425$, between health and aseptic death, and tristable for $0.425 < k_{pg} < 1.5$. We set $k_{pg} = 0.6$ for all of the simulation in this section.

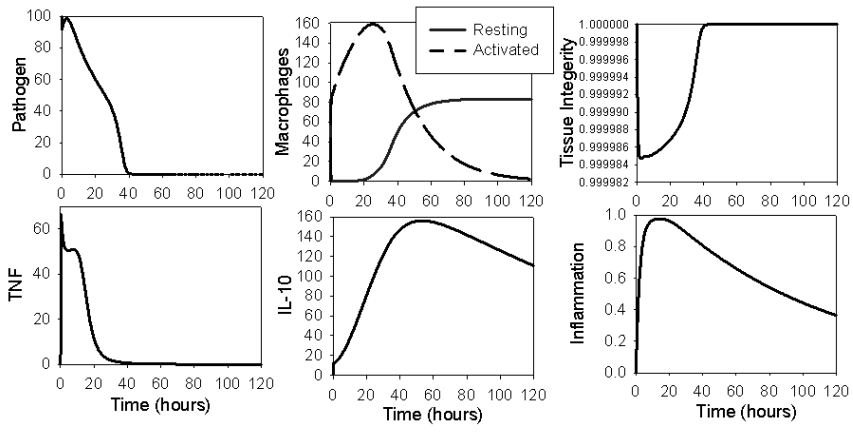

Figure 15: Transients of the tissue immune components from a single unit during a healthy outcome. This insult was triggered by setting initial tissue pathogen to 100 and all other varibales are at background level. Macrophages are the only phagocytes activated during this insult (neutrophil activation was turned off). k_{pg} is set to 0.6/hr.

3.3.1.1 Without neutrophils: We will initially explore the results of the tissue compartment and then add the blood compartment. However, we will not completely isolate the tissue. Diffusion is active, but neutrophils activation is turned off. Figure 15 shows a healthy outcome under these conditions. Note that macrophages reside in the tissue while resting, so tissue damage is not caused by their presence in the cell. Therefore, the only change in tissue integrity is caused the by-products of the macrophage and pathogen interactions. In this simulation there is low pathogen concentration, so we have minimal tissue damage. Also in this simulation, $IL10$ decays to zero after activated macrophages (M^*) do, due to the concentration dependent decay rate of $IL10$. TNF is produced initially, but inhibition of the macrophages by $IL10$ eliminates this production. Therefore, the TNF population drops well before the activated macrophage population.

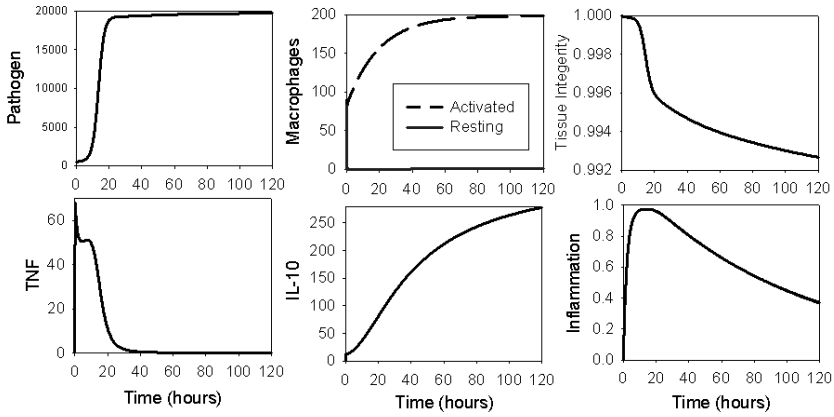

Figure 16: Transients of the tissue immune components from a single unit during a death outcome. This insult was triggered by setting initial tissue pathogen to 500 and all other varibales are at background level. Macrophages are the only phagocytes activated during this insult (neutrophil activation was turned off). k_{pg} is set to 0.6/hr.

During a lethal insult the macrophage population is overwhelmed by the pathogen concentration yielding a state similar to septic death, see Figure 16. This insult was triggered by setting initial pathogen in the tissue to 500. This is not really septic death because $TI \neq 0$. Tissue integrity is not zero, because damage is minimal in the absence of neutrophils. In this simulation, activation by pathogen consumes the resting macrophage population. The TNF transient is very similar to the nonlethal simulation, since it is dependent on early levels of macrophages, which are similar in both the lethal and nonlethal cases. Inflammation is

the same in both cases, since it is dependent on TNF and TI. TI changes are minimal during the lethal insult and TNF is same in both scenarios, therefore inflammation is nearly unchanged from the healthy outcome.

3.3.1.2 With neutrophils: When including the neutrophil population, the insult of an initial tissue pathogen of 500 is survivable, see Figure 17. Tissue integrity is compromised more than in the macrophage only immune response, but it is able to repair itself. Also, $IL10$ does not recover until after neutrophils have reached background levels as is the case with macrophages.

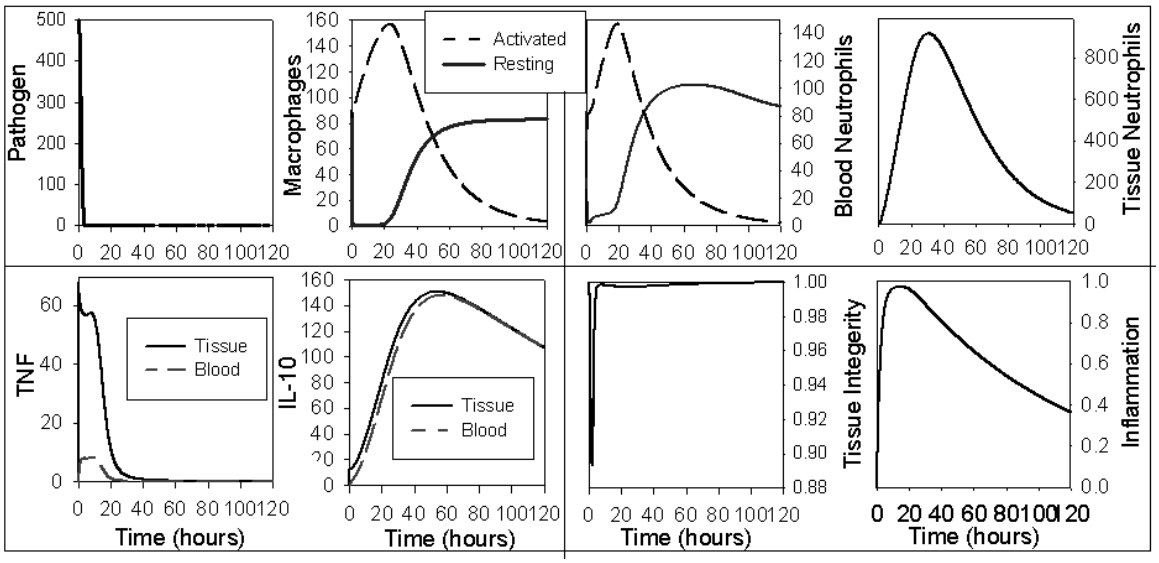

Figure 17: Transients for a healthy outcome in the single unit compartmental model. The insult was triggered by initially setting tissue pathogen to 500 and all other varibales are at background level. k_{pg} is set to 0.6/hr.

Aseptic death occurs when the insult is increased, see Figure 18. This simulation was run with initial tissue pathogen set to 850. Any initial pathogen level less than 842 results in health, between 842 and 1061 results in aseptic death and above 1061 results in septic death. During the aseptic outcome in Figure 18, inflammation does not recover due to the depletion of TI. Here, tissue damage is driven by the $k_{rntp}N^*P\ TI$ term. High initial levels of pathogen as neutrophils become activated cause tissue damage to drop below the threshold for tissue repair.

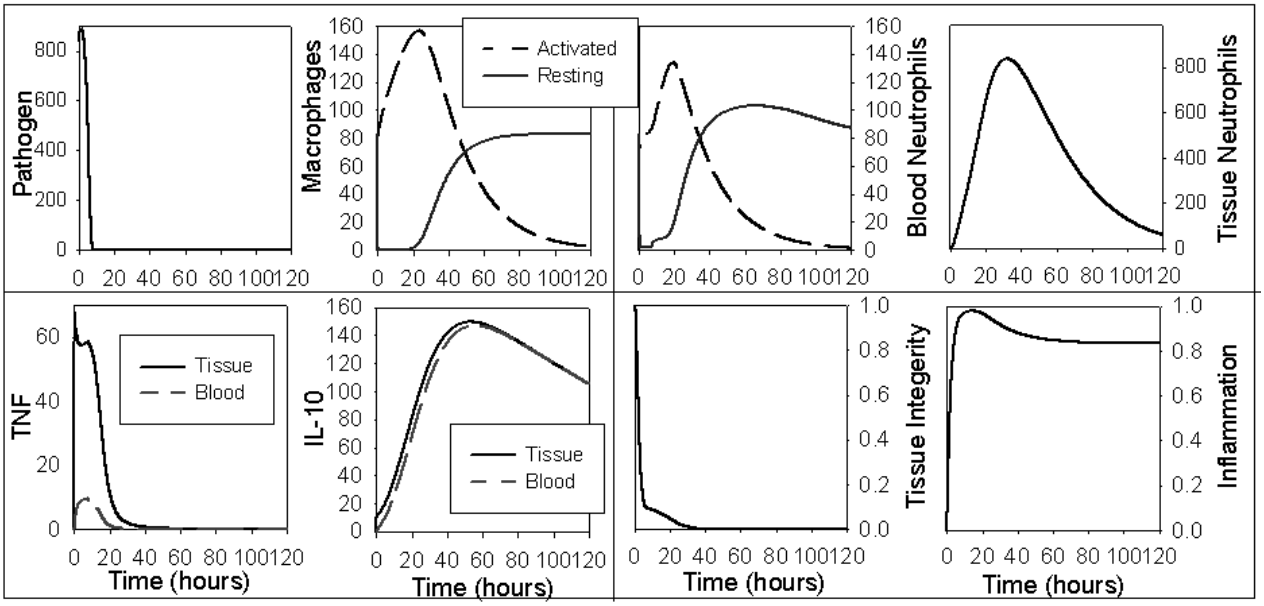

Figure 18: Transients for an aseptic outcome in the single unit compartmental model. The insult was triggered by initially setting tissue pathogen to 850 and all other varibales are at background level. k_{pg} is set to 0.6/hr.

In Figure 19 we see the transients for a septic outcome triggered by an initial tissue pathogen of 1200. High pathogen within the tissue corresponds to high pathogen in the blood, but at significantly lower levels, ≈ 0.73. This is true for all simulations shown here. This huge difference is due to the fact that diffusion of tissue pathogen is dependent on surface area and the relative sizes of the tissue and blood compartments .

Neutrophil levels in Figure 19 are significantly lower than those in Figure 18. This is because of the consumption of neutrophils as pathogen is eliminated term, $-(1-r)k_{pncell}f_{in}(N^*)$ $*f(P, x_{n*p}, h_{n*p})$ in equation 3.25. In the aseptic case, pathogen is eliminated early on and once they are absent neutrophils are able to reach higher levels, since this term is zero. In the septic case pathogen is elevated throughout this term in nonzero lower the level of neutrophils. Despite the lower neutrophil levels, tissue damage is still driven by the term $k_{rntp}N^*P\ TI$ as in the aseptic case. This term contributes throughout the response in the septic case. Therefore, $TI = 0$ occurs more quickly in the septic case, because of the higher initial pathogen and the elevated pathogen levels throughout.

These outcomes can be reached by insults via blood pathogen at drastically lower levels.

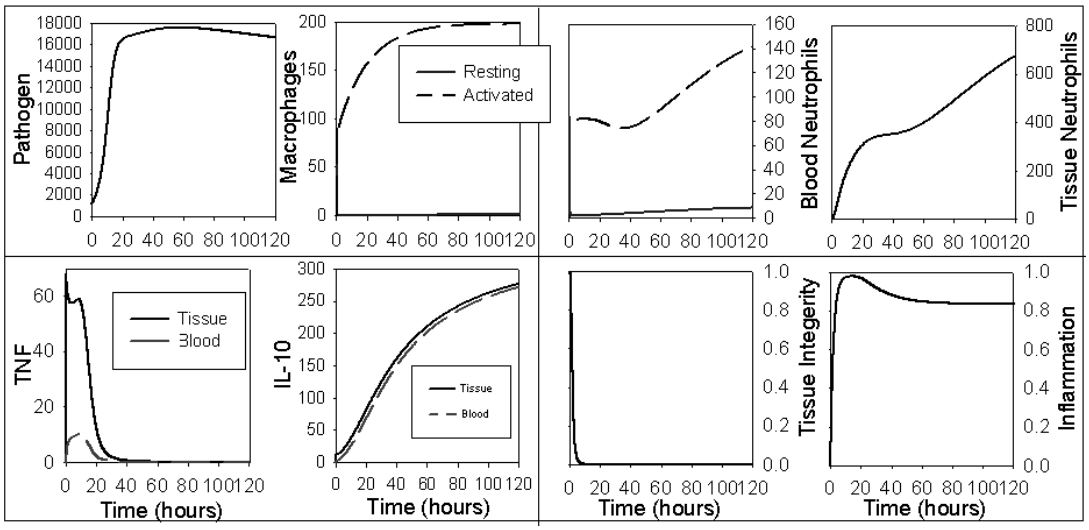

Figure 19: Transients for a septic outcome in the single unit compartmental model. The insult was triggered by initially setting tissue pathogen to 1200 and all other variables are at background level. k_{pg} is set to 0.6/hr.

An insult of $P_{B0} = 8.49$ will cause aseptic death. Due to the large constant for diffusion into the tissue, there is an immediate loss of blood pathogen. Blood pathogen drop drastically to their typical levels during insults via the tissue pathogen. An insult of $P_{B0} = 10.72$ will result in septic death. After the quick initial drop in blood pathogen, transients for all insults are similar to those seen during an insult triggered by tissue pathogen.

3.3.1.3 Summary: This single unit models the immune response within one organ. The local tissue macrophage population can eliminate low pathogen insults. They trigger neutrophil activation and neutrophils enter the tissue. However, there is minimal damage, since the macrophages have eliminated the pathogen present. Neutrophil elimination of pathogen causes more radical production than neutrophil influx. If the local macrophages are overwhelmed, there is a range of initial tissue pathogen for which neutrophils can eliminate pathogen while causing repairable tissue damage. However, at larger initial pathogen, neutrophils influx combined with pathogen elimination can produce enough radicals to fully damage the organ even when the pathogen is eliminated, which is the case in aseptic death. The immune response can also be overwhelmed. Pathogen is not eliminated and immune

components are elevated and cause the organ to fail, the case of septic death.

3.3.2 Multiple units

Linking two organs (tissue units) to the same blood supply, we look at the spread of inflammation as it would be seen during MODS. Differences in organs are evident in function and structure. Therefore, we alter parameters to explore how these difference affect the spread of infection and inflammation. We first consider linking two identical and then linking two organs, where one has altered diffusion of pathogen and neutrophils. We also consider two linked organs, where one has an increased source of resting macrophages.

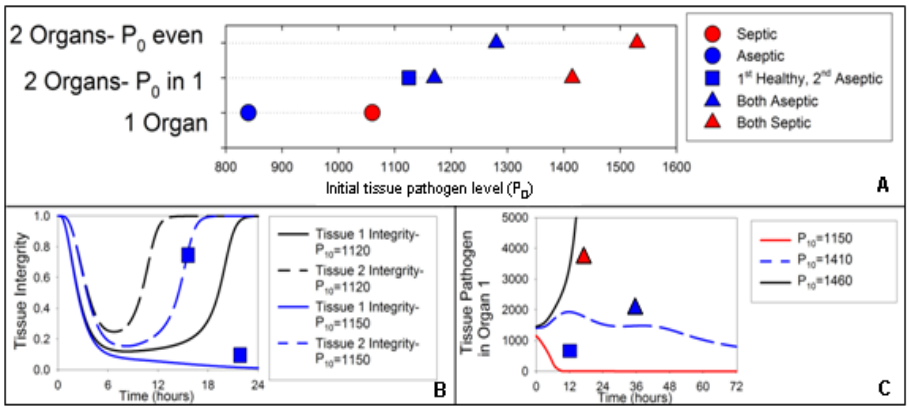

Figure 20: Thresholds for death in the single organ and for two identical organs linked to the same blood supply. A. A plot of the onset of aspetic and septic death versus initial pathogen load for a single organ, two identical organs with the initial tissue pathogen introduced into only one organ (P_0 in 1), and two organs with the initial pathogen evenly distributed between the two organs (P_0-even). B. Tissue integrity during insults to the two organ systems. The tissue pathogen is introduced in only one organ near the threshold for the onset of aseptic death in the first, but not the second organ. C. Tissue pathogen transients when pathogen introduced in one organ. The black curve results in both organs septic, the blue dashed curve results in both organ aseptic, and the red curve results in first organ aseptic and second healthy.

3.3.2.1 Identical organs: Linking two identical organs and initiating the insult via the tissue pathogen in one organ, we see that the threshold for both aseptic and septic death is increased compared to a single unit, see figure 20A. Distribution of the pathogen and inflammation increase the survival of the system. When the insult is introduced into one of the two organs, there is a range of initial tissue pathogen, where the organ that received

the insult is aseptic, but the other organ is healthy, see Figure 20A. Figure 20B shows the transients near the onset of aseptic death in one organ. There is more tissue damage in organ 1, even when both organs result in health (black curves). This is true for both the more and less diffusive cases. As the initial tissue pathogen load in organ 1 (P_{10}) is increased, tissue 1 integrity (TI_1) drops below the level at which it can repair itself ($TI = 0.10$), before the tissue 2 integrity (TI_2) falls this low, therefore aseptic death occurs first in organ 1. Further increases in P_{10} will cause TI_2 to fall below 0.10 and both organs will be aseptic. Therefore, we have captured the spread of inflammation even when the pathogen is eliminated.

In Figure 20C, we have plotted tissue pathogen within organ 1 (P_1) for scenarios were the initial pathogen load is introduced into a single organ. With $P_{10} = 1150$, pathogen is eliminated in both organs, but organ 1 has $TI_1 = 0$. An insult of $P_{10} = 1410$ leads to aseptic death in both organs. This insult is close to the threshold for the onset of septic death. The pathogen population can grow significantly, but is eventually eliminated by the immune response. $P_{10} = 1450$ leads to septic death in both organs. There is no range for P_{10} were organ 1 or 2 is septic while the other is aseptic. When both organs are septic, both P_1 and P_2 increase to nearly 18000 and then drop to their values at septic death, which is 14317 for both organs.

Distributing the initial pathogen between both organs further increases the initial tissue pathogen load survivable by the two organ system. In Figure 20A the upper line is the thresholds for aseptic and septic death versus P_0, where P_0 has been evenly distributed between both organs, $P_{10} = P_{20}$ and $P_0 = P_{10} + P_{20}$. Though the entire system is surviving a higher P_0, when death outcomes occur, each individual organ is dying at a lower initial tissue pathogen than what is survivable by a single unit.

In Figure 21, we look at the cause of this increased sensitivity in the individual organs. We compare the transients for tissue pathogen, neutrophils and radicals from an insult of 650 P units to a single unit (blue dashed curves) and 650 in each organ (black curves), which corresponds to P_0=1300. For the multiple organ simulation, there is only one curve, because results match for both organs, since they are identical with the same initial conditions. More radicals accumulate in tissue during an insult to the two organ system than to the single organ. These high levels of radicals are due to the radical production terms, $k_{rntp1} N_1^* P_1 \, TI_1$

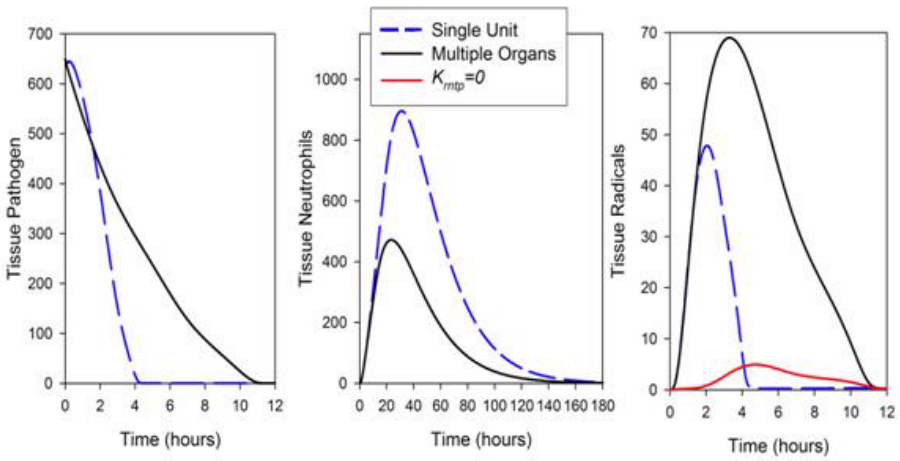

Figure 21: Comparsion of transients from a single organ and multiple organ system with the initial tissue pathogen load evenly distributed. Transients are plotted for tissue pathogen, neutrophils, and radicals for the single (blue dashed) and multiple organs (black) models. Additionally, tissue radicals are plotted with $k_{rntp2} = 0$ and $k_{rntp2} = 0$ (red curve). $k_{rntp1} = k_{rntp2} = 0$ eliminates the production of radicals during the elimination of pathogen by neutrophils in both organs. The multiple organ curves (black) represent the level in both organs. Results match for both organs, since the organs are identical with the same initial conditions.

and $k_{rntp2}N_2^*P_2\ TI_2$, which account for the radicals produced when neutrophils fight pathogen within the tissue. Pathogen does not grow within the tissue during the insult to the two organ system, but is nonzero for nearly 12 hours, where as pathogen is eliminated within six hours after the insult in the single organ. Pathogen is high in the tissue, since less pathogen diffuses from two organs into one blood compartment. This causes the neutrophil population to not reach as high of levels as those seen in the single unit overall, since neutrophils are eliminated during the elimination of pathogen. However, while pathogen is nonzero, we have similar levels of radicals and neutrophils for both the multiple and single organ transients. Once P drops to zero, $k_{rntp}N^*P\ TI$ is zero, and less radicals are produced. We see that this term is the main contributor by plotting the radical levels in the two organ system with $k_{rntp1}N_1^*P_1\ TI_1 = 0$ and $k_{rntp2}N_2^*P_2\ TI_2 = 0$ (see the red curve in Figure 21). Having more significant damage when pathogen is present has been seen experimentally. Neutrophil influx was found to be less harmful in the absence of infection. TNF promotes inflammation without significant injury to the muscle [56].

The septic death threshold of each individual unit is lower than in the single organ,

because septic death is determined by the neutrophil population. The local macrophage population is already overwhelmed before the thresholds of aseptic death are reached. Both organs are calling on the same blood supply of neutrophils and therefore exhausting it at lower levels in the individual, but with sum greater than the level seen in the individual organ.

3.3.2.2 Altered neutrophil and pathogen diffusion: We continue to look at the spread of inflammation by looking at two non-identical organs linked to the same blood supply. First, we explore changes in the diffusive properties. One organ's parameters remain as seen in Tables 5-12. For the other we either increase or decrease the permeability of the tissue to pathogen and neutrophils. Molecule diffusion is not altered. For the less diffusive case we set $d_{bp2} = d_{bp}/20$ and $d_{bn2} = d_{bn}/20$ and for the more diffusive case we set $d_{bp2} = 1.5d_{bp}$ and $d_{bn2} = 1.5d_{bn}$. More significant increases cause septic death to become unstable with the single unit. This minimal change causes septic death to lose stability in the multiple organ case. However, there is a significant change in transients for sufficiently high pathogen (after the both aseptic threshold). Where these this significant change in the transients occurs is referred to as the both "aseptic" threshold In Figure 22, we compare transients which result in the various death outcomes. Above the both "aseptic" threshold transients seem to be going to septic death, but then there is a sudden drop of pathogen to zero. So, even though they technically are aseptic during the early relevant hours of disease the appear to be septic. Therefore, we compare this threshold to the septic threshold.

Single organ: Comparing changes in diffusive properties on a single unit, Figure 23A, we see that there is no aseptic death in the less diffusive case. Neutrophils are not as effective at eliminating disease, since they cannot enter the tissue. Therefore, septic death occurs well before the initial pathogen load is high enough to cause significant tissue damage via the $k_{rntp}N^*P\,TI$ term. Significant levels of radicals are not produced until pathogen is at levels only seen in septic death. Therefore, $TI = 0$ only when septic death occurs. Neutrophils, however, accumulate more in the tissue when the tissue is more diffusive. Therefore, the onset for aseptic death is earlier for the more diffusive organ. Increasing the baseline diffusion pulls this onset of aseptic death even lower. Onset of septic death is at a much higher P_0 due to

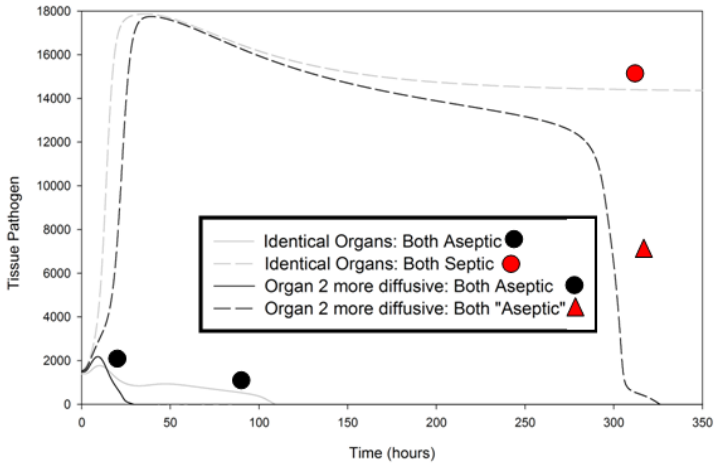

Figure 22: Tissue pathogen transients from the two organ model for the Both Septic, Both Aseptic and "Both Aseptic" outcomes. Insults to the identical organs system were introduced by setting initial tissue pathogen in one organ to 1400 and 1500 resulting in Both Aseptic and Both Septic, respectively. The more diffusive system consists of one normal organ, which has parameter values from Table 1, and a second organ with set $d_{bp} = 1.5d_{bp}$, $d_{bn} = 1.5d_{bn}$, and all other paremeter values unaltered. Insults were caused by setting initial tissue pathogen in the normal organ at 1500 and resulting in Both Aseptic and Both "Aseptic", respectively.

the high tissue neutrophils influx allowing more effective elimination of pathogen.

Two organ system: In Figure 23B we see the effect of linking organs were the second organ is either less diffusive, the same, or more diffusive than the first organ. In this figure the tissue pathogen insult is introduced into the first organ, the normal organ. The less diffusive case only improves the thresholds for aseptic death slightly compared to the single normal organ in Figure 23A. Compared to the two identical organs, the less diffusive organ causes significant decreases in the thresholds for the onset of death. During an insult to the identical case, there is a more significant exchange of pathogen into the second organ. Also, neutrophils are able to diffuse more freely into the second organ to fight the pathogen that diffuses into it. This causes a higher threshold than they are in the less diffusive case, were pathogen cannot diffuse as freely. Limited diffusion into the second organ causes high levels in the normal organ that the immune response is not able to eliminate.

With the more diffusive second organ inflammation can spread causing death in the second organ, but not the first. As in the single unit, increased permeability allows pathogen and neutrophils to diffuse easily into the second organ causing more tissue damage than in

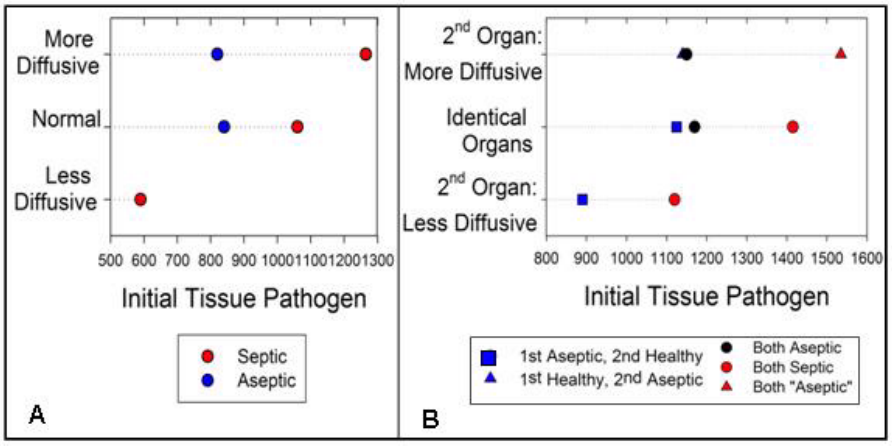

Figure 23: Thresholds for aseptic and septic death in the single and two organ system with various diffusion constants. A. A plot of the onset of aspetic and septic death versus initial pathogen load for a single organ with decreased diffusion, $d_{bp} = d_{bp}/20$ and $d_{bn} = d_{bn}/20$, normal diffusion, and increased diffusion, $d_{bp} = 1.5d_{bp}$ and $d_{bn} = 1.5d_{bn}$. B. Two organs linked to the same blood supply with the second organ less diffusive, normal, and more diffusive. The parameter values for these organs match those of the single organ with comparable diffusion from A. Initial tissue pathogen was introduced into the reference organ.

the first organ. Therefore, the second organ has a lower aseptic death threshold than the first, even though the insult was introduced via the first organ. This is an example of the lethal inflammation in the non-insulted second organ when the insulted organ recovers. This is a common phenomenon in organ failure. MODS typically begins with loss of pulmonary function [42], even when trauma or infection is not introduced into the lung.

In the more diffusive case, both organs go aseptic before both organs go aseptic in the identical case. This is due to higher total tissue neutrophils, which cause more tissue damage. Higher overall neutrophils allow for better elimination of pathogen and therefore both "aseptic" occurs at a higher level than both septic in the identical organ case.

In Figure24 we still are considering a two organ system with one normal organ and the other organ either more or less diffusive. However, for these simulations, we have introduced the insult in the altered organ. In the less diffusive case the threshold for septic death is nearly the same as for a less diffusive single organ, see Figures 23A and 24. Also as in the single tissue there is no aseptic death. The thresholds for the two system is determined by the less diffusive organ, since exchange of neutrophils and pathogen is limited.

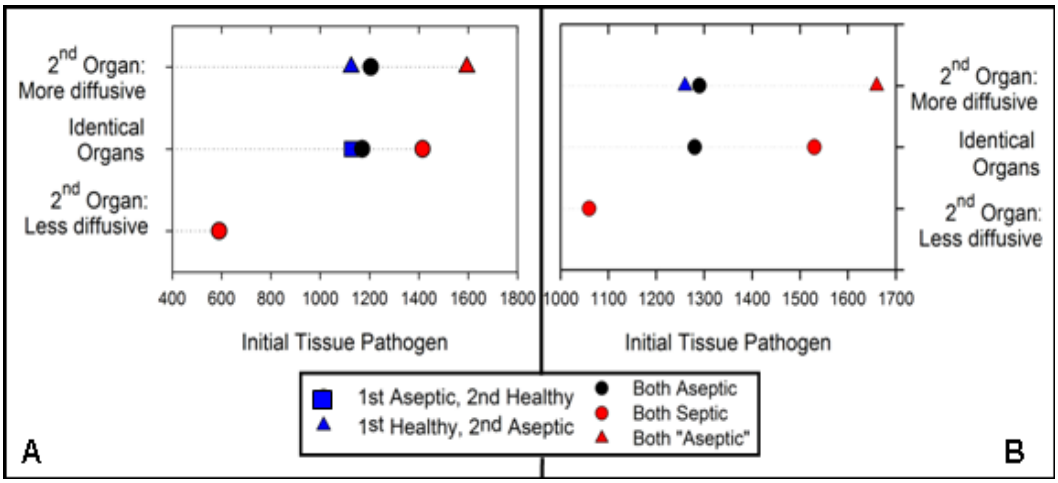

Figure 24: Thresholds for aseptic and septic death in the two organ system with various diffusion constants and initial pathogen in either the second organ or both organs. A. A plot of the onset of aspetic and septic death versus initial pathogen load for a two organs with decreased diffusion, $d_{bp} = d_{bp}/20$ and $d_{bn} = d_{bn}/20$, normal diffusion, and increased diffusion, $d_{bp} = 1.5d_{bp}$ and $d_{bn} = 1.5d_{bn}$. The initial tissue pathogen insult was introduced to the organ with altered diffusion. B. Two organs linked to the same blood supply with the second organ less diffusive, normal and more diffusive. The parameter vaules for these organs match those of from A. Initial tissue pathogen was evenly distributed between both organs.

When we insult the more diffusive organ, as in the normal case, the more diffusive organ goes aseptic before the normal organ. However, this it is not surprising, since the insult was initiated in this organ. Again, increased neutrophils in the overall system buffers against the onset of septic death, so both "aseptic" occurs at a higher initial tissue pathogen than both septic.

In Figure 24B we distributed P_0 in both organs evenly. As in the identical case, overall more P_0 is survived when distributed than when it is introduced to either the normal or altered organs. This holds true for both the more and less diffusive case. However, in all cases, individual units die at lower insults than in they were not linked. This is due to less diffusion of pathogen, since two organs are feeding into the same blood supply. This is causing increased production of radicals during the elimination of pathogen, since pathogen remains nonzero longer. The septic threshold occurs when the blood neutrophils are overwhelmed. It occurs at same level of inflammation in the single and two organ system, since both have the same blood dynamics. Therefore, the slight increases in the septic death threshold for the two organ system are due to the local macrophages. Two local macrophage populations

contribute to the removal of pathogen, so higher initial pathogen is needed to reach the level of inflammation in the blood that will overwhelm the system. These increases are limited by the levels that overwhelm the local macrophages.

3.3.2.3 Altered Source of Macrophages The local macrophages play a large role in determining the thresholds for death. Changes in diffusion only affect the neutrophil population. Therefore, we also introduced heterogeneity in organs by increasing the source of resting tissue marcophages. This allows us to look at the effect of changing the local immune response on overall dynamics. We set $s_m = 2s_m$, which increases the background level of resting macrophage in addition to supplying more resting macrophages during the insult.

Single organ: In Figure 25A, we look at thresholds for a single organ that is normal, more diffusive, and has an increased macrophage source. Also, included is the threshold for the onset of death when the source of macrophages is increased and neutrophils dynamics removed. This threshold is significantly increased compared to the corresponding threshold with a normal s_m level. Here, it is at 960 and with normal source it is only 486. Note that it is labeled with "septic" because unlike actual septic death this outcome has minimal loss of tissue integrity because of the absence of neutrophils.

The increased ability of the local immune system enables higher thresholds for both aseptic and septic death, Figure 25A. Increasing macrophages does not increase damage. Therefore, the onset of aseptic death is at higher P_0 compared to the normal case. Protection against inflammation via high tissue macrophages levels is seen in the liver. The liver has high levels of tissue macrophages and acts as the first line of defense for many insults entering via the gut [55]. Yet, it is rarely becomes inflamed.

The onset of aseptic death in the increased s_m case is actually above the onset of septic death in the normal organ. The main cause of radical production is via neutrophil elimination of pathogen when N^* and P are nonzero, since macrophages are eliminating more pathogen this term is contributing less, avoiding $TI = 0$ until higher P_0.

Two organ system: In Figure 25B, we compare linked organs, where the first organ is normal and the second is either normal or has increased s_m. Introducing the insult into

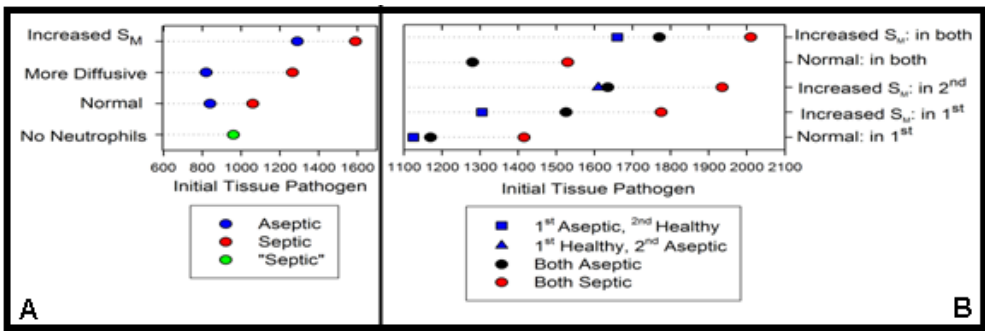

Figure 25: Thresholds for aseptic and septic death in the single and two organ system with the second organ normal, more diffusive or with increased macrophage source. A. A plot of the onset of aseptic and septic death versus initial pathogen load for a single organ with increased macrophage source ($s_m = 2s_m$) and neutrophil activation turned off, normal source and diffusion, increased diffusion ($d_{bp} = 1.5d_{bp}$ and $d_{bn} = 1.5d_{bn}$) and increased macrophage source ($s_m = 2s_m$). B. Two organs linked to the same blood supply with the second normal or increased s_m. The parameter vaules for these organs match those of the single organ with comparable diffusion from A. Initial tissue pathogen was introduced into the normal organ (in 1^{st}), altered organ (in 2^{nd}), and evenly distributed to both (in both).

the normal (first) organ or altered (second) we see an increase in the survival of the system. When the insult is the normal organ the threshold for aseptic death is increased past the onset of aseptic death in both, but not past the onset of septic death. However, insulting the organ with increased macrophages does push the onset of aseptic death past the threshold for both septic in the normal case. Increased elimination of pathogen when the pathogen in introduced to the high macrophage tissue avoids tissue damage, buffering against the onset of aseptic death. This effect continues to drive the late onset of aseptic death when the insult is distributed evenly between both organs.

3.3.2.4 Summary In Figure 26, we compare the parameter changes that were most effective at increasing survival, increasing the source of resting macrophages and diffusion of pathogen and neutrophils. Overall, increasing macrophages is the most effective means to increase survival. A more diffusive second organ allows more influx of neutrophils and pathogen increasing tissue damage. Therefore, this two organ system is more sensitive than if the second organ has an increased source of macrophages. Also, in the more diffusive case, there is a range of $P_{0,}$ where when P_0 is introduced into the normal organ, the normal organ survives and aseptic death occurs in the more diffusive organ. Therefore, even though the

overall system is less sensitive the more diffusive organ itself is more susceptible to the spread of infection. This is not the case for increased macrophages. The system and the organ are both more resist to inflammation.

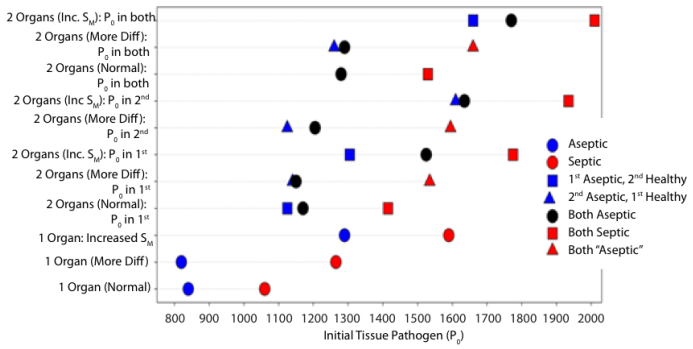

Figure 26: Thresholds for aseptic and septic death in the two organ system with the second organ normal, more diffusive or with increased macrophage source. The onset of aspetic and septic death is ploted versus initial pathogen load for two organ systems where the second is normal, has increased diffusion, $d_{bp} = 1.5d_{bp}$ or $d_{bn} = 1.5d_{bn}$, and increased macrophage source ($s_m = 2s_m$). Initial tissue pathogen (P_0) was introduced into the normal organ (in 1^{st}), altered organ (in 2^{nd}), and evenly distributed to both (in both).

Insults can also be triggered in this multiple organ model also by altering the initial level of blood pathogen. Insults via the blood pathogen are similar to results shown here. The more diffusive organ goes aseptic first. Therefore, if diffusion of the second organ is decreased, the normal organ becomes aseptic first and if the second organ has increased diffusion, it will become aseptic first. With an increase in the source of macrophages the normal organ becomes aseptic first. These outcomes are due the term modeling damaged cause during the elimination of pathogen by neutrophils in the tissue. It is greater in the more diffusive organs therefore, they become aseptic first. In the increased macrophage case, macrophages eliminate more pathogen than in the normal organ and therefore this term contributes less to the production of damage.

Code which simulates the single organ and two organ system is in Appendix C.

3.4 DISCUSSION

We have derived a compartmental model of the acute immune response within an organ. It expands upon the previous reduced model in Chapter 2, Reynolds et al., to include dynamics both in the tissue and blood [58]. As in the reduced model, we have outcomes corresponding to health, aseptic death and septic death. However, we have included TNF and IL-10 as variables and fit their transients to heuristic data. TNF is produced in the initial stages of inflammation and IL-10 is elevated after the activated macrophage population has returned to rest.

The model was developed starting from the tissue and then expanded to included diffusion and neutrophil activation within the blood. Terms were added as needed to properly capture the known biological dynamics. Complexity was minimized, since the model was to be linked with itself to model organ communication. Having more variables and parameters makes understanding the overall behavior of the system less intuitive. Another motivation for minimizing complexity was to implement this compartmental immune system in our pulmonary lung model, presented in the follow chapter.

Once the single organ model was developed and analyzed, we linked two organs together to look at the spread of inflammation. MODS is characterized by the spread of inflammation causing sequential organ failure. Therefore, understanding the spread of infection and inflammation is a first step in developing ways to stop the progression of MODS. We used the linked organ model to look at parameter changes that alter diffusion and the local macrophage population.

Differences in diffusion alter the outcomes of the system. More diffusive organs allow for more influx of neutrophils and therefore protect against the onset of septic death. The damage cause by neutrophils in their elimination of pathogen increases the likelihood of aseptic death. Less diffusive organs can avoid aseptic death, but are highly susceptible to septic death. This is because neutrophils cannot infiltrate and therefore do not cause tissue damage, but they also do not eliminate the pathogen. Linking a normal organ to a less diffusive organ increases the sensitivity of the whole system. Linking to an organ with increased diffusion overall protects the system, but the more diffusive organ itself is more

sensitive to aseptic death.

Changing the local macrophage population by altering their source increases levels of resting macrophage at the onset and throughout the inflammatory response, protecting the tissue. Linking a normal organ to an organ with increased macrophages protects the system from all forms of death. We have seen that the main driver of tissue damage is the elimination of neutrophils by pathogen. This term's effects are increased by changes in diffusion because it alters the levels of pathogen and neutrophils. It is reduced by the increases in macrophages, since macrophages eliminates more pathogen Therefore, even though neutrophil levels rise there is less damage due to lower pathogen levels.

This model gives us the means to explore many aspects of the spread of inflammation. Linking it with our pulmonary model we can look the spread of inflammation to the lung. The lung is typically the first organ to fail during MODS. Linking our full lung model and our two compartmental organ, we can explore what aspects of the lung make it more susceptible to inflammation. Also, we have included specific cytokines in order to have variables that correspond available data. For example, we have included IL-10 rather than simply anti-inflammatories. Therefore, we can further calibrate this model with data. As in the reduced model we can look at the effect of altering the anti-inflammation. However, here we will be altering IL-10, therefore experimentally testing of our hypotheses is more realistic than when using the reduced model. Once we have a greater understanding of acute inflammation, the model can used to explore means by which to hinder its spread.

4.0 PULMONARY GAS EXCHANGE UNDER INFLAMMATORY STRESS

4.1 INTRODUCTION

There is substantial literature on mathematical models of gas exchange, that has focused on different aspects of the process of gas transfer and distribution between ambient air and blood, including distribution of ventilation, transport between alveolar air space and pulmonary capillaries, red blood cell rheology, hemoglobin dynamics and acid-base physiology [7]. These models span different anatomical scales and have generally been useful to study airflow distribution, deposition of particulate drugs in airways, and determine the severity of shunting within the lung.

New imaging techniques ([47], [69]) and cell-type identification tools ([52]) are providing a unique opportunity to construct and calibrate increasingly complex and realistic models that integrate the large body of existing knowledge with these newer data and provide modeling tools with significant translational impact into the understanding, and modification of, human disease. In the realm of critical care medicine, acute lung injury (ALI) is an inflammatory process that can be triggered by chemical, infectious or traumatic stimuli. ALI typically requires mechanical ventilatory support and is the most frequent manifestation of multisystem organ dysfunction, which is the leading cause of death in the ICU ([62]). ALI also has long-term consequences for those who survive the acute phase. Substantial public and corporate resources are devoted to prevent and treat ALI. There are also good animal models of ALI ([20]) and its pathophysiology is increasingly well understood.

To our knowledge, existing modeling efforts have not attempted to describe the progression of ALI following a local or systemic inflammatory stimulus. We therefore describe such an attempt, where the direct effects of inflammatory mediators on lung tissue are modeled,

with their impact on lung volumes, lung water content and gas exchange ability. This is the first step in constructing a truly multiscale representation of gas exchange under inflammatory stress, with an explicit representation of the time evolution of ventilation-perfusion inequalities under such conditions.

4.2 METHODS

4.2.1 Overview

In order to explore changes in lung function during an infection we modeled gas exchange and the inflammatory response within a small portion of the lung. We consider the local dynamics on a respiratory unit (RU), which consists of 25 alveoli and the capillaries surrounding them ([27]). We constructed a model of gas exchange within RU consisting of partial differential equations for oxygen, oxyhemoglobin, carbon dioxide, and bicarbonate. A RU consists of three compartments, the alveolar air space, lung tissue and capillary blood. There are variables expressing the partial pressure of oxygen (PO_2) and carbon dioxide (PCO_2) in all three compartments, while oxyhemoglobin (Hb_4) and bicarbonate (HCO_3^-) are only in the blood. We model the following biological processes: diffusion of oxygen and carbon dioxide, hemoglobin uptake of oxygen, and enzymatic reactions governing carbon dioxide and bicarbonate levels. We assume diffusion occurs across two distinct barriers within the RU, the blood/tissue and tissue/alveolar air space barriers. Tidal breathing regulates alveolar gas pressures of oxygen and carbon dioxide within the alveolar space. Following the development of a model of the gas exchange subsystem, we incorporate a response to an inflammatory stimulus, the inflammation subsystem, leading to the development of ALI. This additional subsystem consists of equations for neutrophils and tumor necrosis factor (TNF), a canonical pro-inflammatory cytokine, in both the blood and tissue compartment. Figure 27 illustrates the interactions included within the single RU.

The RU is modeled as a one-dimensional spatial domain along the length of the capillary. Therefore, variables for the partial pressure of oxygen and carbon dioxide in the blood and tissue and the concentration of saturated hemoglobin in the blood all vary in time and

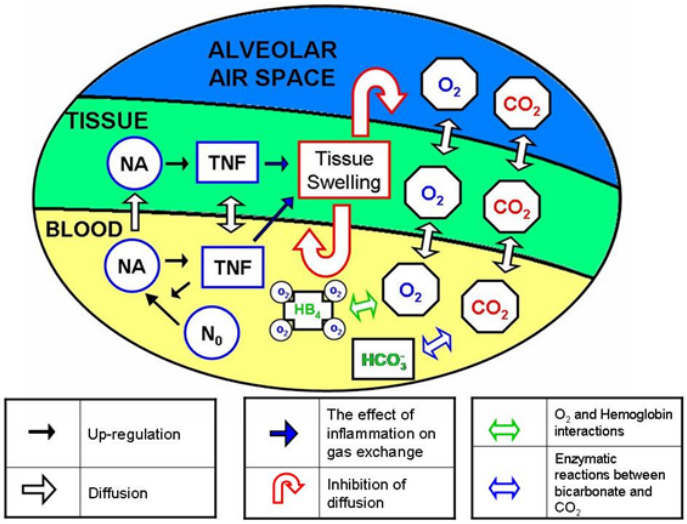

Figure 27: Interactions included within the single RU model. Resting and activated neutrophils are represented by N_0 and NA, respectively.

space. We assume alveolar air space to be well mixed. Under this assumption, variables in this compartment are functions of time only. Space along the compartment is modeled as N units of equal length and variables are modeled on each unit. Therefore, the variable names are oxygen/carbon dioxide in blood on unit i, G_{Bi}/C_{Bi}, in the tissue on unit i, G_{Ti}/C_{Ti}, and in the alveolar air space, G_A/C_A with $i = 1,..N$. For our simulation we have set $N = 20$. Oxyhemoglobin and bicarbonate on unit i, are Hb_{4i} and HCO_{3i}^-, respectively. After developing the gas exchange subsystem, we will derive the immune variables based on their known interactions and effects on gas exchange.

4.2.2 Diffusion

Diffusion, the exchange of molecules and cells across both the alveolar air space/tissue and tissue/blood barriers, is the only form of interaction between the compartments. Previous models for gas exchange depict diffusion as movement from the alveolar space to the blood across a tissue barrier ([7], [28], [36]). However, we consider lung tissue as a compartment, not merely a barrier. We have chosen this approach to better reflect the impact of tissue volume changes caused by inflammation on gas exchange between air and blood. In order

to properly model the effects of inflammation, we derive terms for diffusion driven by PO_2 and PCO_2 gradients across each barrier, tissue/blood and air/tissue.

Gas diffusion across the tissue/blood barrier is described in equations (4.1)-(4.3). Model parameters are described in Tables 13-19. The σ_j^Gparameters scale partial pressure to molar concentration, for example, $[O_2]_j = \sigma_j^G PO_2 = \sigma_j^G G_j$ in compartment j. The parameters expressing diffusion rates from compartments j to k are of the form D_{jk}^G. The volumes of each compartment, blood, tissue, and alveolar air space, are represented by V_{B0}, V_{T0}, and V_{A0}, respectively. Note that, $D_{TB}^G(G_{Ti} - G_{Bi})/N$ expresses the number of oxygen molecules diffusing from tissue to blood per second on the i^{th} unit of space. Division of this type of term by the compartmental volume in that space unit, for example V_{B0}/N, and σ on a given compartment yields the change in partial pressure in that compartment due to diffusion on a given space unit along the capillary.

Diffusion across the tissue/air barrier is more complex because the alveolar air space compartment is assumed to be well mixed while the tissue compartment is not. As in the above derivation, $D_{TA}^G(G_{Ti} - G_A)/N$ is the number of molecules that will diffuse from air to tissue per second on each unit of space. In the tissue compartment this term is multiplied by negative one and divided by $\frac{V_{T0}}{N}$ and σ_T^G. This then simplifies to the second term of equation (4.2). For the air equation, equation (4.3), one sums over all units to account for exchange with each unit of the tissue and then divides by V_{A0}.

$$\frac{dG_{Bi}}{dt} = \frac{D_{TB}^G(G_{Ti} - G_{Bi})}{\sigma_B^G V_{B0}} \tag{4.1}$$

$$\frac{dG_{Ti}}{dt} = \frac{D_{TB}^G(G_{Bi} - G_{Ti})}{\sigma_T^G V_{T0}} + \frac{D_{TA}^G(G_A - G_{Ti})}{\sigma_T^G V_{T0}} \tag{4.2}$$

$$\frac{dG_A}{dt} = \frac{D_{TA}^G}{\sigma_A^G V_{A0} N} \sum_{i=1}^{N} (G_{Ti} - G_A) \tag{4.3}$$

4.2.3 Blood/O_2

As blood traverses the capillary through a RU, oxygen diffuses into the blood and reacts with hemoglobin in the blood. Rather than accounting for the full dynamics of all four oxygen binding sites on hemoglobin tetramers, we consider hemoglobin as being either partially saturated (Hb_m) or fully saturated (Hb_4), where m is a Hill factor derived empirically from

the oxyhemoglobin dissociation curve ([36]). We refer to Hb_m as unsaturated hemoglobin. Oxygen binds to Hb_m to form Hb_4 at the rate k^+ and it detaches at the rate k^- from Hb_4, to return to Hb_m. The reaction between unsaturated and saturated hemoglobin and oxygen is modeled by equations (4.4)-(4.6).

$$\frac{dHb_m}{dt} = -k^+ Hb_m G_B^m + k^- Hb_4 \tag{4.4}$$

$$\frac{dHb_4}{dt} = k^+ Hb_m G_B^m - k^- Hb_4 \tag{4.5}$$

$$\frac{dG_B}{dt} = \frac{D_{TB}^G (G_T - G_B)}{\sigma_B^G V_{B0}} + m \frac{-k^+ Hb_m G_B^m + k^- Hb_4}{\sigma_B^G} \tag{4.6}$$

Total concentration hemoglobin, T_{Hb}, is conserved. Thus, Hb_m can be replaced with $T_{Hb} - Hb_4$. Therefore, equations (4.4)-(4.6) reduce to equations (4.7) and 4.8, with $\frac{d}{dt} T_{Hb} = 0$.

$$\frac{dHb_4}{dt} = k^+ (T_{Hb} - Hb_4) G_B^m - k^- Hb_4 \tag{4.7}$$

$$\frac{dG_B}{dt} = \frac{D_{TB}^G (G_T - G_B)}{\sigma_B^G V_{B0}} + m \frac{-k^+ (T_{Hb} - Hb_4) G_B^m + k^- Hb_4}{\sigma_B^G} \tag{4.8}$$

The temporal dynamics are much faster than the spatial dynamics. We therefore assume quasi steady state for the saturated hemoglobin to determine parameter values. This is necessary to develop an equation for percent saturation of hemoglobin that is dependent on G_B only. Percent saturation of hemoglobin is an increasing sigmoid function of the partial pressure of oxygen. Using the data for this curve we find that $m = 3.6$ and $R_H = \frac{k^-}{k^+} = 177916$ [30]. Incorporating flow of these molecules in the blood and the diffusion terms described earlier yields equations (4.9)-(4.10). Speed of blood (cm/s) is represented by v_0. This subsystem now includes both the spatial and temporal dynamics for O_2 in the blood.

$$\frac{\partial Hb_4}{\partial t} = k^+ (T_{Hb} - Hb_4) G_B^m - k^- Hb_4 - v_0 \frac{\partial Hb_4}{\partial x} \tag{4.9}$$

$$\frac{\partial G_B}{\partial t} = \frac{D_{TB}^G (G_T - G_B)}{\sigma_B^G V_{B0}} + m \frac{-k^+ (T_{Hb} - Hb_4) G_B^m + k^- Hb_4}{\sigma_B^G} - v_0 \frac{\partial G_B}{\partial x} \tag{4.10}$$

4.2.4 Blood/CO_2

As dissolved CO_2 and bicarbonate traverse the RU, bicarbonate releases CO_2 into the blood stream. This occurs by a catalyzed enzymatic reaction in which bicarbonate is the substrate. The reverse reaction is of the same type, however, with CO_2 as the substrate [10]. These reactions are modeled by the first two terms of Equation (4.11)-(4.12).

These terms are Michaelis-Menten type where the k_{cat} parameters represent the maximum rate of the catalytic reaction and k_m is the Michaelis constant, the level of the substrate for which the reaction occurs at half k_{cat}. C_B is the PCO_2, hence the substrate in terms of the equation variables is $\sigma_B^C C_B$, the concentration of CO_2. Finally, we incorporate blood flow and diffusion between tissue and blood in this subsystem as done previously for O_2 in the blood. Therefore, the CO_2/bicarbonate subsystem in the blood including temporal and spatial dynamics is described by equations (4.11) and (4.11).

$$\frac{\partial HCO_3^-}{\partial t} = k_{catCB}\frac{\sigma_B^C C_B}{k_{mCB}+\sigma_B^C C_B} - kc_{atHC}\frac{HCO_3^-}{k_{mHC}+HCO_3^-} - v_0\frac{\partial}{\partial x}HCO_3^- \quad (4.11)$$

$$\frac{\partial C_B}{\partial t} = \frac{1}{\sigma_B^C}\left(kc_{atHC}\frac{HCO_3^-}{k_{mHC}+HCO_3^-} - k_{catCB}\frac{\sigma_B^C C_B}{k_{mCB}+\sigma_B^C C_B}\right) - v_0\frac{\partial}{\partial x}C_B \quad (4.12)$$

4.2.5 Tissue/O_2 & CO_2

Within tissue, the only additional interaction modeled is the diffusion of gas molecules, expressed by the reaction-diffusion equations (4.13)-(4.14).

$$\frac{\partial G_T}{\partial t} = \frac{D_{TB}^G(G_B-G_T)}{\sigma_T^G V_{T0}} + \frac{D_{TA}^G(G_A-G_T)}{\sigma_T^G V_{T0}} - D_{GT}\frac{\partial^2 G_T}{\partial x^2} \quad (4.13)$$

$$\frac{\partial C_T}{\partial t} = \frac{D_{TB}^C(C_B-C_{Ti})}{\sigma_T^C V_{T0}} + \frac{D_{TA}^C(C_A-C_T)}{\sigma_T^G V_{T0}} - D_{CT}\nabla_i^2\frac{\partial^2 C_T}{\partial x^2} \quad (4.14)$$

4.2.6 Air/O_2 & CO_2

An average healthy human breathes about 15 times a minute with an inhalation:expiration time ratio of 1:3. We assumed a total tidal breath of 500 ml, with 150 ml of dead space ventilation, yielding an effective alveolar ventilation of 350 ml per breath, with residual total alveolar volume at the end of expiration 2300 ml [27]. This corresponds to an influx of

$2.92\text{x}10^{-5}$ ml of new gas per RU per breath, termed V_{C0}, and an end expiration (residual) volume of $1.92\text{x}10^{-4}$ ml per RU (V_{Amin0}). In order to develop equations for the changes in partial pressures of O_2 and CO_2 in alveolar gas, we first derive equations for the change in alveolar volume on a RU, equations (4.15)-(4.17).

$$s_h(t) = \frac{1}{1+e^{-\sigma(t_{in}-\text{mod}(t,t_{in}+t_{out}))}} \tag{4.15}$$

$$\frac{dy}{dt} = \frac{V_{C0}s_h(t)}{\tau_1} - \frac{y}{\tau_2} \tag{4.16}$$

$$V_{A0}(y) = V_{A\min 0} + y \tag{4.17}$$

The variable y in equation (4.16) is a measure of the alveolar volume change. During inspiration there is growth in y and it decays during expiration. In order to model the increase and decrease in y we use a smoothed Heaviside function, $s_h(t)$. This function appears in the growth term and is approximately one during inspiration and zero during expiration, see equation (4.15). The length of inspiration is $t_{in} = 1$ second and length of expiration is $t_{out} = 3$ seconds. The parameter, σ, controls the abruptness of the function's switch from one to zero. For our calculation we set σ to 20. Increasing this would increase the abruptness of the change. The τ's are chosen such that in t_{in} seconds y reaches V_{C0} and decays to zero in t_{out} seconds. Therefore, the equation of alveolar air volume, equation (4.17), is V_{Amin0} at end of expiration and $V_{Amin0} + V_{C0}$ at the end of inspiration.

We are now ready to model the change in alveolar air space partial pressures of O_2 and CO_2. We will refer to the partial pressure of the O_2 and CO_2 in the air as G_{air} and C_{air}, respectively. Under normal conditions G_{air} is 150 mmHg and C_{air} is 0 mmHg [27]. In order to properly model the changes in partial pressure, we track the changes in number of molecules and convert to a partial pressure change as we did with diffusion between compartments. The number of oxygen molecules in the alveolar space is the concentration of O_2 times the volume in the alveolar space, $\text{V}_{A0}[\text{O}_2]$. During inspiration the change in number of molecules due to breathing, not diffusion, is from the intake of external air. Therefore, we set the derivative of number of O_2 molecules in the alveolar air space equal to the derivative of to the number of molecules in the inspired air, which results in the equation:

$$\frac{d}{dt}(V_{A0}(y)[O_2]) = \frac{d}{dt}(y[O_2]_{air}).$$

We applied the product rule to both sides of this equation to get:

$$V_{A0}(y)\frac{d}{dt}[O_2] + \frac{d}{dt}(V_{A0}(y))[O_2] = \left(\frac{d}{dt}y\right)[O_2]_{air} + y\frac{d}{dt}[O_2]_{air}.$$

We assumed that there is no change in outside air concentration and solved for $\frac{d}{dt}[O_2]$, which resulted in:

$$\frac{d}{dt}[O_2] = \frac{\left(\frac{d}{dt}y\right)[O_2]_{air} - \frac{d}{dt}(V_{A0}(y))[O_2]}{V_{A0}(y)}.$$

Taking the derivative of equation (4.17) we see that $\frac{d}{dt}V_{A0}(y) = \frac{d}{dt}y$. Therefore the above equation simplifies to:

$$\frac{d}{dt}[O_2] = \frac{\left(\frac{d}{dt}y\right)([O_2]_{air} - [O_2])}{V_{A0}(y)}.$$

Letting $R = \frac{1}{V_{A0}(y)}\frac{d}{dt}y$ through by σ_A we derive for the partial pressure for oxygen in the alveolar air space:

$$\frac{d}{dt}G_A = (G_{air}(t) - G_A)R. \tag{4.18}$$

During expiration we assume that the air within the RU is well mixed; therefore all expired air has the same concentration. With this assumption there is no change in concentration and therefore pressure during expiration. Including diffusion, we model changes in alveolar PO_2 during breathing by equation (4.19). The equation for CO_2 has the same form.

$$\frac{dG_A}{dt} = \frac{D_{TA}^G}{\sigma_A^G V_{A0}}\sum_{i=1}^{N}(G_{Ti} - G_A) + \begin{Bmatrix}\text{Inspiration} & (G_{air}(t) - G_A)R \\ \text{Expiration} & 0\end{Bmatrix} \tag{4.19}$$

4.2.7 Immune subsystem

We use a simple model of the inflammatory response which includes TNF and neutrophils ([1], [53]). TNF activates circulating neutrophils in the blood. Once activated, neutrophils can diffuse into the tissue via migration. Migration or trafficking is the process where neutrophils diffuse into tissue which has elevated levels of inflammatory factors. These inflammatory factors cause a transformation of the tissue layer such that activated circulating neutrophils adhere to the tissue and diffuse locally.

Since we are considering a simple immune response that does not include macrophages or a damage variables, we created a positive feedback loop in the pro-inflammatory response by having activated neutrophils in both the blood and tissue produce TNF. We made this assumption despite the fact that TNF production is mostly due to macrophages in order to keep this immune subsystem as simple as possible. This pro-inflammatory feedback exist in our compartmental model, but it is via the variable RAD.

In this immune subsystem model TNF diffuses between the tissue and blood barrier by passive diffusion. Inflammation is a function of many factors not included in this model which sustain inflammatory effects even after the levels of TNF and activated neutrophils have dropped. Therefore we incorporate into our model a differential equation which tracks the overall level of inflammation. The growth of inflammation is dependent on TNF levels. However, it decays at a slower rate than TNF.

We model these biological interactions with equations (4.20)-(4.24). This subsystem consists of equations for TNF in the blood, TNF_B, and activated neutrophils on each unit of the blood, NA_{Bi}, and for both TNF and activated neutrophils on each unit of the tissue compartment, TNF_i and NA_i. Note that unlike other variables in this subsystem TNF_B is not a function of space, since it is well mixed in the blood. The inflammation variable is a function of space and time. It is a measure of the local tissue inflammation and is represented

by Z_i.

$$\begin{aligned}
\frac{dTNF_B}{dt} &= -\mu_{TB}TNF_B - \frac{\alpha N_0 TNF_B^2}{1+\varepsilon TNF_B^2} + \frac{\sum_{i=1}^{N} r_p(Z_i)(TNF_i - TNF_B)}{NV_{B0}} \\
&\quad +\gamma \sum_{i=1}^{N} NA_{Bi} \qquad (4.20)\\
\frac{dNA_{Bi}}{dt} &= -\mu_{NB}NA_{Bi} + \frac{\beta N_0 TNF_B^2}{1+\varepsilon TNF_B^2} - \frac{r_v(Z_i)N^*_{Bi}}{V_{B0}} - v_0\nabla_i NA_{Bi} \qquad (4.21)\\
\frac{dTNF_i}{dt} &= -\mu_T TNF_i + \frac{r_p(Z_i)(TNF_B - TNF_i)}{V_{T0}} + \gamma NA_i + D_T\nabla_i^2 TNF_i \qquad (4.22)\\
\frac{dNA_i}{dt} &= -\mu_N NA_i + \frac{r_v(Z_i)NA_{Bi}}{V_{T0}} - \chi\nabla_i(NA_i\nabla_i TNF_i) \qquad (4.23)\\
\frac{dZ_i}{dt} &= -\mu_z Z_i + \frac{k_{zg}(TNF_i + TNF_B)^2}{k_{tz}^2 + (TNF_i + TNF_B)^2}(1 - Z_i) \qquad (4.24)\\
\text{Where } r_p(x) &= m_p x + b\\
r_v(x) &= \frac{x^q}{k^q + x^q}
\end{aligned}$$

The first term of all equations models decay of the variable. The second terms of equations (4.20) and (4.21) model the activation of resting neutrophils by TNF in the blood. This reaction is modeled by a Hill type equation with a Hill coefficient of two. This nonlinearity models the need for multiple TNF molecules to activate a neutrophil. A similar term appears as the second term of the TNF_B equation because TNF is consumed during this process. The third term in equations (4.20)-(4.21) and the second terms of equations (4.22)-(4.23) model diffusion. These terms do not have the same form because the mechanisms by which neutrophils and TNF diffuse during an infection are different. Neutrophils diffuse by migration and this is dependent on local inflammation. Once inflammation has accumulated locally there are significant changes in activated neutrophil diffusion, however these effects saturate for higher levels of inflammation, hence there is a maximum rate for the diffusion of neutrophils. Due to these properties of neutrophil diffusion we model this with a Hill type function, $r_v(Z_i)$. Note that resting neutrophils are assumed not to diffuse; therefore, there is no activation of neutrophils within the tissue. Also, once an activated neutrophil diffuses into to the tissue we assume that it does not diffuse back into the blood. TNF diffusion is increased during an infection because tissue becomes more porous to all small molecules.

We take this dependence to be linear and is model with the function $r_p(Z_i)$. Diffusion for both TNF and activated neutrophils are modeled as with the gas molecules with the $r_v(Z_i)$ or $r_p(Z_i)$ taking the role of the diffusion constant.

The final term in equation (4.20) is the production of TNF from activated neutrophils. This sum is an numerical estimate for the integral $\gamma \int_0^L NA_{Bi}(x,t)dx$. This integral accounts for TNF produced by the activated neutrophils throughout the blood compartment. We denote the length of the capillary with L. The final term of equation (4.21) is flow of neutrophils in the blood. The final term of the equation (4.23), represents chemotaxis of tissue neutrophils towards TNF. The final two terms of the tissue TNF equation, equation (4.22), are production from neutrophils and diffusion of TNF within the tissue compartment.

We model the local inflammation with equation (4.24), which consists of two terms, growth and decay. The growth of inflammation is dependent on the local and blood TNF. We model this dependence using a Hill type function. This nonlinearity is used since there must be substantial levels of TNF in the tissue to trigger inflammatory changes and the growth rate of inflammation saturates. The decay term depends on the level of inflammation. Note that the inflammation variable has a maximum value of 1, which corresponds to tissue being severely inflamed.

4.2.8 Full single RU model: Effects of inflammation on gas exchange.

During an inflammatory response there is swelling of the tissue layer. The tissue swells into both the alveolar air space and capillary space. Additionally, inflammation decreases the tidal volume inspired during a breath cycle and increases blood velocity such that constant flow is maintained. In our model we take into account these volume changes and the effects on V_{C0} and v_0. To do this we replace, V_{B0}, V_{T0}, V_{Amin0} and v_0 with V_B, V_T, V_{Amin}, and v respectively. V_B, V_T, and V_{Amin} are functions of the average of the local inflammation variables, $\overline{Z}_i$. V_B is a sigmoidal function that decreases as $\overline{Z}_i$ increases and has maximum V_{B0}, equation (4.25). V_{Amin} is a similar shaped function, but with a maximum of V_{Amin0}, and it a tracks the minimum of the alveolar air space (volume at the end expiration), equation (4.27). As increases the amount volume lost from the blood and alveolar air space is added to the volume

of the tissue giving equation (4.26). Note the parameters are set such that $m_{vta} > m_{vtb}$. This is due to the fact that it is easier for the tissue volume to expand into the alveolar air space than into the blood compartment. As the tissue volume increases this causes a decrease in the lung's ability to increase its volume during inspiration (decrease of V_C) and we model this by Equation 4.28. The velocity of blood is determined by $v = v_0 = \frac{V_{B0}}{V_B}$, in order to maintain constant blood flow during an infection.

$$V_B(\overline{Z}_i) = \frac{V_{B0}}{1 + m_{vtb}\overline{Z}_i} \tag{4.25}$$

$$V_T(\overline{Z}_i) = V_{T0} + V_{B0} - \frac{V_{B0}}{1 + m_{vtb}\overline{Z}_i} + V_{Amin0} - \frac{V_{Amin0}}{1 + m_{vta}\overline{Z}_i} \tag{4.26}$$

$$V_{Amin}(\overline{Z}_i) = \frac{V_{Amin0}}{1 + m_{vta}\overline{Z}_i} \tag{4.27}$$

$$V_c(\overline{Z}_i) = \frac{V_{c0}}{1 + m_{vtc}\overline{Z}_i} \tag{4.28}$$

Taking into account these changes due to inflammation, we have the final form of our model, Equations 4.29-4.42. Note that, we have not included feedback from the breathing subsystem onto the immune subsystem. Therefore, the immune subsystem can be simulated separately. Its output is then used as input to the gas exchange subsystem.

4.2.9 Equations and Parameters

Blood Equations

$$\frac{dG_{Bi}}{dt} = \frac{D^G_{TB}(G_{Ti} - G_{Bi})}{\sigma^G_B V_B(\overline{Z}_i)} + m\frac{-k^+(T_{Hb} - Hb_{4i})G^m_{Bi} + k^- Hb_{4i}}{\sigma^G_B} - v(\overline{Z}_i)\nabla_i G_{Bi} \tag{4.29}$$

$$\frac{dHb_{4i}}{dt} = k^+(T_{Hb} - Hb_{4i})G^m_{Bi} - k^- Hb_{4i} - v(\overline{Z}_i)\nabla_i Hb_{4i} \tag{4.30}$$

$$\text{With } k^- = R_H k^+$$

$$\frac{dC_{Bi}}{dt} = \frac{D^C_{TB}(C_{Ti}-C_{Bi})}{\sigma^C_B V_B(\overline{Z}_i)} - v(\overline{Z}_i)\nabla_i C_B + \frac{1}{\sigma^C_B}\left(kc_{atHC}\frac{HCO^-_{3i}}{k_{mHC}+HCO^-_{3i}} - k_{catCB}\frac{\sigma^C_B C_{Bi}}{k_{mCB}+\sigma^C_B C_{Bi}}\right) \quad (4.31)$$

$$\frac{dHCO^-_{3i}}{dt} = k_{catC_{Bi}}\frac{\sigma^C_B C_{Bi}}{k_{mCB}+\sigma^C_B C_{Bi}} - k_{catHC}\frac{HCO^-_{3i}}{k_{mHC}+HCO^-_{3i}} - v(\overline{Z}_i)\nabla_i HCO^-_{3i} \quad (4.32)$$

$$\frac{dTNF_B}{dt} = -\mu_{_{TB}}TNF_B - \frac{\alpha N_0 TNF_B^2}{1+\varepsilon TNF_B^2} + \frac{\sum_{i=1}^{N} r_p(Z_i)(TNF_i - TNF_B)}{NV_B(\overline{Z}_i)} + \gamma\sum_{i=1}^{N} N^*_{Bi} \quad (4.33)$$

$$\frac{dNA_{Bi}}{dt} = -\mu_{NB}NA_{Bi} + \frac{\beta N_0 TNF_B^2}{1+\varepsilon TNF_B^2} - \frac{r_v(Z_i)NA_{Bi}}{V_B(\overline{Z}_i)} - v(\overline{Z}_i)\nabla_i NA_{Bi} \quad (4.34)$$

$$V_B(\overline{Z}_i) = \frac{V_{B0}}{1+m_{vtb}\overline{Z}_i}$$

$$v(\overline{Z}_i) = v_0\frac{V_{B0}}{V_B(\overline{Z}_i)}$$

Tissue Equation

$$\frac{dG_{Ti}}{dt} = \frac{D^G_{TB}(G_{Bi}-G_{Ti})}{\sigma^G_T V_T(\overline{Z}_i)} + \frac{D^G_{TA}(G_A-G_{Ti})}{\sigma^G_T V_T(\overline{Z}_i)} - D_{_{GT}}\nabla^2_i G_{Ti} \quad (4.35)$$

$$\frac{dC_{Ti}}{dt} = \frac{D^C_{TB}(C_{Bi}-C_{Ti})}{\sigma^C_T V_T(\overline{Z}_i)} + \frac{D^C_{TA}(C_A-C_{Ti})}{\sigma^G_T V_T(\overline{Z}_i)} - D_{CT}\nabla^2_i C_{Ti} \quad (4.36)$$

$$\frac{dTNF_i}{dt} = -\mu_{_T}TNF_i + \frac{r_p(Z_i)(TNF_B - TNF_i)}{V_T(\overline{Z}_i)} + \gamma NA_i + D_T\nabla^2_i TNF_i \quad (4.37)$$

$$\frac{dNA_i}{dt} = -\mu_N NA_i + \frac{r_v(Z_i)NA_{Bi}}{V_T(\overline{Z}_i)} - \chi\nabla_i(NA_i\nabla_i TNF_i) \quad (4.38)$$

$$\frac{dZ_i}{dt} = -\mu_z Z_i + \frac{k_{zg}(TNF_i+TNF_B)^2}{k^2_{tz}+(TNF_i+TNF_B)^2}(1-Z_i) \quad (4.39)$$

$$V_T(\overline{Z}_i) = V_{T0}+V_{B0} - \frac{V_{B0}}{1+m_{vtb}\overline{Z}_i} + V_{A\min 0} - \frac{V_{A\min 0}}{1+m_{vta}\overline{Z}_i}$$

Alveolar Air Space Equations

$$\frac{dG_A}{dt} = \frac{D_{TA}^G}{\sigma_A^G V_A(y,\overline{Z_i})N}\sum_{i=1}^{N}(G_{Ti}-G_A) + \begin{Bmatrix}\text{Inspiration} & (G_{air}(t)-G_A)R\\ \text{Expiration} & 0\end{Bmatrix} \quad (4.40)$$

$$\frac{dC_A}{dt} = \frac{D_{TA}^C}{\sigma_A^C V_T(\overline{Z_i})N}\sum_{i=1}^{N}(C_{Ti}-C_A) + \begin{Bmatrix}\text{Inspiration} & (C_{air}(t)-C_A)R\\ \text{Expiration} & 0\end{Bmatrix} \quad (4.41)$$

$$\frac{dy}{dt} = \frac{V_{C0}s_h(t)}{\tau_1} - \frac{y}{\tau_2} \quad (4.42)$$

$$V_A(y,\overline{Z}_i) = V_{Amin}(\overline{Z}_i) + y$$

$$V_{Amin}(\overline{Z}_i) = \frac{V_{Amin0}}{1+m_{vta}\overline{Z_i}}$$

$$V_c(\overline{Z}_i) = \frac{V_{c0}}{1+m_{vtc}\overline{Z_i}}$$

$$s_h(t) = \frac{1}{1+e^{-\sigma(t_{in}-mod(t,t_{in}+t_{out})}}$$

$$R = \frac{1}{V_{A0}(y,\overline{Z_i})}\frac{d}{dt}y$$

Diffusion Function

$$r_p(x) = m_p x + b$$

$$r_v(x) = \frac{k_v^q}{k^q + x^q}$$

Explanations of parameter values are given in the parameter tables, Table 13-19. Most gas exchange parameters are experimentally well characterized. Remaining parameters were chosen to reproduce known biological behaviors of model subsystems. Parameterization of the gas exchange subsystem was such that hemoglobin and oxygen dynamics stabilize in the first third of the capillary while bicarbonate and carbon dioxide reactions stabilize in the first tenth of the capillary [27]. For the immune subsystem we documented many parameter values from literature and the remaining were estimated ([18], [58]).

Param.	Value	Description	Comments
L	0.22 cm	Length of RU along the capillary	Estimated by assuming that an individual alveolus diameter is 0.02 cm and that as the blood traverses the lung it is in contact with half of the circumference of seven alveoli [27].
H	$L/20$=0.011cm	Length of each unit of space along the capillary	We use 20 spatial units in our calculations
t_{in}	1 second	Length of inspiration	Total time for breathing cycle is assumed to be 4 seconds, 15 breaths per minute. The inhalation time is one forth of the total time.
t_{out}	3 seconds	Length of expiration	See above comment for t_{in}.
v	0.2932 cm/s	Speed of blood	We estimated the range for v, 0.01788-0.4398 cm/sec, by assuming transient times for blood between 0.5 to 12.3 seconds with the capillary length calculated above. We took 0.75 seconds to be our transient time under normal conditions [61].
G_{B0}	40 mmHg	Arterial partial pressure of oxygen	[27]
C_{B0}	45 mmHg	Arterial partial pressure of carbon dioxide	[27]
g_{air}	150 mmHg	Partial pressue of oxygen in the air	[27]
c_{air}	0 mmHg	Partial pressue of carbon dioxide in the air	[27]

Table 13: Table of parameters for the single RU model

Param.	Value	Description	Comments
iHb_4	0.001717 M	Arterial concentration of saturated hemoglobin	Found by fitting our oxyhemoglobin curve such that hemoglobin is 50% saturated at a PO_2 of 27 mmHg and 99% saturated at a PO_2 of 100 mmHg and assuming G_{B0} is 40 mmHg [36].
$iHCO_3^-$	0.024M	Arterial concentration of bicarbonate	[27]
D_{TB}^G	6.75×10^{-12} L/s	Rate constant for the diffusion of oxygen between tissue and blood.	
D_{TA}^G	2.36×10^{-12} L/s	Rate constant for the diffusion of oxygen between tissue and air.	
D_{TB}^C	8.48×10^{-11} L/s	Rate constant for the diffusion of carbon dioxide between tissue and blood.	
D_{TA}^C	7.63×10^{-10} L/s	Rate constant for the diffusion of carbon dioxide between tissue and air.	
$\sigma_B^G = \sigma_T^G$	1.24×10^{-6} M/mmHg	$[O_2]=\sigma_B^G PO_2$ in the blood/ $[O_2]=\sigma_T^G PO_2$ in the tissue.	Calculated from the solubility coefficient for oxygen in water [27].
σ_A^G	5.2×10^{-5} M/mmHg	$[O_2]=\sigma_A^G PO_2$ in the air	Calculated from $nRT = PV$

Table 14: Table of parameters for the single RU model continued

Param.	Value	Description	Comments
$\sigma_B^C = \sigma_T^C$	2.95×10^{-5} M/mmHg	$[CO_2]$=$\sigma_B^C PCO_2$ in the blood/ $[CO_2]$= $\sigma_T^C PCO_2$ in the tissue.	
σ_A^C	5.2×10^{-5} M/mmHg	$[PO_2]$= $\sigma_A^C PCO_2$ in the air	
$Numalv$	1.2×10^{7}	Number of RU's in the lung.	Calculated assuming that there are 3×10^8 alveoli in the lung and that each RU consists of 25 alveoli [27].
V_{B0}	$90\text{mL}/Numalv = 7.5\times10^{-9}$	Blood volume: blood volume in the capillaries of a RU under normal conditions.	There is between 70-140ml of blood in the lung capillaries. For our simulations, we assume under normal condition that the blood volume is 90ml [36].
V_{T0}	$500\text{mL}/Numalv = 4.17\times10^{-8}$	Tissue Volume: tissue volume in a RU under normal conditions.	Calculated assuming that there is 500 ml of tissue in the lung .
V_{A0}	$2300\text{mL}/Numalv = 1.92\times10^{-7}$	Minimum of the alveolar air space: volume of the alveolar air space in a RU at the end of expiration under normal conditions.	Calculated assuming that the minimum volume in the lung is 2300ml [27].
V_{C0}	$350\text{mL}/Numalv = 2.9\times10^{-8}$	Tidal volume: the volume inhaled into a RU during a breath under normal conditions.	Calculated assuming that the tidal volume for the whole lung was 350ml [27].

Table 15: Table of parameters for the single RU model continued

Param.	Value	Description	Comments
$R_H = k^-/k^+$	177916	Ratio of the reverse and forward reaction rates for the saturation of hemoglobin.	This ratio was found by fitting the oxyhemoglobin saturation curve as described for iHB_4 [36].
m	3.6	Number of oxygen molecules need to bind to Hb_m to form Hb_4.	This parameter was found by fitting the oxyhemoglobin saturation curve as described for iHB_4 [36].
k^+	0.0005/s	Rate at which m oxygen molecules bind to Hb_m to form Hb_4.	This parameter was chosen to ensure the hemoglobin and oxygen dynamics stabilize in first third of the capillary [27].
T_{Hb}	0.00224 M	Concentration of total hemoglobin, both Hb_4 and Hb_m.	Whole blood from contains from 14-16 g/dl of hemoglobin. We assumed 15g/dl for our calculations of the total concentration [27].
k_{catCB}	1×10^6/s	Maximum rate of the enzymatic reaction with CO_2 as the substrate.	Fit such that the carbon dioxide and bicarbonate dynamics stabilize in the first tenth of the capillary ([10],[27])
k_{mCB}	0.013 M	Michaelis-Menten Constant, concentration were the reaction occurs at half the maximum rate, for the enzymatic reaction with CO_2 as the substrate.	See comment for k_{catCB}
k_{catHC}	2.18×10^5/s	Maximum rate of the enzymatic reaction with HCO_3^- as the substrate.	See comment for k_{catCB}

Table 16: Table of parameters for the single RU model continued

Param.	Value	Description	Comments
k_{mHC}	0.026 M	Michaelis-Menten Constant, concentration were reaction occurs at half the maximum rate, for the enzymatic reaction with HCO_3^- as the substrate.	See comment for k_{catCB}
D_{GT}	3.24×10^{-5}cm^2/s	The diffusion constant for diffusion of oxygen within the tissue.	
D_{CT}	0.00065 cm^2/s	The diffusion constant for diffusion of carbon dioxide within the tissue.	Diffusion of carbon dioxide is 20 times faster than that of oxygen ([10], [27])
σ	20	This parameter determines the rise in $sh(t)$ our approximation to the Heaviside function.	Increasing this parameter sharpens the rise in $sh(t)$.
τ_1	0.5/s	Time constant for inspiration.	Chosen so that V_{C0} is inhaled in t_{in} seconds.
τ_2	0.7/s	Time constant for expiration.	Chosen so that V_{C0} is exhaled in t_{out} seconds.
μ_{TB}	1.8/s	Decay rate of TNF in the blood.	See comment for k_{catCB}
α	8 /s/TNF units/N units	Rate at which TNF are depleted as neutrophils are activated.	See comment for k_{catCB}

Table 17: Table of parameters for the single RU model continued

Param.	Value	Description	Comments
N_0	1.2 N units	Amount resting neutrophils available for activation.	
ε	1/ (TNF units)^2	Determines level at which the activation term reaches half its maximum rate.	
m_p	1×10^{-5}	Slope of the linear function of z modeling the change of the diffusion rate for TNF.	
B	0.001	Y-intercept of the linear function of z modeling the change in the diffusion rate for TNF.	
γ	3 TNF units/s/N units	Production rate of the TNF from neutrophils	
μ_{NB}	0.05/s	Rate of at which neutrophils are produced.	Decay of activated neutrophils is faster in the blood than in tissue.
k_v	12/s/TNF units	Maximum diffusion rate for activated neutrophils	
k	8 /s/TNF units/N units	Determines the level of average inflammation at which the rate of neutrophil activation is half its maximum.	
μ_T	1.8/s	Decay rate of TNF in the tissue.	TNF in tissue decays slower than TNF in the blood.

Table 18: Table of parameters for the single RU model continued

Param.	Value	Description
μ_N	0.05/s	Decay rate of neutrophil within the tissue.
χ	1 cm^2/TNF units/s	Chemotaxis constant for neutrophils.
μ_z	0.008/s	Decay rate of inflammation.
kzg	0.1 Z units/s	Growth rate of inflammation
k_{tz}	2 TNF units	Determines level of TNF at which the growth rate of inflammation reaches half its maximum.
m_{vtb}	0.4/z units	Determines the effect of inflammation on the swelling of tissue volume into the blood compartment.
m_{vta}	1/z units	Determines the effect of inflammation on the swelling of tissue volume into the blood compartment.
closing	10/z units	Determines the effect of inflammation on the swelling of tissue volume into the alveolar air space.
μ_T	1.8/s	Determines the effect of inflammation on the decrease of tidal volume.

Table 19: Table of parameters for the single RU model continued

4.2.10 Full Lung Model

We next linked the output of multiple RUs under various physiological conditions by the method presented in Figure 28. We assumed that initial compartmental volumes were uniform across RUs. Therefore, all blood variable concentrations at the arterial end and initial compartmental volumes, V_{T0}, V_{B0}, and $V_{A\min 0}$, are the same on each RU. The insult is assumed to start in the blood via TNF. So, the initial level of TNF_B is the same on RUs. We introduced heterogeneity by ranging ventilation/perfusion ratios from 0.31 to 1.15, following a truncated normal distribution N˜(0.73, 0.4). This was achieved by ranging tidal ventilation from 150 ml and 550 ml using N˜(350 ml, 104 ml^2), while holding perfusion constant (480 ml/breath cycle). Ventilation/perfusion ratios refers to the ratio of the change in ventilation to the change in perfusion. Here we alter this ratio on individual RUs in the full lung model by altering ventilation.

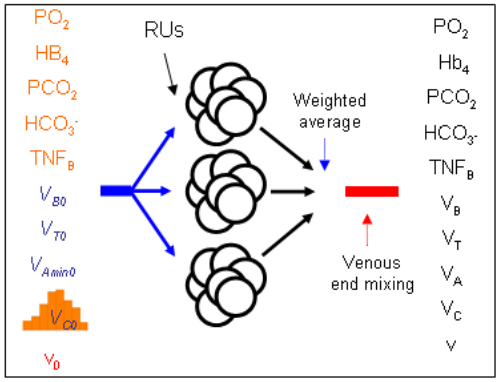

Figure 28: Model schematics for the linking of multiple RUs to create a full lung model. The first column represents entering variable concentrations and partial pressures (orange), initial comparmental and tidal volumes (blue) and blood speed (red) at the onset of inflammation. All of these are the same on all RUs except for the initial tidal volume, V_{C0}. V_{C0} of the RUs were determined by a normal truncated distribution. Simulation are run for the various RUs recording data for both the immune and gas exchange subsystems. A weighted average dependent on the distribution is taken of the blood variables at the venous end. This weighted average is used as the intial conditions for an ODE system that model venous end mixing. The results of this mixing are the output of the full model.

Simulations were run on RU with the local venous partial pressures and concentrations determined by the local inflammation within the RU. Then, at the venous end, mixing of the blood exiting the RUs is accounted for by the system of ODEs, equations (4.43) and (4.44), which include the dynamics between hemoglobin and oxygen. Initial conditions for G_B are

calculated by averaging venous blood PO_2 level from each RU. Initial Hb_4 concentration is calculated by determining the percent saturation of pooled blood. The system, including equations (4.45) and (4.46), is simulated to steady state, yielding mixed PO_2, PCO_2 , HB_4 and HCO_3^-, the outputs of the multiscale full lung model.

$$\frac{dG_B}{dt} = m\frac{-k^+(T_{Hb} - Hb_4)G_B^m + k^- Hb_4}{\sigma_B^G} \tag{4.43}$$

$$\frac{dHb_4}{dt} = k^+(T_{Hb} - Hb_4)G_B^m - k^- Hb_4 \tag{4.44}$$

$$\frac{dC_B}{dt} = \frac{1}{\sigma_B^C}\left(kc_{atHC}\frac{HCO_3^-}{k_{mHC} + HCO_3^-} - k_{catCB}\frac{\sigma_B^C C_B}{k_{mCB} + \sigma_B^C C_B}\right) \tag{4.45}$$

$$\frac{dHCO_3^-}{dt} = k_{catC_B}\frac{\sigma_B^C C_B}{k_{mCB} + \sigma_B^C C_B} - k_{catHC}\frac{HCO_3^-}{k_{mHC} + HCO_3^-} \tag{4.46}$$

4.2.11 Implementing Shunting

In severely inflamed alveoli, fluid accumulates in air space and surfactant production is compromised, resulting in increased surface tension in the alveolar wall, leading to alveolar closure. Thus, supply of fresh alveolar air to the tissue is eliminated. In order to model this effect, the diffusion rate between the air and tissue compartments is set to zero when tidal volume falls below 140 ml, with all other dynamics remaining the same. We refer to this critical value as the alveolar closure threshold. Once this tidal volume falls below this threshold for the remainder of the simulation there are only interactions between the tissue and blood compartments. In our modeling of shunting we have not included a recovery mechanism.

4.3 RESULTS

4.3.1 Gas exchange during tidal breathing

Simulations of equations (4.29)-(4.39) in the absence of inflammation models gas exchange during health and give results similar to those observed experimentally [27]. PO_2 in the blood increases from 40 mmHg at the pulmonary arterial end (G_{B0}) to 101.7 mmHg at the

pulmonary venous end (G_{B20}) as blood crosses the capillary, which is similar to the levels seen in the tissue compartment (Figure 29A, B). Hb_4 becomes saturated in the first third of the capillary, Figure 29C. The oscillations arise in Figure 29(A, B, C) due to varying PO_2 levels in the alveolar air space during breathing. PO_2 levels in alveolar air space oscillates between 96.2 and 101.7 mmHg during the four-second breath cycle, see Figure 29D.

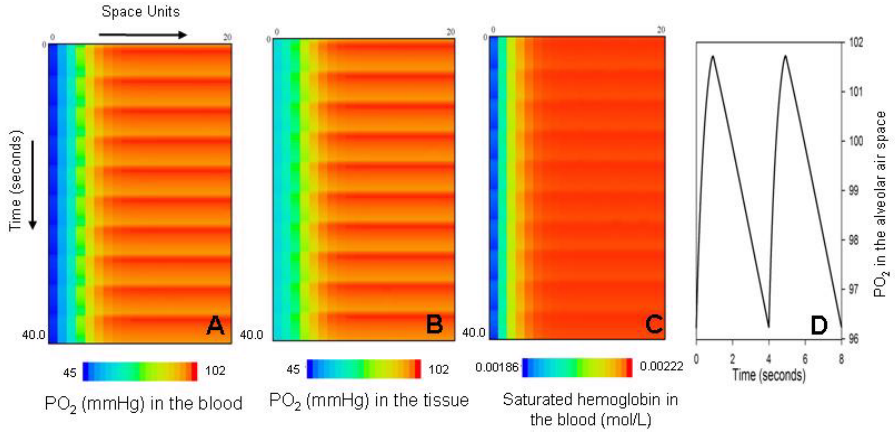

Figure 29: Tissue, blood, and air oxygen and saturated hemoglobin levels under normal conditions. A. PO_2 (mmHg) levels in blood. Zero on the X-axis represents the pulmonary arterial end of the capillary, while, moving right in space, 20 is the pulmonary venous end. Y-axis is time, therefore the columns represent the capillary PO_2 levels in a space unit as time progresses. B. PO_2 levels in the tissue with the same orientation. C. Saturated hemoglobin in the blood with the same orientation.

Blood PCO_2 drops from 45 to 40.7 mmHg as the blood transverses the capillary, see Figure 30A. Enzymatic reactions between Bicarbonate and CO_2 stabilize in the first few space units (Figure 30C). PCO_2 in the alveolar space oscillates between 40.70 and 43.16 mmHg, similar oscillations occur in the tissue, see Figures 30B, D. The oscillations of PCO_2 in the tissue occur over the entire length of the tissue unlike those of PO_2 in the tissue. This is due to the higher diffusion coefficient for carbon dioxide in the tissue. Carbon dioxide decreases during inspiration, since inspired air has a PCO_2 of zero.

4.3.2 The Immune Subsystem

The immune subsystem is bistable between health and sustained inflammation. In health, TNF_i, TNF_B, NA_i, NA_{Bi} and Z_i return to zero in all compartments. For sustained inflammation, corresponding to an outcome of death, these variables evolve to a persistently

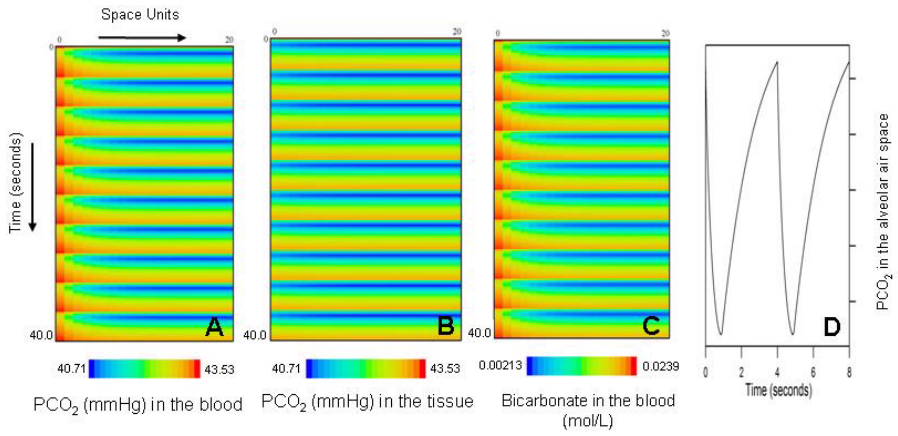

Figure 30: Tissue, blood, and air oxygen and saturated hemoglobin levels under normal conditions. A. PCO_2 (mmHg) levels in blood. Zero on the X-axis represents the pulmonary arterial end of the capillary, while, moving right in space, 20 is the pulmonary venous end. Y-axis is time, therefore the columns represent the capillary PCO_2 levels in a space unit as time progresses. B. PCO_2 levels in the tissue with the same orientation. C. Bicarbonate in the blood with the same orientation.

elevated value. Given an initial dose of TNF_B below 2.23 this immune subsystem will resolve itself to health. Above this level the outcome is death [22]. In our model, inflammation can also be triggered by initializing one of the other immune variables above its threshold for survival (data not shown).

The dynamics of this subsystem determine the volumes of the compartments and the tidal volume in the alveolar space during an inflammatory response within a RU with normal initial compartmental volumes. In Figure 31 , we display the effects of inflammation on the compartmental volumes: tissue swelling is accompanied by a corresponding reduction in other compartmental volumes. Figure 31A illustrates the volumes during an insult of $TNF_B(0) = 2$ (all other immune variables initially zero). The inflammatory response triggered by this insult resolves to health. Tissue volume is initially 0.5 L and swells to approximately 0.522 ml before returning to baseline. The alveolar airspace volume at the end of expiration is initially 2.3 ml and drops to approximately 2.228 L before returning to baseline. Blood volume was initially 0.090 L and reaches a minimum of 0.088 L before returning to baseline. The tissue swells mostly into the alveolar air space. The tidal volume has dynamics similar to those of the blood volume. It starts at 0.35 L and reaches a minimum of 0.264 L.

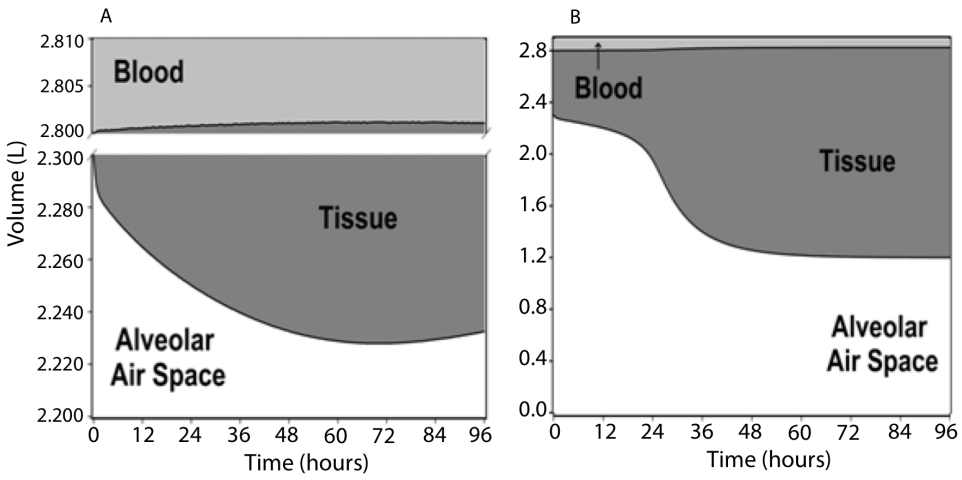

Figure 31: Compartment volumes during insults initiated in the blood. A. Initial levels of TNF in the blood (TNF_B)=2. All variables recover to a healthy outcome levels. Note that in this plot the y-axis starts are 2.2L and ends at 2.89L, the total initial unscaled lung volume, which corresponds to $\frac{2.2L}{\#\text{ of alveoli}}$ to $\frac{2.89L}{\#\text{ of alveoli}}$. B. Initial levels of TNF in the blood (TNF_B) = 4. A death state is reached, where immune variables remain elevated and lung volumes impaired. In this plot the unscaled volumes are plot from 0 to 2.89 L, , which corresponds to 0 to $\frac{2.89L}{\#\text{ of alveoli}}$.

Following a larger insult ($TNF_B(0) = 4$), the subsystem evolves to death (Figure 31B). All volumes have the same baseline volumes. Tissue volumes swells to 1.63 L, blood volume drops to 0.0658 L and alveolar air space at the end at the expiration drops to 1.2 L. Tidal volume dynamics are again similar to blood volume with minimum of 34.5 L. Velocity of the blood increases with similar dynamics to those of the tissue volume with a maximum 0.297 cm/s following the survivable challenge, and 0.400 cm/s following the lethal challenge.

4.3.3 Simulations of a Single RU

Combining both the gas exchange and immune subsystems simulates the effects of inflammation on gas exchange. During a lethal insult ($TNF_B(0) = 4$) PO_2 drops to 43.3 mmHg at the venous end, hemoglobin no longer saturates in the capillary, and PCO_2 also still drops significantly to 41.1 mmHg at the venous end. A non-lethal response ($TNF_B(0) = 2$) is accompanied by minimal changes in the gas exchange subsystem. Transients for inflammation on single units are shown in Figure 34 and will be discussed in detail in comparison to the

full lung model.

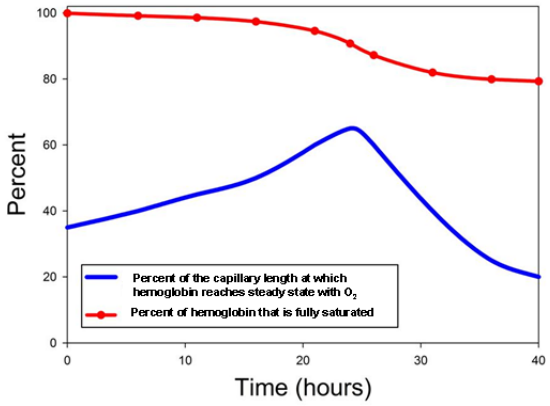

Figure 32: The effects of lethal inflammation on hemoglobin saturation. The bottom curve (blue) is the percent of the capillary transversed before saturation with hemoglobin is complete. The top curve (red-dotted) is the percent of the total hemoglobin that is fully saturated Hb_4.

In Figure 32 we see the effects of inflammation on hemoglobin during a lethal insult in the absence of shunting. At low PO_2 hemoglobin is unable to saturate with O_2. This is shown in the top curve (red-dotted) of Figure 32, which is the percent of total hemoglobin that is fully saturated, $100\frac{Hb_4}{T_{HB}}$, versus time. This curve drops significantly in the second half of the insult when the supply of O_2 is limited. In the lower curve of Figure 32 we have plotted the percent of the capillary transversed by the blood before steady state is reached between O_2 and Hb_4 versus time. Before PO_2 drops below levels at which hemoglobin saturates, the point of steady state moves further along the capillary. Once there are insufficient levels O_2 for full saturation to occur the point where steady state occur moves back along the capillary, since the limited O_2 is absorbed quickly by hemoglobin.

4.3.4 Full lung model

The time evolution of the distribution of RU volumes N˜(350 ml, 104 ml) for a lethal insult predicts that a significant proportion of RUs will reach closing volume within 12 hours and all are below closing volume by 24 hours (Figure 33) The overall structure of the distribution remains unchanged as the average decreases, but its variance decreases in time. We display

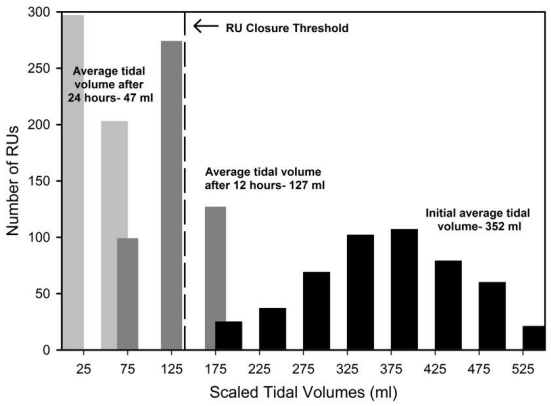

Figure 33: Distributions of the tidal volume at times 0, 12 and 24 hours. Initially, 500 RUs are normally distributed with scaled tidal volumes between 150 and 550 ml (mean = 350 ml) (black bars). After 12 hours the mean scaled volume has dropped to 127 ml (dark gray bars). At 24 hours the mean scaled tidal volume average is 47 ml (pale grey bars). The dotted vertical line at 140 ml represents the scaled tidal volume below which shunting is implemented.

predictions of venous PO_2 of the full lung, and of transients of single RU (scaled to total tidal volume) with lower limit (150 ml), mean (350 ml) and upper limit (550 ml) initial tidal volumes in Figure 34. The full lung transient is always below the transient with initial tidal volume 350 ml due to mixing of the pulmonary blood in the proximal pulmonary veins, in accordance to experimental observations [27]. As we wished to evaluate the relative impact of changes in lung volumes and shunting on gas exchange, we also displayed the prediction of a model where shunting was not implemented, confirming the major role of shunting in the rapid deterioration of gas exchange during a lethal inflammatory stimulus ([49]).

Code used for implementing the model presented here in Appendix D.

4.4 DISCUSSION

Our model for gas exchange contains an immune subsystem and explicit lung tissue layer. This model therefore is used to simulate inflammation within a respiratory unit and determine the effect of inflammation on the ability for gas exchange to occur. A variety of stimuli can trigger inflammation, including infection and activated neutrophils ([1], [21], [20]). A

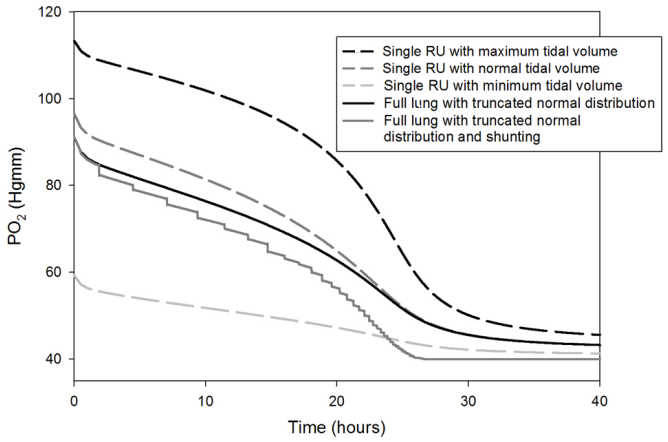

Figure 34: Transients during a lethal insult of TNF in the blood with and without shunting. The dashed lines are transient for single RU with minimum scaled tidal volume, 150 ml (gray), normal scaled tidal volume, 350 ml (dark gray), and maximum scaled tidal volume, 550 ml (black). The black, smooth curve is the transient for the full lung with the distribution shown in Figure 4 without shunting. The solid dark gray curve is the transient for full lung with shunting and the same distribution.

mild inflammatory stimulus does not result in a significant change in partial pressure for either oxygen or carbon dioxide. Larger stimuli lead to a significant reduction in partial pressure of oxygen at the pulmonary venous end, and therefore systemic arterial circulation. This effect is driven by (1) impaired gas diffusion caused by tissue swelling, (2) closure of alveoli below a critical respiratory unit volume, and (3) oxygen remixing in the pulmonary veins.

This model is the first to incorporate a tissue layer allowing the explicit stimulation of immune effector cells or molecular mediators. Other mathematical models of the lung have concentrated on lung mechanics, pulmonary circulation [72], gas exchange with the tissue layer treated as a barrier ([7], [29], [28]), airway mechanics [39], and drug deposition in the tracheo-bronchial tree ([77],[37]). With the exception of mycobacterial granuloma formation modeling ([40], [41]), attempts at mathematical simulation of lung injury have been sparse, although pulmonary immunity and injury are of immense clinical interest and relevance. Immune-mediated lung injury has typically only been approached with experimental models. These experiments include both insults from the blood and those directly introduced into the lung in the form of lipopolysaccharide instillation, chemical injury, and pathogen

deposition ([8], [21]). Although our primary goal was to model pulmonary response to a systemic challenge, our model could capture these different modes of local injury, once RUs are explicitly linked. We have built a road map to achieve this goal. The PDE formulation of the RU model is computationally intensive to simulate, owing to the spatial description and the wide range of time-scales involved. Yet, a detailed picture of gas exchange in the capillary circulation is of limited value to a macroscopic description of the progression of lung injury. It appears quite possible to derive, at the RU scale, an ODE approximation with states of partial pressures of both gases in the alveolar air space, tissue, and at the pulmonary venous end of the capillary. Once the numerical accuracy of this approximation is confirmed, we will have derived a computationally efficient model that allows multiple RU's under heterogeneous conditions seen in the lung to be linked using a physiologically reasonable implementation of diffusion (simulating extension of a process to neighboring RUs) and advection (simulating lymphatic transport of bacteria for example).

Our model is limited in a number of ways. Although the characterization of physicochemical parameters describing gas exchange is adequate, quantification of parameters characterizing the immune response is difficult. Our model contains only a very rudimentary representation of innate immunity and should be expanded accordingly for a more realistic representation of pulmonary immune physiology. Yet, there is a dearth of suitable datasets to properly estimate these parameters. Such datasets would ideally contain information on local concentrations of relevant immune mediators, counts of activated immune cells and relative volume distribution of alveolar air space, capillary blood and lung tissue. We assumed fixed boundary conditions for pulmonary arterial gas and acid-base status. Clearly, a closed loop model that included a metabolic component would be preferable, since, for example, decreased oxygen delivery may result in increased extraction and lower input oxygen partial pressures on the pulmonary arterial boundary. Accordingly, we would expect model predictions to be more optimistic than observations for extreme hypoxia. We also assumed an oxyhemoglobin dissociation curve that was independent of blood pH. Both of these simplifications could be addressed in extensions of our models. We achieved heterogeneity in ventilation-perfusion by allowing ventilation to vary, while keeping perfusion constant on each of the RUs in the full lung model. This resulted in a range of ventilation-perfusion

ratios with in the full lung model which is typically less than that encountered experimentally ([2], [45], [49]). The likely impact of a wider range of ventilation-perfusion ratios would be to accelerate the deterioration of gas exchange impairment in mixed pulmonary venous blood. Interestingly, promising experimental techniques allow less invasive and repetitive measurement of ventilation-perfusion ratios ([59], [60]), offering exciting new possibilities to compare prediction of multiscale organ physiology to experimental paradigms of acute lung injury.

5.0 REDUCTION OF THE LUNG MODEL

5.1 INTRODUCTION

In the previous chapter, we developed a full lung model in order to model the effect of inflammation on the lung. We developed a single respiratory unit (RU) model, which includes dynamics within three compartments: the blood, tissue and alveolar air space. Space along the capillary was included in the tissue and blood compartments due to the uptake of oxygen and release of carbon dioxide as the blood transverses the capillary. We assumed that the air space was well mixed. Therefore, the gas exchange subsystem of the model consists of PDEs for the partial pressure of oxygen (PO_2) and carbon dioxide (PCO_2) in both the tissue and blood and ODEs for PO_2 and PCO_2 in the alveolar air space. These ODEs include a breathing mechanism, which consists of inspiration for one second during which air volume increases and expiration for three seconds during which air volume returns to its level at the beginning of inspiration. In this form the single RU model has excessive computation times. Therefore, we have developed reduction methods that decrease computation time.

In the discretized form of single respiratory unit (RU) there are numerous equations due to space along the capillary, equations (5.1) and (5.9). These equations are the gas exchange subsystem from the previous chapter. To reduce this system, we created a spatial reduction which eliminated space while retaining the pressure levels at the end of the capillary. It is necessary to retain these spatial values, since partial pressure levels at the end of the capillary are needed in determining the output of the full lung model.

We also eliminated the breathing mechanism in order reduce computation times. The switches between inspiration and expiration require small step sizes, which slows simulations. This mechanism was originally included so that variability in breathing cycle could

be implemented into the model. At this time, we prefer to use the model to introduce more accurate ventilation perfusion mismatch. Ventilation perfusion mismatch is an imbalance in ventilation versus perfusion. This occurs in the lung during health conditions. For example, when an individual is standing upright the upper part of the lung has high ventilation with relatively low blood flow resulting in the ventilation perfusion mismatch [27]. In the previous chapter, heterogeneity between RUs in the full lung model was due to changes in ventilation. With the breathing mechanism removed we explore the effects of altering both ventilation and perfusion (changes in blood volumes). We refer to our model with the breathing mechanism removed as the non-breathing model.

The equations for the immune system in the lung are not altered by these reductions. Computation times for the immune subspace are reasonable even when space is included. Therefore, space is not removed from these equations. There is no feedback from the gas exchange subsystem to the immune subsystem, so temporal reductions on the gas exchange subsystem do not affect the immune subsystem.

Once the temporal reduction was applied to the model, we created a closed loop single RU model in order to more accurately model the lung. We include whole body interaction that involve the consumption of oxygen and production of carbon dioxide during metabolic processes. This consumption of oxygen and production of carbon dioxide is not included in the original or non-breathing form of the RU model. In these forms of the model arterial (entering the lung) gas levels are fixed and set to their levels in the absence of inflammation. Therefore, we have included metabolic reactions to determine the arterial gas levels from the venous gas levels in the non-breathing model. This forms a closed loop model of the lung, which we refer to as the closed RU model.

Equations for the original full lung model

$$\frac{dG_A}{dt} = \frac{D^G_{TA}}{\sigma^G_A V_A(y,\overline{Z_i})}\sum_{i=1}^{N}(G_{Ti}-G_A) + \begin{Bmatrix} \text{Inspiration} & (G_{air}(t)-G_A)R \\ \text{Expiration} & 0 \end{Bmatrix} \tag{5.1}$$

$$\frac{dG_{Ti}}{dt} = \frac{D^G_{TB}(G_{Bi}-G_{Ti})}{\sigma^G_T V_T(\overline{Z_i})} + \frac{D^G_{TA}(G_A-G_{Ti})}{\sigma^G_T V_T(\overline{Z_i})} - D_{_{GT}}\nabla^2_i G_{Ti} \tag{5.2}$$

$$\frac{dG_{Bi}}{dt} = \frac{D^G_{TB}(G_{Ti}-G_{Bi})}{\sigma^G_B V_B(\overline{Z_i})} + m\frac{-k^+(T_{Hb}-Hb_{4i})G^m_{Bi}+k^-Hb_{4i}}{\sigma^G_B} - v(\overline{Z_i})\nabla_i G_{Bi} \tag{5.3}$$

$$\frac{dHb_{4i}}{dt} = k^+(T_{Hb}-Hb_{4i})G^m_{Bi} - k^-Hb_{4i} - v(\overline{Z_i})\nabla_i Hb_{4i} \tag{5.4}$$

$$\text{With } k^- = R_H k^+$$

$$\frac{dC_A}{dt} = \frac{D^C_{TA}}{\sigma^C_A V_A(y,\overline{Z_i})}\sum_{i=1}^{N}(C_{Ti}-C_A) + \begin{Bmatrix} \text{Inspiration} & (C_{air}(t)-C_A)R \\ \text{Expiration} & 0 \end{Bmatrix} \tag{5.5}$$

$$\frac{dC_{Ti}}{dt} = \frac{D^C_{TB}(C_{Bi}-C_{Ti})}{\sigma^C_T V_T(\overline{Z_i})} + \frac{D^C_{TA}(C_A-C_{Ti})}{\sigma^G_T V_T(\overline{Z_i})} - D_{CT}\nabla^2_i C_{Ti} \tag{5.6}$$

$$\frac{dC_{Bi}}{dt} = \frac{1}{\sigma^C_B}\left(k_{catHC}\frac{HCO^-_{3i}}{k_{mHC}+HCO^-_{3i}} - k_{catCB}\frac{\sigma^C_B C_{Bi}}{k_{mCB}+\sigma^C_B C_{Bi}}\right) - v(\overline{Z_i})\nabla_i C_B \tag{5.7}$$

$$\frac{dHCO^-_{3i}}{dt} = k_{catCB}\frac{\sigma^C_B C_{Bi}}{k_{mCB}+\sigma^C_B C_{Bi}} - k_{catHC}\frac{HCO^-_{3i}}{k_{mHC}+HCO^-_{3i}} - v(\overline{Z_i})\nabla_i HCO^-_{3i} \tag{5.8}$$

$$\frac{dy}{dt} = \frac{V_{C0}s_h(t)}{\tau_1} - \frac{y}{\tau_2} \tag{5.9}$$

$$\text{with } V_A(y,\overline{Z_i}) = V_{A\min}(\overline{Z_i}) + y$$

$$V_{A\min}(\overline{Z_i}) = \frac{V_{A\min 0}}{1+m_{vta}\overline{Z_i}}$$

$$V_c(\overline{Z_i}) = \frac{V_{c0}}{1+m_{vtc}\overline{Z_i}}$$

$$s_h(t) = \frac{1}{1+e^{-\sigma(t_{in}-\mathrm{mod}(t,t_{in}+t_{out})}}$$

$$R = \frac{1}{V_{A0}(y,\overline{Z_i})}\frac{d}{dt}V_{A0}(y,\overline{Z_i})$$

$$V_T(\overline{Z_i}) = V_{T0}+V_{B0}-\frac{V_{B0}}{1+m_{vtb}\overline{Z_i}}+V_{A\min 0}-\frac{V_{A\min 0}}{1+m_{vta}\overline{Z_i}}$$

$$V_B(\overline{Z_i}) = \frac{V_{B0}}{1+m_{vtb}\overline{Z_i}}$$

$$v(\overline{Z_i}) = v_0\frac{V_{B0}}{V_B(\overline{Z_i})}$$

Note that $\overline{Z_i}$ is the spatial average of the variable which tracks inflammation, Z. Inflammation levels are determined by the immune subsystem, see equations 4.20 and 4.24.

5.2 SPATIAL REDUCTION

Our first attempt at shortening computation times of the RU model consisted of removing space, significantly reducing the number of equations in the discretized form of the model. With space removed from the single RU model, the model consists of four differential equations and two functions f and g, see equations (5.10)-(5.16). The function f determines from look up tables the values of G_B at the end of the capillary, G_B^{end}, and the spatial average of G_B over the length of the capillary, G_B^{avg}. The function g has similar output, but for C_B. The schematic for this reduction is illustrated in Figure 35. Recall that G_x and C_x represent oxygen and carbon dioxide gas pressures on compartment x, respectively. The subscript x is either B for blood, T for tissue, or A for alveolar air space. Individual parameter explanations are given in Table 13 of Chapter 3.

To develop equations (5.10)-(5.16) we first assumed that the pressure for tissue oxygen (G_T) and tissue carbon dioxide (C_T) are both uniform in space, step 1 in Figure 35. This eliminates the diffusion within the tissue terms in equations (5.2) and (5.6). Also in equations (5.1) and (5.5), G_{Ti} and C_{Ti} is replaces with G_T and C_T, respectively, since there is now no spatial discretization in the tissue compartment.

$$\frac{dG_A}{dt} = \frac{D_{TA}^G}{\sigma_A^G V_A(y,\overline{Z_i})}(G_T - G_A) + \begin{Bmatrix} \text{Inspiration} & (G_{air}(t) - G_A)R \\ \text{Expiration} & 0 \end{Bmatrix} \tag{5.10}$$

$$\frac{dG_T}{dt} = \frac{D_{TB}^G(G_B^{avg} - G_T)}{\sigma_T^G V_T(\overline{Z_i})} + \frac{D_{TA}^G(G_A - G_T)}{\sigma_T^G V_T(\overline{Z_i})} \tag{5.11}$$

$$\left[G_B^{avg}, G_B^{end}\right] = f(V_B(y,\overline{Z_i}), v(y,\overline{Z_i}), G_T) \tag{5.12}$$

$$\frac{dC_A}{dt} = \frac{D_{TA}^C}{\sigma_A^C V_A(y,\overline{Z_i})}(C_T - C_A) + \begin{Bmatrix} \text{Inspiration} & (C_{air}(t) - C_A)R \\ \text{Expiration} & 0 \end{Bmatrix} \tag{5.13}$$

$$\frac{dC_T}{dt} = \frac{D_{TB}^C(C_B^{avg} - C_T)}{\sigma_T^C V_T(\overline{Z_i})} + \frac{D_{TA}^C(C_A - C_T)}{\sigma_T^G V_T(\overline{Z_i})} \tag{5.14}$$

$$\left[C_B^{avg}, C_B^{end}\right] = g(V_B(y,\overline{Z_i}), v(y,\overline{Z_i}), C_T) \tag{5.15}$$

$$\frac{dy}{dt} = \frac{V_{C0}s_h(t)}{\tau_1} - \frac{y}{\tau_2} \tag{5.16}$$

In order to remove space from the blood we cannot simply use spatial averaging. We need the levels G_B^{end} and C_B^{end} on each RU to determine the output of the full lung model. In order

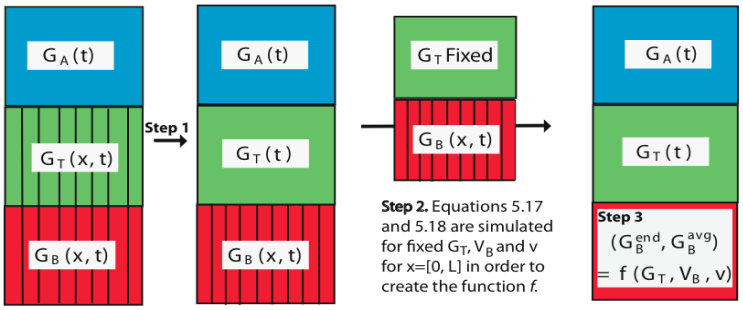

Figure 35: Schematic for the spatial reduction along the length of the capillary. In the original model the air compartment is assumed to well mixed (blue) while the tissue (green) and blood (red) compartments include space along the capillary (first column). In step 1 of the reduction, we assume that the tissue compartment is well mixed removing removed space along the capillary in the tissue. In step 2, we simulated the subsystem 5.17 and 5.18 with ranges of fixed levels of oxygen in the tissue (G_T), blood volume (V_B) and blood speed (v) for $x = [0, L]$, where L is the length of the capillary in order to create, f. From each of the combinations of G_T, V_B, and v simulated we recorded venous end PO_2 (G_B^{end}) and the spatial average of PO_2 along the capillary (G_B^{avg}). In step 3, we replaced the G_B equation with the function f and G_B in the diffusion term of the G_T equation with G_B^{avg}. During simulations of the full model, $f(G_T, V_B, v)$ detemines G_B^{avg} and G_B^{end} from the data collected in step 2.

to calculate G_B^{end}, C_B^{end}, G_B^{avg}, and C_B^{avg}, we assume steady state in the blood compartment and that there is a constant input from the tissue compartment to the blood compartment for both gases, G_T and C_T, during the time the blood transverses the capillary. Blood transverses the length of the capillary in 3/4 of a second and the breath cycle is four seconds under normal conditions. In the full model PO_2 and PCO_2 tissue levels oscillate due to the breathing mechanism in the alveolar air space, but these oscillations have fairly small amplitude and a four second period. Therefore, during the time the blood transverses the capillary it is reasonable to assume constant levels of PO_2 and PCO_2 in the tissue.

Also, we assume that blood velocity (v) and volume (V_B) are constant during the time the blood transverses the capillary. This is also a reasonable assumption given that their values are determined by immune system where changes occur a significantly shorter timescale. These assumptions allow us to rewrite the equations for blood variables, equations (5.3), (5.4), (5.7) and (5.8), as ODE's with space as the only independent variable, see equations (5.17)-(5.20).

$$\frac{\partial G_B}{\partial x} = \frac{1}{v}\left(\frac{D_{TB}^G(G_T - G_B)}{\sigma_B^G V_B} + m\frac{-k^+(T_{Hb} - Hb_4)G_B^m + k^- Hb_4}{\sigma_B^G}\right) \quad (5.17)$$

$$\frac{\partial Hb_4}{\partial x} = \frac{1}{v}\left(k^+(T_{Hb} - Hb_{4i})G_B^m - k^- Hb_4\right) \quad (5.18)$$

$$\frac{\partial C_B}{\partial x} = \frac{1}{v\sigma_B^C}\left(\frac{D_{TB}^C(C_T - C_B)}{\sigma_B^C V_B} + k_{catHC}\frac{HCO_3^-}{k_{mHC} + HCO_3^-}\right) - \frac{k_{catCB}}{v\sigma_B^C}\frac{\sigma_B^C C_B}{k_{mCB} + \sigma_B^C C_B} \quad (5.19)$$

$$\frac{\partial HCO_3^-}{\partial x} = \frac{1}{v}\left(k_{catCB}\frac{\sigma_B^C C_B}{k_{mCB} + \sigma_B^C C_B} - k_{catHC}\frac{HCO_3^-}{k_{mHC} + HCO_3^-}\right) \quad (5.20)$$

Step two of the reduction is to simulate equations 5.17-5.20 for ranges of G_T, V_b, and v in order to create the look-up tables used in determining G_B^{end} and G_B^{avg}.Before simulating over the various levels of G_T, v and V_B, we simulated this system with these parameters set to their baseline values. Oxygen and carbon dioxide levels are uncoupled in this system, so we can simulate equations (5.17) and (5.18) separately from equations (5.19) and (5.20). We first focused on oxygen. Normal conditions for these parameters are $v = 0.2933$ cm/s, $V_B = 7.5 \times 10^{-9}$L, which is 90 ml/(# of alveoli) and $G_T = 100$ mmHg. $G_T = 100$ mmHg is approximately the value that the full model G_T oscillates around after the hemoglobin and oxygen have reached steady state in the blood. With this parameter set, the hemoglobin becomes saturated and G_B reaches the G_T level early along the capillary. Under normal conditions hemoglobin saturates in approximately the first 1/3 of the capillary. The diffusion rate for oxygen crossing the tissue/blood barrier in the full model was fit such that hemoglobin saturates at an appropriate point along of the capillary. This is one of the few free parameters in the full lung model. Given how this rate was determined for the full model, we adjusted the diffusion rate in the spatial reduction, such that G_B reaches the level of G_T further along the capillary (see the new diffusion constant curve in the Figure 36).

Once the diffusion constant was adjusted, equations (5.17) and (5.18) were simulated with a range of G_T, v and V_B and both G_B^{end}, G_B^{avg} were recorded. In Figure 37 we look at a sample of the data collected. We have plotted the G_B^{avg} and G_B^{end} with G_T=100 mmHg, V_B ranging from 20 ml/(# of alveoli) to 120 ml/(# of alveoli) and v from 0.055 to 1.47 cm/s. Note that for ease of plotting, unscaled blood volumes are used, 20 ml to 120 ml. Under

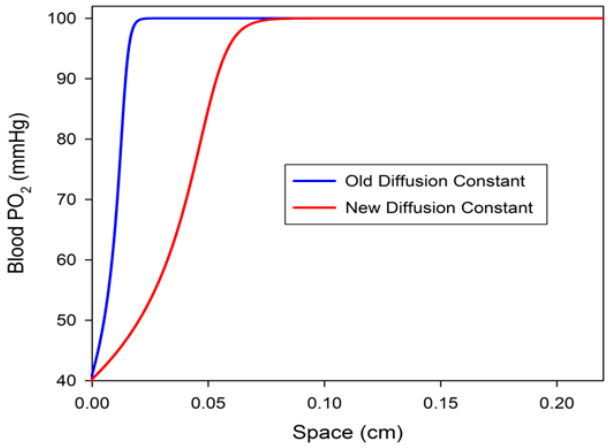

Figure 36: Transients from the blood compartment with the same fixed oxygen tissue, blood velocity and blood volume, but with different diffusion constants. The diffusion constant is set to the value from the full model, 6.7483×10^{-12} L/s, for the curve labeled old diffusion constant. Diffusion constant is set to the value from the spaceless model, 1.8×10^{-12} L/s, for the new diffusion constant curve.

most conditions G_B^{end} reaches G_T. G_B^{end} is affected most by the changes in the blood speed. When the blood is too fast the hemoglobin does not saturate and venous PO_2 levels do not increase to the levels seen in the tissue. Changes in V_B affect the diffusion term, but if the speed of the blood is slow enough this does not affect the end blood level. Changes in both V_B and v, however, both do effect the G_B^{avg}, since these change where hemoglobin steady state occurs. Later saturation decreases G_B^{avg}. Only when saturation does not occur is G_B^{end} affected.

The data collected for G_B^{avg} and G_B^{end} from range G_T between 20 and 165 mmHg and the ranges of v and V_B mentioned above and stored in matrices. These matrices are used to determine the value of f at a given $V_B(t)$, $v(t)$, and $G_T(t)$. $G_T(t)$ determines which matrix of G_B^{end} values is called . We then linearly interpolate for G_B^{end}, from the four matrix values corresponding the closest simulated v and V_B above and below the actual $v(t)$ and $V_B(t)$. The same method is used to determine G_B^{avg}. Once f is determined, the final step of the reduction is to eliminate the PDE for G_B and determine venous PO_2 with f. We also replaced G_B by G_B^{avg} in the G_T equation, which was also determined by f. This creates the spaceless form of the model, equations 5.10-5.16.

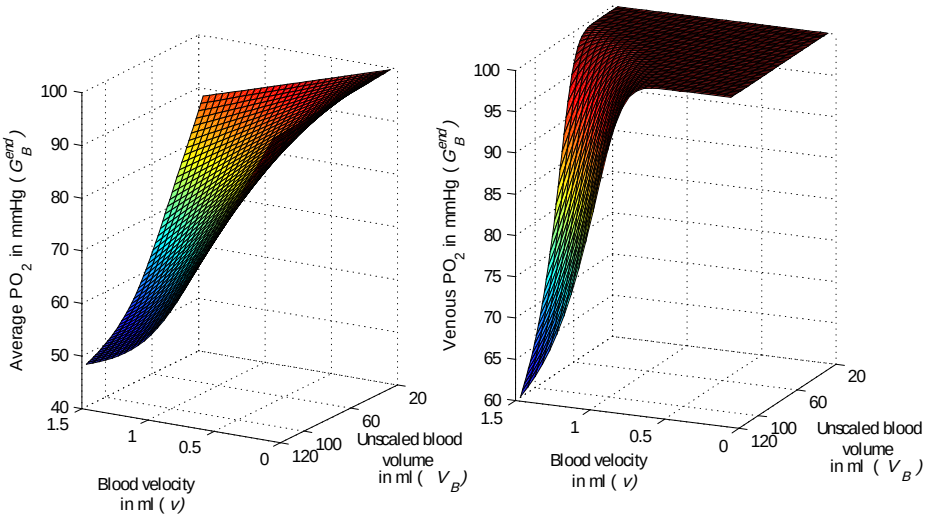

Figure 37: Average PO_2 and end PO_2 in the blood versus the speed of blood (v) and unscaled blood volume (V_B) with fixed tissue PO_2. PO_2 in the tissue (G_T) is set to 100 mmHg. Actual volume used of the blood was 1.7×10^{-9}L $\left(\frac{20\text{ml}}{\#\text{ of alveoli}}\right)$ to 1×10^{-8}L$\left(\frac{120\text{ ml}}{\#\text{ of alveoli}}\right)$. For plotting purposes unscaled volumes, 20-120 ml, were used. On the left is the plot for average oxygen in the blood (G_B^{avg}) versus v and V_B. On the right is the plot for venous PO_2 in the blood (G_B^{end}) versus v and V_B.

We first simulated this model in the absence of inflammation. These simulation resulted in a $G_B^{end} = 95$ mmHg, $G_B^{avg} = 86.5$ mmHg, $G_T = 90.34$ mmHg and $G_A = 96.95$ mmHg (at the end of expiration). In the full model with space along the capillary with the same condition we had $G_B^{end} = 97$ mmHg, $G_T = 96.82$ mmHg, and $G_A = 96.77$ mmHg. Therefore, during health the spatial reduction reproduces results similar to that in the original model. The running time for the first 120 seconds during lethal inflammation ($TNF_B = 4$) of the original RU model is 91.73 seconds for the model with space along the capillary. With spatial reductions the same insult ran in 31.67 seconds. The same lethal insult used in the previous chapter was also simulated here ($TNF_B = 4$). During the initial stages of this insult the spatial reduction method decreased computation times minimally. However, when inflammation accumulates the matrices used to determine G_B^{avg} and G_B^{end} changes. This is due to the changes in G_T during the insult. When the matrices change there was a significant increase in computation times. The non-spatial model actually had a longer running time than the full method. Given the effectiveness of the temporal reduction, this spatial reduction was not applied to the model.

5.3 TEMPORAL REDUCTION

The main cause of long computation times in the single RU model is the breathing mechanism. Therefore, we removed this mechanism, altering the equations for alveolar PO_2 (G_A) and PCO_2 (C_A) (equations (5.1) and (5.5)), and eliminating the y variable (equation (5.9)). The last terms in equations (5.1) and (5.5) are replaced by a source term in G_A equation and a decay term in the C_A, see the last terms in equations 5.21 and 5.25. This change is equivalent to introducing a source for G_A, since $G_A < G_{air0}$ in lung, and a decay of C_A, since we assume $C_{air0} = 0$. The effects of inflammation are still applied to this term via the ratio $V_C(\overline{Z_i})/V_{C0normal}$, where $V_C(\overline{Z_i})$ is the tidal volume and $V_{Cnormal} = 350$ ml/$(\#ofalveoli)$. When V_C decreases there is less new air introduced on a breath cycle reducing the ability of the alveolar space to supply O_2 and remove CO_2.

$$\frac{dG_A}{dt} = P_{va}(V_G(\overline{Z_i}))\frac{D^G_{TA}}{\sigma^G_A}\sum_{i=1}^{N}(G_{Ti} - G_A) + k_G(G_{air0} - G_A)\frac{V_C(\overline{Z_i})}{V_{C0}} \tag{5.21}$$

$$\frac{dG_{Ti}}{dt} = \frac{D^G_{TB}(G_{Bi} - G_{Ti})}{\sigma^G_T V_T(\overline{Z_i})} + \frac{D^G_{TA}(G_A - G_{Ti})}{\sigma^G_T V_T(\overline{Z_i})} - D_{_{GT}}\nabla^2_i G_{Ti} \tag{5.22}$$

$$\frac{dG_{Bi}}{dt} = \frac{D^G_{TB}(G_{Ti} - G_{Bi})}{\sigma^G_B V_B(\overline{Z_i})} + m\frac{-k^+(T_{Hb} - Hb_{4i})G^m_{Bi} + k^- Hb_{4i}}{\sigma^G_B} - v(\overline{Z_i})\nabla_i G_{Bi} \tag{5.23}$$

$$\frac{dHb_{4i}}{dt} = k^+(T_{Hb} - Hb_{4i})G^m_{Bi} - k^- Hb_{4i} - v(\overline{Z_i})\nabla_i Hb_{4i} \tag{5.24}$$

$$\text{With } k^- = R_H k^+$$

$$\frac{dC_A}{dt} = P_{va}(V_C(\overline{Z_i}))\frac{D^C_{TA}}{\sigma^C_A}\sum_{i=1}^{N}(C_{Ti} - C_A) + k_C(C_{air0} - C_A)\frac{V_C(\overline{Z_i})}{V_{C0}} \tag{5.25}$$

$$\frac{dC_{Ti}}{dt} = \frac{D^C_{TB}(C_{Bi} - C_{Ti})}{\sigma^C_T V_T(\overline{Z_i})} + \frac{D^C_{TA}(C_A - C_{Ti})}{\sigma^G_T V_T(\overline{Z_i})} - D_{CT}\nabla^2_i C_{Ti} \tag{5.26}$$

$$\frac{dC_{Bi}}{dt} = \frac{1}{\sigma^C_B}\left(k_{catHC}\frac{HCO^-_{3i}}{k_{mHC} + HCO^-_{3i}} - k_{catCB}\frac{\sigma^C_B C_{Bi}}{k_{mCB} + \sigma^C_B C_{Bi}}\right) - v(\overline{Z_i})\nabla_i C_B \tag{5.27}$$

$$\frac{dHCO^-_{3i}}{dt} = k_{catCB}\frac{\sigma^C_B C_{Bi}}{k_{mCB} + \sigma^C_B C_{Bi}} - k_{catHC}\frac{HCO^-_{3i}}{k_{mHC} + HCO^-_{3i}} - v(\overline{Z_i})\nabla_i HCO^-_{3i} \tag{5.28}$$

$$
\begin{aligned}
V_{A\min}(\overline{Z_i}) &= \frac{V_{A\min 0}}{1+m_{vta}\overline{Z_i}} \\
V_c(\overline{Z_i}) &= \frac{V_{c0}}{1+m_{vtc}\overline{Z_i}} \\
V_T(\overline{Z_i}) &= V_{T0}+V_{B0}-\frac{V_{B0}}{1+m_{vtb}\overline{\overline{Z_i}}}+V_{A\min 0}-\frac{V_{A\min 0}}{1+m_{vta}\overline{Z_i}} \\
V_B(\overline{Z_i}) &= \frac{V_{B0}}{1+m_{vtb}\overline{\overline{Z_i}}} \\
v(\overline{Z_i}) &= v_0\frac{V_{B0normal}}{V_B(\overline{Z_i})}
\end{aligned}
$$

We then eliminated the variable y. Recall that y tracks the changes in the alveolar air space volume during a breath cycle. Changes in the alveolar air space volume caused by inflammation are retained in this reduction. To eliminate y in the equation for G_A and C_A we took the temporal average of $\frac{1}{V_A(t,\overline{Z_i})}$ over a breath cycle. Recall that $V_A(t,\overline{Z_i}) = V_{A\min}(\overline{Z_i})+y$, where $V_{A\min}(\overline{Z_i})$ is the minimal alveolar volume and y grows from $V_{A\min}(\overline{Z_i})$ to $V_{A\min}(\overline{Z_i})+V_C(\overline{Z_i})$ during inspiration (one second) and decays back to $V_{A\min}(\overline{Z_i})$ during expiration (three seconds). $V_{A\min}(\overline{Z_i})$ and $V_C(\overline{Z_i})$ are output of the immune subsystem and we assume here they fixed for a given breath cycle, since the immune subsystem runs of the order of hours and the breath cycle is 4 seconds. With the breathing mechanism replaced by the source/decay term, y only remains in the diffusion terms in the alveolar air space compartment (RU model equations 5.1 and 5.5). Therefore, the diffusion term $\frac{1}{V_A(t,\overline{Z_i})}$ was replaced with its average over the breath cycle, which equals $\frac{1}{4}\int_0^4 \frac{1}{V_{A\min}(\overline{Z_i})+y}dt$.

Note that, y is defined by equation 5.9 and that $V_{A\min}(\overline{Z_i})$ and $V_C(\overline{Z_i})$ are assumed to be constant the breathing cycle. Replacing $sh(t)$ with the Heaviside function in the y equation, on a single breath cycle we can rewrite this y equation as

$$
\begin{aligned}
\frac{dy_1}{dt} &= \frac{Vc(\overline{Z_i})}{\tau_1}-\frac{y_1}{\tau_2}, \text{ with } y_1(0)=0 \text{ for } 0\le t<1 \\
\frac{dy_2}{dt} &= \frac{y_2}{\tau_2}, \text{ with } y_2(1)=y_1(1) \text{ for } 1\le t\le 4.
\end{aligned}
$$

Solving these ODEs we rewrite the average as

$$\begin{aligned}\frac{1}{4}\int_0^4 \frac{1}{V_{A\min}(\overline{Z_i})+y}dt &= \frac{1}{4}\left(\int_0^1 \frac{1}{V_{A\min}(\overline{Z_i})+y_1}dt+\int_1^4 \frac{1}{V_{A\min}(\overline{Z_i})+y_2}dt\right)\\ &= \frac{1}{4}\int_0^1 \frac{1}{V_{A\min}(\overline{Z_i})+\frac{V_c(\overline{Z_i})\tau_2}{\tau_1}(1-e^{-t/\tau_2})}dt\\ &\quad +\frac{1}{4}\int_1^4 \frac{1}{V_{A\min}(\overline{Z_i})+y_1(1)e^{-(t-1)/\tau_2}}dt.\end{aligned}$$

Setting parameters to their values from Tables 13-19 of Chapter 3 and integrating we get the average as a function of $V_{A\min}(\overline{Z_i})$ and $V_C(\overline{Z_i})$,

$$\begin{aligned}\frac{1}{4}\int_0^4 \frac{1}{V_{A\min}(\overline{Z_i})+y}dt &= 0.875\frac{\ln(5V_{A\min}(\overline{Z_i})+5.322Vc(\overline{Z_i}))-\ln(V_{A\min}(\overline{Z_i}))-0.181}{5V_{A\min}(\overline{Z_i})+7V_C(\overline{Z_i})}\\ &\quad +0.175\frac{\ln(1\times10^9V_{A\min}(\overline{Z_i})+1.465\times10^7V_C(\overline{Z_i}))+4.286}{V_{A\min}(\overline{Z_i})}\\ &\quad -0.175\frac{\ln(1\times10^9V_{A\min}(\overline{Z_i})+1.064\times10^9V_C(\overline{Z_i}))}{V_{A\min}(\overline{Z_i})}.\end{aligned}$$

We refer to this function as $P_{va}(\overline{Z_i})$. Replacing $\frac{1}{V_A(t,\overline{Z_i})}$ with $P_{va}(\overline{Z_i})$ and the breathing mechanism term with the source/decay term in the G_A and C_A equations, we have the model for a single until RU without the breathing mechanism, equations (5.21)-(5.28).

Computation times are dramatically decreased with this reduction. To simulate 96 hours of gas exchange with the same lethal inflammation took only 19.07 seconds. Recall that in the full model to simulate 120 seconds of lethal inflammation took 91.73 seconds. In Figure 38 we compare the results of the RU model with and without breathing during a lethal insult of TNF_B=4. For the breathing model we have plotted G_B^{end} at the end of expiration, which is the minimum during the breath cycle. However, in the non-breathing model, the parameter K_G in the source term was fit so that our healthy level for G_B^{end} is approximately the average G_B^{end} over a breath cycle in the full model, ≈100 mmHg. Hence in Figure 38, the non-breathing model is initially above the breathing model. The effects of inflammation are slightly greater in the non-breathing case. This is likely due to change in the implementation of inflammatory effects on the intake of oxygen. The accumulation of inflammation eventually causes the non-breathing curve to fall below the breathing curve. However, overall the

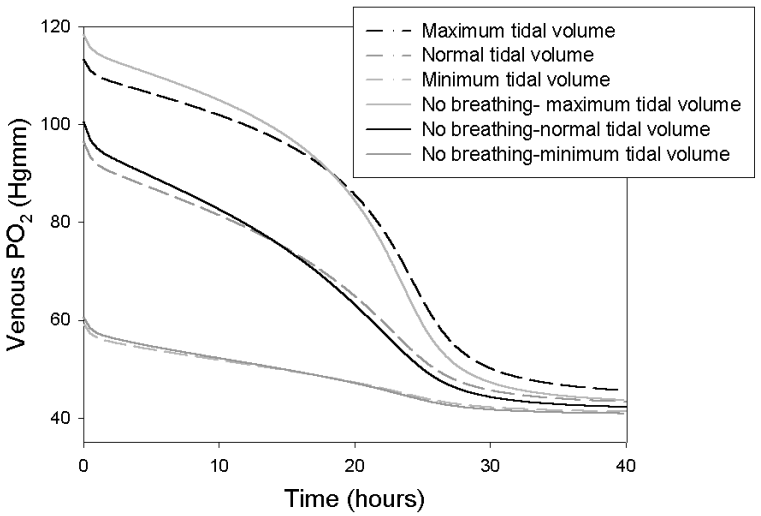

Figure 38: Comparsion of venous PO_2 from the single RU model with and without the breathing mechanism for various tidal volumes, during a lethal insult. Dashed transients are the results from the single RU model with the breathing mechanism. The insult was trigger by setting $TNF_B = 4$. The minimum , normal and maximum tidal volume are 150 ml/(# of alveoli), 350 ml/(# of alveoli) and 550 ml/(# of alveoli), respectively.

temporal reduction gives similar results to the full model. For the sake of computation times, oxygen was separated from carbon dioxide and only the oxygen subsystem was simulated for the breathing model. Therefore, there is no comparison presented here between these model for PCO_2. With the temporal reduction, simulations for both gases are run simultaneously and the results for PCO_2 are presented in a later figure.

5.4 FULL LUNG

As with the breathing RU model, multiple non-breathing RU models were linked to create a full lung model. Again, we introduced ventilation perfusion mismatch into the full lung model by implementing a truncated normal distribution in the initial tidal volume levels of the linked RUs. Previously, we only considered oxygen. Here, we will study results for both oxygen and carbon dioxide. This type of heterogeneity in the lung is caused by changes in the ventilation. However, perfusion also differs from RU to RU. Therefore, we also consider a lung which has a normal truncated distribution in the initial blood volumes of the RUs.

Finally, we considered altering both ventilation and perfusion simultaneously as seen in an actual lung. For this we introduced a uncorrelated bivariate truncated normal distribution in the initial tidal and blood volumes of the linked RUs.

In all of our full lung models we considered the full lung with and without shunting. Recall that shunting is when the alveolar air space collapses during severe inflammation. Shunting is typically assumed to be the main cause of PO_2 drops during acute lung injury, rather than changes in diffusion. As we did in the breathing model, when tidal volume drops below 40% of the normal tidal volume diffusion across the tissue barrier is eliminated, by taking $D_{TA}^G = 0$, $D_{TA}^C = 0$, if $V_C(\overline{Z_i})/V_{C0Normal} < 0.4$, where $V_{C0Normal} = 350$ ml/(# of alveoli). When shunting is included in both the non-breathing and breathing models the shunting curve is exactly the same as the results without shunting until $V_C(\overline{Z_i})/V_{C0Normal}$ falls below 0.4. Note that, the time point where shunting occurs is determined by the immune subsystem, so there is no difference in the closure times for the breathing and non-breathing model.

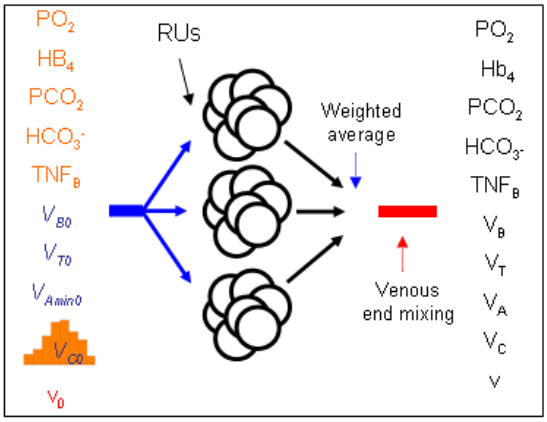

Figure 39: Model schematics for the linking of multiple RUs to create the Full lung-V_C model. The first column represents entering variable concentrations and partial pressures (orange), initial comparmental and tidal volumes (blue) and blood speed (red) at the onset of inflammation. All of these are the same on all RUs except for the initial tidal volume, V_{C0}. V_{C0} of the RUs were determined by a normal truncated distribution. Simulation were run for the various RUs. A weighted average dependent on the distribution is taken of the blood variable values at the venous end. This weighted average is used as the intial conditions for an ODE system that models venous end mixing. The results of this system are the output of the full model.

5.4.1 Full Lung-V_C

We linked multiple RU models with various initial tidal volumes (V_{C0}) to form a full lung model, which we will refer to as the Full lung-V_C model. With this method the ventilation perfusion mismatch is introduced via differences in air supply. No change were made to account for difference in blood supply. A schematic for creating the Full lung-V_C model is given Figure 39.

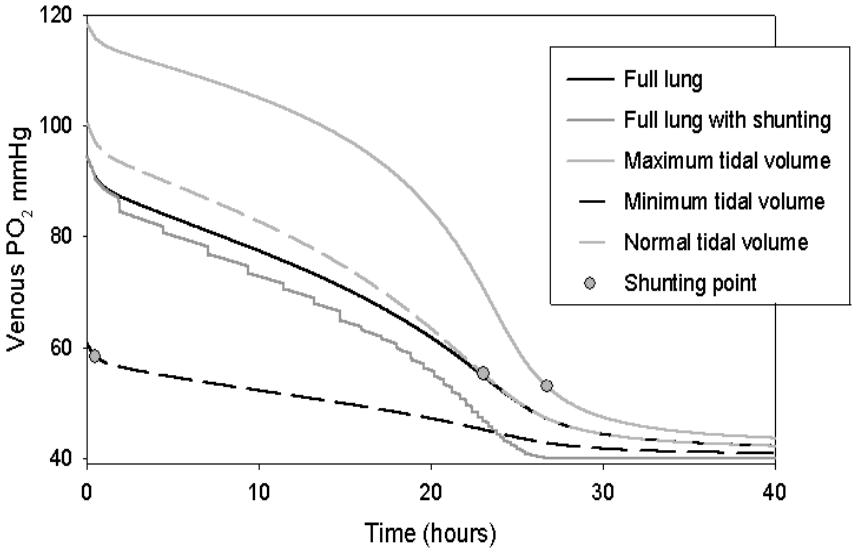

Figure 40: Venous PO_2 from the non-breathing single RU model and Full lung-V_C model with and without shunting during a lethal insult. The insult was triggered by setting $TNF_B = 4$. The minimum, normal and maximum tidal scaled volume are $\frac{150ml}{\#\text{ of alveoli}}$, $\frac{350ml}{\#\text{ of alveoli}}$ and $\frac{550ml}{\#\text{ of alveoli}}$, respectively. Each single unit transient is mark with a gray circle where shunting for that curve occurred.

As in the breathing model, each RU has the same compartmental volumes, entering blood concentrations for HB_4 and HCO_3^-, entering PO_2 and PCO_2 and initial blood velocity (left column of Figure 39). We took the same sample set from the truncated normal distribution we used in the previous chapter, with minimum scaled volume, 150 ml, maximum scaled volume, 550 ml, and the scaled mean, ≈350 ml. To model the full lung, the single RU model is simulated over a range of tidal volumes. We then take weighted averages for G_B^{end}, Hb_4^{end}, C_B^{end}, and HCO_3^{-end} from the output of these single units. The weights for the average were determined by the distribution. The weighted averages are then used as the initial conditions

for a system of ODEs consisting of G_B, Hb_4, C_B, and HCO_3^- reactions from equations (5.23), (5.24), (5.27), and (5.28) without the diffusion and advection terms. This system models the mixing of the blood when it leaves the lung.

In Figure 40 we compare the results from scaled 150 ml, scaled 350 ml, scaled 550 ml and the Full lung-V_C model with and without shunting. As in the breathing model there is significant PO_2 loss during inflammation. All transients approach the fixed arterial blood PO_2 level, 40 mmHg. This value was fixed throughout the simulation.

Each transient for the single RUs is marked with a circle where shunting occurred. At this circle PO_2 on that RU will drop to approximately 40 mmHg when shunting is included. The higher the initial tidal volume the later the RU shunts. We binned the sample set such that the simulations were run with initial tidal volume incremented by 10 ml from 150 to 550 ml. Therefore, all RUs in a bin shunt at the same time. This is what causes the "steps" in the shunting curve. The full lung shunting curve has more severe drops in venous PO_2 than without shunting. However, in the absence of shunting there are still significant drops due to limited diffusion of oxygen during inflammation.

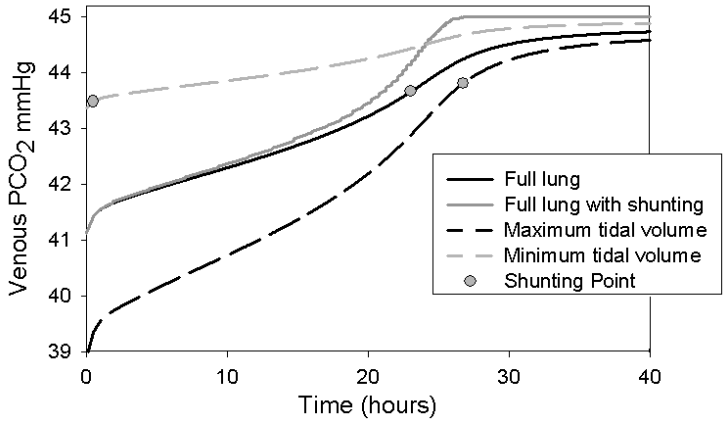

Figure 41: Venous PCO_2 from the non-breathing single RU model and Full lung-V_C model with and without shunting during a lethal insult. The insult was triggered by setting $TNF_B = 4$. The minimum and maximum tidal scaled volume are $\frac{150ml}{\#\text{ of alveoli}}$ and $\frac{550ml}{\#\text{ of alveoli}}$, respectively. Each single unit transient is mark with a gray circle where shunting for that curve occurred.

Figure 41 shows results for venous PCO_2 from the non-breathing RU model for various tidal volumes and the Full lung-V_C model with and without shunting during the same insult.

Inflammation hinders the removal of PCO_2 from the blood. Therefore, for all tidal volumes PCO_2 increase during inflammation. As in the simulations for PO_2, curves approach the fixed arterial PCO_2 level, 45 mmHg. Again, where shunting occurs for the single RU transients is marked with a gray circle. When shunting occurs the PCO_2 rises to approximately 45 mmHg. The curve for the full lung model with shunting shows more severe increases than the curve without shunting.

5.4.2 Full Lung-V_B

Next we considered a lung where heterogeneity in the lung is introduced via changes in perfusion. This was modeled by introducing a distribution in the initial blood volumes (V_{B0}) of the RUs with initial tidal volumes equal on all units. We refer to this full model as the Full lung-V_B model. Overall schematics for the linking of the RUs is the same as in Figure 39, but with the distribution now in V_{B0}. The truncated normal distribution used to determine the initial blood volumes of the RUs was assumed to have minimum, scaled 30 ml, maximum ,scaled 150 ml, and average scaled 90 ml.

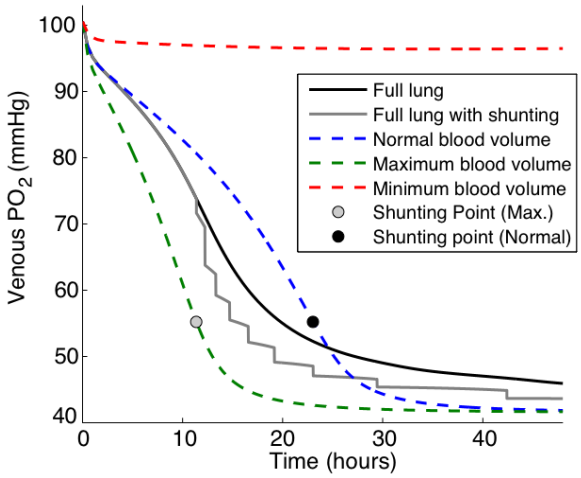

Figure 42: PO_2 level for various blood volumes and the full lung model which has a truncated normal distribution in the blood volume, Full lung-V_B model. PO_2 transients from RUs with maximum (scaled 150 ml), normal (scaled 90 ml), and minimum (scaled 30 ml) blood volume and from full model which has the blood volumes of the RUs from a normal distrubition truncated at the minimum and maximum volumes and average approximately the normal blood volume.

In Figures 42 and 43 we see the effect of implementing mismatch via a truncated normal distribution in V_B on venous PO_2 and PCO_2. Inflammation was introduced via the same $TNF_B = 4$ insult. For both oxygen and carbon dioxide results are similar to those seen when tidal volume is varied. Due to the conservation of flow all RUs have the same initial conditions. In each RU flow is conserved by adjusting blood speed for the differences in the blood volume. This allows the saturation of hemoglobin and sufficient uptake of oxygen as the blood transverses in all RUs.

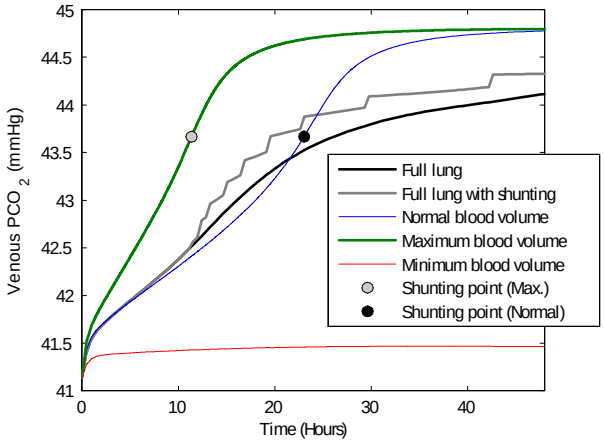

Figure 43: PCO_2 level for various blood volumes and the full lung model which has a truncated normal distribution in the blood volume, Full lung-V_B model. PCO_2 transients from RUs with maximum (scaled 150 ml), normal (scaled 90 ml), and minimum (scaled 30 ml) blood volume and from full model which has the blood volumes of the RUs from a normal distrubition truncated at the minimum and maximum volumes and average approximately the normal blood volume.

Though changes in blood do not alter the initial level of PO_2 and PCO_2, the levels of inflammation on the RUs differ during an insult. Changes in blood volume affect the diffusion of the immune variables, effecting the inflammation levels. Therefore, in Figures 42 and 43 transients for individual RUs differ despite having the same initial PO_2 level. For the minimum volume case an insult of $TNF_B = 4$ is a non-lethal. When shunting is included this unit does not shunt, since there are low levels of inflammation on this unit. The normal and minimum blood volume RUs shunt and their transients in Figures 42 and 43 are marked with circles at the point when it occurs. This does not occur at the same point, despite the fact that both units start with the same tidal volume, since inflammation levels differs

on these units. Difference in inflammation levels between RUs does not occur in the Full lung-V_C model, since changes to the alveolar air space do not affect the immune subsystem, which is modeled in only the tissue and blood compartments.

As seen in Full lung-V_C model, the Full lung-V_B with shunting had more significant drops in venous PO_2 (Figure 42) than without shunting. However, shunting effects overall are seen later in the Full lung-V_B model. With or without shunting, the Full lung-V_B model does not drop to the arterial PO_2 level as seen in the Full lung-V_C model. This is due to the RUs that do not have significant levels of inflammation to cause severe drops in venous PO_2. Results are similar for PCO_2, but with increasing PCO_2 levels during inflammation (Figure 43).

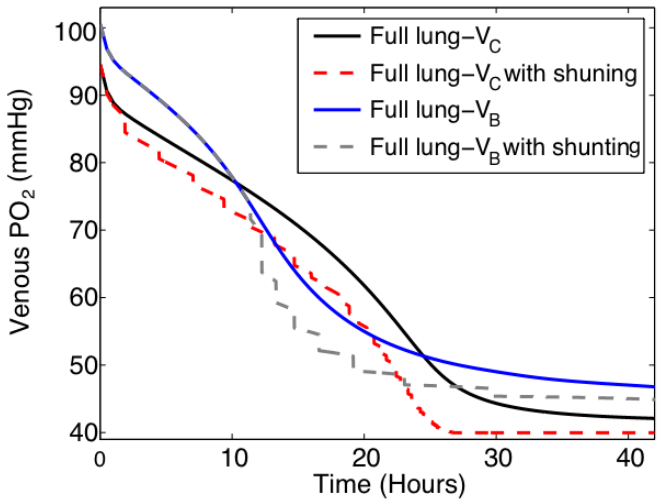

Figure 44: Venous PO_2 for Full lung-V_C and Full lung-V_B models with and without shunting during a lethal insult. In both full lung models the insult was triggered by $TNF_B = 4$.

In Figure 44 we compare the full models with and without shunting for the Full lung-V_C and Full lung-V_B models. Without shunting the Full lung-V_B model has more significant drops in PO_2 in the first 24 hours, since the differences is V_{B0} effect the inflammation variable. In the late stages of the insult the Full lung-V_B model remains elevated due to RUs that did not accumulate significant inflammation. With shunting we see that the Full lung-V_B model begins shunting at about 11 hours, which is much later that the Full lung-V_C model.

5.4.3 Full Lung-$V_C V_B$ Model

Within the lung ventilation perfusion mismatch is caused by both heterogeneity in the blood and air supply. Therefore, we created a full lung model following the schematic in Figure 39 but with both initial tidal and blood volumes varying between RUs. This heterogeneity was introduced via an uncorrelated, bivariate, truncated normal distribution in V_{B0} and V_{C0}, with the same maximums, minimums, and averages used in the previous full models. We refer to the model as the Full lung-$V_B V_C$ model. In Figure 45A is the sample set used from this distribution. Figure 45B shows the initial conditions for venous PO_2 that arise from this distribution.

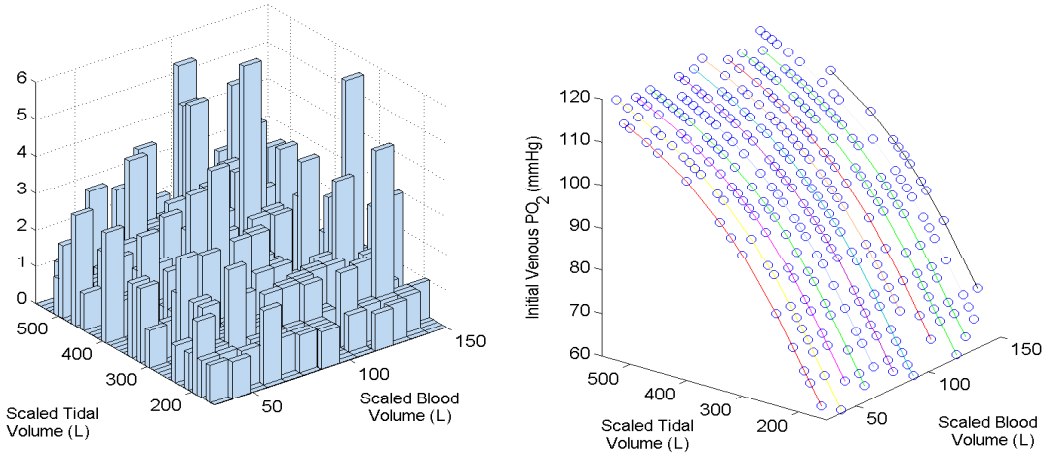

Figure 45: The distrubtion used in the Full-$V_C V_B$ and the associated initial conditions for venous PO_2. A. Realization of the bivariate truncated normal used in the full model with ventilation perfusion mismatch introduced by varying both the tidal volume and blood volume. The height of the bar determines the portions of RUs in the full model with that associated tidal and blood volume. B The initial condition associated with each tidal and blood volume combination. Altering these volumes affects the normal level of venous PO_2. The normal level is used as the initial condition for PO_2 when inflammation is introduced. The blue circles represent the intial conditions assocated with a nonzero bar from A.

As seen in the previous full lung model initial venous PO_2 is dependent only on V_{C0}. Following the lines in Figure 45B we see the effect of increasing V_{C0} at a fixed initial blood volume. The circles plotted in Figure 45B correspond to the initial venous levels actually used. Each circle corresponds to one for the bars in Figure 45A. In this realization, the ratio of initial tidal volumes to initial blood volume on the RUs varied from 1.21 to 17 and had

an average of 4.7. On a RU with normal $V_{C0} = 350$ and $V_{B0} = 90$ this ratio is 3.89. For ranges of V_{C0} and V_{B0} considered in this distribution this ratio could have ranged from 1 to 18.33. Note that in the Full lung-V_C and Full lung-V_B models this ratio ranged from 1.67 to 6.1 and 2.33 to 11.67, respectively.

We compare the transients for the lethal inflammation on various RUs in Figure 46. The curve with the minimum initial venous PO_2 has the minimum initial tidal volume. This initial PO_2 is comparable to the minimum initial PO_2 level seen in the Full lung-V_C model. The circles on the curves mark the time point when shunting occurs for that given curve. Shunting is determined by the both V_{C0} and V_{B0} levels. As in the Full lung-V_B model there are units that do not shunt.

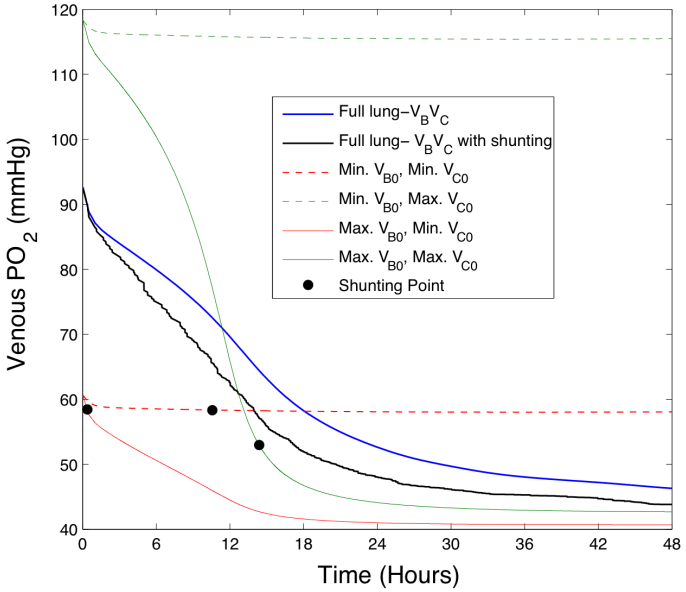

Figure 46: Transients from single RUs and the Full lung-V_BV_C model. Transients for single RUs with with various tidal and blood volume combinations are plotted for an insult triggerd by $TNF_B = 4$. Circles indicate the time point where shunting occured. Also included is the Full lung-V_BV_C model with and without shunting.

In Figure 47 we compare the three full lung models with shunting. Venous PO_2 level for the Full lung-V_BV_C and Full lung-V_C model are similar during early stages of the insult since both models have RUs that shunt early. However, since all RUs are shunting in the Full lung-V_C model and there are non-shunting units in the Full lung-V_BV_C model, these curves eventually pull farther apart. In the later stages of the insult the Full lung-V_B and Full

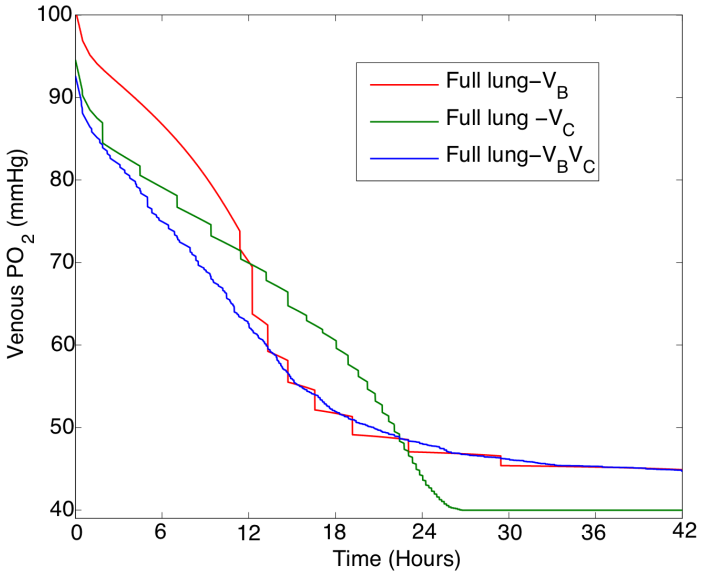

Figure 47: Comparsion of Full lung-V_B, Full lung-V_C, and Full lung-V_BV_C models with shunting. For all model the insult was triggered by an insult of $TNF_B = 4$.

lung-V_BV_C are similar, since they both have non-shunting RUs with high PO_2 levels. Results for carbon dioxide follow the same trends as PO_2 with increases rather than decreases.

In all full lung models we see that shunting causes more severe drops during the time-course of the insult. However, there are drops in the PO_2 due to the changes in diffusion due to swelling of the tissue compartment. The Full lung-V_BV_C model is more accurate lung model, since it accounts for difference in both perfusion and ventilation and will be used in future modeling of the full lung.

5.5 CLOSED LOOP RU MODEL

Once the temporal reduction is implemented the RU model runs with reasonable computation times. However, as we saw in the above simulations venous PO_2 levels fall at most to 40 mmHg and venous PCO_2 levels rise to at most 45 mmHg. In order to have a more accurate model we need to include variable arterial levels in the model. Up to this point we have assumed that blood enters the lung with a PO_2 of 40 mmHg and PCO_2 of 45 mmHg, their healthy levels. To correct this we have to created a closed loop RU model where arterial

pressures G_B^0 and C_B^0 are dependent on venous pressures, G_B^{end} and C_B^{end}.

In the absence of inflammation, blood leaves the lung with PO_2 approximately 100 mmHg and CO_2 approximately 40 mmHg. Metabolic processes consume O_2 and produce CO_2 when the blood is not in the lung. Therefore, the blood levels during healthy conditions drop to approximately 40 mmHg and 45 mmHg for O_2 and CO_2, respectively [27]. Once again, in modeling the metabolic process we focused on oxygen first. We calculate arterial PO_2 by first determining content of oxygen at the venous end (ϕ_V). Oxygen content accounts for oxygen both free and bound to hemoglobin in the blood and has units ml/100cc. Content is determined by a standard formula dependent on PO_2 and hemoglobin [27]. Using normal cardiac output (co) of 5000 ml/min and a constant metabolic rate of consumption of oxygen (λ), 150cc/min, we determine arterial content of O_2 (ϕ_A) with the formula $\phi_A = \left(\phi_{_V} - 100\lambda/co\right)$. With ϕ_A we numerically determine arterial PO_2 and hemoglobin from the content formula and the oxyhemoglobin dissociation curve.

For more accurate results we refit our hemoglobin parameters m, k^+, and k^- from equations (5.23) and (5.24). We then fit K_G, the parameter in the source term of the G_A equation, so that under normal condition arterial (entering the RU) and venous PO_2 (exiting the RU) match levels seen clinically for a normal lung, 40 mmHg and 100 mmHg, respectively. After fitting, in the closed model arterial PO_2 (G_B^0) is 39.20 mmHg and venous (G_B^{end}) PO_2 is 100.06 mmHg with no inflammation.

When modeling hemoglobin we considered two states for hemoglobin: fully saturated, Hb_4, and hemoglobin that has needs m oxygen to bind to it in order to become saturated , Hb_m. Not modeling a completely unsaturated hemoglobin does not properly capture the hemoglobin dynamics when PO_2 levels drop below the 40 mmHg (its minimum level in previous results). In the future we will account for completely unsaturated PO_2. At this time we will compare the non-breathing and closed RU models for a nonlethal level of insult of TNF_B, $TNF_B = 2$ (see Figure (48)). Results show that arterial PO_2 now drops as venous PO_2 drops during inflammation. Overall there is a more significant drop in venous PO_2 in the closed RU model than in the non-breathing RU model. Once the hemoglobin equations are reformulated we will implement the effects of metabolism on PCO_2.

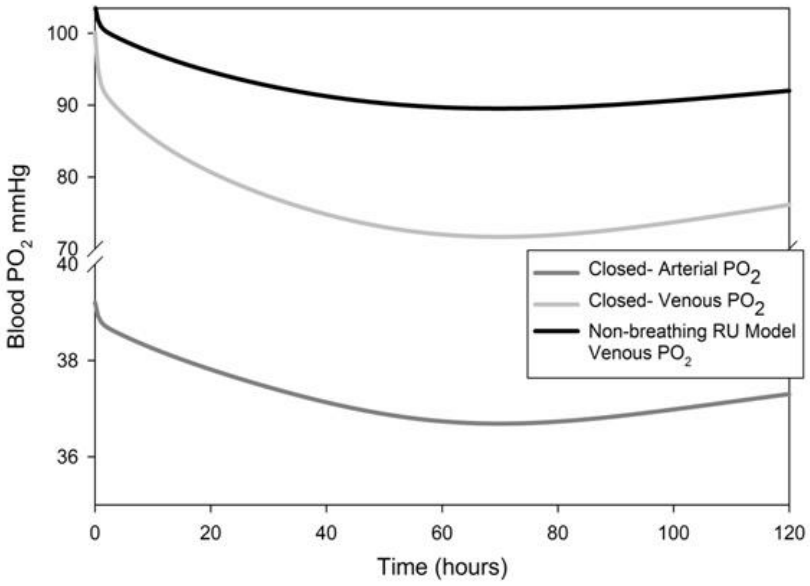

Figure 48: Venous and arterial blood PO_2 levels from the closed RU model. The closed venous and arterial PO_2 are from a simulation of the closed model was with an insult of $TNF_B = 2$. The non-breathing RU model- venous PO_2 curve is from the same insult to the non-breathing model.

5.6 DISCUSSION

We have reduced the RU model developed in the previous chapter in order to more efficiently simulate the full lung with ventilation perfusion mismatch. We developed a spatial reduction that eliminated space along the capillary and a temporal reduction that eliminated the breathing mechanism in the RU model. The spatial reduction method was designed such that gas pressure levels at the end of the capillary were retained. However, the spatial reduction as is was not an effective method to eliminate long computation times. Therefore, we only implemented a temporal reduction, which consisted of temporal averaging over the breathing cycle. This eliminated the breathing mechanism, which consisted of switching back and forth from inspiration (increasing alveolar air space volume) to expiration (decreasing alveolar air space volume) with a period of four seconds. This drastically reduced computation times and allowed us to implement more accurate ventilation perfusion mismatch.

In the breathing RU model we only considered mismatch introduced by varying the

initial tidal volumes of the RUs, which alters only ventilation . However, within the actual lung ventilation and perfusion, both can differ [27]. With the non-breathing model, we are able to easily introduce any initial compartmental and tidal volumes on the RUs. The Full lung-V_BV_C model has the most accurate full lung model we considered because it accounts for changes in perfusion and ventilation. However, first considering the Full lung-V_C and Full lung-V_B models allowed us to explore how changing perfusion and ventilation contribute to overall dynamics. We see that the changes in V_{B0} do not affect the initial levels of PO_2. However, significant decreases in V_{B0} give rise to RUs which do not have significant drops in PO_2. Also, the effects of shunting are observed in the later stages of the insult compared to the Full lung-V_C model. Changes in V_{C0} affect the initial conditions with higher initial tidal volume causing higher initial PO_2 levels and shunting effects are seen throughout the insult. In the Full lung-V_BV_C we see a combination of these effects with initial conditions similar to those of the Full lung-V_C model and venous levels slightly above the fixed arterial level of 40 mmHg at the end of the insult as seen in the Full lung-V_B model. Due to more variety in the closing times of the RUs in the Full lung-V_BV_C model there is a more gradual decrease in the shunting transient than in the other full lung models. There is a more gradual separation of the with and without shunting transients than in the previous full lung models, since there is more variety in the closing time among the RUs (Figure 47). Results are similar for PCO_2 but with increasing instead of decreasing levels.

Once we had explored the effects of altering perfusion and ventilation, we increased the biological accuracy of the model by implementing feedback from venous PO_2 onto arterial PO_2. Therefore, the arterial level is no longer fixed and decreases due to drops in the venous PO_2. This causes more significant drops in PO_2 than seen in previous versions of the model. During severe inflammation these more significant drops nullify an assumption we made regarding the saturation levels of hemoglobin. Therefore, with the hemoglobin equations as is, the closed model is only effective at low levels of inflammation. Reformulating our derivation of the hemoglobin equation will create a model that is accurate during severe inflammation.

We have created a method to model the full lung with inflammation and heterogeneity within its units. This model allowed us to explore overall lung and single RU unit results

during an insult. Once the closed RU unit is adjusted to account for severe drops in PO_2, we will look at the closed full lung model by linking the multiple closed RUs with the distribution used in Full lung-V_BV_C model. With this model we can alter the immune subsystem so that we model a specific disease, such as pneumonia and influenza. In this form we can explore the effect of these diseases on PO_2 and PCO_2 levels. Additionally, ventilation and perfusion ratios (rate of ventilation over the rate of perfusion), PO_2 and PCO_2 levels are measurable in patients. This provides data during these insults for which we can calibrate and verify are full model once metabolic consumption of oxygen is included.

The lung is a common site for secondary infections and typically the first organ to fail during MODS, even when the insult is not initially via the lungs. Therefore, we will also consider the spread of inflammation to and from the lung by connecting the closed full lung model and the compartmental model. To increase the biological fidelity of the innate immune responses within the lung, we can replace the simplified immune subsystem used in these simulations with the compartmental model. With this more accurate immune system we can explore PO_2 levels during inflammation that results in health, aseptic or septic death.

6.0 CONCLUSION

6.1 THESIS SUMMARY

We have developed and analyzed three mathematical models of acute inflammation. These models were developed in order to look at various aspects of multiple organ dysfunction syndrome (MODS). This disease is the leading cause of death in ICU patients [11]. The treatment options for MODS are limited and do not focus on the elimination of inflammation or stopping its spread from one organ to the next. These models serve as an initial step in understanding the dynamics that drive the spread of inflammation. Understanding these complex interactions will facilitate the development of effective treatment options for MODS.

Our first model includes pro- and anti- inflammation with pathogen as an initiating event. Giving anti-inflammatory therapy as a treatment for MODS were experimentally tested with little success ([63], [65]). Therefore, we use this simple model to explore the role of anti-inflammatories during the immune response. The model was developed via a subsystem approach. This allowed us to ensure that proper dynamics were captured between interacting variables. These subsystems were combined to form the four variable ODE model, which we refer to as the reduced model. This model has clinically relevant outcomes represented by fixed points (health, aseptic and septic death).

In order to analyze the effects of anti-inflammatories, we used this model to determine the basins of attraction in various scenarios and to model the administration of an anti-inflammatory treatment. The results from these simulations showed that anti-inflammatories play a significant role in restoring health during an infection. Our results also illustrate that altering the levels of anti-inflammatories either at a given time point or by fixing their levels during the response to an infection may compromise outcomes. This result has been

observed clinically. Administration of steroids, an anti-inflammatory mediator, to severely septic patients has clearly decreased survival. ([63], [65]). Our model shows that repeatedly administering anti-inflammatories as a treatment is not effective, since this eliminates the dynamics in the anti-inflammatory population, increasing sensitivity to secondary insults.

The reduced model gave us insight into the overall dynamics between pro- and anti-inflammation. However, to model the spread of inflammation we needed a model that included variables from specific pro- and anti- inflammatory mediators and cells in both the blood and tissue. Therefore, we expanded this model into our compartmental model, which consists of immune components in the blood and tissue and has variables corresponding to TNF and IL-10 levels. Modeling specific mediators will allow for calibration of the model to data. Separating the blood and tissue allows us to explore the effects of manipulating both the local (tissue) and systemic (blood) responses on the spread of inflammation between multiple tissue units linked to the same blood unit. Complexity was added to the equations as needed to capture known biological behavior of the system. Adding complexity to these models makes the overall behavior of the system less intuitive.

The interactions between the tissue and blood are essential in eliminating the pathogen and restoring homeostasis. This two compartment ODE model accounts for the communication between the tissue and blood and has the same outcomes as the reduced model. This model is a minimal model of an organ. Therefore, we explore the spread of inflammation between organs by linking two tissue compartments to the same blood supply. We considered linked organs with the same parameter values, with various levels of pathogen and neutrophil diffusion, and with difference in their source of resting macrophages. This allows us to explore the effect of altering the local versus the innate immune response initiated in the blood.

Changing diffusive properties within an organ alters the communication between compartments. When the organ is more diffusive there is an increase in the influx of neutrophils, this causes tissue damage to accumulate more readily while the infection is being eliminated. Therefore, more diffusive organs are more likely to enter aseptic death, but their increased neutrophil levels protect them against septic death. When a normal and more diffusive organ are linked, the onset of death occurs at higher pathogen loads compared to a single

normal organ. The more diffusive organ accumulates more damage than the normal organ. Therefore, there is a range of initial tissue pathogen of which inflammation spreads to the second organ despite a healthy outcome in the insulted organ. Exploring this phenomenon further will likely give insight into why the lung is typically the first organ to fail during MODS, even when the initial insult is not in the lung [42].

Changing diffusion alters the response via the blood. In order to study the effects of changing the immune response within the tissue we increased the levels of resting macrophages in an organ. This increased the overall response without the damage associated with high neutrophil influx to an infected organ, since the local macrophages have eliminated more of the pathogen than in a normal organ. Linking a normal organ and an organ with increased macrophages to the same blood supply increases the thresholds for death without increasing tissue damage and therefore is the more effective means of protecting an organ. We hypothesize that protection via tissue macrophages allows the liver to be highly resistant to infection, rarely becoming inflamed despite being the first organ to provide an immune response to many types of insults via the gut [55].

Differences in the accumulation of damage during the local and innate response is what allows increases in local response to be more beneficial. Minimal damage is produced when pathogen is eliminated by macrophages compared to neutrophils. Validity of this assumption need to be established before making conclusions of the effectiveness of increasing the local macrophages.

The lung is highly likely to be affected during MODS. However, modeling the lung with the compartmental model does not account for interaction with the air, which is essential to the function of the lung. Therefore, we have developed a full lung model that accounts for gas exchange and inflammatory effects that accounts for the air, blood and tissue compartment dynamics. This model is multiscale in that it takes into account gas exchange within a single respiratory unit (RU) and combines the output of single RUs to determine the full lung model results. Heterogeneity between RUs was introduced by altering their compartment volumes.

To our knowledge, this is the first gas exchange model to treat tissue as a compartment. This allowed us to simulate the swelling of the tissue due to the immune response. Other mathematical models of the lung have concentrated on many aspects of the lung function

such as mechanics, gas exchange, drug deposition, and circulation. The models that include gas exchange treat the tissue layer as a simply the barrier between the air and blood ([7], [28], [29], [39], [46]).

In its original form the full model lung was computational expensive due to the breathing mechanism. Both a temporal and spatial reduction were applied to the model. The temporal average on the breathing cycle reduced running times drastically and allows the model to be used with ease in various scenarios of ventilation perfusion mismatch. The spatial reduction was not effective compared to the temporal reduction and, in the end, was not applied to the full lung model.

In the original breathing full model we only introduced ventilation perfusion mismatch via a distribution in the initial tidal volumes on the single RUs. However, heterogeneity in the lung is due to RUs differences in air and blood supply. With the non-breathing we introduced various distributions in the initial tidal and/or blood volumes of the RUs. Our Full lung-V_BV_C model best mimics the conditions within the lung, since it accounts for heterogeneity in both perfusion and ventilation. However, looking at the Full lung-V_C and Full lung-V_B models allowed us to explore the effects of changing perfusion and ventilation independently. Changes in the initial blood volume do not affect the initial levels of PO_2. However, significant decreases in V_{B0} give rise to RUs which do not have significant drops in PO_2, since changes in blood volume affect the inflammation variable. Also, the effects of shunting are seen in the later stages of the insult compared to the Full lung-V_C model. Changes in V_{C0} affect the initial conditions with higher initial tidal volume causing higher initial PO_2 levels and shunting effects are seen throughout the insult. In the Full lung-V_BV_C we see the a combination of these effects with initial conditions similar to those of the Full lung-V_C model and venous levels slightly above the fixed arterial level of 40 mmHg at the end of the insult as seen in the Full lung-V_B model. More variety in the closing time among the RUs in the Full lung-V_BV_C model causes a more gradual decrease in the shunting than the other full lung models (Figure 47).

In all simulations of the breathing and non-breathing model, the venous PO_2 and PCO_2 approach their fixed arterial levels. Dropping venous PO_2 does not affect the level of arterial PO_2 and rising PCO_2 does not affect arterial PCO_2. However, outside of the lung metabolic

process consume oxygen and produce carbon dioxide ([27]). A fixed arterial level assume that these metabolic processes are adjusted throughout inflammation, so that the arterial level is maintain. In actuality, the metabolic processes cause drops in venous PO_2 to give rise to drops in arterial PO_2 and the opposite holds for PCO_2. We have modeled this metabolic process forming a close loop lung model. This model shows correlated arterial and venous levels. This now allows PO_2 levels to drop to levels which correspond to nearly unsaturated hemoglobin. These levels were not seen in previous simulation and nullify the assumptions made regarding hemoglobin dynamics. Therefore, this model is effective for non-lethal insults to the lung.

Once hemoglobin in the closed loop model is corrected we can consider a closed full lung model. With this model we can assume a more accurate distribution that accounts for position of RUs within lung and compare results to experimental data collected for ventilation perfusion during respiratory distress ([17], [59], [60], [2]). Additionally, the immune subsystem can be replaced with a model of a specific disease, such as pneumonia or influenza. With this we can explore changes in PO_2 and PCO_2 levels during a specific disease.

With these three model we have explored main aspects of inflammation. We have investigated the role of anti-inflammation, the interactions between the blood and tissue during an immune response, communication between organs, and inflammatory effects on the gas exchange within a RU and on overall lung function during a lethal insult. All of these are various aspects of inflammation that play a role in the progression of MODS. These are model are an initial step in developing models which can facilitate the advancement of treatment development for MODS. They provided insight into the role of inflammation and interaction between the local and innate immune response. Using mathematical models to gain insight into the underlying mechanisms of the immune response may provide a means by which to steer the development of treatments such that they address the cause of the organ failure, an overactive immune response. Also using the compartmental and lung models to explore the spread of inflammation to the lung and between organs may give hope to halting the progression of organ failure which will increase the survivability of MODS.

6.2 FUTURE DIRECTIONS

In order to create a usable closed lung model during severe inflammation, we will augment the hemoglobin equations, so that they are accurate during the more severe drop in PO_2. With this closed lung model we will simulate the lung with more accurate ventilation perfusion distributions and compare results to the available data mentioned above.

We would also like to model in lung the spread of inflammation from RU to RU via the tissue rather than the blood. We would have to implement diffusion between the tissue units of RUs if they are spatially close to the inflammation. More elaborate modeling techniques are required to capture this phenomenon. Additionally, mathematical analysis for the resulting tissue interactions may give insight to the spread of inflammation within the lung.

We plan to implement the compartmental model as the immune system within the lung model. This will increase the biological fidelity of the lung model and give more accurate time courses for the inflammation feeding into the gas exchange subsystem. We will then examine venous PO_2 during infection that results in health, aseptic and septic death. Also, with the shortened computation times it is now possible to include feedback from the gas exchange system onto the immune system, such as decreases in neutrophil function at low PO_2 [25]. This form of the model easily allows users to alter parameters within an RU and evaluate their effect on the full lung model.

The compartmental model was fit to heuristics for TNF and IL-10. These cytokines were included, since they are often measured experimentally. We will use data to further calibrate this model. When using this model to explore organ to organ interaction, we will introduce heterogeneity to model specific organs. This will allow us to study the spread of inflammation between specific organs, for example, the liver and kidneys.

After further calibration we hope to use these models as predictive tools and guide experimentation to obtain a greater understanding of interactions on both the cellular and organ levels.

APPENDIX A

PARAMETER EXPLANATION FOR THE REDUCED MODEL

The standard parameter values for both the subsystems and the reduced model from Chapter 2, equations A.1-A.4 (equations 4.9-**??**), are supplied in the tables provided. These parameter values are selected to remain within the given ranges and constraints found in the experimental literature as well as in unpublished data. Details on the derivation of these ranges are given below. Parameters that could not be documented from existing data were estimated such that the subsystems behave in a biologically appropriate manner for all physiologically relevant levels of the anti-inflammatory mediator. Furthermore, when the pathogenic insult is replaced by endotoxin as an initiating event, as presented in Day et al. [18], the resulting model exhibits observed biological behaviors of the immune mediators during repeated endotoxin administrations

Units for N^*, C_A, and D cannot be determined, since they represent various types of cells, signaling proteins such as cytokines, and/or other mediators concurrently. These variables quantify the response of the immune function they represent rather than, for example, an exact cell count. Correspondingly, units of most parameters related to these variables are not in conventional form, but rather in terms of the associated variable. How parameters are estimated in relation to a given subsystem is detailed below along with comments for documented parameters.

Equations:

$$\frac{dP}{dt} = k_{pg}(\left(1 - \frac{P}{P_\infty}\right) - \frac{k_{pm}s_m P}{\mu_m + k_{mp}P} - k_{pn}f(N^*)P \quad \text{(A.1)}$$

$$\frac{dN^*}{dt} = \frac{s_{nr}R}{\mu_{nr} + R} - \mu_n N^* \quad \text{(A.2)}$$

$$\frac{dD}{dt} = k_{dn}f_s(f(N^*)) - \mu_d D \quad \text{(A.3)}$$

$$\frac{dC_A}{dt} = s_c + \frac{k_{cn}f(N^* + k_{cnd}D)}{1 + f(N^* + k_{cnd}D)} - \mu_c C_A \quad \text{(A.4)}$$

$$\text{Where } R = f(k_{nn}N^* + k_{np}P + k_{nd}D) \text{ and}$$

$$fs(V) = \frac{V^6}{x_{dn}^6 + V^6}$$

Tables:

Name	Range	Value	Description	Comments	Sources
k_{pm}	Estimated	0.6/Munits/ hr	Rate at which the non-specific local response (M) eliminates pathogen (P)	1, 5	
k_{mp}	Estimated	0.011/Punits/ hr	Rate at which the non-specific local response (M) is exhausted by pathogen (P)	1,6	
s_m	Estimated	0.005 Munits/hr	Source of non-specific local response (M)	1, 7	
μ_m	0.0013 - 0.0048/hr	0.002/hr	Decay rate for the non-specific local response	1, 8	([34] [80])
k_{pg}	0.021-2.44/hr	Various	The growth rate of pathogen	1, 9	([64]; [70])
p_∞	Estimated	20×10^6 pg/cc	Maximum pathogen population	1, 10	Vodovotz, personal communication
k_{pn}	Maximum 2.5/N-units/hr	1.81/N^*units/ hr	Rate at which activated phagocytes (N^*) consume pathogen	2, 11	[13]

Table 20: Parameters for the reduced model of acute inflammation

Comments:

Name	Range	Value	Description	Comments	Sources
k_{np}	Estimated	$0.1/N^*$units/ hr	Activation of resting phagocytes (N_R) by pathogen	2, 3	
k_{nn}	Estimated	$0.01/N^*$units/ hr	Activation of resting phagocytes by already activated phagocytes and their cytokines	2, 3, 12	
s_{nr}	Estimated	$0.08/N_R$units/ hr	Source of resting phagocytes	2, 3, 13.	
μ_{nr}	0.069-0.12/hr	0.12/hr	Decay rate of resting phagocytes (macrophages and neutrophils)	2, 3, 14	[14]
μ_n	Less than μ_{nr}	0.05/hr	Decay rate of activated phagocytes (macrophages and neutrophils)	2, 3, 15	[14]
k_{nd}	Less than k_{np}	$0.021/D$ units/hr	Activation of phagocytes by tissue damage (D)	3, 16	[3]
k_{dn}	Estimated	$0.35/D$ units/ hr	Max rate of damage production by activated phagocytes (and/or associated cytokines/free radicals)	3	
x_{dn}	Estimated	$0.06/N^*$ units/ hr	Determines level of activated phagocytes (N^*) needed to bring damage production up to half its maximum	3	
μ_d	0.017 minimum	0.02/hr	Decay rate of damage; combination of repair, resolution, and regeneration of tissue	3, 17	[76]
c_∞	Estimated	0.28 $C_A$units	Controls the strength of the anti-inflammatory response	4, 18	[32]
s_c	Estimated	0.0125 $C_A$units/hr	Source of the anti-inflammatory mediator	4, 19	
k_{cn}	Estimated	0.04 $C_A$units/hr	Maximum production rate of the anti-inflammatory mediator	4	
k_{cnd}	Estimated	48 N^*units/Dunits	Relative effectiveness of activated phagocytes versus damage in inducing the production of anti-inflammatory mediators	4	
μ_c	0.15-2.19/hr	0.1/hr	Decay rate of the anti-inflammatory mediator	4, 20	[6], [12], [24], [31]
Hill coeff. for f_s	Postive integers	6	The Hill coefficient used in the production term of tissue damage from the activated phagocytes	3, 21	

Table 21: Table of parameters continued.

1) The non-specific local immune response/pathogen (M/P) subsystem with the M equation in quasi state gave rise to the first two terms of the pathogen equation, equation A.1. The parameters in these terms were fit such that the pathogen equation is bistable for k_{pg} below 1.5/hr, which is where the health state loses stability. The k_{pg} level 1.5 was chosen such that for most physically observed pathogen growth rates the outcome of health is stable.

2) The activated phagocytes/pathogen (N^*/P) subsystem was fit such that for low pathogen growth rate (k_{pg}) health is the only stable state, and at a moderately high k_{pg} septic death exists and is stable. Parameters in this subsystem were first estimated so that these general dynamics occurred for a significant range of the physiologically possible levels of the anti-inflammatory mediator. They were then adjusted so that the reduced model and the altered model for endotoxin [18] exhibited observed biological behaviors of the immune mediators in the presence of pathogen (see comment 4) and endotoxin, respectively.

3) The activated phagocytes/tissue damage (N^*/D) subsystem was initially fit such that for physiologically relevant levels of the anti-inflammatory mediator the system is bistable between health and aseptic death with a reasonable basin of attraction for the health state. Adjustments were then made so that the reduced model and the altered model for endotoxin [18] exhibited observed biological behaviors of the immune mediators the presence of pathogen (see comment 4) and endotoxin, respectively.

4) Once the anti-inflammatory mediator (C_A) was incorporated in the model as a dynamic variable, the parameters where adjusted so that the reduced model now has the following behavior (1) the model is bistable between the health and aseptic death states for low k_{pg} with a plausible basin of attraction for the health state, (2) for moderate to high k_{pg} all three states (health, aseptic death, and septic death) are stable, and (3) as k_{pg} continues to increase the health state and the aseptic death state lose stability.

5) The parameter, k_{pm}, quantifies the ability of the local non-specific immune response to clear pathogen. This response is comprised of local factors such as defensins, local macrophages, and non-specific antibodies (e.g. IgA's). This response is considered to be less efficient than the phagocyte driven response, which yields the constraint $k_{pm}<k_{pn}$. The value of this parameter was estimated such that the local non-specific immune response can

be overwhelmed with a modest to large inoculum of pathogen.

6) The rate at which the local non-specific immune response is exhausted, k_{mp}, was set so that $\frac{k_{pm}s_m}{\mu_m} = 1.5/\text{hr}$.

7) The parameter, s_m, representing the source of the local non-specific immune response (M) was estimated to balance, μ_m, the decay rate of M. These parameters are closely related since the ratio $\frac{k_{pm}s_m}{\mu_m} = 1.5/\text{hr}$ and at health state $M = \frac{s_m}{\mu_m}$.

8) The range for the decay rate of the non-specific local immune response, μ_m, was based on the reported half-lives of immunoglobulin G and A, which are non-specific antibodies probably key in this response. These half-lives were documented in the textbook Immunobiology Fig. 4.16 on page 143 [34] and Table 1 of Zouali et al. [80].

9) Though changed throughout our simulations, the physiologically relevant range for the growth rate of pathogen, k_{pg}, was taken from Todar's Online Textbook of Bacteriology [70], which uses references from Spector's textbook, Handbook of Biological Data [64].

10) The maximum pathogen level, p_∞, was estimated from a lethal model of E.coli rat peritonitis from unpublished data received via personal communication with Y. Vodovotz.

11) We based our estimation for the maximum of k_{pn}, the rate at which activated phagocytes consume pathogen, on the observed mean rate of phagocytosis by macrophages in the presence of unlimited supply of particles up to 20 microns. This result is from the abstract of Branwood et al. [13]. This is taken as the maximum since the supply of pathogen is limited under normal circumstances.

12) The parameter, k_{nn}, corresponding to the rate of activation of resting phagocytes by those previously activated, was estimated while to ensure $\mu_n > \frac{s_{nr}k_{nn}}{\mu_{nr}}$. This inequality must hold for the health state to be stable.

13) The source of resting phagocytes, s_{nr}, was set to ensure a stable concentration of resting phagocytes (N_R) in the health state. As with the other source parameter, s_m, this s_{nr} was adjusted to balance the decay rate of resting phagocytes. These parameters are related since at health $N_R = \frac{s_{nr}}{\mu_{nr}}$.

14) The range for the decay rate of the resting phagocytes, μ_{nr}, was calculated from the half-lives (6-20 hours) of circulating neutrophils presented in Coxon et al. [14].

15) The half-life of activated phagocytes, μ_n, is longer than the half-life of resting phago-

cytes, μ_{nr} , due to delayed apoptosis in the activated population; therefore $\mu_n < \mu_{nr}$ [14].

16) The peak of the activated phagocyte response elicited from pathogen, k_{np}, is greater than that triggered by damage, k_{nd}; therefore, $k_{nd} < k_{np}$.

17) The minimum for μ_d, which represents tissue repair, resolution, and regeneration, was estimated from data in Wang et al. [76]. We used the half-life of HMG-1 (HMGb-1), since it is a histone tethering protein leaked by damaged cells as a surrogate for the many danger molecules that perpetuate the inflammatory signal. Wang and colleagues give data for HMG-1 levels during an inflammatory response to bacterial lipopolysaccharide (LPS). Therefore, we estimated the lower limit as the slope of the data shown in Fig. 1C of Wang et al. [76] during the decay phase of HMG-1. It would be unrealistic to set μ_d to a value higher than the time constant of a recognized marker of cellular injury.

18) The value for c_∞ was set such that corresponds to ≈75% inhibition, i.e. , when C_A reaches maximum value in response to an insult. We set this to be approximately 75% because Fig. 6B in Isler et al. [32] shows that when the anti-inflammatory mediator, IL-10, is blocked with anti-IL10 there is approximately a 75% increase in the production of IL-12 (a pro-inflammatory cytokine produced by activated phagocytes).

19) Organisms have constitutive levels of anti-inflammatory effectors. Therefore the source parameter, sc, was chosen to balance the corresonding documented half-life, μ_c. These parameters are related because at the health state $C_A = \frac{s_c}{\mu_c}$.

20) Anti-inflammatory signals have downstream cellular effects not explicitly modeled herein, lasting longer than the effector cytokines or molecules producing them. Therefore, the value for μ_c was set at the lower limit of reported half-lives of anti-inflammatory effectors, which were estimated from pg. 130 of Bacon et al. [6], Table 1 on pg. 277 of Bocci [12], pg. 291 of Fuchs et al. [24], and the abstract of Huhn et al. [31].

21) The Hill coefficient for Equation A.3 was set to six so that the response of tissue damage to activated phagocytes is not hypersensitive. A lower Hill coefficient would not appropriately represent this. In other words, it is biologically plausible that low levels of activated phagocytes do not trigger significant amounts of damage that could lead to a positive feedback capable of sustaining aseptic death. Also, for values six and higher, there was not a significant difference in the sensitivity of damage to the activated phagocytes.

Contrary to the common inference regarding the use of Hill coefficients in enzymatic kinetics, we are not implying that a cooperativity-based mechanism is at work.

APPENDIX B

XPP CODE OF THE REDUCED MODEL AND ITS SUB-SYSTEMS

XPPAUT code for the development and analysis of the reduced model. Followed by the code for the reduced model.

B.1 ACTIVATED PHAGOCYTES AND PATHOGEN SUBSYSTEM:

#Code:

key: #-comment, par-parameter, x'-differential equation for variable x, @-numeric command

#Parameters

par ca=0, d=0

par kpm=0.6, pinf=20, sm=.005, kmp=.01, mum=.002, kpg=.3, kpn=1.8

par mun=.05, snr=.08, munr=.12, knd=0.02, knp=0.1, knn=.01

par mud=.02, kdn=.35, xdn=.06, qna=6

par sc=0.0125, cinf=0.28

par muc=.1, kcn=.04, kcnd=48

#Notes:

#1) qna=Hill coefficient

#2) μ in equations from the main text was replaced by mu in the code above.

#3) d and ca are treated as parameters.

```
# Function Definitions
f(x,y)=x/(1+y^2)
R=f((knd*d+knp*p+knn*na),ca/cinf)

#Equations

p' =kpg*p*(1-p/pinf)-kpm*sm*p/(mum+kmp*p)-kpn*f(na,ca/cinf)*p

na'=snr*R/(munr+R)-mun*na

#Initial Conditions
na(0.0)=0.0
p(0.0)=0.0

#Numerical Specifications
@ method=rk, tol=0.0001, dt=0.1, total=200.0, bounds=10000000
@ xlo=0, xhi=3, ylo=0, yhi=3, bell=0
@ maxstore=100000
done
```

B.2 ACTIVATED PHAGOCYTES/ TISSUE DAMAGE SUBSYSTEM:

#Code:

```
# key: #-comment, par-parameter, x'-differential equation for variable x, @-numeric command

#Parameters
```

```
par p=0, ca=0
par kpm=0.6, pinf=20, sm=.005, kmp=.01, mum=.002, kpg=.3, kpn=1.8
par mun=.05, snr=.08, munr=.12, knd=0.02, knp=0.1, knn=.01
par mud=.02, kdn=.35, xdn=.06, qna=6
par sc=0.0125, cinf=0.28
par muc=.1, kcn=.04, kcnd=48

#Notes:
#1) qna= Hill coefficient
#2) μ in equations from the main text was replaced by mu in the code above.
#3) d and ca are treated as parameters.

#Function Definitions
fs(x,v,hill)=x^hill/(v^hill+x^hill)
f(x,y)=x/(1+y^2)
R=f((knd*d+knp*p+knn*na),ca/cinf)

#Equations

na'=snr*R/(munr+R)-mun*na

d'=kdn*fs(f(na,ca/cinf),xdn,qna)-mud*d

#Initial Conditions
d(0.0)=0.0
na(0.0)=0.0

#Numerical Specifications
@ method=rk, tol=0.0001, dt=0.1, total=200.0, bounds=10000000
@ xlo=0, xhi=3, ylo=0, yhi=3, bell=0
```

@ maxstore=100000

done

B.3 ACTIVATED PHAGOCYTES, PATHOGEN, AND TISSUE DAMAGE SUBSYSTEM (THREE VARIABLE SUBSYSTEM):

#Code:

key: #-comment, par-parameter, x'-differential equation for variable x, @-numeric command

#Parameters

par ca=0

par kpm=0.6, pinf=20, sm=.005, kmp=.01, mum=.002, kpg=.3, kpn=1.8

par mun=.05, snr=.08, munr=.12, knd=0.02, knp=0.1, knn=.01

par mud=.02, kdn=.35, xdn=.06, qna=6

par sc=0.0125, cinf=0.28

par muc=.1, kcn=.04, kcnd=48

#Notes:

#1) qna=hill coefficient

#2) μ in equations from the main text was replaced by mu in the code above.

#3) ca is treated as parameters

Function Definitions

fs(x,v,hill)=x^hill/(v^hill+x^hill)

f(x,y)=x/(1+y^2)

R=f((knd*d+knp*p+knn*na),ca/cinf)

#Equations

p' =kpg*p*(1-p/pinf)-kpm*sm*p/(mum+kmp*p)-kpn*f(na,ca/cinf)*p

na'=snr*R/(munr+R)-mun*na

d'=kdn*fs(f(na,ca/cinf),xdn,qna)-mud*d

#Initial Conditions
d(0.0)=0.0
na(0.0)=0.0
p(0.0)=0.0

#Numerical Specification
@ method=rk, tol=0.0001, dt=0.1, total=200.0, bounds=10000000
@ xlo=0, xhi=2, ylo=0, yhi=2, bell=0
@ maxstore=100000
done

B.4 REDUCED MODEL (FULL MODEL):

#Code

key: #-comment, par-parameter, x'-differential equation for variable x, @-numeric command

#Parameters
par kpm=0.6, pinf=20, sm=.005, kmp=.01, mum=.002, kpg=.3, kpn=1.8
par mun=.05, snr=.08, munr=.12, knd=0.02, knp=0.1, knn=.01
par mud=.02, kdn=.35, xdn=.06, qna=6
par sc=0.0125, cinf=0.28
par muc=.1, kcn=.04, kcnd=48

```
#Notes:
#1) qna=hill coefficient
#2) μ in equations from the main text was replaced by mu in the code.

#Function Definitions
fs(x,v,hill)=x^hill/(v^hill+x^hill)
f(x,y)=x/(1+y^2)
R=f((knd*d+knp*p+knn*na),ca/cinf)

#Equations

p' =kpg*p*(1-p/pinf)-kpm*sm*p/(mum+kmp*p)-kpn*f(na,ca/cinf)*p

na'=snr*R/(munr+R)-mun*na

d'=kdn*fs(f(na,ca/cinf),xdn,qna)-mud*d

ca'=-muc*ca+sc+kcn*f(na+kcnd*d,ca/cinf)/(1+f(na+kcnd*d,ca/cinf))

#Initial Conditions
ca(0.0)=0.125
d(0.0)=0.0
na(0.0)=0.0
p(0.0)=0.0

#Numerical Specifications
@ method=rk, tol=0.0001, dt=0.1, total=200.0, bounds=10000000
@ xlo=0, xhi=200, ylo=0, yhi=10, bell=0
@ maxstore=100000
done
```

APPENDIX C

XPP CODE FOR THE COMPARTMENTAL MODEL

XPP-AUT code for the compartmental model and the two organ system created by linking two tissue compartments to the same blood supply.

C.1 SINGLE TISSUE UNIT CODE:

%CODE:

% KEY %-comments, par-parameters, x'-differential equation for variable x, @-numeric commands

C.1.1 %PARAMETERS

% Source and decay rates

par sm=10, snb=10, sb=0.0075, sbb=0.0075

par mum=0.12, muma=0.05, mul=3, mulb=3, mut=1.8, mutb=1.8

par munb=0.12, munba=0.05, muna=0.05, muimin=0.005, muimax=.34

par muibmin=0.005, muibmax=0.34, mur=4, murb=4

% Growth rate and population maximum for pathogen in the tissue and the blood

par kpg=0.6, pinf=20000, pbinf=20

% Tissue repair rate and the maximum of tissue integrity is set to one.

par ktg=2, tinf=1

% Diffusion baseline (db_) and facilitate (df_)

par dbmol=10, dfmol=1, dbn=.005, dfn=50, dbp=1, dfp=1

% Portion of the neutrophil and macrophage population that remains when neutrophils and macrophages fit pathogen.

% For example, r1=0.98 means that the depletion term in the tissue neutrophils equation for their interaction with pathogen is

% multiplied by (1-r1).

par r1=0.98,r2=0.98, q=1

% Background immune system parameters

par kpb=.46,kpbb=.46, mub=0.0023,mubb=0.0023,kbp=0.0001,kbbp=0.02

% Activation of macrophages and neutrophils

par kmp=40, kmtcell=20, kmtmol=5, kmrcell=0.01, knpbcell=5, knlbmol=0

par kntbcell=2, kntbmol=0.8, knrbcell=0.1

% Cytokine production

par kmai=1000

par kmat=3000

% Depletion of pathogen

par kmappath=2.8, kmapcell=0

par knappath=5.8,knapbpath=.04, knapcell=5, knapbcell=5

% Tissue depletion from radicals

par krtt=0.01

%Radical production terms

par krtr=0.1, knar=0.01, knarb=0.01, knatr=0.01, krntp=0.2, krtmp=0.00001

% Inflammation growth rate, decay rate, and Hill constant

par ktz=0.5, b=.01, xtz=20, kzti=0.1, thillz=2

% Threshold for tissue integrity. If TI falls below parameter a, TI cannot repair itself.

par a=.1

% Hill parameters for activation triggered by TNF

par xtb=2, xt=20, thill=2

% Inhibition parameters

par il10bar=200, ci=.05, il10bbar=200,cib=.05, il10tbar=60,cit=.000001

par il10tbbar=15,citb=.000001,il10nbar=80,cin=.15,il10nbbar=80,cinb=.15

par fie=3, fite=5, fibe=3, fitbe=3, fine=1, finbe=1

% Parameters for the increase of resting neutrophil source during inflammation

par ksnb=3, xsnb=200, hillsnb=2

% Hill parameters for the interactions involving pathogen

par xpma=200, xpna=1500, phill=3, xpb=.1, pbhill=1

%Diffusion parameters

par utexp=2,ltexp=1

par at=50, bt=0.8, ab=2000

par b1=1, c1=1

% Compartmental volume

par vb=50

par vt=.5

% Hill parameters for the production of TNF

par xma=80, mahill=2

% Hill parameters for the production of IL-10 and the changes in the decay rate of IL-10 during inflammation

par vi=8, hilli=2, xmi=140,hillmi=2, pro=1, vib=8

% This parameter is set to zero to turn off all neutrophil interactions

par naonoff=1

% This parameter is set to zero to turn off all macrophage interactions

par maonoff=1

C.1.2 % FUNCTION DEFINITIONS

% Hill equation

f(x,v,hill)=x^hill/(v^hill+x^hill)

% Inhibition functions

fi(x,y)=x*((1-ci)/(1+(y/il10bar)^fie)+ci)

fin(x,y)=x*((1-cin)/(1+(y/il10nbar)^fine)+cin)

fit(x,y)=x*((1-cit)/(1+(y/il10tbar)^fite)+cit)

fitb(x,y)=x*((1-citb)/(1+(y/il10tbbar)^fitbe)+citb)

fib(x,y)=x*((1-cib)/(1+(y/il10bbar)^fibe)+cib)

finb(x,y)=x*((1-cinb)/(1+(y/il10nbbar)^finbe)+cinb)

% Diffusion functions

dmol=dbmol*(1+z*dfmol)

dn=dbn*(1+z*dfn)

dp=dbp*(1+z*dfp)

% growth rate of the pathogen is assumed to be the same in the tissue and blood.

kpbg=kpg

% Diffusion of pathogen from the blood to the tissue

pbdiff(x,a)=a*x

% To reduce computation times p13(x) is used to estimate the cube root of x.

p13(x)=1.02*(1+x)^(1/3)*x/(.5+x)

% Diffusion of pathogen from the tissue into the blood is dependent on surface area of the population

ptdiff(x,a,b,upperexp,lowerexp)=a*p13(x)*p13(x)/(1+b*p13(x))

% Allows you to plot the activation of macrophages due to TNF during simulations

aux tnfact=kmtcell*fi(m*f(tnf,xt,thill),il10)

% Allows you to plot the activation of macrophages due to pathogen during simulations

aux pact=kmp*fi(m,il10)*f(p,xpma,phill)

% Allows you to plot the decay rate of IL-10 in the tissue during simulations

aux mui=(muimax-pro*(muimax-muimin)*(il10^hilli)/(vi^hilli+il10^hilli))

% Allows you to plot the source rate of neutrophils during simulations

aux sourcen=snb+ksnb*f(b1*nba+c1*na,xsnb,hillsnb)

C.1.3 %EQUATIONS: b-denotes blood

```
% PATHOGEN EQUATIONS
    p'=kpg*p*(1-p/pinf)-kmappath*fi(ma*f(p,xpma,phill),il10)
    -knappath*fin(na*f(p,xpna,phill),il10)-sb*kpb*p/(mub+kbp*p)
    +dp*pbdiff(pb,ab)/vt-dp*ptdiff(p,at,bt,utexp,ltexp)/vt

    pb'=kpbg*pb*(1-pb/pbinf)-knapbpath*finb(nba*f(pb,xpb,pbhill),il10b)
    +dp*ptdiff(p,at,bt,utexp,ltexp)/vb -dp*pbdiff(pb,ab)/vb
    -sbb*kpbb*pb/(mubb+kbbp*pb)

    % MACROPHAGE EQUATIONS
    m'=sm-mum*m-maonoff*(kmp*fi(m*f(p,xpma,phill),il10)
    +kmtcell*fi(m*f(tnf,xt,thill),il10) +kmrcell*fi(m,il10)*rad)

    ma'=-muma*ma+maonoff*(kmp*fi(m*f(p,xpma,phill),il10)
    +kmtcell*fi(m*f(tnf,xt,thill),il10) +kmrcell*fi(m,il10)*rad)
    -(1-q)*kmapcell*fi(p*ma,il10)

    % TNF EQUATIONS
    tnf'= -mut*tnf+dmol*(tnfb-tnf)/vt-kmtmol*fi(m*f(tnf,xt,thill),il10)
    +kmat*fit(f(ma,xma,mahill),il10)

    tnfb'= -mutb*tnfb+dmol*(tnf-tnfb)/vb-kntbmol*finb(nb*f(tnfb,xtb,thill),il10b)

    % NEUTROPHIL EQUATIONS
    nb'=(snb+ksnb*f(b1*nba+c1*na,xsnb,hillsnb))-munb*nb
    -naonoff*(kntbcell*finb(nb*f(tnfb,xtb,thill),il10b)+knrbcell*finb(nb*radb,il10b)
    +knpbcell*fib(nb*f(pb,xpb,pbhill),il10b))

    na'= -muna*na+dn*nba/vt-(1-r1)*knapcell*fin(na*f(p,xpna,phill),il10)
```

```
nba'=-munba*nba-dn*nba/vb+naonoff*(knpbcell*finb(nb*f(pb,xpb,pbhill),il10b)
+kntbcell*finb(nb*f(tnfb,xtb,thill),il10b)+knrbcell*finb(nb*radb,il10b)
-(1-r2)*knapbcell*finb(nba*f(pb,xpb,pbhill),il10b))

% IL-10 EQUATIONS
il10'= -(muimax-pro*(muimax-muimin)*(il10^hilli)/(vi^hilli+il10^hilli))*il10
+dmol*(il10b-il10)/vt+kmai*fi(f(ma,xmi,hillmi),il10)

il10b'= -(muibmax-pro*(muibmax-muibmin)*(il10b^hilli)/(vib^hilli+il10b^hilli))*il10b
+dmol*(il10-il10b)/vb

% RADICAL EQUATIONS
rad'= -mur*rad+dmol*(radb-rad)/vt+krtr*rad*(ti)+knar*fin(na,il10)+knatr*na*(ti)
+krntp*na*p*(ti)+krtmp*ma*p*(ti)

radb'=-murb*radb+dmol*(rad-radb)/vb+knarb*finb(nba,il10b)

% TISSUE INTEGRITY EQUATION
ti'=ktg*ti*(1-ti/tinf)*(ti-a)-krtt*rad*ti

% INFLAMMATION EQUATIONS
z'=ktz*(f(tnf,xtz,thillz)+kzti*(tinf-ti))*(1-z)-b*z

% INITIAL CONDITION FOR TISSUE INTEGRITY
ti(0)=1
```

C.1.4 %NUMERICS

```
@ method=qrk, tol=0.0001, dt=0.1, total=200.0, bounds=10000000
    @ xp=t,yp=p, xlo=0, xhi=200, ylo=0, yhi=20, bell=0
    @ maxstore=10000
```

C.2 TWO ORGAN SYSTEM

The following XPP-AUT code simulates of multiple tissue compartments connected to the same blood compartment.

%CODE:

% KEY %-comments, par-parameters, x'-differential equation for variable x, @-numeric commands

% Up to three tissue units connected to one blood unit

C.2.1 %PARAMETERS: b-denotes blood

% Source and decay rates

par sm1=10, sm2=10,sm3=10, snb=10, sb1=0.0075, sb2=0.0075,sb3=0.0075,sbb=0.0075

par mum1=0.12, mum2=0.12, mum3=0.12, muma1=0.05, muma2=0.05,muma3=0.05

par mul1=3, mul2=3, mul3=3, mulb=3, mut1=1.8, mut2=1.8, mut3=1.8,mutb=1.8

par munb=0.12, munba=0.05, muna1=0.05, muna2=0.05, muna3=0.05,mui1min=0.005

par mui1max=.34,mui2min=0.005, mui2max=.34,mui3min=0.005, mui3max=.34

par muibmin=0.005, muibmax=.34, mur1=4,mur2=4, mur3=4, murb=4

% Growth rate and population maximum for pathogen in the tissue and the blood

par kpg1=0.6, kpg2=0.6, kpg3=.6, kpbg=.6

par pinf1=20000, pinf2=20000, pinf3=20000, pbinf=20

% Tissue repair rate and the maximum of tissue integrity is set to one.

par ktg1=2,ktg2=2,ktg3=2, tinf1=1,tinf2=1, tinf3=1

% Diffusion baseline (db_) and facilitate (df_)

par dbmol1=10,dbmol2=10, dbmol3=10, dfmol1=1,dfmol2=1, dfmol3=1

par dbn1=0.005, dbn2=0.005, dbn3=0.005, par dfn1=50, dfn2=50, dfn3=50

par dbp1=1,dbp2=1,dbp3=1, dfp1=1, dfp2=1, dfp3=1

% Portion of the neutrophil and macrophage population that remains when neutrophils and macrophages fit pathogen.

% For example, r1=0.98 means that the depletion term in the tissue neutrophils equation for their interaction with pathogen is

% multiplied by (1-r1).

par r1=0.98,r2=0.98,r3=0.98,rb=0.98, q1=1, q2=1, q3=1

% Background immune system parameters

par kpb1=.46,kpb2=.46,kpb3=.46, kpbb=.46, mub1=0.0023,mub2=0.0023,mub3=0.0023

par mubb=0.0023, kbp1=0.0001,kbp2=0.0001, kbp3=0.0001,kbbp=0.02

% Activation of macrophages and neutrophils

par kmp1=40, kmp2=40, kmp3=40, kmtcell1=20, kmtcell2=20, kmtcell3=20

par kmrcell1=.01, kmrcell2=0.01, kmrcell3=0.01

par kmtmol1=5, kmtmol2=5, kmtmol3=5, knlbcell=0, knlbmol=0

par kntbcell=2, kntbmol=0.8, knrbcell=0.1, knpbcell=5

% Cytokine production

par kmai1=1000,kmai2=1000,kmai3=1000

par kmat1=3000,kmat2=3000,kmat3=3000

% Depletion of pathogen

par kmappath1=2.8,kmappath2=2.8,kmappath3=2.8

par kmapcell1=0,kmapcell2=0,kmapcell3=0

par knappath1=5.8, knappath2=5.8, knappath3=5.8, knapbpath=0.04

par knapcell1=5, knapcell2=5, knapcell3=5, knapbcell=5,

% Tissue depletion from radicals

par krtt1=0.01, krtt2=0.01, krtt3=0.01

%Radical production terms

par krtr1=0.1,krtr2=0.1,krtr3=0.1,knar1=0.01,knar2=0.01,knar3=0.01,knarb=0.01

par knatr1=0.01, knatr2=0.01, knatr3=0.01, krntp1=0.2, krntp2=0.2, krntp3=0.2

par krtmp1=1e-5, krtmp2=1e-5, krtmp3=1e-5

% Inflammation growth rate, decay rate, and Hill constant

par ktz1=.5, ktz2=.5, ktz3=.5, b1=.01, b2=.01,b3=.01, xtz1=20, xtz2=20, xtz3=20

% Threshold for tissue integrity. If TI falls below parameter a, TI cannot repair itself.

par a1=.1, a2=.1,a3=.1

% Hill parameters for activation triggered by TNF

par xtb=2, xt1=20,xt2=20, xt3=20, thill1=2, thill2=2, thill3=2,tbhill=2

% Inhibition parameters

par il10bar1=200,il10bar2=200,il10bar3=200, ci1=0.05,ci2=0.05, ci3=0.05

par il10bbar=200,cib=0.05, il10tbar1=60, il10tbar2=60,il10tbar3=60

par cit1=0.000001, cit2=0.000001, cit3=0.000001, il10tbbar=15, citb=.000001

par il10nbbar=80, cinb=.15, il10nbar1=80, cin1=.15, il10nbar2=80, cin2=.15

par il10nbar3=80,cin3=.15

par fie1=3, fite1=5,fie2=3, fite2=5,fie3=3, fite3=5, fibe=3, fitbe=3

par fine1=1,fine2=1,fine3=1, finbe=1

% Parameters for the increase of resting neutrophil source during inflammation

par ksnb=3, xsnb=200, hillsnb=2, b11=1, c1=1

% Hill parameters for the interactions involving pathogen

par xpma1=200, xpma2=200. xpma3=200, xpna1=1500,xpna2=1500 , xpna3=1500

par phill1=3, phill2=3, phill3=3, xpb=0.1, pbhill=1

%Diffusion parameters

par utexp=2,ltexp=1

par at=50, bt=0.8, ab=2000, bb=0

% Compartmental Volume

par vb=50

par vt1=.5, vt2=.5, vt3=.5

% Hill parameters for the production of TNF

par xma1=80,xma2=80,xma3=80, mahill1=2, mahill2=2, mahill3=2

% Hill parameters for the production of IL-10 and the changes in the decay rate of IL-10 during inflammation

par vi1=8, vi2=8,vi3=8, vib=8, hilli1=2, hilli2=2,hilli3=2,hillib=2

par xmi1=140, xmi2=140, xmi3=140, hillmi1=2, hillmi2=2, hillmi3=2

par pro1=1, pro2=1, pro3=1, prob=1

par thillz1=2, thillz2=2, thillz3=2

par kzti1=0.1, kzti2=0.1, kzti3=0.1

% These parameters control whether there are two or three organs connected to the blood supply

par y2=1, y3=1

% These parameters are set to zero to turn off all neutrophil interactions in associate organ

par na1onoff=1,na2onoff=1,na3onoff=1

% These parameters are set to zero to turn off all macrophage interactions in associate organ

```
par ma1onoff=1,ma2onoff=1,ma3onoff=1

% This parameter is set to zero to turn off all neutrophil interactions in the blood
par nbonoff=1

% Controls the relative diffusion of each organ
par d1=1,d2=1,d3=1
```

C.2.2 % FUNCTION DEFINITIONS

```
% hill equation
f(x,v,hill)=x^hill/(v^hill+x^hill)

% Inhibition functions
fi1(x,y)=x*((1-ci1)/(1+(y/il10bar1)^fie1)+ci1)
fi2(x,y)=x*((1-ci2)/(1+(y/il10bar2)^fie2)+ci2)
fi3(x,y)=x*((1-ci3)/(1+(y/il10bar3)^fie3)+ci3)
fib(x,y)=x*((1-cib)/(1+(y/il10bbar)^fibe)+cib)
fin1(x,y)=x*((1-cin1)/(1+(y/il10nbar1)^fine1)+cin1)
fin2(x,y)=x*((1-cin2)/(1+(y/il10nbar2)^fine2)+cin2)
fin3(x,y)=x*((1-cin3)/(1+(y/il10nbar3)^fine3)+cin3)
fit1(x,y)=x*((1-cit1)/(1+(y/il10tbar1)^fite1)+cit1)
fit2(x,y)=x*((1-cit2)/(1+(y/il10tbar2)^fite2)+cit2)
fit3(x,y)=x*((1-cit3)/(1+(y/il10tbar3)^fite1)+cit3)
fitb(x,y)=x*((1-citb)/(1+(y/il10tbbar)^fitbe)+citb)
finb(x,y)=x*((1-cinb)/(1+(y/il10nbbar)^finbe)+cinb)

% Diffusion functions
dmol1=d1*dbmol1*(1+z1*dfmol1)
```

dmol2=d2*dbmol2*(1+z2*dfmol2)

dmol3=d3*dbmol3*(1+z3*dfmol3)

dn1=d1*dbn1*(1+z1*dfn1)

dn2=d2*dbn2*(1+z2*dfn2)

dn3=d3*dbn3*(1+z3*dfn3)

dp1=d1*dbp1*(1+z1*dfp1)

dp2=d2*dbp2*(1+z2*dfp2)

dp3=d3*dbp3*(1+z3*dfp3)

% Diffusion of pathogen from the blood to the tissue

pbdiff(x,a)=a*x

% To reduce computation times p13(x) is used to estimate the cube root of x.

p13(x)=1.02*(1+x)^(1/3)*x/(.5+x)

% Diffusion of pathogen from the tissue into the blood is dependent on surface area of the population

ptdiff(x,a,b,upperexp,lowerexp)=a*p13(x)*p13(x)/(1+b*p13(x))

C.2.3 % BLOOD EQUATIONS

% TNF EQUATION

tnfb'= -mutb*tnfb+dmol1*(tnf1-tnfb)/vb+y2*dmol2*(tnf2-tnfb)/vb

+y3*dmol3*(tnf3-tnfb)/vb-kntbmol*finb(nb*f(tnfb,xtb,tbhill),il10b)

% RESTING NEUTROPHILS EQUATION

nb'=nbonoff*((snb+ksnb*f(b11*nba+c1*(na1+y2*na2+y3*na3),xsnb,hillsnb))-munb*nb

-knpbcell*fib(nb*f(pb,xpb,pbhill),il10b-kntbcell*finb(nb*f(tnfb,xtb,tbhill),il10b)

-knrbcell*finb(nb*radb,il10b))

% ACTIVATED NEUTROPHILS EQUATION

nba'=nbonoff*(-munba*nba-dn1*nba/vb-y2*dn2*nba/vb-y3*dn3*nba/vb
+knpbcell*finb(nb*f(pb,xpb,pbhill),il10b)+kntbcell*finb(nb*f(tnfb,xtb,tbhill),il10b)
+knrbcell*finb(nb*radb,il10b)-(1-rb)*knapbcell*finb(nba*f(pb,xpb,pbhill),il10b))

% IL-10 EQUATION

il10b'= -(muibmax-prob*(muibmax-muibmin)*(il10b^hillib)/(vib^hillib+il10b^hillib))*il10b
+dmol1*(il101-il10b)/vb+y2*dmol2*(il102-il10b)/vb+y3*dmol3*(il103-il10b)/vb

% RADICAL EQUATION

radb'=-murb*radb+dmol1*(rad1-radb)/vb+y2*dmol2*(rad2-radb)/vb
+y3*dmol3*(rad3-radb)/vb+knarb*finb(nba,il10b)

% PATHOGEN EQUATION

pb'=kpbg*pb*(1-pb/pbinf)-nbonoff*knapbpath*finb(nba*f(pb,xpb,pbhill),il10b)
+dp1*ptdiff(p1,at,bt,utexp,ltexp)/vb-dp1*pbdiff(pb,ab)/vb
+y2*(dp2*ptdiff(p2,at,bt,utexp,ltexp)/vb-dp2*pbdiff(pb,ab)/vb)
+y3*(dp3*ptdiff(p3,at,bt,utexp,ltexp)/vb-dp3*pbdiff(pb,ab)/vb)-sbb*kpbb*pb/(mubb+kbbp*pb)

C.2.4 % TISSUE 1 EQUATIONS

% PATHOGEN EQUATION

p1'=kpg1*p1*(1-p1/pinf1)-ma1onoff*kmappath1
*fi1(ma1*f(p1,xpma1,phill1),il101)
-na1onoff*knappath1*fin1(na1*f(p1,xpna1,phill1),il101)
-sb1*kpb1*p1/(mub1+kbp1*p1)-dp1*ptdiff(p1,at,bt,utexp,ltexp)/vt1
+dp1*pbdiff(pb,ab)/vt1

% RESTING MACROPHAGE EQUATION

m1'= ma1onoff*(sm1-mum1*m1-kmp1*fi1(m1*f(p1,xpma1,phill1),il101)

```
-kmtcell1*fi1(m1*f(tnf1,xt1,thill1),il101)-kmrcell1*fi1(m1*rad1,il101))

% ACTIVATED MACROPHAGE EQUATION
ma1'=ma1onoff*(-muma1*ma1+kmp1*fi1(m1*f(p1,xpma1,phill1),il101)
+kmtcell1*fi1(m1*f(tnf1,xt1,thill1),il101)+kmrcell1*fi1(m1*rad1,il101)
-(1-q1)*kmapcell1*fi1(p1*ma1,il101))

%TNF EQUATION
tnf1'= -mut1*tnf1+dmol1*(tnfb-tnf1)/vt1
-ma1onoff*kmtmol1*fi1(m1*f(tnf1,xt1,thill1),il101)
+ma1onoff*kmat1*fit1(f(ma1,xma1,mahill1),il101)

% ACTIVATED NEUTROPHIL EQUATION
na1'= -muna1*na1
+dn1*nba/vt1-(1-r1)*na1onoff*knapcell1*fin1(na1*f(p1,xpna1,phill1),il101)

% IL-10 EQUATION
il101'= -(mui1max-pro1*(mui1max-mui1min)
*(il101^hilli1)/(vi1^hilli1+il101^hilli1))*il101
+dmol1*(il10b-il101)/vt1+ma1onoff*kmai1*fi1(f(ma1,xmi1,hillmi1),il101)

% RADICAL EQUATION
rad1'= -mur1*rad1+dmol1*(radb-rad1)/vt1+krtr1*rad1*ti1
+na1onoff*knar1*fin1(na1,il101)
+na1onoff*knatr1*na1*(ti1)+na1onoff*krntp1*na1*p1*(ti1)
+ma1onoff*krtmp1*ma1*p1*(ti1)

% TISSUE INTEGRITY EQUATION
ti1'=(ktg1*ti1*(1-ti1/tinf1)*(ti1-a1)-krtt1*rad1*ti1)

% INFLAMMATION EQUATION
```

z1'=ktz1*(f(tnf1,xtz1,thillz1)+kzti1*(tinf1-ti1))*(1-z1)-b1*z1

C.2.5 % TISSUE 2 EQUATIONS

% PATHOGEN EQUATION

p2'=y2*(kpg2*p2*(1-p2/pinf2)-ma2onoff*kmappath2*fi2(ma2*f(p2,xpma2,phill2),il102)
-na2onoff*knappath2*fin2(na2*f(p2,xpna2,phill2),il102)-sb2*kpb2*p2/(mub2+kbp2*p2)
-dp2*ptdiff(p2,at,bt,utexp,ltexp)/vt2+dp2*pbdiff(pb,ab)/vt2)

% RESTING MACROPHAGE EQUATION

m2'=y2*ma2onoff*(sm2-mum2*m2-kmp2*fi2(m2*f(p2,xpma2,phill2),il102)
-kmtcell2*fi2(m2*f(tnf2,xt2,thill2),il102)-kmrcell2*fi2(m2,il102)*rad2)

% ACTIVATED MACROPHAGE EQUATION

ma2'=y2*ma2onoff*(-muma2*ma2+kmp2*fi2(m2*f(p2,xpma2,phill2),il102)
+kmtcell2*fi2(m2*f(tnf2,xt2,thill2),il102)-(1-q2)*kmapcell2*fi2(p2*ma2,il102)
+kmrcell2*fi2(m2,il102)*rad2)

%TNF EQUATION

tnf2'=y2*(-mut2*tnf2+dmol2*(tnfb-tnf2)/vt2
-ma2onoff*kmtmol2*fi2(m2*f(tnf2,xt2,thill2),il102)
+ma2onoff*kmat2*fit2(f(ma2,xma2,mahill2),il102))

% ACTIVATED NEUTROPHIL EQUATION

na2'=y2*(-muna2*na2+dn2*nba/vt2
-na2onoff*(1-r2)*knapcell2*fin2(na2*f(p2,xpna2,phill2),il102))

% IL-10 EQUATION

il102'=y2*(-(mui2max-pro2*(mui2max-mui2min)*(il102^hilli2)/(vi2^hilli2+il102^hilli2))*il102
+dmol2*(il10b-il102)/vt2+ma2onoff*kmai2*fi2(f(ma2,xmi2,hillmi2),il102))

% RADICAL EQUATION

rad2'=y2*(-mur2*rad2+dmol2*(radb-rad2)/vt2+krtr2*rad2*ti2+na2onoff*knatr2*na2*ti2

+na2onoff*knar2*fin2(na2,il102)+na2onoff*krntp2*na2*p2*(ti2)

+ma2onoff*krtmp2*ma2*p2*(ti2))

% TISSUE INTEGRITY EQUATION

ti2'=y2*((ktg2*ti2*(1-ti2/tinf2)*(ti2-a2)-krtt2*rad2*ti2))

% INFLAMMATION EQUATION

z2'=y2*(ktz2*(f(tnf2,xtz2,thillz2)+kzti2*(tinf2-ti2))*(1-z2)-b2*z2)

%TISSUE 3 EQUATIONS

% PATHOGEN EQUATION

p3'=y3*(kpg3*p3*(1-p3/pinf3)

-ma3onoff*kmappath3*fi3(ma3*f(p3,xpma3,phill3),il103)

-na3onoff*knappath3*fin3(na3*f(p3,xpna3,phill3),il103)

-sb3*kpb3*p3/(mub3+kbp3*p3)

-dp3*ptdiff(p3,at,bt,utexp,ltexp)/vt3+dp3*pbdiff(pb,ab)/vt3)

% RESTING MACROPHAGE EQUATION

m3'=y3*(sm3-mum3*m3-ma3onoff*kmp3*fi3(m3*f(p3,xpma3,phill3),il103)

-ma3onoff*kmtcell3*fi3(m3*f(tnf3,xt3,thill3),il103)

-ma3onoff*kmrcell3*fi3(m3,il103)*rad3)

% ACTIVATED MACROPHAGE EQUATION

ma3'=y3*(-muma3*ma3+ma3onoff*kmp3*fi3(m3*f(p3,xpma3,phill3),il103)

+ma3onoff*kmtcell3*fi3(m3*f(tnf3,xt3,thill3),il103)

-ma3onoff*(1-q3)*kmapcell3*fi3(p3*ma3,il103)

+ma3onoff*kmrcell3*fi3(m3,il103)*rad3)

%TNF EQUATION

```
tnf3'=y3*(-mut3*tnf3+dmol3*(tnfb-tnf3)/vt3
-ma3onoff*kmtmol3*fi3(m3*f(tnf3,xt3,thill3),il103)
+ma3onoff*kmat3*fit3(f(ma3,xma3,mahill3),il103))

% ACTIVATED NEUTROPHIL EQUATION
na3'=y3*(-muna3*na3+dn3*nba/vt3
-(1-r3)*na3onoff*knapcell3*fin3(na3*f(p3,xpna3,phill3),il103))

% IL-10 EQUATION
il103'=y3*(-(mui3max-pro3*(mui3max-mui3min)*(il103^hilli3)
/(vi3^hilli3+il103^hilli3))*il103
+dmol3*(il10b-il103)/vt3
+ma3onoff*kmai3*fi3(f(ma3,xmi3,hillmi3),il103))

% RADICAL EQUATION
rad3'=y3*(-mur3*rad3+dmol3*(radb-rad3)/vt3+krtr3*rad3*ti3
+na3onoff*knatr3*na3*ti3+na3onoff*knar3*fin3(na3,il103)
+na3onoff*krntp3*na3*p3*(ti3)
+ma3onoff*krtmp3*ma3*p3*(ti3))

% TISSUE INTEGRITY EQUATION
ti3'=y3*((ktg3*ti3*(1-ti3/tinf3)*(ti3-a3)-krtt3*rad3*ti3))

% INFLAMMATION EQUATION
z3'=y3*(ktz3*(f(tnf3,xtz3,thillz3)+kzti2*(tinf3-ti3))*(1-z3)-b3*z3)

% Initial condition for tissue integrity
ti2(0)=1
ti1(0)=1
ti3(0)=1
```

C.2.6 %NUMERICS

@ method=gear, tol=0.0001, dt=0.1, total=200.0, bounds=10000000

@ xlo=0, xhi=200, ylo=0, yhi=10, bell=0

@ maxstore=10000

APPENDIX D

CODE FOR THE FULL LUNG MODEL

This appendix contains the Matlab code for the immune subsystem, single respiratory unit and full lung. It also contains the XPP-AUT code for the immune subsystem and single respiratory unit and pseudo code for the implementation of the full lung with a distribution in the initial tidal volumes. The XPP-AUT code for the single respiratory unit requires tab files created from the immune subsystem. These table are only created when the immune subsystem is run in Matlab. Therefore, to run the single RU in XPP you must first run the immune subsystem Matlab Code in the directory that the XPP code will run from. The Matlab immune subsystem code must also be run before the single RU Matlab code. This code requires as input the matrix data, which is produced from the immune subsystem Matlab code.

D.1 IMMUNE SUBSYSTEM

D.1.1 Matlab code for the immune subsystem:

D.1.1.1 immunepde.m: (main m-file of the system) This code must be run before using the single RU is simulated in either XPP or Matlab.

CODE:

function [data,NewIC,v]=immunepde(ic,t0,tfinal,tinc,vtidal0)

% This code solves the system of ODE defined in dximmunepde.m with builtin Matlab solver ode15s for stiff systems.

% Input parameters:

% ic is the initial conditions vector, which is of length 81. Changing ic(21) introduces the inflammtion in the blood by increasing tnfb. The lethal insult used throughout the simulations of this thesis were initiated by setting ic(21)=4 in the command line.

% t0- is the initial time and this typically set to zero.

% tfinal- is the total time the immune subsystem will run. (This system runs in hours)

% tinc- is the increment in time used when returning the data matrix. To use the data matrix in XPP set this to 0.5.

%vtidal0- initial scaled tidal volume. In the normal RU we assume this is 350 ml. The code will scale this to its corresponding volume on a sinlge RU. In the full lung this ranges between 150 and 550 by increments of 10.

% Output paramters:

% data- matrix of the solutions to the ODE in dximmunepde

% The following entry in the command line of Matlab when in the directory that this m-file exist will run the immune subsystem with no inflammation and normal volumes. The matrix data produced is needed in the single RU code to find the initial conidition at health from the vb0, vc0, vamin0 chosen.

% ic=zeros(1,81) followed by [data,NewIC,v]=immunepde(ic,0,2,.5,350,90,2300);

close all;

%following sets initial conditions and tolerences

k=ones(1,81);

nba1=ic(1);nba2=ic(2);nba3=ic(3);nba4=ic(4);nba5=ic(5);nba6=ic(6);nba7=ic(7);

```
nba8=ic(8);nba9=ic(9);nba10=ic(10);nba11=ic(11);nba12=ic(12);nba13=ic(13);
nba14=ic(14);nba15=ic(15);nba16=ic(16);nba17=ic(17);nba18=ic(18);
nba19=ic(19);nba10=ic(10);nba20=ic(20);
tnfb=ic(21);
na1=ic(22);na2=ic(23);na3=ic(24);na4=ic(25);na5=ic(26);na6=ic(27);na7=ic(28);
na8=ic(29);na9=ic(30);na10=ic(31);na11=ic(32);na12=ic(33);na13=ic(34);
na14=ic(35);na15=ic(36);na16=ic(37);na17=ic(38);na18=ic(39);na19=ic(40);
na20=ic(41);tnf1=ic(42);tnf2=ic(43);tnf3=ic(44);tnf4=ic(45);tnf5=ic(46);tnf6=ic(47);
tnf7=ic(48);tnf8=ic(49);tnf9=ic(50);tnf10=ic(51);tnf11=ic(52);tnf12=ic(53);
tnf13=ic(54);tnf14=ic(55);tnf15=ic(56);tnf16=ic(57);tnf17=ic(58);tnf18=ic(59);
tnf19=ic(60);tnf20=ic(61);z1=ic(62);z2=ic(63);z3=ic(64);z4=ic(65);z5=ic(66);
z6=ic(67);z7=ic(68);z8=ic(69);z9=ic(70);z10=ic(71);z11=ic(72);z12=ic(73);
z13=ic(74);z14=ic(75);z15=ic(76);z16=ic(77);z17=ic(78);
z18=ic(79);z19=ic(80);z20=ic(81);

options = odeset('RelTol',1e-8,'AbsTol',(1e-8).*k);

% This solves the ode system defined by the in dximmunepde.m from t0 to tfinal with
ode solver ode15s
[T,Y] = ode15s(@dximmunepde,[t0:tinc:tfinal],[nba1,nba2,nba3,nba4, nba5,nba6, nba7,
nba8,nba9,nba10,nba11,nba12,nba13,nba14,nba15, nba16,nba17,nba18, nba19, nba20,
tnfb, na1, na2,na3,na4,na5,na6,na7,na8,na9,na10,na11,na12, na13,na14,na15,na16,na17,
na18,na19,na20, tnf1, tnf2,tnf3,tnf4,tnf5,tnf6,tnf7,tnf8,tnf9,tnf10,tnf11,tnf12, tnf13,tnf14,
tnf15,tnf16,tnf17,tnf18,tnf19, tnf20, z1,z2,z3,z4,z5,z6,z7,z8,z9,z10,z11,z12,z13,z14,z15,
z16,z17,z18,z19,z20],options);

% plots results
figure;
plot(T,Y(:,1),'-');YLABEL('nba1');xLABEL('time');figure;
plot(T,Y(:,21),'-.');ylabel('tnfb');xLABEL('time');figure;
```

```
plot(T,Y(:,41),'.');YLABEL('na20');xLABEL('time');figure;
plot(T,Y(:,61),'+');YLABEL('tnf20');xLABEL('time');figure;
plot(T,Y(:,81),'*');YLABEL('z20');xLABEL('time');figure;
```

%creates tables for the single RU XPP code and the data maxtrix for the single RU Matlab code. Also, the following code plots the compartmental volumes.

```
mvtb=.4; mvta=1; auc=.12e8;
vamin0=2300/(.12e8); vbnormal=90/(.12e8); vtnormal=500/(.12e8);
vachange0=vtidal0;closing=10;
vb=auc*(vbnormal./(1+(mvtb.*(sum(Y(:,62:81)')/20))))';
%plot(T,vb(:,1),'*');YLABEL('vb');xLABEL('time');figure;
vt=auc*(vtnormal+vbnormal-vbnormal./(1+(mvtb.*(sum(Y(:,62:81)')/20)))
+vamin0-vamin0./(1+(mvta.*(sum(Y(:,62:81)')/20))))';
%plot(T,vt(:,1),'*');YLABEL('vt');xLABEL('time');figure;
vamin=auc*(vamin0./(1+mvta.*(sum(Y(:,62:81)')/20)))';
%plot(T,vamin(:,1),'*');YLABEL('vamin');xLABEL('time');figure;
vc=(vachange0./(1+(closing.*(sum(Y(:,62:81)')/20))))';
%plot(T,vc(:,1),'*');YLABEL('vchange');xLABEL('time');figure;
v0=.2932;
v=v0*90./vb;
%plot(T,v(:,1),'*');YLABEL('v');xLABEL('time');
data=[T,Y,vb,vt,vamin,vc];
NewIC=Y(end,:);
na1v=[tfinal*(1/tinc)+1; 0; tfinal; data(:,23)];
na2v=[tfinal*(1/tinc)+1; 0; tfinal; data(:,24)];
na3v=[tfinal*(1/tinc)+1; 0; tfinal; data(:,25)];
na4v=[tfinal*(1/tinc)+1; 0; tfinal; data(:,26)];
na5v=[tfinal*(1/tinc)+1; 0; tfinal; data(:,27)];
na6v=[tfinal*(1/tinc)+1; 0; tfinal; data(:,28)];
na7v=[tfinal*(1/tinc)+1; 0; tfinal; data(:,29)];
```

```
na8v=[tfinal*(1/tinc)+1; 0; tfinal; data(:,30)];
na9v=[tfinal*(1/tinc)+1; 0; tfinal; data(:,31)];
na10v=[tfinal*(1/tinc)+1; 0; tfinal; data(:,32)];
na11v=[tfinal*(1/tinc)+1; 0; tfinal; data(:,33)];
na12v=[tfinal*(1/tinc)+1; 0; tfinal; data(:,34)];
na13v=[tfinal*(1/tinc)+1; 0; tfinal; data(:,35)];
na14v=[tfinal*(1/tinc)+1; 0; tfinal; data(:,36)];
na15v=[tfinal*(1/tinc)+1; 0; tfinal; data(:,37)];
na16v=[tfinal*(1/tinc)+1; 0; tfinal; data(:,38)];
na17v=[tfinal*(1/tinc)+1; 0; tfinal; data(:,39)];
na18v=[tfinal*(1/tinc)+1; 0; tfinal; data(:,40)];
na19v=[tfinal*(1/tinc)+1; 0; tfinal; data(:,41)];
na20v=[tfinal*(1/tinc)+1; 0; tfinal; data(:,42)];
length(na1v)
dlmwrite('na1.tab', na1v, '\line')
dlmwrite('na2.tab', na2v, '\line')
dlmwrite('na3.tab', na3v, '\line')
dlmwrite('na4.tab', na4v, '\line')
dlmwrite('na5.tab', na5v, '\line')
dlmwrite('na6.tab', na6v, '\line')
dlmwrite('na7.tab', na7v, '\line')
dlmwrite('na8.tab', na8v, '\line')
dlmwrite('na9.tab', na9v, '\line')
dlmwrite('na10.tab', na10v, '\line')
dlmwrite('na11.tab', na11v, '\line')
dlmwrite('na12.tab', na12v, '\line')
dlmwrite('na13.tab', na13v, '\line')
dlmwrite('na14.tab', na14v, '\line')
dlmwrite('na15.tab', na15v, '\line')
dlmwrite('na16.tab', na16v, '\line')
```

```
dlmwrite('na17.tab', na17v, '\line')
dlmwrite('na18.tab', na18v, '\line')
dlmwrite('na19.tab', na19v, '\line')
dlmwrite('na20.tab', na20v, '\line')
vtv=[tfinal*(1/tinc)+1; 0; tfinal; vt];
vbv=[tfinal*(1/tinc)+1; 0; tfinal; vb];
vaminv=[tfinal*(1/tinc)+1; 0; tfinal; vamin];
vcv=[tfinal*(1/tinc)+1; 0; tfinal; vc];
dlmwrite('vt.tab', vtv, '\line')
dlmwrite('vb.tab', vbv, '\line')
dlmwrite('vamin.tab', vaminv, '\line')
dlmwrite('vc.tab', vcv, '\line')
```

D.1.1.2 dximmunepde.m (equations for the right-hand side on the immune subsystem)

CODE:

```
function r = dximmunepde(t,X)
r=zeros(81,1);

% defines variables
nba1=X(1);nba2=X(2);nba3=X(3);nba4=X(4);nba5=X(5);nba6=X(6);
nba7=X(7);nba8=X(8);nba9=X(9);nba10=X(10);nba11=X(11);
nba12=X(12);nba13=X(13);nba14=X(14);nba15=X(15);nba16=X(16);
nba17=X(17);nba18=X(18);nba19=X(19);nba10=X(10);nba20=X(20);
tnfb=X(21);na1=X(22);na2=X(23);na3=X(24);na4=X(25);na5=X(26);
na6=X(27);na7=X(28);na8=X(29);na9=X(30);na10=X(31);na11=X(32);
na12=X(33);na13=X(34);na14=X(35);na15=X(36);na16=X(37);na17=X(38);
na18=X(39);na19=X(40);na20=X(41);tnf1=X(42);tnf2=X(43);tnf3=X(44);
tnf4=X(45);tnf5=X(46);tnf6=X(47);tnf7=X(48);tnf8=X(49);tnf9=X(50);
tnf10=X(51);tnf11=X(52);tnf12=X(53);tnf13=X(54);tnf14=X(55);
```

```
tnf15=X(56);tnf16=X(57);tnf17=X(58);tnf18=X(59);tnf19=X(60);
tnf20=X(61);z1=X(62);z2=X(63);z3=X(64);z4=X(65);
z5=X(66);z6=X(67);z7=X(68);z8=X(69);z9=X(70);z10=X(71);
z11=X(72);z12=X(73);z13=X(74);z14=X(75);z15=X(76);z16=X(77);
z17=X(78);z18=X(79);
z19=X(80);z20=X(81);

% Parameters
% decat rate:
munba=.05;
muna=.05;
mutb=1.8;
mut=1.8;

%parameters in the activation of neutrophil terms
beta=12;
n0=1.2;
alpha=8;
eps=1;

% Diffusion between compartments
kv=0.0001;
q=2;
k=0.7;
m=1e-5;
b=.001;

%production of TNF by neutrophils
gamma=3;

% Inflammation parameters
```

```
kzg=.1 ;
muz=0.008;
ktz=2;

%chemotaxsis
xi=1;

%Diffustion of TNF within the tissue
dtnf=1;

%number of space units
spaceunits=20;

% tissue length is .2199 cm so h=.2199/20
h=0.011;

% Speed of Blood
v0=.2932;

% Changes in compartmental volumes due to increasing inflammation
mvtb=.4; mvta=1 ;
hillz=1;

% Initial Volumes (in liters)
vamin0=2300/(.12e8);
vbnormal=90/(.12e8) ;
vtnormal=500/(.12e8);

%Compartmental volumes
vamin=inline('vamin0/(1+mvta*x)','x','vamin0','mvta');
```

```
vb=inline('vbnormal/(1+mvtb*x)','x','vbnormal','mvtb');
vt=inline('vtnormal+vbnormal-vbnormal/(1+mvtb*x)
+vamin0-vamin0/(1+mvta*x)','x','vtnormal','vbnormal','mvta','mvtb','vamin0');

% Diffusion functions
rv=inline('(kv*x^q)/(k^q+x^q)','x','k','kv','q');
rp=inline('m*x+b','x','m','b');

% hill function
fh=inline('x^hill/(x^hill+const^hill)','x','hill','const');

v=v0*90/vb(sum(X(62:81,1))/20,vbnormal,mvtb);

%DE's for neutrophils in the blood
r(1)=-munba*nba1+(beta*n0*tnfb^2)/(1+eps*tnfb^2)
-rv(z1,k,kv,q)*nba1/vb(sum(X(62:81,1))/20,vbnormal,mvtb)-v*((nba1-nba1)/h);
for i=2:20
r(i)=-munba*X(i)+(beta*n0*tnfb^2)/(1+eps*tnfb^2)
-rv(X(i+61),k,kv,q)*X(i)/vb(sum(X(62:81,1))/20,vbnormal,mvtb)
-v*((X(i)-X(i-1))/h);
end

%DE for TNF in the blood
r(21)=-mutb*tnfb-(alpha*n0*tnfb^2)/(1+eps*tnfb^2)
+(rpsum(X,tnfb,m,b)/20)/vb(sum(X(62:81,1))/20,vbnormal,mvtb)
+gamma*sum(X(1:20,1))*h;

% DE's for Neutrophils in the tissue
r(22)=-muna*na1
+rv(z1,k,kv,q)*nba1/vt(sum(X(62:81,1))/20,vtnormal,vbnormal,mvta,mvtb,vamin0)
```

```
+xi*(-(tnf1+tnf2)*na1+(tnf1)*(na1+na2));
for i=23:40
r(i)=-muna*X(i)
+rv(X(i+40),k,kv,q)*X(i-21)/vt(sum(X(62:81,1))/20,vtnormal,
vbnormal,mvta,mvtb,vamin0)
+xi*(-(X(i+19)+X(i+21))*X(i)+X(i+20)*(X(i-1)+X(i+1)));
end
r(41)=-muna*na20
+rv(z20,k,kv,q)*nba1/vt(sum(X(62:81,1))/20,vtnormal,vbnormal,mvta,mvtb,vamin0)
+xi*(-(tnf19+tnf20)*na20+(tnf20)*(na19+na20));

% DE's TNF in the tissue
r(42)=-mut*tnf1
+rp(z1,m,b)*(tnfb-tnf1)/vt(sum(X(62:81,1))/20,vtnormal,vbnormal,mvta,mvtb,vamin0)
+gamma*na1+dtnf*(tnf2-2*tnf1+tnf1)/(h^2);
for i=43:60
r(i)=-mut*X(i)
+rp(X(i+20),m,b)*(tnfb-X(i))/vt(sum(X(62:81,1))/20,vtnormal,vbnormal,
mvta,mvtb,vamin0)
+gamma*X(i-20)+dtnf*(X(i+1)-2*X(i)+X(i-1))/(h^2);
end
r(61)=-mut*tnf20
+rp(z20,m,b)*(tnfb-tnf20)/vt(sum(X(62:81,1))/20,vtnormal,vbnormal,mvta,
mvtb,vamin0)
+gamma*na20+dtnf*(tnf20-2*tnf20+tnf19)/(h^2);

% DE's for inlfammation
r(62)=kzg*fh(tnf1,hillz,ktz)*(1-z1)-muz*z1;
for i=63:80
r(i)=kzg*fh(X(i-20),hillz,ktz)*(1-X(i))-muz*X(i);
```

end

r(81)=kzg*fh(tnf20,hillz,ktz)*(1-z20)-muz*z20;

D.1.2 XPP-AUTO- Immune Subsystem

% Immune Parameters

% We have 20 space units and tissue length is .2199 cm, so h=.2199/20

par h=0.011

% decay rate of neutrophils in tissue and blood

par munba=.05, muna=.05

% rate of activation of a neutrophil, source of resting neutrophils, consumption of tnf during activiation, hill constant

par beta=12, n0=1.2, alpha=8, eps=1

% rate constant, hill coeff, hill constant for velcro diffusion, slope and intersect for molecule diffusion

par kv=0.0001, q=2, k=.7, m=1e-5, b=.001

% Diffusion functions

rv(x,q)=(kv*x^q)/(k^q+x^q)

rp(x)=m*x+b

% decay rate of TNF in tissue and blood

par mutb=1.8, mut=1.8

% production of tnf from neutrophils

par gamma=3

% Inflammation growth rate, inflamation decay rate, hill constant with dependence on TNF,

par kzg=.1, muz=.008, ktz=2

% consumption of oxygen by neutophils

par delta=0

% space parameter

%chemotaxis, diffusion of tnf

par xi=1, dtnf=1,

%Chemotaxis function

f(x)=x

%numerical parameter

% time step for derivative approx., number of space units

par dt=.1, spaceunits=20

% Tissue and blood starting volumes for whole lung, converstion from total ml to ml on a RU

par vtstart=500, vbstart=90, auc=12000000, vaminstart=2300

%function of on RU

vbnormal=vbstart/auc

vtnormal=vtstart/auc

vamin0=vaminstart/auc

% Volume changes during an infection for blood and air. Tissue volume increases by what the

% other two compartments lose.

par mvtb=.4, mvta=1

vt(x)=vtnormal+vbnormal-vbnormal/(1+mvtb*x)+vamin0-vamin0/(1+mvta*x)

vb(x)=vbnormal/(1+mvtb*x)

aux vtf=auc*(vt(sum(0,19)of(shift(z1,i'))/spaceunits))

aux vbf=auc*(vb(sum(0,19)of(shift(z1,i'))/spaceunits))

% the effect of the unit closing: the change in alveolus volume decreases

par closing=10

% the vachange and vamin are altered during an infection. The change is an effect of the

% closing. The vamin decreases as the vloume of the tissue increases.

vamin=vamin0/(1+mvta*sum(0,19)of(shift(z1,i'))/spaceunits)

vamax=vamin+(vachange0/(1

+closing*(vt(sum(0,19)of(shift(z1,i'))/spaceunits)-vtnormal)))/auc

aux vc=(vachange0/(1+closing*(sum(0,19)of(shift(z1,i'))/spaceunits)))

```
aux vam=auc*(vamin0/(1+mvta*sum(0,19)of(shift(z1,i'))/spaceunits))
% hill function used for inflamation's dependence on TNF
fh(x,const,hill)=x^hill/(x^hill+const^hill)
% Boundary Conditions
nba0=nba1
nba21=nba20
na0=na1
na21=na20
tnf0=tnf1
tnf21=tnf20
z0=0
z21=z20
par kvol=1, hillz=1
par v0=.2932
v=kvol*v0*(90/(vb(sum(0,19)of(shift(z1,i'))/spaceunits)))
vachange0'=0
% Inflammation
z[1..20]'=kzg*fh(tnf[j],ktz,hillz)*(1-z[j])-muz*z[j]
%%blood equations with nba(x,t) and tnfb(t)
nba[1..20]'=-munba*nba[j]+(beta*n0*tnfb^2)/(1+eps*tnfb^2)
-rv(z[j],q)*nba[j]/vb(sum(0,19)of(shift(z1,i'))/spaceunits)-v*((nba[j]-nba[j-1])/h)
tnfb'=-mutb*tnfb-(alpha*n0*tnfb^2)/(1+eps*tnfb^2)
+(1/spaceunits)*sum(0,19)of(rp(shift(z1,i'))*(shift(tnf1,i')-tnfb))
/vb(sum(0,19)of(shift(z1,i'))/spaceunits)
+gamma*sum(0,19)of(shift(nba1,i')*h)
%%Tissue equations
na[1..20]'=-muna*na[j]+rv(z[j],q)*nba[j]/vt(sum(0,19)of(shift(z1,i'))/spaceunits)
+xi*(-f(tnf[j-1]+tnf[j+1])*na[j]+f(tnf[j])*(na[j-1]+na[j+1]))
tnf[1..20]'=-mut*tnf[j]+rp(z[j])*(tnfb-tnf[j])/vt(sum(0,19)of(shift(z1,i'))/spaceunits)
+gamma*na[j]+dtnf*(tnf[j+1]-2*tnf[j]+tnf[j-1])/(h^2)
```

vachange0(0)=350

@ meth=gear,xp=t, dt=.01, yp=tnfb,xlo=0,xhi=100,ylo=0,yhi=20, total=100,

bound=500000

done

D.2 CODE FOR THE SINGLE RESPIRATORY UNIT

D.2.1 Matlab code for the single RU

D.2.1.1 breathingpde.m (main m-file) Code for a single respiratory unit:

function [va,T,Y]=breathingpdenew(ic,t0,tfinal,data)

% Inputs:

% the matrix data is created when the immune subsystem is run in Matlab (immunepde.m)

% ic is a vector of length 123. To find the proper initial conditions for this system, immunepde should be run with no inflammation for an hour and then feed in to this function with ic=zeros(1,123) and run until it reaches a fixed oscillation in the ga and ca. Then take end point as your new starting initial conditions by setting ic=Y(end, :).

% t0=0 (initial time must conicide with the starting point for the immune system usually 0)

%tfinal- end time (this system runs in seconds, so tfinal=40 is 10 breathing cycles of 4 seconds)

%outputs:

% va is the alveolar airspace volume

% is a vector of times for the matrix of variable values Y during inflammation

```
close all;
k=ones(1,123);

%initial conditions
y=ic(1);ga=ic(2);
gt1=ic(3);gt2=ic(4);gt3=ic(5);gt4=ic(6);gt5=ic(7);gt6=ic(8);gt7=ic(9);gt8=ic(10);
gt9=ic(11);t10=ic(12);gt11=ic(13);gt12=ic(14);gt13=ic(15);gt14=ic(16);gt15=ic(17);
gt16=ic(18);gt17=ic(19);gt18=ic(20);gt19=ic(21);gt20=ic(22);
gb1=ic(23);gb2=ic(24);gb3=ic(25);gb4=ic(26);gb5=ic(27);gb6=ic(28);gb7=ic(29);
gb8=ic(30);gb9=ic(31);gb10=ic(32);gb11=ic(33);gb12=ic(34);gb13=ic(35);
gb14=ic(36);gb15=ic(37);gb16=ic(38);gb17=ic(39);gb18=ic(40);gb19=ic(41);
gb20=ic(42);hb41=ic(43);hb42=ic(44);hb43=ic(45);hb44=ic(46);hb45=ic(47);
hb46=ic(48);hb47=ic(49);hb48=ic(50);hb49=ic(51);hb410=ic(52);hb411=ic(53);
hb412=ic(54);hb413=ic(55);hb414=ic(56);hb415=ic(57);hb416=ic(58);hb417=ic(59);
hb418=ic(60);hb419=ic(61);hb420=ic(62);ca=ic(63);ct1=ic(64);ct2=ic(65);
ct3=ic(66);ct4=ic(67);ct5=ic(68);ct6=ic(69);ct7=ic(70);ct8=ic(71);ct9=ic(72);
ct10=ic(73);ct11=ic(74);ct12=ic(75);ct13=ic(76);ct14=ic(77);ct15=ic(78);ct16=ic(79);
ct17=ic(80);ct18=ic(81);ct19=ic(82);ct20=ic(83);cb1=ic(84);cb2=ic(85);
cb3=ic(86);cb4=ic(87);cb5=ic(88);cb6=ic(89);cb7=ic(90);cb8=ic(91);cb9=ic(92);
cb10=ic(93);cb11=ic(94);cb12=ic(95);cb13=ic(96);cb14=ic(97);
cb15=ic(98);cb16=ic(99);cb17=ic(100);cb18=ic(101);cb19=ic(102);cb20=ic(103);
hco31=ic(104);hco32=ic(105);hco33=ic(106);hco34=ic(107);hco35=ic(108);
hco36=ic(109);hco37=ic(110);hco38=ic(111);hco39=ic(112);hco310=ic(113);
hco311=ic(114);hco312=ic(115);hco313=ic(116);hco314=ic(117);
hco315=ic(118);hco316=ic(119);hco317=ic(120);hco318=ic(121);
hco319=ic(122);hco320=ic(123);

% Alveolor count
auc=.12e11;
% Tolerances
```

options = odeset('RelTol',1e-11,'AbsTol',(1e-11).*k);

% This function solve the system of ODES defined in dxbreathingnew with the ode solver ode15s. [t0:40:tfinal] reports output only every 40 seconds. This can be changed to [t0:tfinal] and output will be every second.

[T,Y] = ode15s(@dxbreathingpdenew,[t0: 40: tfinal],[y, ga, gt1,gt2,gt3,gt4,gt5,gt6,gt7, gt8,gt9,gt10,gt11,gt12,gt13,gt14,gt15,gt16,gt17,gt18,gt19, gt20, gb1,gb2,gb3,gb4,gb5, gb6,gb7,gb8,gb9,gb10,gb11,gb12,gb13,gb14,gb15,gb16,gb17,gb18,gb19,gb20, hb41, hb42,hb43,hb44,hb45,hb46,hb47,hb48,hb49,hb410,hb411,hb412,hb413,hb414,hb415, hb416,hb417,hb418,hb419,hb420,ca, ct1,ct2,ct3,ct4,ct5,ct6,ct7,ct8,ct9,ct10,ct11,ct12, ct13,ct14,ct15,ct16,ct17,ct18,ct19,ct20, cb1,cb2,cb3,cb4,cb5,cb6,cb7,cb8,cb9,cb10, cb11,cb12,cb13,cb14,cb15,cb16,cb17,cb18,cb19,cb20,hco31,hco32,hco33,hco34,hco35, hco36,hco37,hco38,hco39,hco310,hco311,hco312,hco313,hco314,hco315,hco316, hco317,hco318,hco319,hco320],options,data);

%plots of several variables

figure;

plot(T,Y(:,1),'*');YLABEL('y');xlabel('time');figure;

plot(T,Y(:,2),'-');YLABEL('ga');xLABEL('time');figure;

plot(T,Y(:,22),'-'),YLABEL('gt20');xlabel('time');figure;

plot(T,Y(:,42),'-.');ylabel('gb20');xLABEL('time');figure;

plot(T,Y(:,62),'.');YLABEL('hb420');xLABEL('time');figure;

plot(T,Y(:,63),'+');YLABEL('ca');xLABEL('time');figure;

plot(T,Y(:,83),'*');YLABEL('ct20');xLABEL('time');figure;

plot(T,Y(:,103),'*');YLABEL('cb20');xLABEL('time');figure;

plot(T,Y(:,123),'*');YLABEL('hco320');xLABEL('time');figure;

% Determines alveolar air space volume from the data matrix

g=size(data);

max=g(1);

va=zeros(length(T),1);

```
for i=1:length(T)
for counter=1:max
if data(counter,1)>=T(i,1)/(60^2)
va(i)=data(counter,g(2)-1)/auc;
else
counter=counter+1;
end
end
end
plot(T,auc*(va(:,1)+Y(:,1)),'*');xlabel('time');ylabel('va');
```

D.2.1.2 dxbreathingpdenew.m (m-file of the right-hand side)

Code:

```
function r = dxbreathingpdenew(t,X,data)
r=zeros(123,1);

% tissue length is .2199 cm so h=.2199/20
h=0.011;

% time for inspir and time for expir
tin=1;
tout=3;

%controls smoothness of the smooth Heaviside function
sh=20;
% Sets up variables
y=X(1);ga=X(2);
gt1=X(3);gt2=X(4);gt3=X(5);gt4=X(6);gt5=X(7);gt6=X(8);gt7=X(9);gt8=X(10);
gt9=X(11);gt10=X(12);gt11=X(13);gt12=X(14);gt13=X(15);gt14=X(16);
gt15=X(17);gt16=X(18);gt17=X(19);gt18=X(20);gt19=X(21);gt20=X(22);
gb1=X(23);gb2=X(24);gb3=X(25);gb4=X(26);gb5=X(27);gb6=X(28);gb7=X(29);
```

```
gb8=X(30);gb9=X(31);gb10=X(32);gb11=X(33);gb12=X(34);gb13=X(35);gb14=X(36);
gb15=X(37);gb16=X(38);gb17=X(39);gb18=X(40);gb19=X(41);gb20=X(42);
hb41=X(43);hb42=X(44);hb43=X(45);hb44=X(46);hb45=X(47);hb46=X(48);
hb47=X(49);hb48=X(50);hb49=X(51);hb410=X(52);hb411=X(53);hb412=X(54);
hb413=X(55);hb414=X(56);hb415=X(57);hb416=X(58);hb417=X(59);hb418=X(60);
hb419=X(61);hb420=X(62);
ca=X(63);
ct1=X(64);ct2=X(65);ct3=X(66);ct4=X(67);ct5=X(68);ct6=X(69);ct7=X(70);ct8=X(71);
ct9=X(72);ct10=X(73);ct11=X(74);ct12=X(75);ct13=X(76);ct14=X(77);ct15=X(78);
ct16=X(79);ct17=X(80);ct18=X(81);ct19=X(82);ct20=X(83);cb1=X(84);cb2=X(85);
cb3=X(86);cb4=X(87);cb5=X(88);cb6=X(89);cb7=X(90);cb8=X(91);cb9=X(92);
cb10=X(93);cb11=X(94);cb12=X(95);cb13=X(96);cb14=X(97);cb15=X(98);cb16=X(99);
cb17=X(100);cb18=X(101);cb19=X(102);cb20=X(103);hco31=X(104);hco32=X(105);
hco33=X(106);hco34=X(107);hco35=X(108);hco36=X(109);hco37=X(110);hco38=X(111);
hco39=X(112);hco310=X(113);hco311=X(114);
hco312=X(115);hco313=X(116);hco314=X(117);hco315=X(118);hco316=X(119);
hco317=X(120);hco318=X(121);hco319=X(122);hco320=X(123);

% Hemglobin and bicarbonate parameters
hbtotal=2.24e-3;
ihb4=.001717;
fith=3.6;
ihco3=.024;
ratio=177916;
kplus0=0.0005;
boff=1;
kminus=88.96;
kcatcb=880000;
kmcb=.01;
kcathco3=199800;
```

kmhco3=0.0225;

% Partial pressure of Oxygen and Carbon Dioxide of the blood entering the RU

lowo2=40;

highco2=45;

% speed of the blood. Assuming 1 respiratory unit is crossed in 0.8secs and the length scale is

% as above .22cm. Speed is cm/sec and applies to RBC. Plasma may be flowing faster.

v0=.2932;

% Diffusion

dgt=3.24e-5;

dct=0.00065;

%Sigmas such that []=σP for oxygen and carbon dioxide in the blood (tissue is the same σ) and the alveolar air space

sigmagBT=1.24e-6;

sigmacBT=2.95e-5;

sigmaair=5.2e-5;

% Diffusion across the barrier

gtbb=0;

sf=1;

gtbm=6.7483e-12;

ctbb=0;

ctbm=8.477e-11;

gtab=0;

gtam=2.362e-12;

ctab=0;

ctam=7.6293e-10;

```
% Gas levels in the air that is being inhaled
gair0=150;
cair0=0;

% time constants for the breathing mechanism
tau1=.5;
tau2=.7;

% Speed during inflammation
v=90*(7.5e-09)/vbfunc(t,data);

% Alveolus count
auc=.12e8;

%DE for y-breathing variable
r(1)=(g(t,data,sh,auc,tin,tout)/tau1-y/tau2);

%DE for oxygen in the alveolar air space
r(2)=gtam*(1/20)*(sum(X(3:22),1)-20*ga)/(sigmaair*va(t,data,y))
+max(rv(t,data,sh,auc,tin,tout,tau1,tau2,y),0)*(gair0-ga);

% vtfunc is a function that determines the tidal volume from the data matrix
vtt=vtfunc(t,data);
% vbfunc is a function that determines the blood volume from the data matrix
vbb=vbfunc(t,data);

%DE's for oxygen in the tissue
r(3)=((gb1-gt1)*gtbm+(ga-gt1)*gtam)/(sigmagBT*vtt)+dgt*(gt2-2*gt1+gt1)/(h^2);
for i=4:21
r(i)=((X(i+20)-X(i))*gtbm+(ga-X(i))*gtam)/(sigmagBT*vtt)+dgt*(X(i+1)-2*X(i)+X(i-
1))/(h^2);
```

```
end
r(22)=((gb20-gt20)*gtbm+(ga-gt20)*gtam)/(sigmagBT*vtt)
+dgt*(gt19-2*gt20+gt20)/(h^2);

%DE's for oxygen in the blood
r(23)=(gt1-gb1)*gtbm/(sigmagBT*vbb)+(fith/sigmagBT)*
(-kplus0*(hbtotal-hb41)*gb1^fith
+kminus*hb41)-v*((gb1-lowo2)/h);
for i=24:41
r(i)=(X(i-20)-X(i))*gtbm/(sigmagBT*vbb)+(fith/sigmagBT)
*(-kplus0*(hbtotal-X(i+20))*X(i)^fith
+kminus*X(i+20))-v*((X(i)-X(i-1))/h);
end
r(42)=(gt20-gb20)*gtbm/(sigmagBT*vbb)+(fith/sigmagBT)*
(-kplus0*(hbtotal-hb420)*gb20^fith
+kminus*hb420)-v*((gb20-gb19)/h);

%DE for Saturated Hemoglobin
r(43)=kplus0*(hbtotal-hb41)*gb1^fith-kminus*hb41
-v*((hb41-ihb4)/h);
for i=44:61
r(i)=kplus0*(hbtotal-X(i))*X(i-20)^fith-kminus*X(i)
-v*((X(i)-X(i-1))/h);
end
r(62)=kplus0*(hbtotal-hb420)*gb20^fith-kminus*hb420
-v*((hb420-hb419)/h);

%DE for carbon dioxide in the alveolar air space
r(63)=ctam*(1/20)*(sum(X(65:84),1)-20*ca)/(sigmaair*va(t,data,y))
+max(rv(t,data,sh,auc,tin,tout,tau1,tau2,y),0)*(cair0-ca);
```

```
%DE's for Carbon Dioxide in the tissue
r(64)=((X(84)-X(64))*ctbm+(ca-X(64))*ctam)/(sigmacBT*vtt)
+dct*(X(63)-2*X(64)+X(64))/(h^2);
for i=65:82
r(i)=((X(i+20)-X(i))*ctbm+(ca-X(i))*ctam)/(sigmacBT*vtt)
+dct*(X(i+1)-2*X(i)+X(i-1))/(h^2);
end
r(83)=((X(103)-X(83))*ctbm+(ca-X(83))*ctam)/(sigmacBT*vtt)
+dct*(X(83)-2*X(83)+X(82))/(h^2);

%DE's for Carbon Dioxide in the blood
r(84)=(X(64)-X(84))*ctbm/(sigmacBT*vbb)
+(kcathco3*X(104)/(kmhco3+X(104))
-(kcatcb*sigmacBT*X(84)/(kmcb+sigmacBT*X(84))))/sigmacBT
-v*((X(84)-highco2)/h);
for i=85:102
r(i)=(X(i-20)-X(i))*ctbm/(sigmacBT*vbb)
+(kcathco3*X(i+20)/(kmhco3+X(i+20))-
(kcatcb*sigmacBT*X(i)/(kmcb+sigmacBT*X(i))))/sigmacBT
-v*((X(i)-X(i-1))/h);
end
r(103)=(X(83)-X(103))*ctbm/(sigmacBT*vbb)
+(kcathco3*X(123)/(kmhco3+X(123))
-(kcatcb*sigmacBT*X(103)/(kmcb+sigmacBT*X(103))))/sigmacBT
-v*((X(103)-X(102))/h);

%DE's for hco3 in the blood
r(104)=(kcatcb*sigmacBT*X(84)/(kmcb+sigmacBT*X(84)))
-(kcathco3*X(104)/(kmhco3+X(104)))
-v*(X(104)-ihco3)/h;
```

```
for i=105:122
r(i)=(kcatcb*sigmacBT*X(i-20)/(kmcb+sigmacBT*X(i-20)))
-(kcathco3*X(i)/(kmhco3+X(i)))-v*(X(i)-X(i-1))/h;
end
r(123)=(kcatcb*sigmacBT*cb20/(kmcb+sigmacBT*cb20))
-(kcathco3*hco320/(kmhco3+hco320))-v*(hco320-hco319)/h;
```

D.2.1.3 Additional m-files: These files extract volume levels from the data matrix by interpolating and implement shunting.

Blood volume:

```
function [vbb]=vbfunc(t,data)
auc=.12e11;
g=size(data);
max=g(1);
for counter=1:max
if data(counter,1)>=t/(60^2)
if counter==1
vbb=data(counter,g(2)-3)/auc;
return
else
vbb=(((data(counter,g(2)-3)-data(counter-1,g(2)-3))/(data(counter,1)-data(counter-1,1)))
*(t/(3600)-data(counter,1))+data(counter,g(2)-3))/auc;
return
end
else
counter=counter+1;
end
end
```

Tissue Volume:

```
function [vtb]=vtfunc(t,data)
auc=.12e8;
g=size(data);
max=g(1);
for counter=1:max
if data(counter,1)>=t/(60^2)
if counter==1
vtb=data(counter,g(2)-2)/(1000*auc);
return
else
vtb=(((data(counter,g(2)-2)-data(counter-1,g(2)-2))
/(data(counter,1)-data(counter-1,1)))
*(t/(3600)-data(counter,1))+data(counter,g(2)-2))/(1000*auc);
return
end
else
counter=counter+1;
end
end
```

Alveolar air space volume:

```
function x=va(t,data,y)
auc=.12e11;
x=(vafunc(t,data))+y;
(vafunc(t,data));
y;
```

and

```
function [vaminb]=vafunc(t,data)
auc=.12e11;
g=size(data);
maxdata=g(1);
for counter=1:maxdata
if data(counter,1)>=t/(60^2)
if counter ==1
vaminb=(data(1,g(2)-1))/auc;
return
else
vaminb=(((data(counter,g(2)-1)-data(counter-1,g(2)-1))
/(data(counter,1)-data(counter-1,1)))
*(t/(3600)-data(counter,1))+data(counter,g(2)-1))/auc;
return
end
else
counter=counter+1;
end
end
```

Tidal volume:

```
function [vcb]=vcfunc(t,data)
auc=.12e11;
g=size(data);
max=g(1);
for counter=1:max
if data(counter,1)>=t/(60^2)
```

```
if counter==1
vcb=data(counter,g(2))/auc;
return
else
vcb=(((data(counter,g(2))-data(counter-1,g(2)))
/(data(counter,1)-data(counter-1,1)))
*(t/(3600)-data(counter,1))+data(counter,g(2)))/auc;
return
end
else
counter=counter+1;
end
end
```

For the breathing mechanism:

```
function y=g(t,data, sh, auc, tin, tout)
y=(vcfunc(t,data))/(1+exp(-sh*(tin-mod(t,tin+tout))));
```

and

```
function rvf=rv(t,data,sh,auc,tin,tout,tau1,tau2,y)
rvf=(g(t,data,sh,auc,tin,tout)/tau1-y/tau2)/(va(t,data,y));
```

Diffusion of TNF:

```
function sum=rpsum(X,tnfb,m,b)
sum=0;
rp=inline('m*x+b','x','m','b');
for i=1:20
```

```
sum=sum+rp(X(i+61),m,b)*(X(i+41)-tnfb);
end
```

and

sum of inflammation function:

```
function y=rvsum(z,spaceunits)
sum=0;
for i=1:spaceunits
sum=sum+z(i);
end
y=sum/spaceunits;
```

D.2.2 XPP-AUTO code for single RU

```
% Parameters

    % length of spactial unit
    par h=0.011

    % time for inpiration and expiration
    par tin=1, tout=3

    % Hemoglobin and bicarbonate parameters
    par hbtotal=2.24e-3, ihb4=.001717, fith=3.6 ,ihco3=0.024
    par ratio=177916, kplus0=0.0005, kplus1=0
    kminus=ratio*kplus0
    par kcatcb=900000, kmcb=0.01, kcathco3=188000, kmhco3=0.0225

    %Partial pressures for the O2 and CO2 in the entering blood.
```

par lowo2=40, highco2=45,

%speed of blood

par v0=.2932

% Diffusion within the tissue

par dgt=3.24e-5, dct=0.00065,

%Sigmas such that []=σP for oxygen and carbon dioxide in the blood (tissue is the same σ) and the alveolar air space

par sigmagBT=1.24e-6, sigmacBT=2.95e-05, sigmaair=5.2e-5

%Diffusion between compartmentsl

par gtbm=6.7483e-12, ctbm=9e-11, gtam=2.362e-12, ctam=9e-10

% Gas levels in new breath

par gair0=150, cair0=0

%time constants for the breathing mechanims

par tau1=.5, tau2=.7

% Alveolar breathing functions

sheav(x)=1/(1+exp(-sh*x))

par sh=20, auc=.12e8

sv(t)=sheav(tin-t)

g(t)=((vc(t/3600)/1000)/auc)*sv(mod(t,tin+tout))

% DE for the change in volume during a breathing cycle

y'=(g(t)/tau1-y/tau2)

% derivative of alveolar air space volume. we assume that that this is y'

```
vap(x,t)=(g(t)/tau1-x/tau2)

%ratio between the y' and actual alveolar air space volume
rvol(x,t)=vap(x,t)/va(x,t)

% this allows you to plot this ratio
aux r=rvol(y,t)

%alveolar air space volume
va(x,t)=x+(vamin(t/3600)/1000)/auc

% plots scaled alveolar air volume
aux vf=auc*va(y,t)

%number of space units
par spaceunits=20

% fixes outside to gair0=150
gair(t)=gair0
% hill functioin
fh(x,const,hill)=x^hill/(x^hill+const^hill)

%Following Sets up the tables from the tab files created in Matlab
table vamin vamin.tab
table vc vc.tab
table vt vt.tab
table vb vb.tab

% Boundary Conditions
gt0=gt1
```

gt21=gt20

hb40=ihb4

hb421=hb420

gb0=lowo2

gb21=gb20

ct0=ct1

ct21=ct20

cb0=highco2

cb21=cb20

hco30=ihco3

hco321=hco320

%speed of blood during inflammation

v(t)=v0*90/vb(t/3600)

aux speed=v0*vb(t/3600)/90

% Blood equations

%oxygen

gb[1..20]'=(gt[j]-gb[j])*gtbm/(sigmagBT*(vb(t/3600)/1000)/auc)-v(t)*((gb[j]-gb[j-1])/h)

+(fith/sigmagBT)*(-kplus0*(hbtotal-hb4[j])*gb[j]^fith+kminus*hb4[j])

%Hemoglobin

hb4[1..20]'=-v(t)*((hb4[j]-hb4[j-1])/h)+kplus0*(hbtotal-hb4[j])*gb[j]^fith-kminus*hb4[j]

%Carbon Dioxide

cb[1..20]'=(ct[j]-cb[j])*ctbm/(sigmacBT*(vb(t/3600)/1000)/auc)

-v(t)*((cb[j]-cb[j-1])/h)+(kcathco3*hco3[j]/(kmhco3+hco3[j])

-(kcatcb*sigmacBT*cb[j]/(kmcb+sigmacBT*cb[j])))/sigmacBT

%Bicarbonate

```
hco3[1..20]'=(kcatcb*sigmacBT*cb[j]/(kmcb+sigmacBT*cb[j]))
-(kcathco3*hco3[j]/(kmhco3+hco3[j]))-v(t)*(hco3[j]-hco3[j-1])/h

%Tissue equations
%Oxygen
gt[1..20]'= ((gb[j]-gt[j])*gtbm+(ga-gt[j])*gtam)/(sigmagBT*(vt(t/3600)/1000)/auc)
+dgt*(gt[j+1]-2*gt[j]+gt[j-1])/(h^2)

%Carbon Dioxide
ct[1..20]'= ((cb[j]-ct[j])*ctbm+(ca-ct[j])*ctam)/(sigmacBT*(vt(t/3600)/1000)/auc)
+dct*(ct[j+1]-2*ct[j]+ct[j-1])/(h^2)
%Alveolar Airspace
% Oxygen
ga'= gtam*(1/spaceunits)*sum(0,19)of(shift(gt1,i')-ga)/(sigmaair*va(y,t))
+max(rvol(y,t),0)*(gair0-ga)
%Carbon Dioxide
ca'= ctam*(1/spaceunits)*sum(0,19)of(shift(ct1,i')-ca)/(sigmaair*va(y,t))
+max(rvol(y,t),0)*(cair0-ca)

% Initial Conditions
gb[0..20](0)=lowo2
gt[0..20](0)=lowo2
hb4[0..20](0)=ihb4
%Numerics
@ meth=gear,xp=t, dt=.001, yp=ga,xlo=0,xhi=200,ylo=90,yhi=110, total=200, bound=500000
done
```

D.3 PSEUDO CODE FOR THE FULL LUNG MODEL

1) From the normal truncated distribution of tidal volume select N random numbers and bin these numbers using bins that have centers 150 to 550 incrementing by 10.

2) To get the correct initial conditions for each bin:

a) Simulate immune subsystem with each of the centers of the bins, 150, 160, 170,..540, 550 with icbreathing=zeroes(81), t0=0, tfinal=2 and tinc=0.5

b) Feed each data file created in step 2 into to the breathingpde.m file with ic=zeros(123), t0=0, tfinal=2*3600 (2 hours) and the associated unscaled tidal volume. The code will convert to the actual volume on an RU.

c) Save the end level of the Y vector for each created to use as you initial condition from now on. For example, set icbreathing350=Y(:,end) for simulation ran with the tidal volume of 350.

3) Run the immune subsystem on each bin with the same insult. Use ic=zereos(81), ic(21)=4, to get a lethal insult.

4) Feed the data matrix and initial conditions saved in 2c in breathingpde.m for each bin.

5) the weighted average determined by your bid count of the results for oxygen in the blood Y(:,41) and saturated hemoglobin Y(:,61)

6) use these average at each time point as the initial conditions to mixing.m

7) the weighted average determined by your bin counts of the results for oxygen in the blood Y(:,103) and saturated hemoglobin Y(:,123)

8) use these average at each time point as the initial conditions to mixingc.m

9) the results of mixing.m and mixingc.m are the outputs of the full lung model

Mixing.m

```
function [T]=mixing(output)
m=size(output);
ic=output(1,2:3)
```

```
[filenameT1, filenameY1]=breathingend1(ic,0,0.1);
T=[output(1,1) filenameY1(end,:)];
for i=1:m(1)
ic=output(i,2:3);
[filenameT1, filenameY1]=breathingend1(ic,0,0.1);
T=[T;output(i,1) filenameY1(end,:)];
end
```

Mixingc.m

```
function [T]=mixingc(output)
m=size(output);
ic=output(1,2:3)
[filenameT1, filenameY1]=breathingend1c(ic,0,0.1);
T=[output(1,1) filenameY1(end,:)];
for i=40:40:m(1)
ic=output(i,2:3);
[filenameT1, filenameY1]=breathingend1c(ic,0,0.1);
T=[T;output(i,1) filenameY1(end,:)];
end
```

BIBLIOGRAPHY

[1] E. Abraham, K. Reinhart, D. Opal, S., C. I., Doig, A. Rodriguez, R. Beale, P. Svoboda, P. Laterre, S. Simon, B. Light, H. Spapen, J. Stone, A. Seibert, C. Peckelsen, C. de Deyne, R. Postier, V. Pettila, A. Artigas, S. Percell, V. Shu, C. Zwingelstein, J. Tobias, L. Poole, J. Stolzenbach, and A. Creasey, *Efficacy and safety of tifacogin (recombinant tissue factor pathway inhibitor) in severe sepsis: a randomized controlled trial.*, JAMA, 290 (2003), pp. 238–247.

[2] V. Alfaro, J. Roca-Acin, L. Palacios, and R. Guitart, *Multiple inert gas elimination technique for determining ventilation/perfusion distributions in rat during normoxia, hypoxia and hyperoxia.*, Clin. Exp. Pharmacol. Physiol., 28 (2001), pp. 419–424.

[3] U. Andersson, H. Wang, K. Palmblad, A. Aveberger, O. Bloom, H. Erlandsson-Harris, A. Janson, R. Kokkola, M. Zhang, H. Yang, and K. Tracey, *High mobility group 1 protein (hmg-1) stimulates proinflammatory cytokine synthesis in human monocytes*, J. Exp. Med., 192 (2000), pp. 565–570.

[4] D. Annane, *Corticosteroids for septic shock*, Crit Care Med, 29 (2001), pp. 117–20.

[5] D. Annane, V. Sebille, C. Charpentier, P. Bollaert, B. Francois, J. Korach, G. Capellier, Y. Cohen, E. Azoulay, G. Troche, P. Chaumet-Riffaut, and E. Bellissant, *Effect of treatment with low doses of hydrocortisone and fludrocortisone on mortality in patients with septic shock*, JAMA, 288 (2002).

[6] G. Bacon, F. Kenny, H. Murdaugh, and C. Richards, *Prolonged serum half-life of cortisol in renal failure.*, Johns. Hopkins. Med.J., 132 (1973), pp. 127–131.

[7] A. Ben-Tal, *Simplified models for gas exchange in the human lungs.*, J. Theor. Biol., 238 (2006), pp. 474–495.

[8] Y. Bergeron, N. Ouellet, A. Deslauriers, M. Simard, M. Olivier, and M. Bergeron, *Cytokine kinetics and other host factors in response to pneumococcal pulmonary infection in mice.*, Infect. Immun., 66 (1998), pp. 912–922.

[9] G. Bernard, J. Vincent, P. Laterre, S. LaRosa, J. Dhainaut, A. Lopez-Rodriguez, J. Steingrub, G. Garber, J. Helterbrand, E. Ely, and J. Fisher,

C.J., *Efficacy and safety of recombinant human activated protein c for severe sepsis.*, N. Engl. J. Med., 344 (2001), pp. 699–709.

[10] A. Bidani and E. Crandall, *Velocity of co_2 exchanges in the lungs.*, Annu. Rev. Physiol., 50 (1988), pp. 639–652.

[11] E. Bilevicius, D. Dragosavac, S. Dragosavac, S. Araújo, A. Falcão, and R. Terzi, *Multiple organ failure in septic patients*, Braz J Infect Dis, 5 (2001), pp. 103–110.

[12] V. Bocci, *Interleukins. clinical pharmacokinetics and practical implications.*, Clin. Pharmacokinet., 21 (1991), pp. 274–284.

[13] A. Branwood, K. Noble, and K. Schindhelm, *Phagocytosis of carbon particles by macrophages in vitro.*, Biomaterials, 19 (1992), pp. 646–648.

[14] A. Coxon, T. Tang, and T. Mayadas, *Cytokine-activated endothelial cells delay neutrophil apoptosis in vitro and in vivo. a role for granulocyte/macrophage colony-stimulating factor.*, J. Exp. Med., 190 (1999), pp. 923–934.

[15] A. Cross and S. Opal, *A new paradigm for the treatment of sepsis: is it time to consider combination therapy?*, Ann. Intern. Med., 138 (2003), pp. 502–505.

[16] A. D'Andrea, M. ste Amezaga, N. Valiante, X. Ma, M. Kubin, and G. Trinchieri, *Interleukin 10 (il-10) inhibits human lymphocyte interferon gamma-production by suppressing natural killer cell stimulatory factor/il-12 synthesis in accessory cells.*, J. Exp. Med., 178 (1993), pp. 1041–1048.

[17] D. Dantzker, C. Brook, P. Dehart, J. Lynch, and J. Weg, *Ventilation-perfusion distributions in the adult respiratory distress syndrome*, Am. Rev. Respir. Dis., 120 (1979), pp. 1039–1052.

[18] J. Day, J. Rubin, Y. Vodovotz, C. Chow, A. Reynolds, and G. Clermont, *A reduced mathematical model of the acute inflammatory response ii. capturing scenarios of repeated endotoxin administration*, Journal of Theoretical Biology, 242 (2006), pp. 237–256.

[19] R. de Waal Malefyt, J. Abrams, B. Bennett, C. Figdor, and J. de Vries, *Interleukin 10(IL-10) inhibits cytokine synthesis by human monocytes: an autoregulatory role of IL-10 produced by monocytes*, J. Exp. Med., 174 (1991), pp. 1209–1220.

[20] C. Delclaux, S. Rezaiguia-Delclaux, C. Delacourt, C. Brun-Buisson, C. Lafuma, and A. Harf, *Alveolar neutrophils in endotoxin-induced and bacteria-induced acute lung injury in rats*, Am. J. Physiol., 273 (1997), pp. L104–112.

[21] L. Domenici-Lombardo, C. Adembri, M. Consalvo, R. Forzini, M. Meucci, P. Romagnoli, and G. Novelli, *Evolution of endotoxin induced acute lung injury in the rat.*, Int. J. Exp. Pathol., 76 (1995), pp. 381–390.

[22] P. Eichacker, W. Hoffman, A. Farese, S. Banks, G. Kuo, T. MacVittie, and C. Natanson, *TNF but not IL-1 in dogs causes lethal lung injury and multiple organ dysfunction similar to human sepsis*, J. Appl. Physiol., 71 (1991), pp. 1979–1989.

[23] G. B. Ermentrout, *Simulating, analyzing, and animating dynamical systems: A guide to XPPAUT for researchers and students.*, Soc. for Industrial & Applied Math, Philadelphia, 1 ed., 2002.

[24] A. Fuchs, E. Granowitz, L. Shapiro, E. Vannier, G. Lonnemann, J. Angel, J. Kennedy, A. Rabson, E. Radwanski, M. Affrime, D. Cutler, P. Grint, and C. Dinarello, *Clinical, hematologic, and immunologic effects of interleukin-10 in humans.*, J. Clin. Immunol., 16 (1996), pp. 291–303.

[25] C. Gabka, P. Benhaim, S. Mathes, H. Scheuenstuhl, A. Chan, K. Fu, and T. Hunt, *An experimental model to determine the effect of irradiated tissue on neutrophil function*, Plast. Reconstr. Surg., 96 (1995), pp. 1676–1688.

[26] R. Goris, T. te Boekhorst, J. Nuytinck, and J. Gimbrere, *Multiple-organ failure. generalized autodestructive inflammation?*, Arch. Surg., 120 (1985), pp. 1109–1115.

[27] A. Guyton and J. Hall, *Textbook of Medical Physiology.*, W.B. Saunders Company, Philadelphia, PA, 2000.

[28] C. Hahn, A. Black, S. Barton, and I. Scott, *Gas exchange in a three-compartment lung model analyzed by forcing sinusoids of n2o.*, J. Appl. Physiol., 75 (1993), pp. 1863–1876.

[29] E. Hill, G. Power, and L. Longo, *Mathematical simulation of pulmonary o_2 and co_2 exchange.*, American Journal of Physiology, 224 (1973), pp. 904–917.

[30] Hlastala, *Complexity in Structure and Function of the Lung (Lung Biology in Health and Disease)*, Informa Healthcare, 1st ed., 8 1998.

[31] R. Huhn, E. Radwanski, J. Gallo, M. Affrime, R. Sabo, G. Gonyo, A. Monge, and D. Cutler, *Pharmacodynamics of subcutaneous recombinant human interleukin-10 in healthy volunteers.*, Clin. Pharmacol. Ther., 62 (1997), pp. 171–180.

[32] P. Isler, B. de Rochemonteix, F. Songeon, N. Boehringer, and L. Nicod, *Interleukin-12 production by human alveolar macrophages is controlled by the autocrine production of interleukin-10.*, Am. J. Respir. Cell Mol. Biol., 20 (1999), pp. 270–278.

[33] C. Janeway and R. Jr.and Medzhitov, *Innate immune recognition.*, Annu. Rev. Immunol., 20 (2002), pp. 197–216.

[34] C. Janeway, P. Travers, M. Walport, and M. Shlomchik, *Immunobiology: The immune system in health and disease*, Garland Publishing, New York, 5 ed., 2001.

[35] D. Joyce and B. Grinnell, *Recombinant human activated protein c attenuates the inflammatory response in endothelium and monocytes by modulating nuclear factor-kappab.*, Crit. Care. Med., 30 (2002), pp. S288–S293.

[36] J. Keener and J. Sneyd, *Mathematical Physiology.*, Springer-Verlag, New York, 1998.

[37] J. Kimbell, R. Segal, B. Asgharian, B. Wong, J. Schroeter, J. Southall, C. Dickens, G. Brace, and F. Miller, *Characterization of deposition from nasal spray devices using a computational fluid dynamics model of the human nasal passages*, J Aerosol Med, 20 (2007), pp. 59–74.

[38] R. Kumar, G. Clermont, Y. Vodovotz, and C. Chow, *The dynamics of acute inflammation.*, J. Theor. Biol., 230 (2004), pp. 145–155.

[39] C. Liu, S. Niranjan, J. J. Clark, K. San, J. Zwischenberger, and A. Bidani, *Airway mechanics, gas exchange, and blood flow in a nonlinear model of the normal human lung.*, J. Appl. Physiol., 84 (1998), pp. 1447–1469.

[40] S. Marino and D. Kirschner, *The human immune response to mycobacterium tuberculosis in lung and lymph node.*, J. Theor. Biol., 227 (2004), pp. 463–486.

[41] S. Marino, D. Sud, H. Plessner, P. Lin, J. Chan, J. Flynn, and D. Kirschner, *Differences in reactivation of tuberculosis induced from anti-tnf treatments are based on bioavailability in granulomatous tissue.*, PLoS Comput. Biol., 3 (2007), pp. 1909–1924.

[42] J. Marshall, *Clinical trials of mediator-directed therapy in sepsis: what have we learned?*, Intensive Care Med., 26, Suppl 1 (2000), pp. 75–83.

[43] ——, *Such stuff as dreams are made on: mediator-directed therapy in sepsis*, Nat Rev Drug Discov, 2 (2003), pp. 391–405.

[44] J. Mathison, E. Wolfson, and R. Ulevitch, *Participation of tumor necrosis factor in the mediation of gram negative bacterial lipopolysaccharide-induced injury in rabbits*, J. Clin. Invest., 81 (1988), pp. 1925–1937.

[45] H. Maurenbrecher, M. Lamy, G. by Dupont, P. Frascarolo, and G. Hedenstierna, *An animal model of response and nonresponse to inhaled nitric oxide in endotoxin-induced lung injury.*, Chest, 120 (2001), pp. 573–581.

[46] T. Menges, P. Hermans, S. Little, T. Langefeld, O. Boning, J. Engel, M. Sluijter, R. de Groot, and G. Hempelmann, *Plasminogen-activator-inhibitor-1 4g/5g promoter polymorphism and prognosis of severely injured patients.*, Lancet, 357 (2001).

[47] H. Moller, X. Chen, B. Saam, K. Hagspiel, G. Johnson, T. Altes, E. de Lange, and H. Kauczor, *Mri of the lungs using hyperpolarized noble gases.*, Magn. Reson. Med., 47 (2002), pp. 1029–1051.

[48] H. Movat, M. Cybulsky, I. Colditz, M. Chan, and C. Dinarello, *Acute inflammation in gram-negative infection: endotoxin, interleukin 1, tumor necrosis factor, and neutrophils*, Fed. Proc., 46 (1987), pp. 97–104.

[49] P. Neumann and G. Hedenstierna, *Ventilation-perfusion distributions in different porcine lung injury models*, Acta Anaesthesiol Scand, 45 (2001), pp. 78–86.

[50] J. Nick, C. Coldren, M. Geraci, K. Poch, B. Fouty, J. O'Brien, M. Gruber, S. Zarini, Murphy, K. R.C., R. K., K. D., Kast, and E. Abraham, *Recombinant human activated protein c reduces human endotoxin-induced pulmonary inflammation via inhibition of neutrophil chemotaxis.*, Blood, 104 (13) (2004), pp. 3878–3885.

[51] A. Ochsenbein and R. Zinkernagel, *Natural antibodies and complement link innate and acquired immunity.*, Immunol. Today, 21 (2000), pp. 624–630.

[52] T. Olson, K. Singbartl, and K. Ley, *L-selectin is required for fmlp- but not c5a-induced margination of neutrophils in pulmonary circulation.*, Am. J. Physiol. Regul. Integr. Comp. Physiol., 282 (2002), pp. R1245–R1252.

[53] I. Pallister, C. Dent, and N. Topley, *Increased neutrophil migratory activity after major trauma: a factor in the etiology of acute respiratory distress syndrome?*, Crit. Care Med., 30 (2002), pp. 1717–1721.

[54] F. Paulsen, T. Pufe, L. Conradi, D. Varoga, M. Tsokos, J. Papendieck, and W. Petersen, *Antimicrobial peptides are expressed and produced in healthy and inflamed human synovial membranes.*, J. Pathol., 198 (2002), pp. 369–77.

[55] M. Peters, *Animal models of autoimmune liver disease*, Immunol. Cell Biol., 80 (2002), pp. 113–116.

[56] J. Peterson, K. Feeback, J. Baas, and F. Pizza, *Tumor necrosis factor-alpha promotes the accumulation of neutrophils and macrophages in skeletal muscle*, J. Appl. Physiol., 101 (2006), pp. 1394–1399.

[57] P. Raj and A. Dentino, *Current status of defensins and their role in innate and adaptive immunity.*, FEMS Microbiol. Lett., 206 (2002), pp. 9–18.

[58] A. Reynolds, J. Rubin, G. Clermont, J. Day, and B. Ermentrout, *A reduced mathematical model of the acute inflammatory response: I. derivation of the model and analysis of anti-inflammation.*, J .Theor. Biol., 242 (2006), pp. 220–236.

[59] C. Rhodes, S. Valind, L. Brudin, P. Wollmer, T. Jones, P. Buckingham, and J. Hughes, *Quantification of regional v/q ratios in humans by use of pet. ii. procedure and normal values.*, J. Appl. Physiol., 66 (1989), pp. 1905–1913.

[60] J. Roca and P. Wagner, *Contribution of multiple inert gas elimination technique to pulmonary medicine. 1. principles and information content of the multiple inert gas elimination technique.*, Thorax, 49 (1994), pp. 815–824.

[61] F. Roughton, *The average time spent by the blood in the human lung capillary and its relation to the rates of co uptake and elimination in man.*, American Journal of Physiology, 143 (1945), pp. 621–633.

[62] G. Rubenfeld and M. Herridge, *Epidemiology and outcomes of acute lung injury*, Chest, 131 (2007), pp. 554–562.

[63] W. Schumer, *Steroids in the treatment of clinical septic shock.*, Ann. Surg., 184 (1976), pp. 333–341.

[64] W. S. Spector, *Handbook of biological data.*, W.B. Saunders Company, London, 1956.

[65] C. Sprung, P. Caralis, E. Marcial, M. Pierce, M. Gelbard, W. Long, R. Duncan, M. Tendler, and M. Karpf, *The effects of high-dose corticosteroids in patients with septic shock. a prospective, controlled study.*, N. Engl. J. Med., 311 (1984), pp. 1137–1143.

[66] S. H. Strogatz, *Nonlinear dynamics and chaos: With application to physics, biology, chemistry, and engineering.*, Westview Press, Cambridge, 1994.

[67] V. Stvrtinova, J. Jakubovsky, and I. Hulin, *The acute phase reactants.*, Inflammation and Fever Academic Electronic Press., (1995).

[68] A. Takala, I. Jousela, S. Jansson, K. Olkkola, O. Takkunen, A. Orpana, S. Karonen, and H. Repo, *Markers of systemic inflammation predicting organ failure in community-acquired septic shock.*, Clin Sci.(Lond), 97 (1999), pp. 529–538.

[69] M. Tawhai and K. Burrowes, *Developing integrative computational models of pulmonary structure.*, Anat. Rec. B. New. Anat., 275 (2003), pp. 207–218.

[70] K. Todar, *Growth of bacterial populations*, Todar's online textbook of bacteriology. Date Accessed: 10-21-2005. http://www.textbookofbacteriology.net., (2002).

[71] K. Tsukaguchi, L. de Lange, and W. Boom, *Differential regulation of ifn-gamma, tnf-alpha, and il-10 production by cd4(+) alphabetatcr+ t cells and vdelta2(+) gammadelta t cells in response to monocytes infected with mycobacterium tuberculosis-h37ra.*, Cell Immunol., 194 (1999), pp. 12–20.

[72] M. Ursino and E. Magosso, *Acute cardiovascular response to isocapnic hypoxia. I. A mathematical model*, Am. J. Physiol. Heart Circ. Physiol., 279 (2000), pp. H149–165.

[73] L. Vane, D. Prough, M. Kinsky, C. Williams, J. Grady, and G. Kramer, *Effects of different catecholamines on the dynamics of volume expansion of crystalloid infusion*, Anesthesiology, 101 (2004), pp. 1136–1144.

[74] J. Vincent, Y. Sakr, C. Sprung, V. Ranieri, K. Reinhart, H. Gerlach, R. Moreno, J. Carlet, J. Le Gall, and D. Payen, *Sepsis in European intensive care units: results of the SOAP study*, Crit. Care Med., 34 (2006), pp. 344–353.

[75] Y. Vodovotz, C. Chow, J. Bartels, C. Lagoa, J. Prince, R. Levy, R. Kumar, J. Day, J. Rubin, G. Constantine, T. Billiar, M. Fink, and G. Clermont, *In silico models of acute inflammation in animals*, Shock, 26 (2006), pp. 235–244.

[76] H. Wang, O. Bloom, M. Zhang, J. Vishnubhakat, M. Ombrellino, J. Che, A. Frazier, H. Yang, S. Ivanova, L. Borovikova, K. Manogue, E. Faist, E. Abraham, J. Andersson, U. Andersson, P. Molina, N. Abumrad, A. Sama, and K. Tracey, *HMG-1 as a late mediator of endotoxin lethality in mice*, Science, 285 (1999), pp. 248–251.

[77] H. Yeh and G. Schum, *Models of human lung airways and their application to inhaled particle deposition*, Bull. Math. Biol., 42 (1980), pp. 461–480.

[78] F. Zeni, B. Freeman, and C. Natanson, *Anti-inflammatory therapies to treat sepsis and septic shock: a reassessment*, Crit. Care Med., 25 (1997), pp. 1095–1100.

[79] J. Zimmerman, W. Knaus, X. Sun, and D. Wagner, *Severity stratification and outcome prediction for multisystem organ failure and dysfunction*, World J Surg, 20 (1996), pp. 401–405.

[80] M. Zouali, *Antibodies in Encyclopedia of life science.*, Nature Publishing Group, www.els.net, 2001.